UMTRI-86-14

AD-A169 563

# Analysis of Head and Neck Dynamic Response of the U.S. Adult Military Population

A.C. Bosio
B.M. Bowman

DTIC
SELECTE
JUL 0 8 1986
S D
D

APRIL 1986

**UMTRI** The University of Michigan Transportation Research Institute

*A169563*

**Technical Report Documentation Page**

| 1. Report No.  UMTRI-86-14 | 2. Government Accession No. | 3. Recipient's Catalog No. |
|---|---|---|
| 4. Title and Subtitle  Analysis of head and neck dynamic response of the U. S. adult military population | | 5. Report Date  April 15, 1986 |
| | | 6. Performing Organization Code  UMTRI, IST (5670) |
| 7. Author's)  A. C. Bosio and B. M. Bowman | | 8. Performing Organization Report No.  UMTRI-86-14 |
| 9. Performing Organization Name and Address  Transportation Research Institute  University of Michigan  Ann Arbor, Michigan 48109-2150 | | 10. Work Unit No.  019286 |
| | | 11. Contract or Grant No.  N00014-81-K-0603 |
| 12. Sponsoring Agency Name and Address  Naval Medical Research and Development Command  National Naval Medical Center  Bethesda, Maryland 20814 | | 13. Type of Report and Period Covered  Final Technical Report  1 Oct. 1984 - 1 Feb. 1986 |
| | | 14. Sponsoring Agency Code |
| 15. Naval Biodynamics Laboratory  Box 29407, Michoud Station  New Orleans, Louisiana 70129 | | |

16. Abstract. Mechanisms of head/neck dynamic response were investigated for NBDL volunteer data in −Gx and +Gy acceleration vectors with the MVMA 2-D and VOM 3-D Crash Victim Simulation models. Computer simulation of human subject response yielded mechanical constants pertinent to the design of a Biofidelic Manikin (BFM). Improved biofidelity for a two-joint neck model was achieved by relocating the lower neck pivot point inferior and posterior to anatomic T1. In −Gx, the magnitude and duration for condyles extension, in particular, was improved while satisfactory acceleration response was maintained. Exercising the neck model at −6Gx and −15Gx showed that it was necessary to use nonlinear stiffnesses for the lower neck joint in flexion.

Two modes of extension motion at the occipital condyles were seen in the volunteer subjects. The first mode was extension with rebound (some subjects demonstrating flexion). The second mode was peak extension followed by further increase in the extension motion. The two modes of condyles extension appear to depend on some pre-test condition — probably muscle tensing — since the short duration of the head and neck motion in a test (300 ms) should not allow muscular reaction beginning after the onset of the test to be a factor. Simulations with a model that has passive neck elements give only the extension with rebound response, i.e., mode one response. Thus, on the basis of simulations, it can probably be said that mode one response results for subjects who are not pretensed and mode two response results for pre-tensed subjects.

| 17. Key Words  Anthropomorphic dummy  Impact  Manikin  Neck Model  Simulation | | 18. Distribution Statement  Unlimited | | |
|---|---|---|---|---|
| 19. Security Classif. (of this report)  Unclassified | | 20. Security Classif. (of this page)  Unclassified | 21. No. of Pages  136 | 22. Price |

/

## TABLE OF CONTENTS

QUALITY
INSPECTED
1

Accesion For

| | | |
|---|---|---|
| NTIS CRA&I | | ☑ |
| DTIC TAB | | ☐ |
| Unannounced | | ☐ |
| Justification | | |

By ..............................
Distribution /

Availability Codes

| Dist | Avail and / or Special |
|---|---|
| A-1 | |

i

# LIST OF FIGURES

# I. INTRODUCTION

The Biosciences Division of the Transportation Research Institute has completed Phase III of a study conducted in cooperation and conjunction with the Naval Biodynamics Laboratory: "Analysis of Head and Neck Dynamic Response of the U.S. Adult Military Population" (Contract No. N00014-81-K-0603).

This study has two primary goals:

1) to develop a better understanding of the mechanisms involved in head and neck dynamic response;

2) to develop guidance for the design of the neck module for a Bio-Fidelic Manikin (BFM).

The basic methodology applied in this study is computer simulation of human subject response in sled tests carried out at the Naval Biodynamics Laboratory.

## II. BACKGROUND

The program of impact acceleration tests being conducted at NBDL (1-10) has been of particular importance among efforts over the past twenty-five years to gain an understanding of human impact response. This effort has resulted in the most extensive body of experimental data that exists for human head/neck dynamic response. The work has involved precise measurement of the dynamic response of the head, neck, and first thoracic vertebra. A significant part of the total effort was the development of data acquisition and data processing systems.

Study of NBDL experimental data through application of simulation models has made possible the determination of biomechanical properties of the neck structure of human test subjects (11-20). This approach has made it possible to establish relationships that exist between dynamic response and the mechanical parameters of the neck.

The MVMA 2-D and VOM 3-D Crash Victim Simulation models (20-23) were exercised with NBDL data to refine neck model parameters in each phase of this work. In Phases I and II of this study, methods and required computer codes were established for investigation of data provided by NBDL. Phase I effort utilized pre-1976 data for −Gx vector tests. Initial investigations of +Gy data were carried out as well. Phase II effort utilized NBDL data of improved quality for both −Gx and +Gy and led to refined analysis methods and refined results. In Phase III, NBDL data of still better quality have been used and better analysis methods have been developed, building upon the methods established in the earlier work. Important questions relating to the mechanisms of head/neck dynamic response and resulting from Phase II work have been investigated in Phase III.

Because of funding delays and time required by NBDL for processing of requested data, Phase III effort was not begun until approximately eighteen months after the end of primary Phase II work. In the interim, UMTRI prepared and presented a technical paper on Phase II findings (19).

5

# III. METHODS AND PROCEDURES

The following tasks were defined for Phase III effort.

Task 1. Determine the nature of nonlinearities in the biomechanical properties of the human neck.

Task 2. Simulate + Gz tests being run at NBDL.

Task 3. Refine understanding of head/neck biomechanics through continued simulation analysis of NBDL tests in all vector directions.

Task 4. Investigate, to the extent possible, the relationship between injury potential, dynamic response levels, and dynamic response mechanisms.

Task 5. Carry out a formal parameter sensitivity study for the established "baseline" analytical neck model.

Task 6. Establish a maximally simplified set of model parameters which can serve as a design plan for a neck for an anthropomorphic dummy.

Work on the above tasks was begun only after a considerable amount of effort given to "restart" activities. Because of the funding discontinuity between Phase II and Phase III, a staff member who had been instrumental in the earlier work was no longer available and a new staff member had to be trained in the various specific aspects of data handling, computer simulation, and analysis of simulation results. Additionally, a not insignificant effort was required in reconstituting data and program files and re-establishing techniques developed in the course of Phase II work.

A brief summary of Phase III activity relevant to the above tasks is given below. Presentation of results is given in Section V.

## SUMMARY OF ACTIVITY:

on Task 1 — Simulations were designed and carried out for the purpose of determining whether nonlinear material properties need to be represented in manikin neck design. Nonlinear material properties at C7/T1 were necessary to improve the biofidelity of simulation results at $-6Gx$ and $-15Gx$.

on Task 2 — Simulations in the +Gz vector were not carried out because data were not provided by NBDL.

7

on Task 3 — Response mechanisms were investigated through simulation of −Gx and +Gy tests. Of major importance was achieving a condyles extension of sufficient magnitude and duration in simulations. Modification of the joint parameter data provided only small improvements in the condyles extension motion. Relocating the upper and lower pivot points, however, provided a significant modification of motion and moments at the neck joints. A two-joint model is described which has the upper pivot point at the occipital condyles and the lower pivot point inferior and posterior to anatomic T1.

on Task 4 — At the request of NBDL, no effort was expended toward an attempt to determine information relevant to injury thresholds. Since no NBDL tests with human subjects are at high enough impact levels to cause injury, such a study could at best have determined lower bounds on injury thresholds.

on Task 5 — A formal parameter sensitivity study was not carried out since a "baseline" neck model has not been established. Such a study will be meaningful only after +Gz data have been investigated and further investigation is done in parallel in the −Gx and +Gy vectors. Nonetheless, parameter sensitivity information of some usefulness is determined as an implicit part of every series of computer simulations carried out with non-final (i.e., "non-baseline") neck model data.

on Task 6 — Recommendation of a maximally simplified set of model parameters similarly cannot be given until after a "baseline" neck model is established. Simulation effort has proceeded, however, with a goal of establishing a parsimonious neck model in mind. Parameter sensitivity information and study of response mechanisms are both pertinent to this goal.

# IV. DATA PREPARATION

## NBDL Time-Averaged Data for −Gx and +Gy

NBDL data for multi-vectorial acceleration response was received for subjects H00118 through H00142 in September, 1985. Test data were selected for −Gx and +Gy for forcing inputs and impact reponse data. The volunteer test data were plotted for all test subjects for −6Gx, −10Gx, −15GX, and +5Gy to assess the data for anomalies and outlier response characteristics. Examples of the volunteer data are presented below prior to the averaging of results to illustrate characteristics of the experimental data.

−6Gx Volunteer Response Data. In Figures 1-10, the response data for −6Gx impacts of subjects H00118 and H00130 are shown. T1 x- and z-axis accelerations (Figures 1-2) are averaged for forcing inputs for simulations of −Gx tests. In some tests, however, large acceleration spikes were observed in the time history data. The T1 z-axis acceleration-time histories in Figure 2, for example, show large positive spikes. Acceleration peaks that exceeded the average peak accelerations by a factor two or more in the T1-x and T1-z acceleration forcing inputs were considered anomalous. Tests that demonstrated this response were not included in time averaging.

Figures 3-6 show the response data for the head angular position, head angular velocity, head angular acceleration, and head resultant acceleration for subjects H00118 and H00130, respectively. Head angular motion and linear acceleration response data were used in Phase II to assess the biofidelity of the neck model response for volunteer T1 forcing inputs. In Phase III, response data were determined for the head origin x-and z-axis displacement relative to T1 (Figures 7-8), and the joint relative angles at the condyles and T1 (Figures 9-10). The condyles relative angle is defined as neck angle minus head angle. T1 relative angle is torso angle minus neck angle. Since all motion takes place in the midsagittal plane, negative relative angles are seen when the head angle is greater than neck angle at the condyles or the neck angle is greater than torso angle at T1.

For −6Gx simulations, data used as forcing input to the models and for comparison with model predicted dynamic responses were obtained by averaging the time histories of 15 individual tests of NBDL volunteers. The tests used were: LX3856 (Subject 118), LX3875(118), LX3880 (118), LX3851 (120), LX3852 (127), LX3854 (130), LX3876 (130), LX3857 (131), LX3885 (131), LX3858 (132), LX3887 (132),

9

LX3869 (133), LX3870 (134), LX3871 (135), LX3872 (136). These tests were selected from the eighteen −6Gx runs on computer tapes prepared for UMTRI by NBDL in September 1985. Although there was more than one run for some subjects, no subject was represented more than once in final averaged results. An intermediate averaging step produced an "average run" for each subject so that the ten subjects could be represented with equal weight.

With the approach of averaging across runs, responses that may reflect individual differences in the test subjects were weighted against the responses of all other subjects. Anomalous response characteristics were therefore de-emphasized by averaging. It is felt that neck model parameters determined from simulations with averaged subject response data will successfully model a hypothetical subject who is "average" for the group in terms of strength and anthropometry.

−10Gx Volunteer Response Data. In Figures 11–20, the response data for −10Gx impacts of subjects H00132, H00133, and H00135 are shown. The time histories for NBDL volunteer response at −10Gx show the following types of response. Large T1 z-acceleration spikes, both positive and negative, are present at −10Gx (Figure 12). The bimodal head angular acceleration shown in Figure 15 is an "atypical" test subject response for subject H00132, test LX3989. It should be noted that an "atypical" response is seen only for head angular acceleration, i.e., the time histories for test LX3989 are similar to other subjects' with the exception of head angular acceleration. In Figure 19, subject H00133 displays two distinct modes of condyles extension. Subject H00133 displayed extension with rebound in test LX3913, while no significant rebound occurred in test LX3998. It seems unusual that the condyles extension angle becomes increasingly negative after the first peak in test LX3998. (This response, i.e., extreme extension, was seen in other subjects as well at −10Gx and −15Gx and a discussion of condyles extension in the volunteer response is given below in the section "-Gx NBDL Volunteer Data: Two Modes of Condyles Extension.")

For −10Gx simulations, data were obtained by averaging the time histories of 14 individual tests of NBDL volunteers. The tests used were: LX3903 (Subject 118), LX3985(118), LX3906 (120), LX3995 (120), LX3904 (127), LX3928 (130), LX3991 (130), LX3908 (131), LX3999 (131), LX3909 (132), LX3998 (133), LX3913 (133), LX3916 (135), LX3918 (136).

−15Gx Volunteer Response Data. Volunteer data for subjects H00127, H00132, and H00133 are shown for −15Gx in Figures 21-30. In Figures 21 and 22, large positive and negative spikes are observed in both the T1-x and T1-z acceleration responses. It is difficult identify the source of the acceleration spikes in the −Gx data, but it is present in the data at −6Gx, −10Gx, and −15Gx for certain tests. These data were eliminated from the time-averaged volunteer data. Subject H00133 once more demonstrated two modes of condyles extension at −15Gx (Figure 29), similar to the subject's response at −10Gx (Figure 19). In test LX3986, the extension at the condyles exceeds 100 degrees for subject H00133 at −15Gx. It is interesting to note that there is a larger range of variation among test subjects in joint relative angles than in inertial head angles, which have a relatively narrow corridor (Figure 23).

For −15Gx simulations, data were obtained by averaging the time histories of 13 individual tests of NBDL volunteers. The tests used were: LX3958 (Subject 118), LX3969(118), LX3972 (120), LX3987 (131), LX3990 (131), LX3959 (127), LX3982 (132), LX3957 (132), LX3963 (133), LX3986 (133), LX3983 (134), LX3965 (135), LX3970 (135).

+5Gy Volunteer Response Data. The volunteer data for subjects H00130, H00131, H00132, and H00133 are shown for +5Gy in Figures 31-39. The forcing inputs for T1 are shown in Figures 31-33. The components of the head linear acceleration response and the Euler angles for head yaw, pitch, and roll are shown in Figures 34-39, respectively.

The forcing inputs for simulations of NBDL +5Gy tests were obtained by averaging the time histories of eight tests of NBDL volunteers. The averaged tests were: LX4088 (Subject 130), LX4089 (131), LX4093 (133), LX4100 (139), LX4094 (141), LX4097 (134), LX4095 (135), and LX4098 (138). In general, there was a greater amount of variation in the +Gy response variables than in the corresponding data for −Gx.

Stick Figure Plots for 3-D Motion. A new feature was added to the VOM CVS post-processor prior to Phase III startup. A Fortran program was written for obtaining "stick figure" printer plots of the head/neck motion predicted by the VOM model. Up to five views of a 3-D stick figure are plotted at a minimum time interval of 10 ms between plots. The program calculates the 3-D rotation matrix for the head and projects contours and landmarks onto a 2-D view plane defined by the user. Each view plane is normal to a vector from the T1 origin. An example of 3-D

11

stick figure plotting is shown in Figure 40. The view plane is normal to the laboratory x-axis for a +5Gy simulation. Head contours and eyes, ears, and nose provide information for assessing both planar and nonplanar head motion. The neck cord extends from anatomic T1 to the occipital condyles. A triaxial head target on the top of the head (visible in two frames) further aids in following nonplanar head motion.

## -Gx NBDL Volunteer Data: Two Modes of Condyles Extension

The data shown in Figures 1–30 for the volunteer response in − Gx generally demonstrate a high degree of similarity in waveform for the time histories for different subjects. One notable exception to the marked similarity of the results was the time history for the condyles relative angle.

It was observed for − Gx tests that the waveform of condyles relative angle response differed significantly after the first peak. At − 6Gx and − 10Gx, a majority of the subjects show condyles extension with rebound, but a few subjects show extension with little or no rebound. At − 15Gx, the extension with rebound motion and extension with no rebound are both more pronounced. The two modes of extension are of interest in that a two-joint passive neck model simulates one mode of extension response (extension with rebound), but it does not simulate the other mode (no rebound). In addition, the pattern of these two types of extension motion suggest that it is controlled by the subject, probably by pre-test muscle tensing.

Condyles Extension at − 6Gx. In Figures 41–46, the time histories of − 6Gx joint relative angles are plotted. The condyles joint displays an extension motion in all cases followed by largely varying amounts of rebound from extension. In Figure 41, subject H00118 shows no significant rebound from extension in test LX3875 (solid line) while the same subject shows a significant rebound in tests LX3856 and LX3880. In Figure 43, subject 131 (LX3857) demonstrates no rebound after the peak extension. The other tests in Figure 43 all show a peak extension with rebound. The T1 joint relative angle in Figure 44 shows that the subjects experiencing the largest angulations for condyles extension also show large T1 joint angulations. The converse is also shown in that smaller condyles angulation is paired with smaller T1 angulation. In Figure 45, subject 134 (LX3870) shows no rebound after peak extension while the other four tests show rebound. (It is interesting to note that only subject 127 shows flexion at the end of the impact in Figure 45.)

12

## 1-T1 X-ACCELERATION
### NBDL SUBJECTS 118, 130; -GX AT 6.2 G'S
### T1 MOTION FORCED
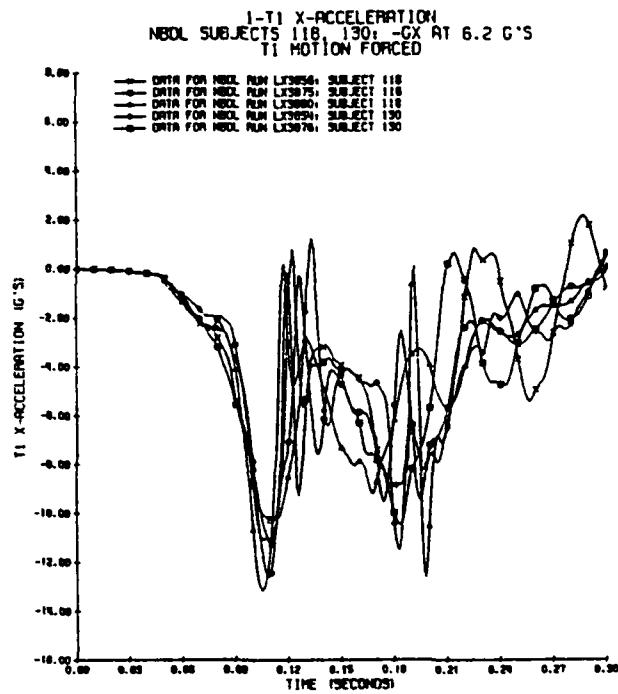


Figure 1. T1 X-Axis Acceleration-Time History at -6Gx for NBDL Subjects 118 and 130.

## 2-T1 Z-ACCELERATION
### NBDL SUBJECTS 118, 130; -GX AT 6.2 G'S
### T1 MOTION FORCED
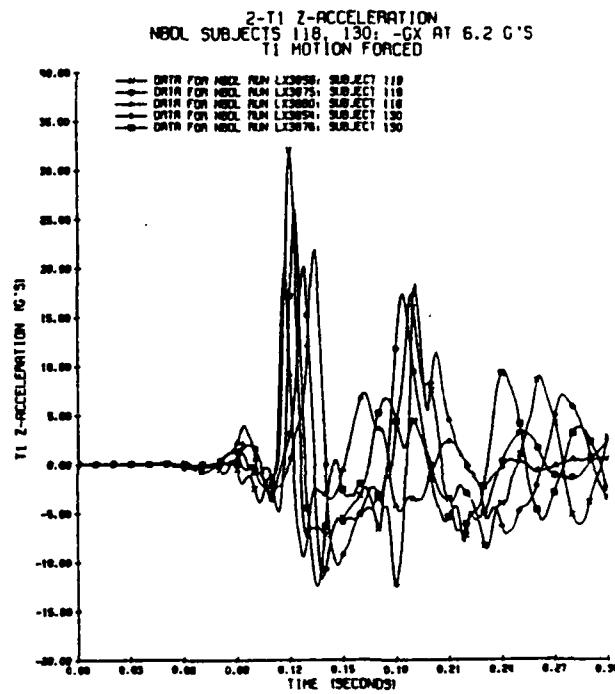


Figure 2. T1 Z-Axis Acceleration-Time History at -6Gx for NBDL Subjects 118 and 130.

## 3-HEAD ANGULAR POSITION
### NBDL SUBJECTS 118, 130; -GX AT 6.2 G'S
### T1 MOTION FORCED
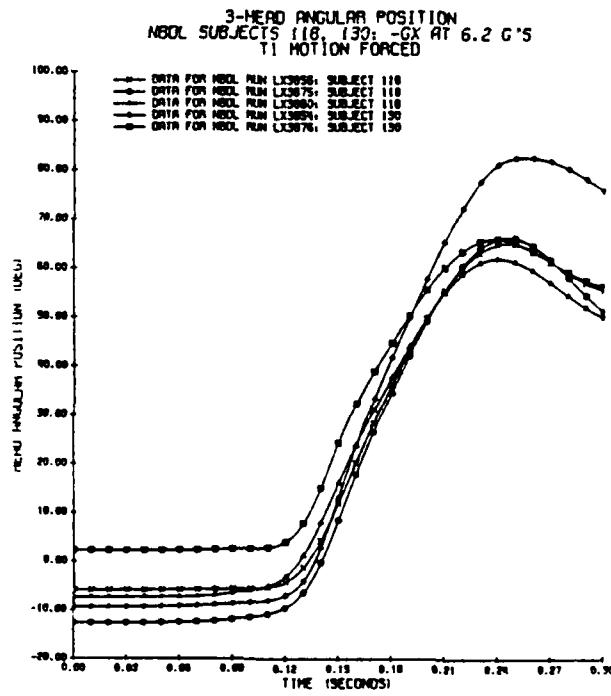


Figure 3. Head Angular Position-Time History at -6Gx for NBDL Subjects 118 and 130.

## 4-HEAD ANGULAR VELOCITY
### NBDL SUBJECTS 118, 130; -GX AT 6.2 G'S
### T1 MOTION FORCED
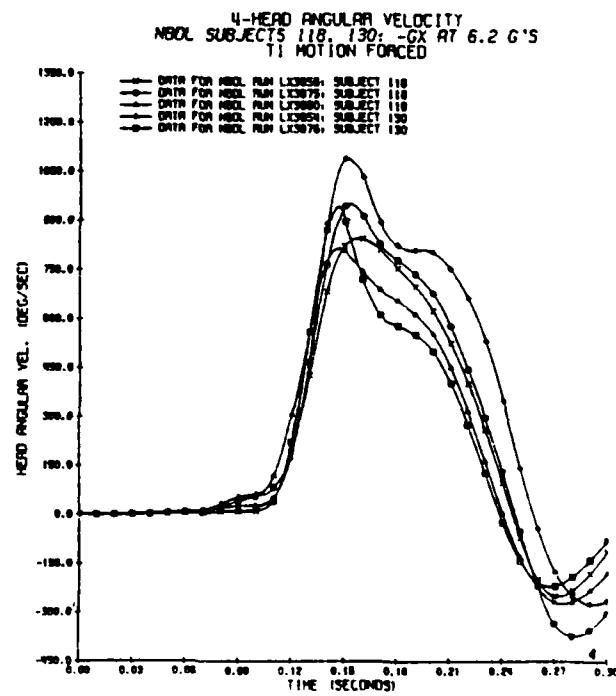


Figure 4. Head Angular Velocity-Time History at -6Gx for NBDL Subjects 118 and 130.

13

## 5-HEAD ANGULAR ACCELERATION
### NBDL SUBJECTS 118, 130: -GX AT 6.2 G'S
### T1 MOTION FORCED
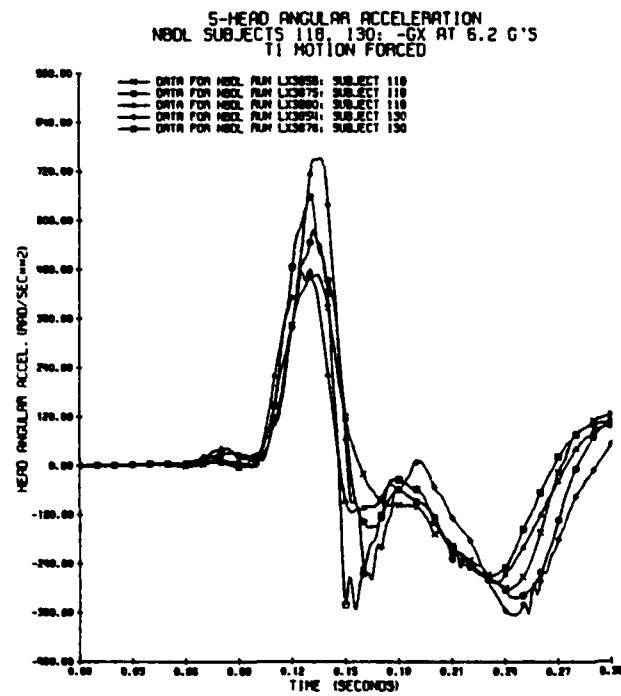
Figure 5. Head Angular Acceleration-Time History at -6Gx for NBDL Subjects 118 and 130.

## 6-RESUL. LINEAR ACCEL. OF HEAD ANATOMICAL ORIGIN
### NBDL SUBJECTS 118, 130: -GX AT 6.2 G'S
### T1 MOTION FORCED
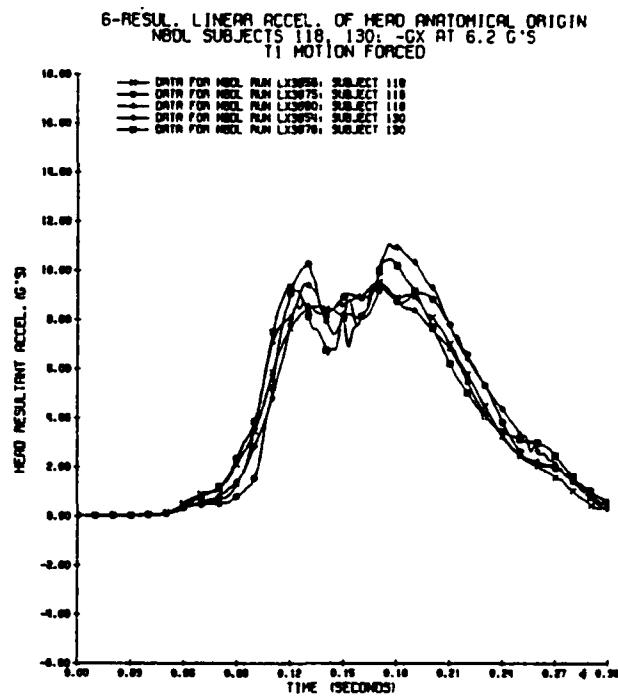
Figure 6. Head Resultant Acceleration-Time History at -6Gx for NBDL Subjects 118 and 130.

## 7-HEAD X-DISPL. REL. TO T1
### NBDL SUBJECTS 118, 130: -GX AT 6.2 G'S
### T1 MOTION FORCED
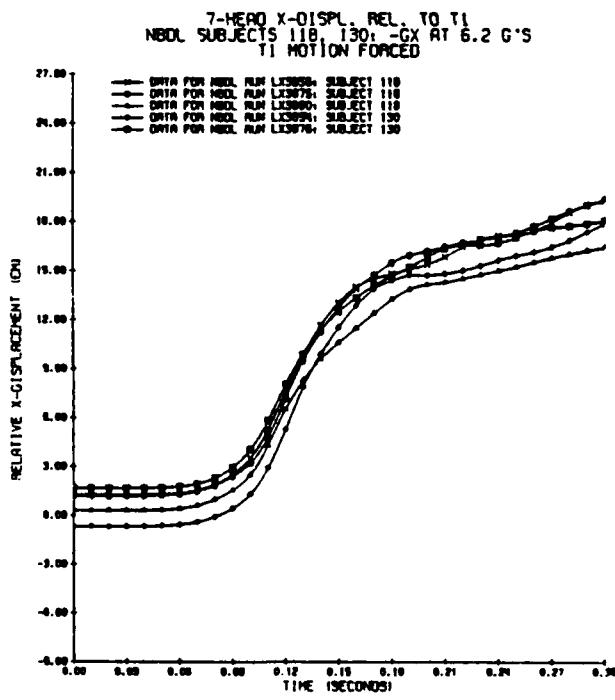
Figure 7. Head Origin X-Axis Displacement-Time History at -6Gx for NBDL Subjects 118 and 130.

## 8-HEAD Z-DISPL. REL. TO T1
### NBDL SUBJECTS 118, 130: -GX AT 6.2 G'S
### T1 MOTION FORCED
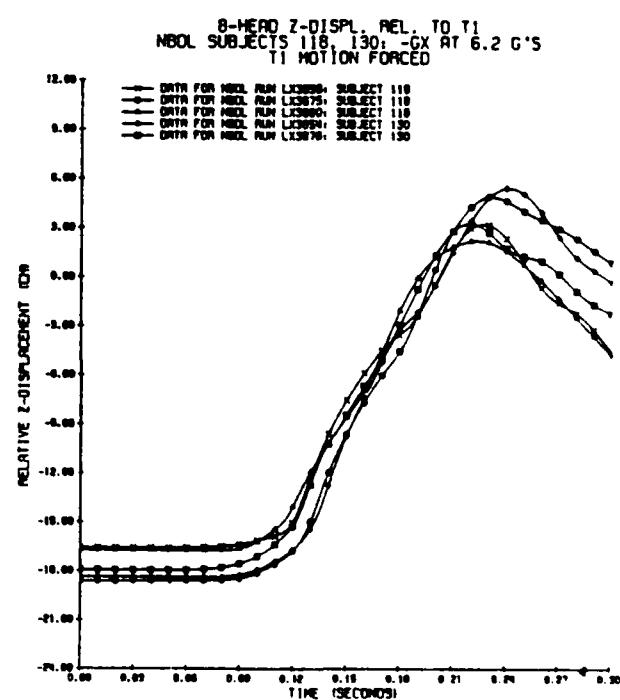
Figure 8. Head Origin Z-Axis Displacement-Time History at -6Gx for NBDL Subjects 118 and 130.

14

22-CONDYLES RELATIVE ANGLE
NBDL SUBJECTS 118, 130; -GX AT 6.2 G'S
T1 MOTION FORCED
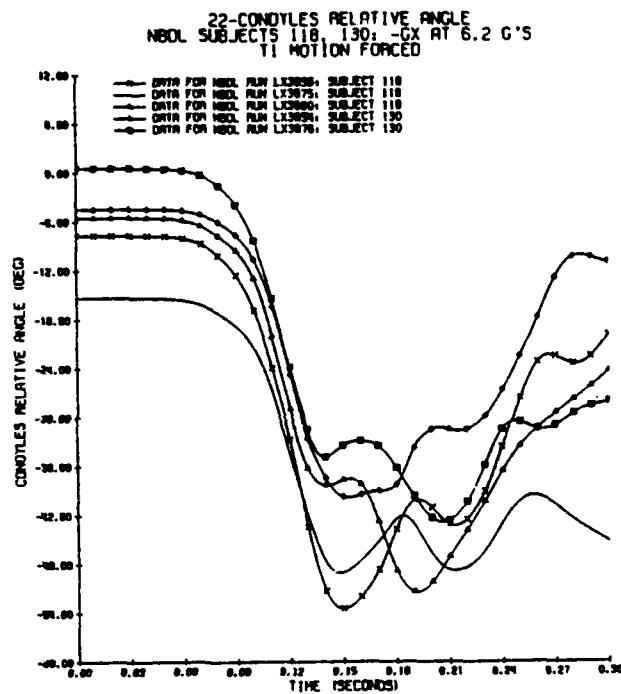
Figure 9. Condyles Relative Angle-Time History at -6Gx for NBDL Subjects 118 and 130.



23-T1 RELATIVE NECK ANGLE
NBDL SUBJECTS 118, 130; -GX AT 6.2 G'S
T1 MOTION FORCED
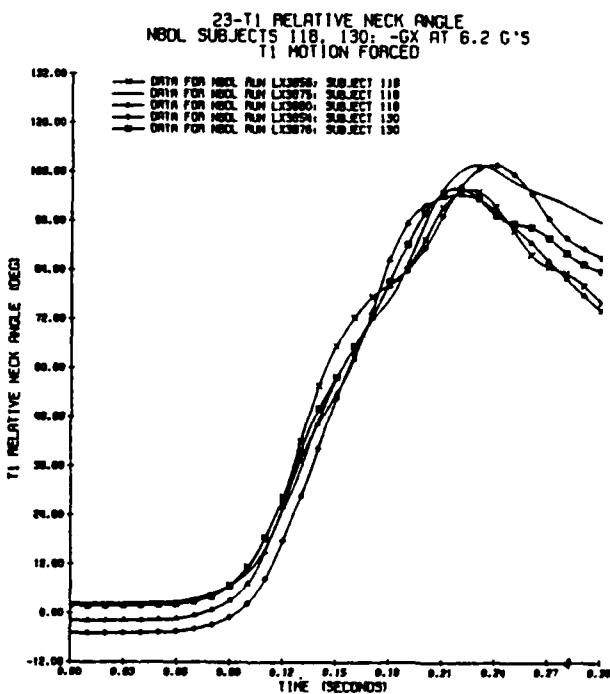
Figure 10. T1 Relative Angle-Time History at -6Gx for NBDL Subjects 118 and 130.

15
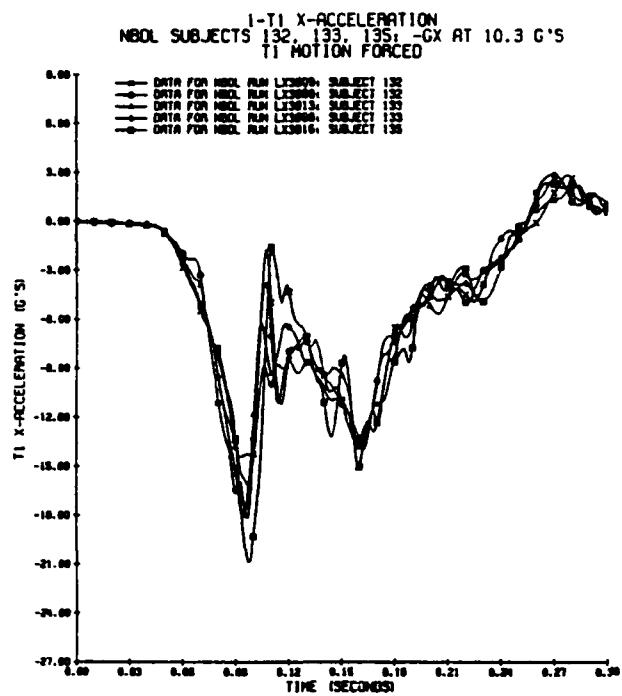
Figure 11. T1 X-Axis Acceleration-Time History at -10Gx, NBDL Subjects 132, 133, and 135.
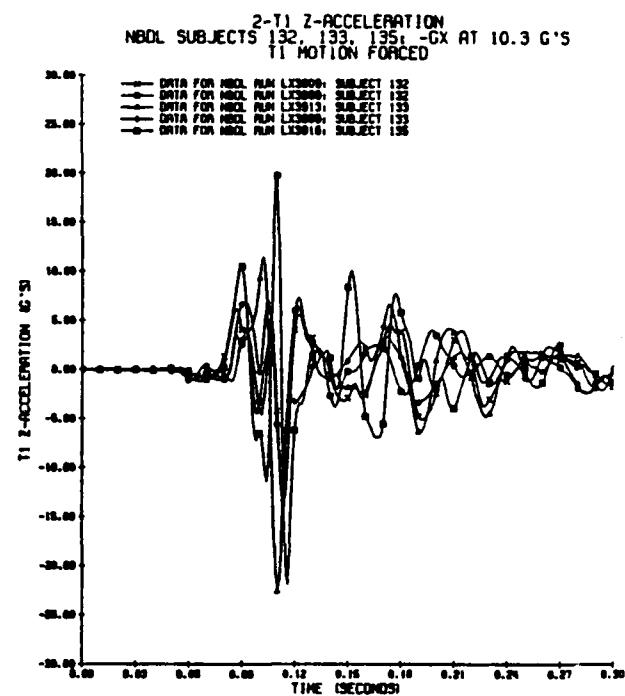


Figure 12. T1 Z-Axis Acceleration-Time History at -10Gx, NBDL Subjects 132, 133, and 135.
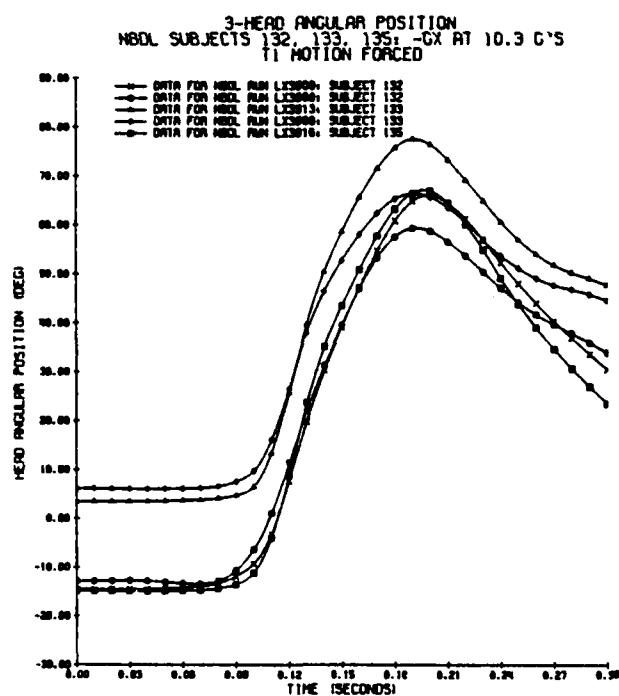


Figure 13. Head Angular Position-Time History at -10Gx, NBDL Subjects 132, 133, and 135.
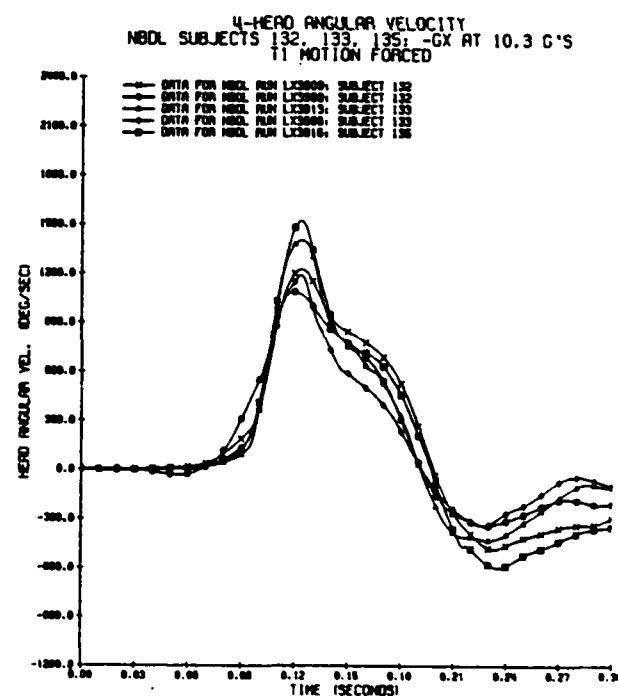


Figure 14. Head Angular Velocity-Time History at -10Gx, NBDL Subjects 132, 133, and 135.

16
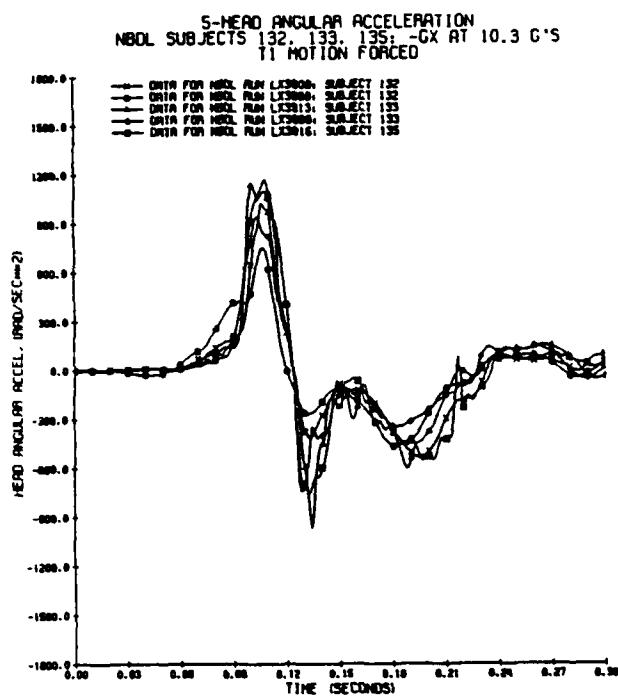
Figure 15. Head Angular Acceleration-Time
History at -10Gx, NBDL Subjects 132, 133, and 135.
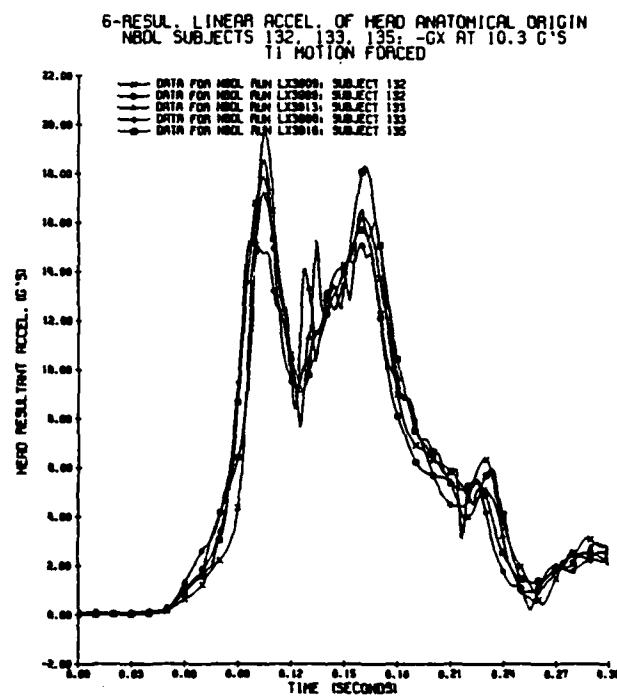


Figure 16. Head Resultant Acceleration-Time
History at -10Gx, NBDL Subjects 132, 133, and
135.
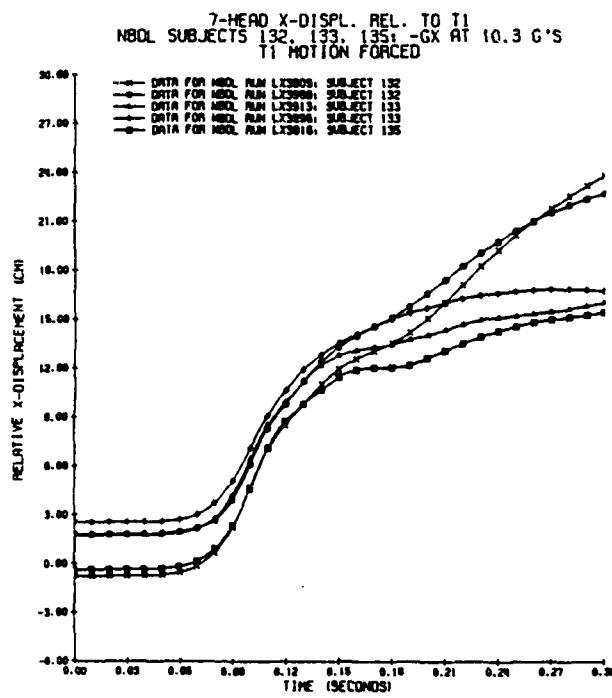


Figure 17. Head Origin X-Axis Displacement-Time
History at -10Gx, NBDL Subjects 132, 133, and
135.
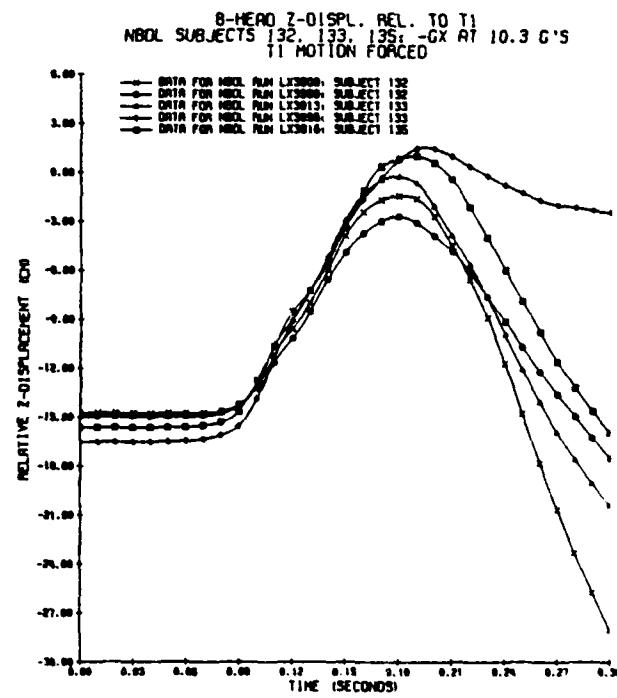


Figure 18. Head Origin Z-Axis Displacement-Time
History at -10Gx, NBDL Subjects 132, 133, and
135.
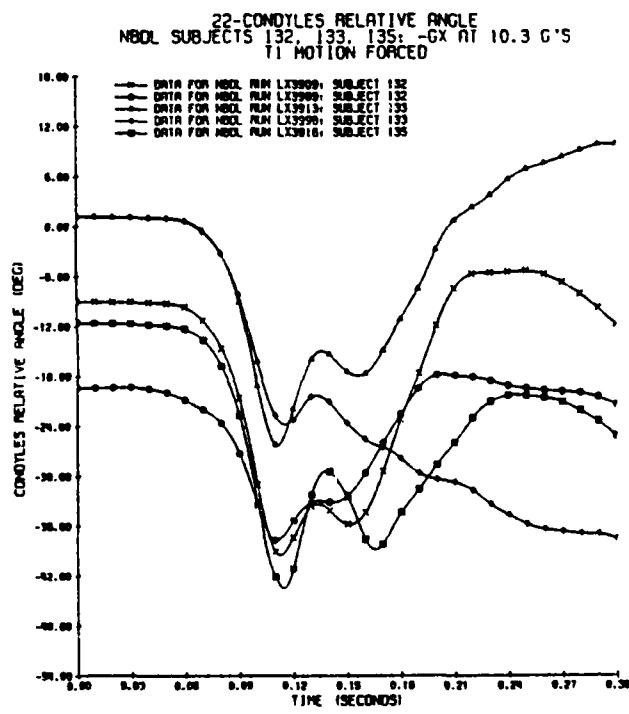
Figure 19.   Condyles Relative Angle-Time History at -10Gx, NBDL Subjects 132, 133, and 135.
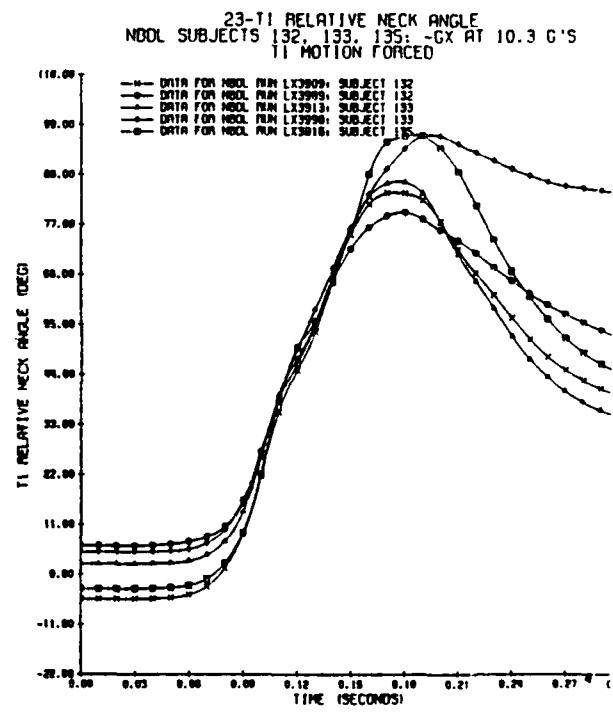
Figure 20.   T1 Relative Angle-Time History at -10Gx, NBDL Subjects 132, 133, and 135.

18
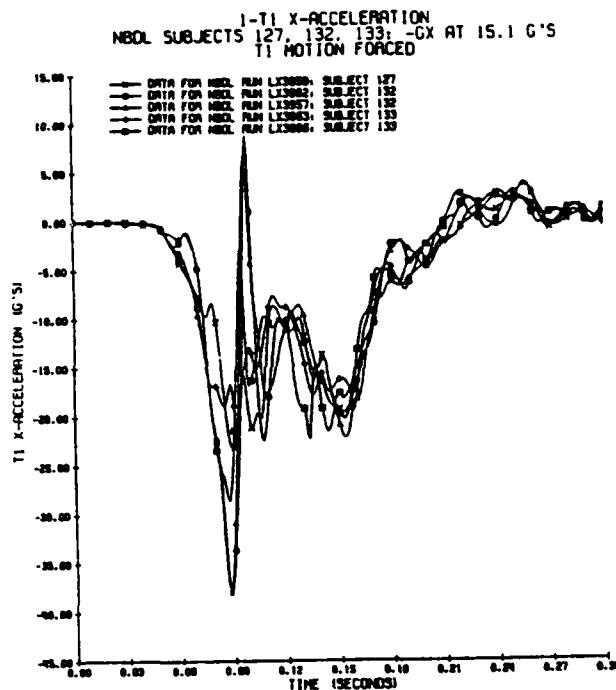
Figure 21. T1 X-Axis Acceleration-Time History at -15Gx, NBDL Subjects 127, 132, and 133.
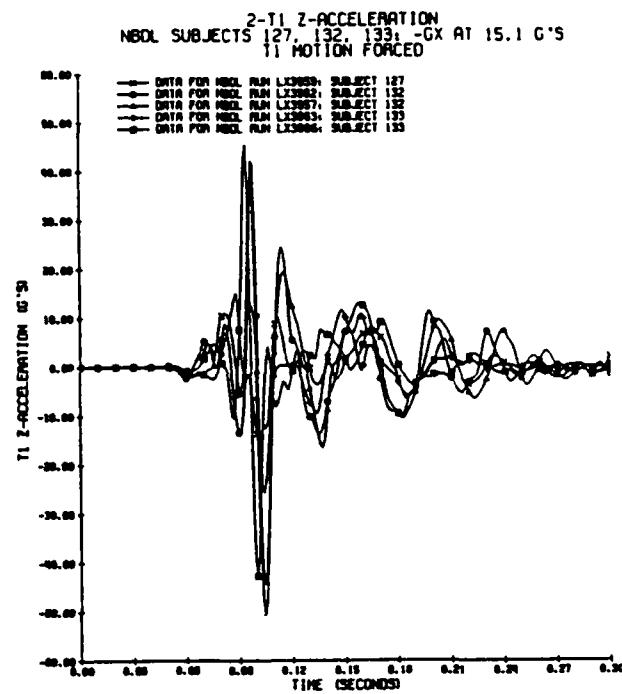


Figure 22. T1 Z-Axis Acceleration-Time History at -15Gx, NBDL Subjects 127, 132, and 133.
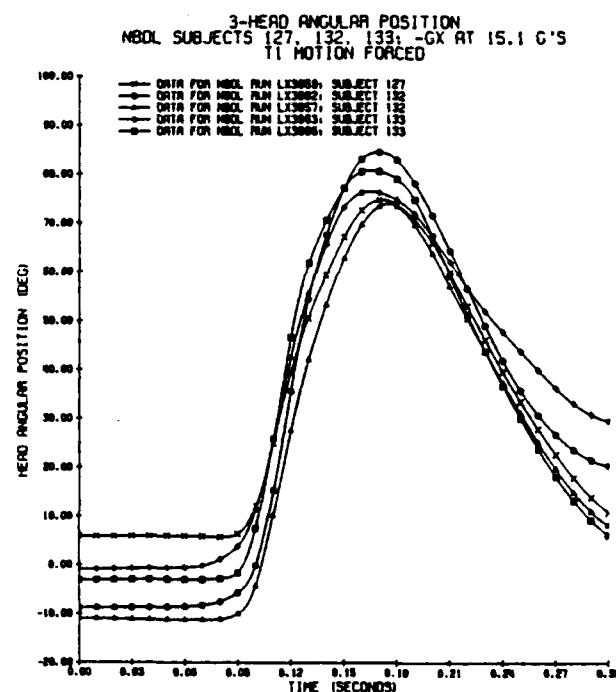


Figure 23. Head Angular Position-Time History at -15Gx, NBDL Subjects 127, 132, and 133.
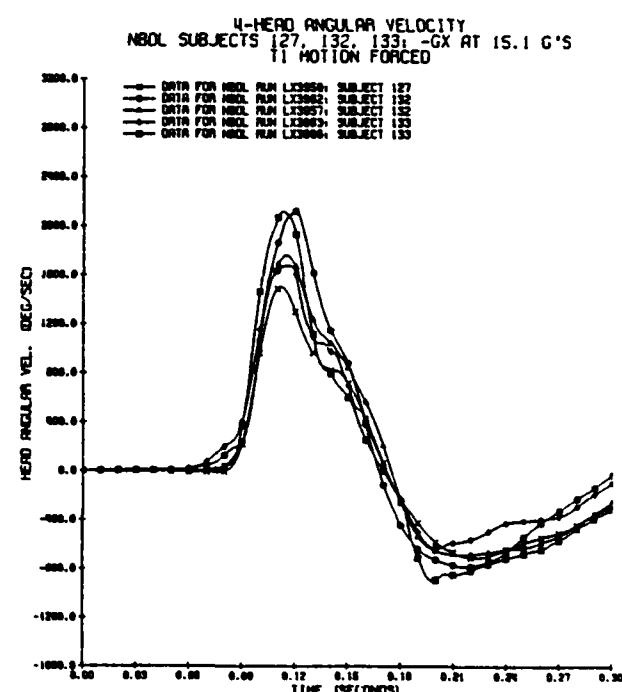


Figure 24. Head Angular Velocity-Time History at -15Gx, NBDL Subjects 127, 132, and 133.
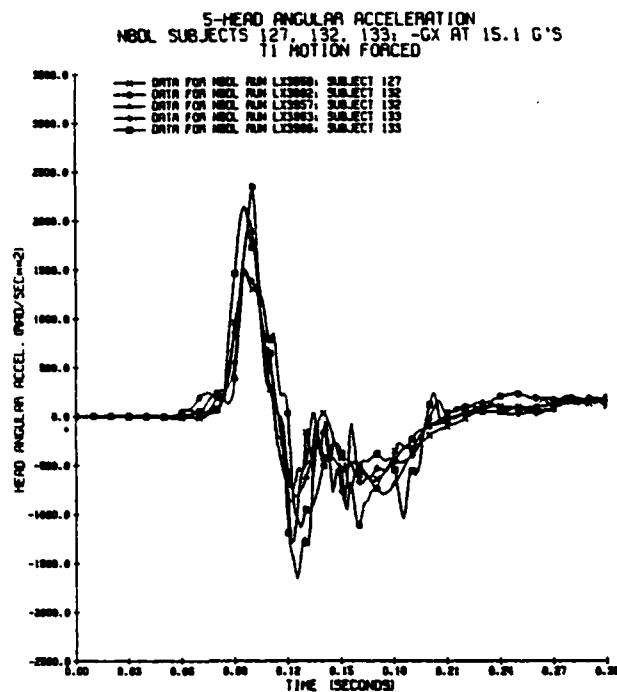
Figure 25. Head Angular Acceleration-Time History at -15Gx, NBDL Subjects 127, 132, and 133.
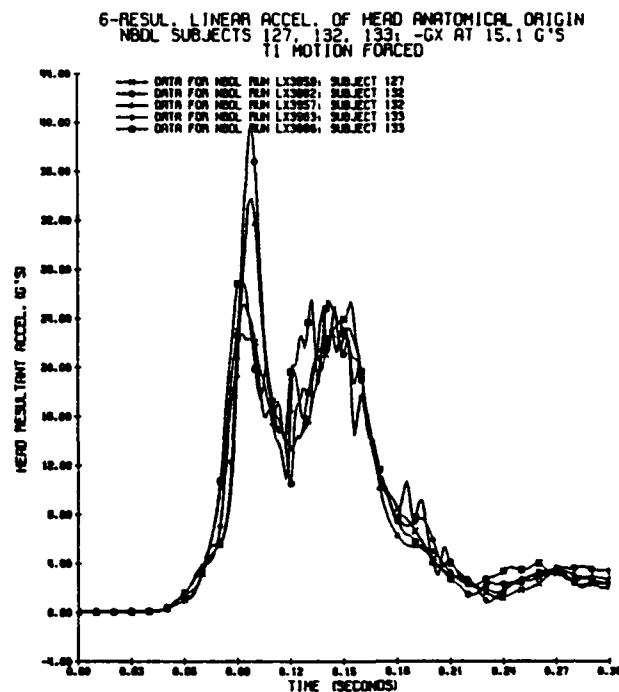


Figure 26. Head Resultant Acceleration-Time History at -15Gx, NBDL Subjects 127, 132, and 133.
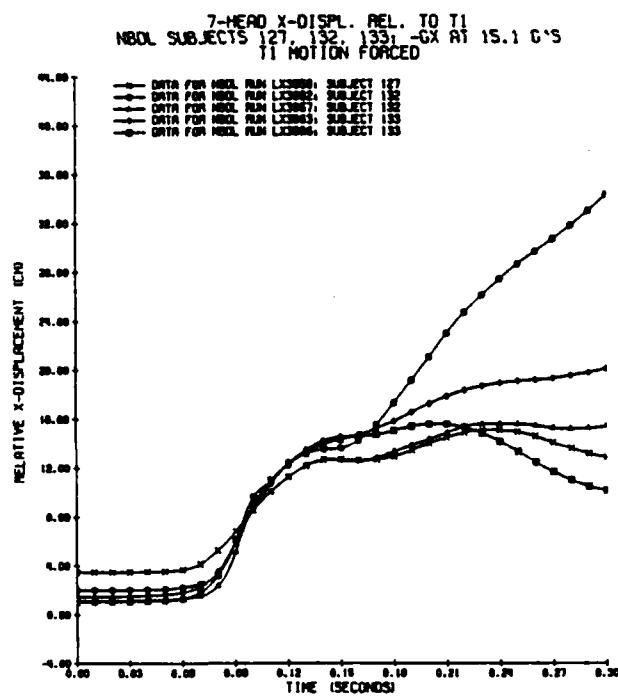


Figure 27. Head Origin X-Axis Displacement-Time History at -15Gx, NBDL Subjects 127, 132, and 133.
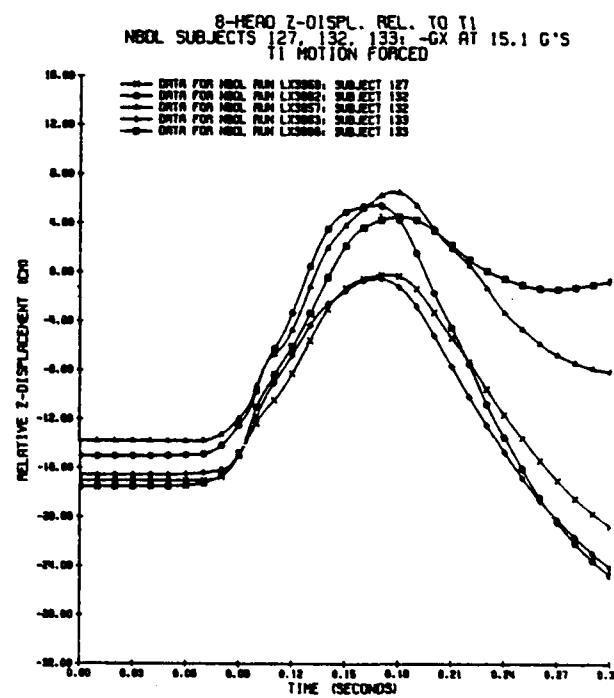


Figure 28. Head Origin Z-Axis Displacement-Time History at -15Gx, NBDL Subjects 127, 132, and 133.

20
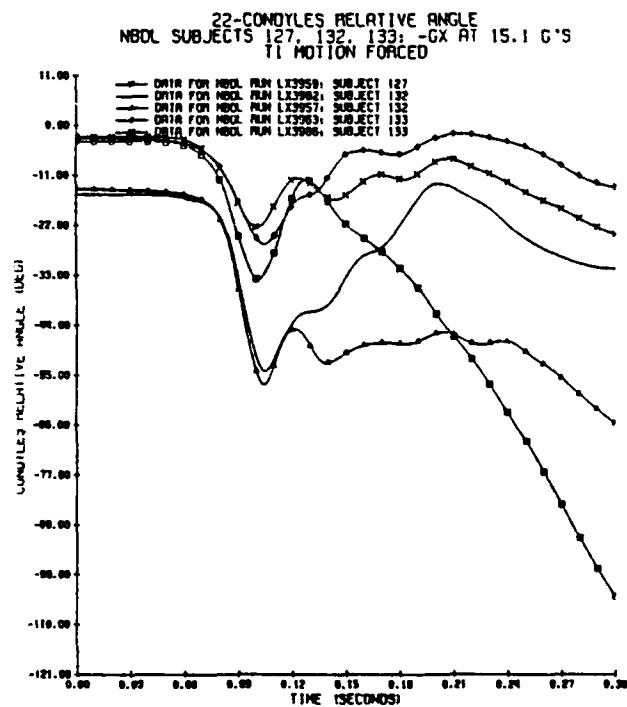
Figure 29.  Condyles Relative Angle-Time History at -15Gx, NBDL Subjects 127, 132, and 133.
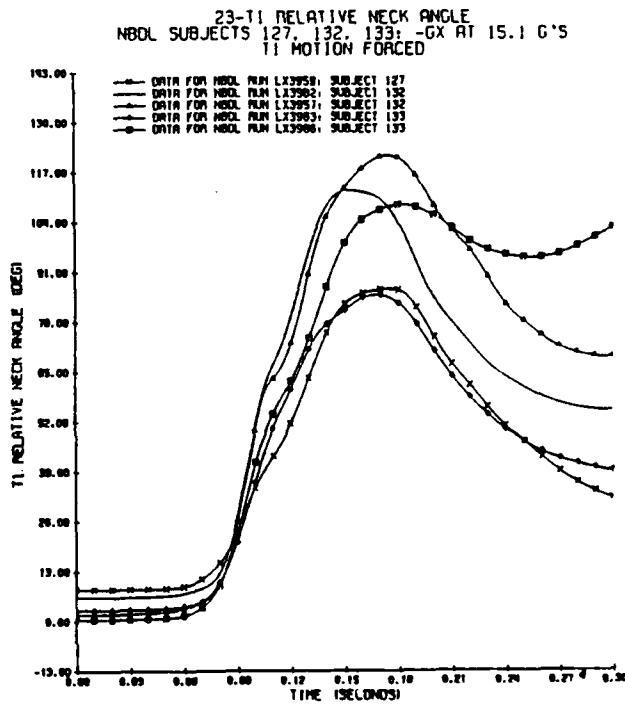
Figure 30.  T1 Relative Angle-Time History at -15Gx, NBDL Subjects 127, 132, and 133.
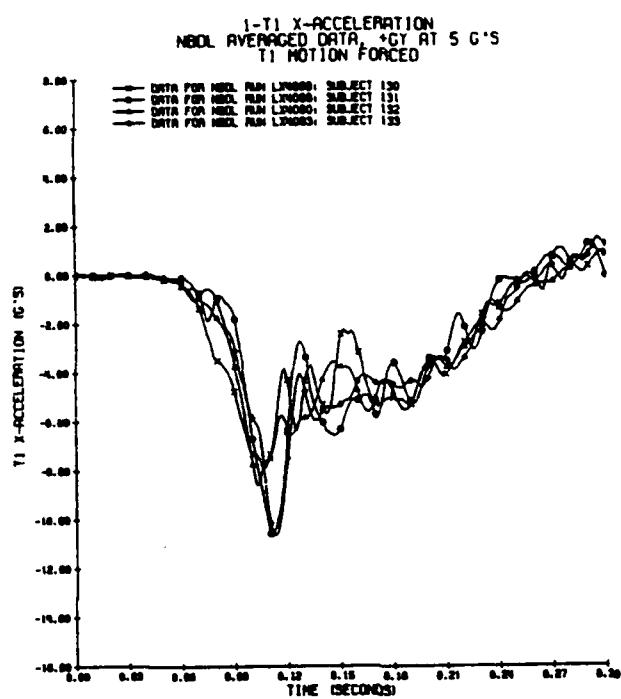
Figure 31.  T1 X-Axis Acceleration-Time History at +5Gy for NBDL Subjects 130, 131, and 132.
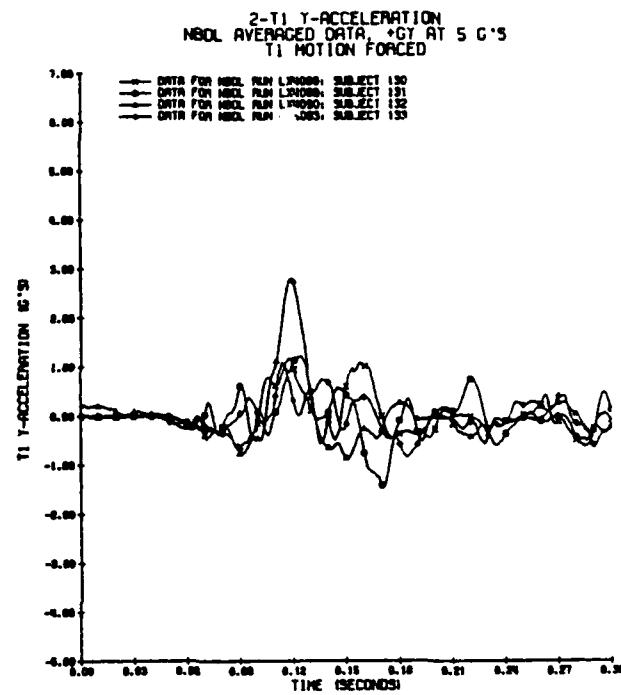


Figure 32.  T1 Y-Axis Acceleration-Time History at +5Gy for NBDL Subjects 130, 131, and 132.
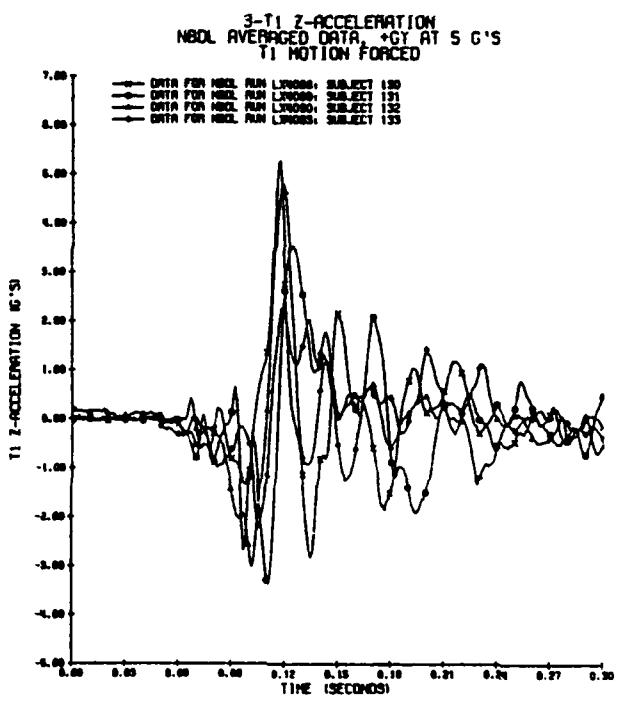


Figure 33.  T1 Z-Axis Acceleration-Time History at +5Gy for NBDL Subjects 130, 131, and 132.

22

**4-HEAD ORIGIN X-ACCEL.**
**NBDL AVERAGED DATA, +GY AT 5 G'S**
**T1 MOTION FORCED**
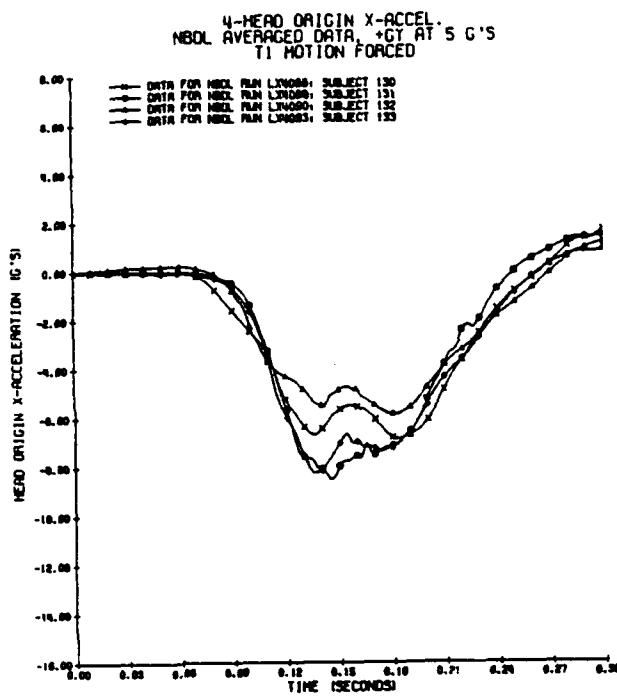


Figure 34. Head Origin X-Axis Acceleration-Time History at +5Gy for NBDL Subjects 130, 131, and 132.

**5-HEAD ORIGIN Y-ACCEL.**
**NBDL AVERAGED DATA, +GY AT 5 G'S**
**T1 MOTION FORCED**
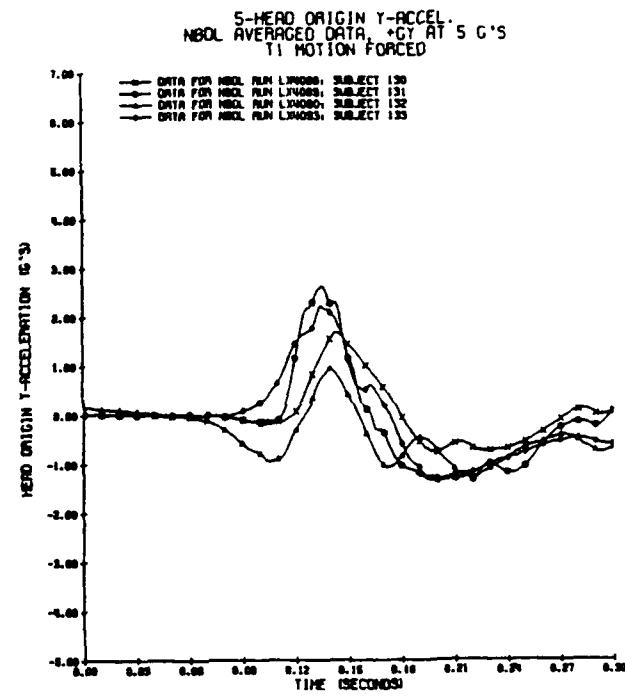


Figure 35. Head Origin Y-Axis Acceleration-Time History at +5Gy for NBDL Subjects 130, 131, and 132.

**6-HEAD ORIGIN Z-ACCEL.**
**NBDL AVERAGED DATA, +GY AT 5 G'S**
**T1 MOTION FORCED**
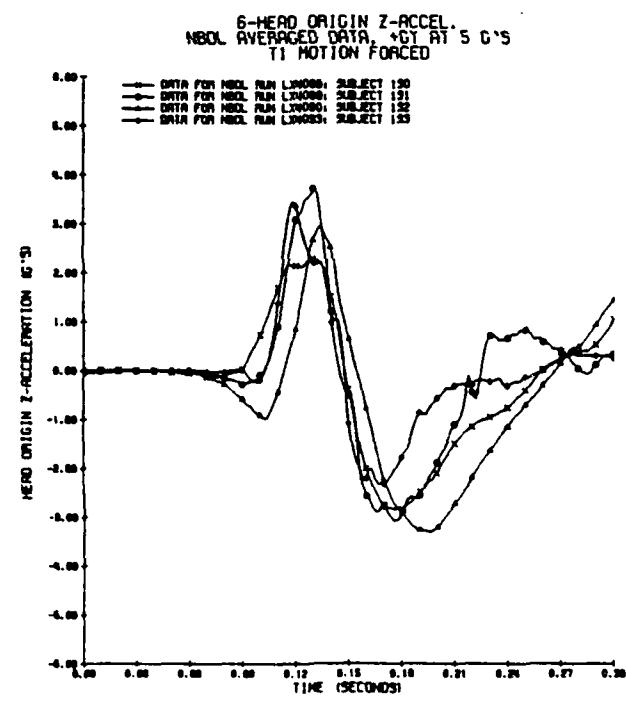


Figure 36. Head Origin Z-Axis Acceleration-Time History at +5Gy for NBDL Subjects 130, 131, and 132.

23
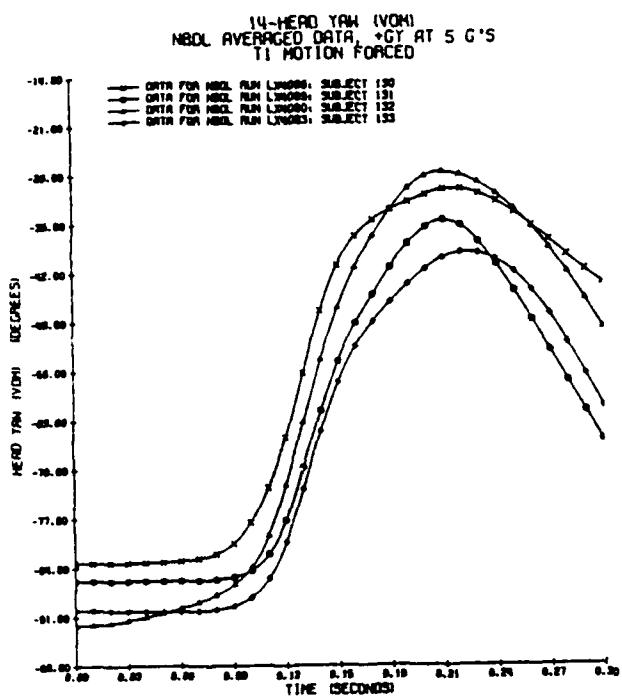
Figure 37. Head Yaw Angle-Time History at +5Gy for NBDL Subjects 130, 131, and 132.
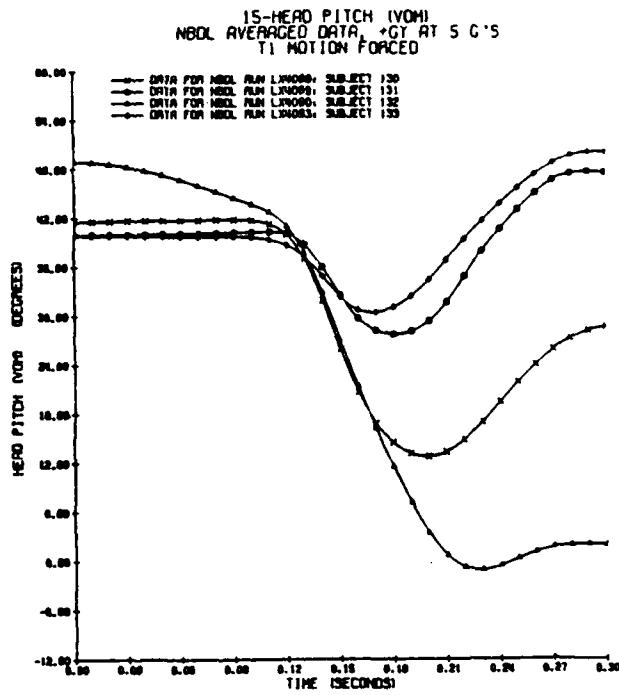


Figure 38. Head Pitch Angle-Time History at +5Gy for NBDL Subjects 130, 131, and 132.
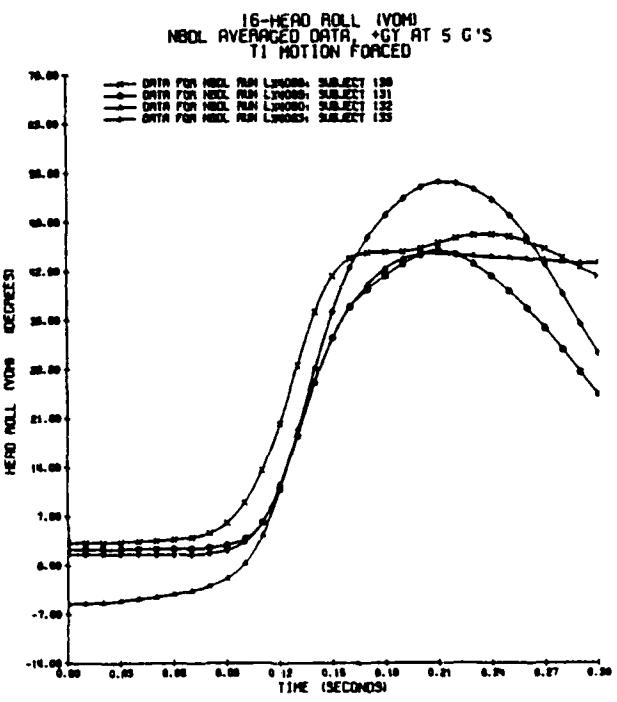


Figure 39. Head Roll Angle-Time History at +5Gy for NBDL Subjects 130, 131, and 132.

24
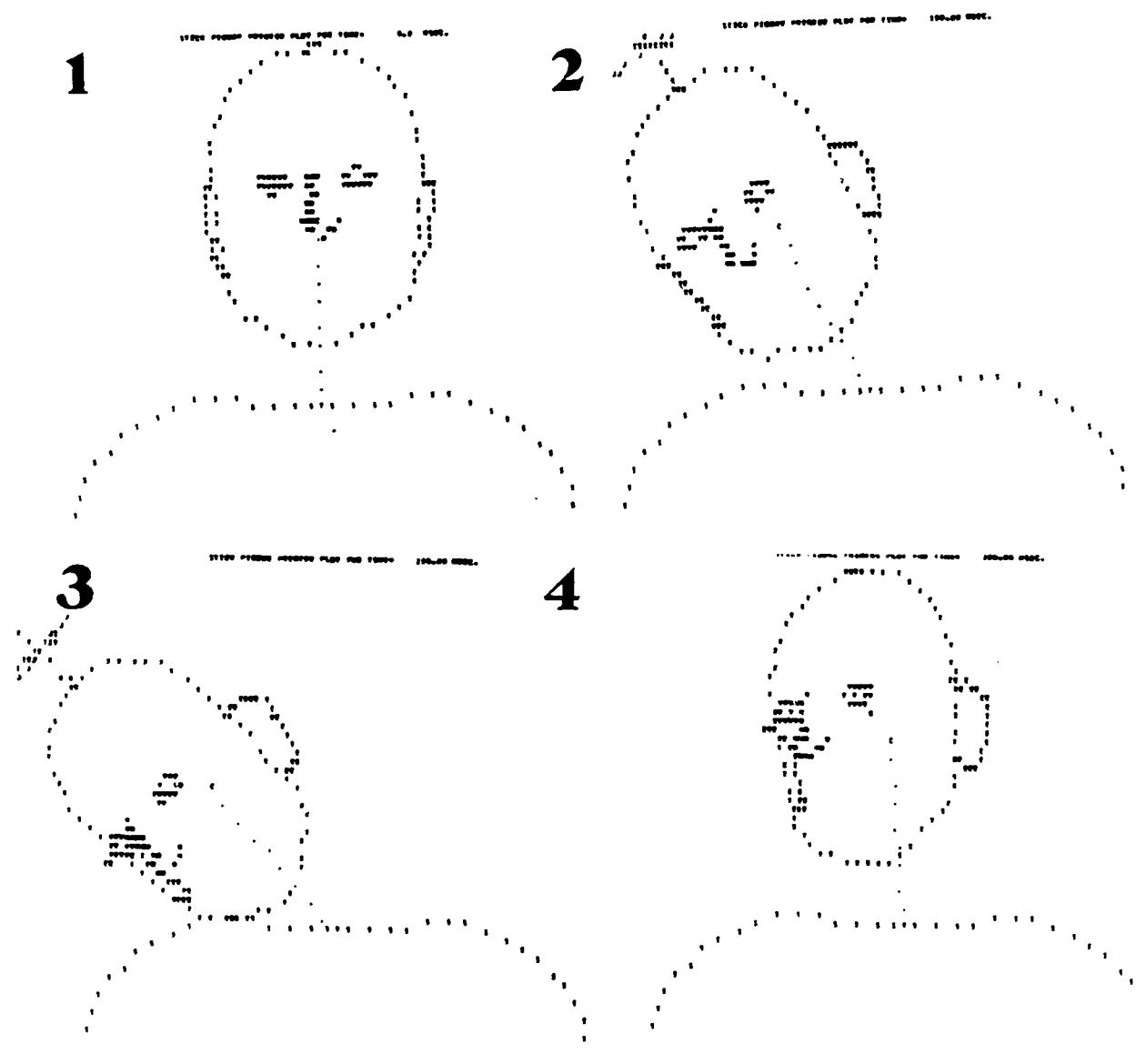
Figure 40.   Stick Figure Printer Plots of Lateral Flexion
for VOM model at 1) 0 ms, 2) 150 ms, 3) 210 ms, and 4) 300 ms.

At − 6Gx, the majority of the test subjects displayed an extension peak at the occipital condyles followed by greater or lesser amounts of rebound from peak extension. In four out of fifteen tests, the subjects showed no significant rebound after the extension peak.

Condyles Extension at − 10Gx. At − 10Gx, the test subjects in Figure 47 show a peak condyles extension similar to − 6Gx extension, but the rebound is not as pronounced as for − 6Gx. In Figures 47 and 48, it is seen that the two tests showing the largest condyles angulations also have the largest T1 joint angulations. (The neck chord for subject 118 (LX3903) and (LX3985) is thirty degrees below the horizontal at peak T1 joint relative angulation.)

In Figure 49, three subjects in − 10Gx tests show extension with rebound (subject 136 shows flexion at the condyles after approximately 180 ms) and subject H00130 shows a continuously increasing extension motion. The corresponding lower joint relative angle in Figure 50 reaches 30 to 40 degrees below the horizontal and remains near this condition for the duration of the test. Figure 49 illustrates clearly the two modes of subject response that will be called, respectively, "extension with rebound" and "no-rebound" extension. In the rebound mode of condyles extension, the initial extension is followed by rebound at both the condyles joint and the T1 joint after 180 milliseconds.

The − 10Gx test subjects in Figures 51 and 52 show "no-rebound" extension in only one test (LX3998) and extension with rebound in the remaining four. It is interesting to note that subject H00133 shows condyles extension with rebound in test LX3913 (resulting in flexion) and "no-rebound" extension in test LX3998. The condition for extension with rebound occurs at − 10Gx in 10 cases and "no-rebound" extension occurs in five cases. This is similar to the ratio seen for − 6Gx (11:4).

Condyles Extension at − 15Gx. At − 15Gx, the two modes of condyles extension motion are more definite than at − 6Gx and − 10Gx. In addition, the numbers of subjects showing extension rebound and "no-rebound" extension are more nearly the same at − 15Gx: seven tests show extension with rebound and six show "no-rebound" extension. In Figure 53, subject 120 displays a significant rebound followed by condyles flexion. Subject 120 also experienced the smallest angulation at the T1 joint and the largest rebound from flexion among the test subjects. At the other extreme, subject 131 (LX3987) shows a significant angulation

26

in extension that approaches ninety degrees relative to the horizontal. At the end of the impact event, little rebound for the T1 joint deflection has occurred (Figure 54).

In Figure 55, three − 15Gx tests show extension with rebound and two tests show "no-rebound" condyles extension. In Figures 57, subjects 134 and 135 show the "no-rebound" extension response in all three tests. At − 15Gx, the extension with rebound motion shows tests with the condyles joint proceeding into flexion. The no-rebound mode of condyles extension was also more pronounced for test subjects at − 15GX than at − 6Gx and − 10Gx.

Significance of Condyles Extension Modes. There does not appear to be any strong pattern involved in the subject response for these two modes of condyles extension. At − 6Gx and − 10Gx, "no-rebound" condyles extension is "atypical" in the sense that only one-third of the reponses are of this type. At − 15Gx, however, nearly half of the tests show the "no-rebound" response. The two modes of condyles rebound seem to depend on some pre-test condition of the subject, since one subject can display both modes; e.g., subject H00133 at − 10Gx and − 15Gx.

Muscle tensing prior to the impact may allow the subject to control the type of extension rebound that is exhibited in the impact. It is felt that tensing before onset of the impact is a factor for two reasons: 1) "no-rebound" response, when it occurs, becomes evident by about 150 milliseconds, which is much less than muscle response time, and 2) two distinct response modes are seen, thus suggesting that there is no condition intermediate between "tensed before onset" and "not tensed before onset".

This raises a question of whether pretest muscle tensing is an infrequent occurrence that is characterized by Subject H00132 in test LX3989 (− 10Gx), which shows a bimodal head angular acceleration, or whether muscle tensing is a relatively common phenomenon that is indicated by the condyles extension rebound signature. Seemann has already considered this in simulations with a Becker linkage (12). (See Appendix.) It seems appropriate to repeat the simulations of neck muscle tensing and bimodal head angular acceleration response with a two-joint neck model other than the Becker neck to study the dynamic effect of a pre-test "condyles lock-up" situation. Perhaps further insight could be gained by simulation of pre-test neck muscle tensing with a neck model with the upper pivot point at the occipital condyles. The "condyles locked" condition could then be met for the upper pivot point by specifying a friction element that remains locked until

27

sufficient force is applied to the head to free the condyles joint. It could be argued that a bimodal head angular acceleration should appear for the neck model with occipital condyles upper pivot point if the bimodal acceleration signature is characteristic for the "condyles locked" pre-test condition.

With regard to the neck model, it is useful to identify in the volunteer data two distinguishable modes of condyles angulation because the first mode can be reproduced with a passive neck model whereas the second mode is not reproducible without significant modification of the upper neck joint element by inclusion of active elements.
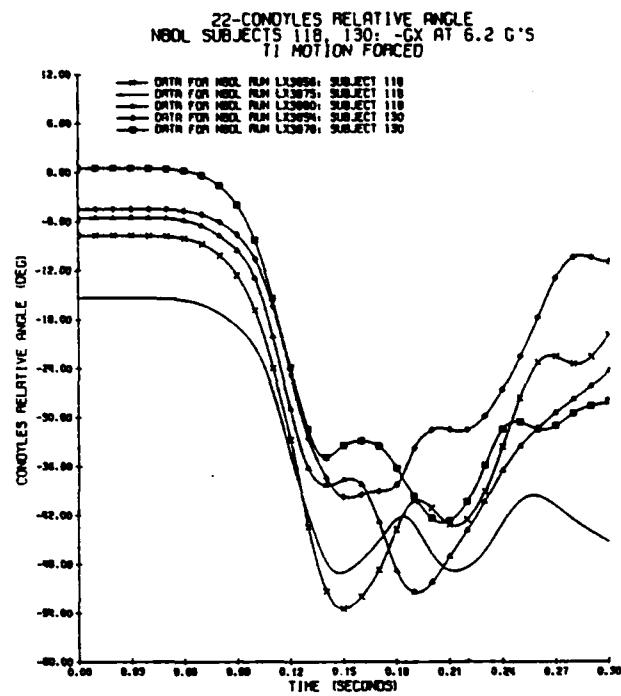
Figure 41. Condyles Relative Angle-Time History at -6Gx, NBDL Subjects 118 and 130.
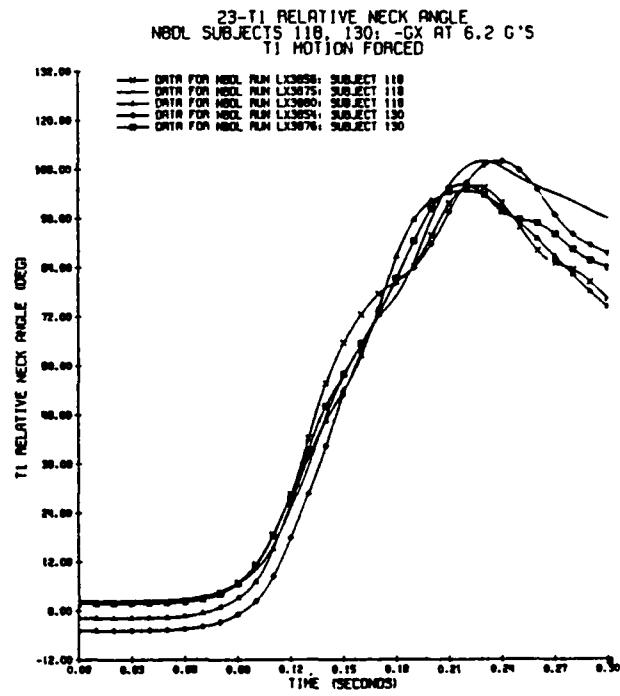


Figure 42. T1 Relative Angle-Time History at -6Gx, NBDL Subjects 118 and 130.
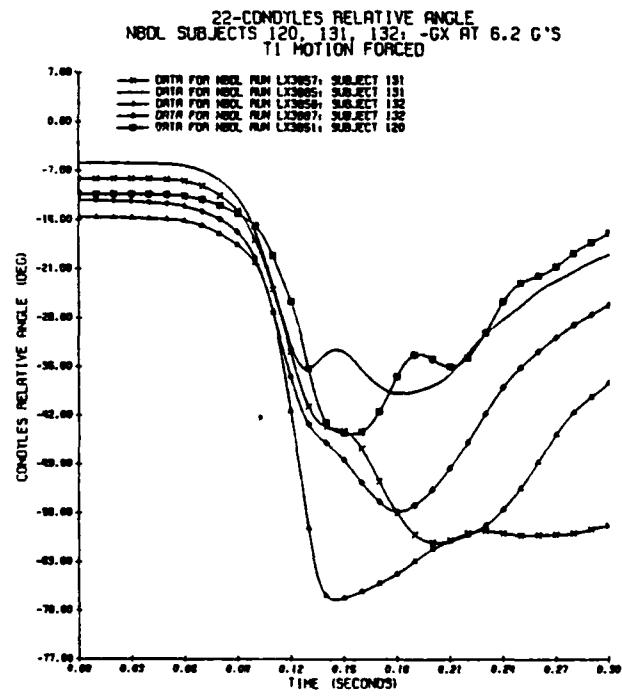


Figure 43. Condyles Relative Angle-Time History at -6Gx, NBDL Subjects 120, 131, and 132.
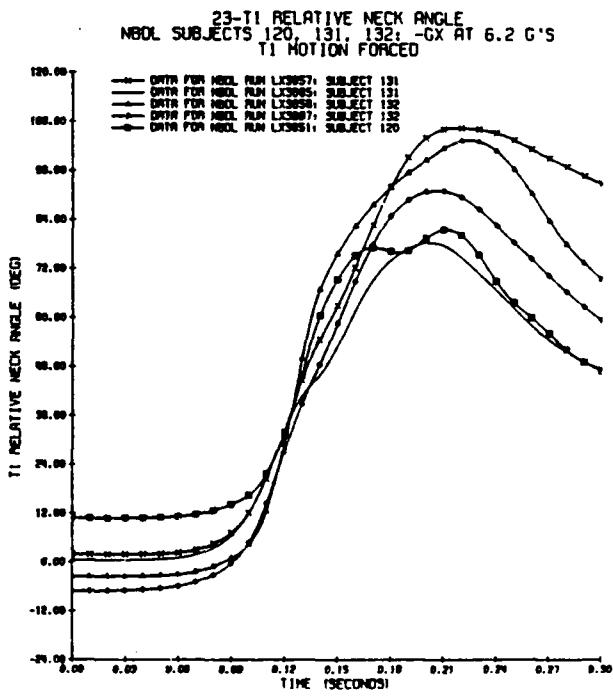


Figure 44. T1 Relative Angle-Time History at -6Gx, NBDL Subjects 120, 131, and 132.

29
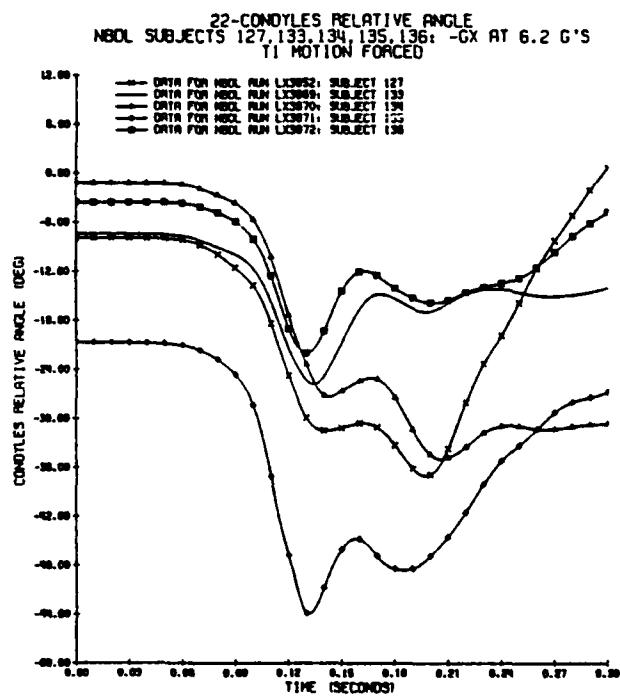
Figure 45. Condyles Relative Angle-Time History at -6Gx, NBDL Subjects 127, 133, 135, and 136.
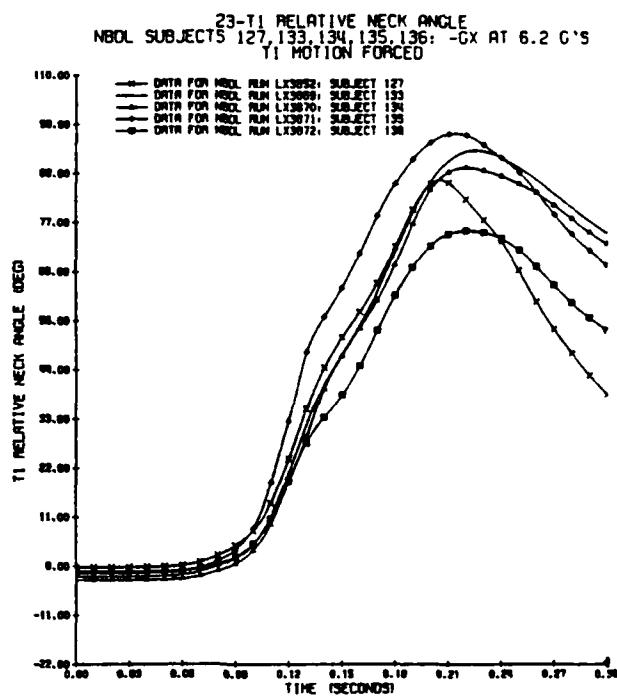
Figure 46. T1 Relative Angle-Time History at -6Gx, NBDL Subjects 127, 133, 135, and 136.
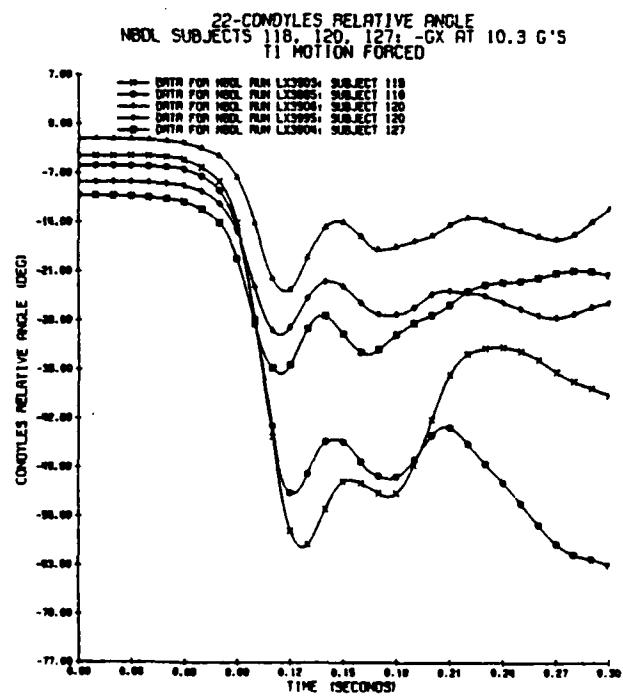


Figure 47. Condyles Relative Angle-Time History at -10Gx, NBDL Subjects 118, 120, and 127.
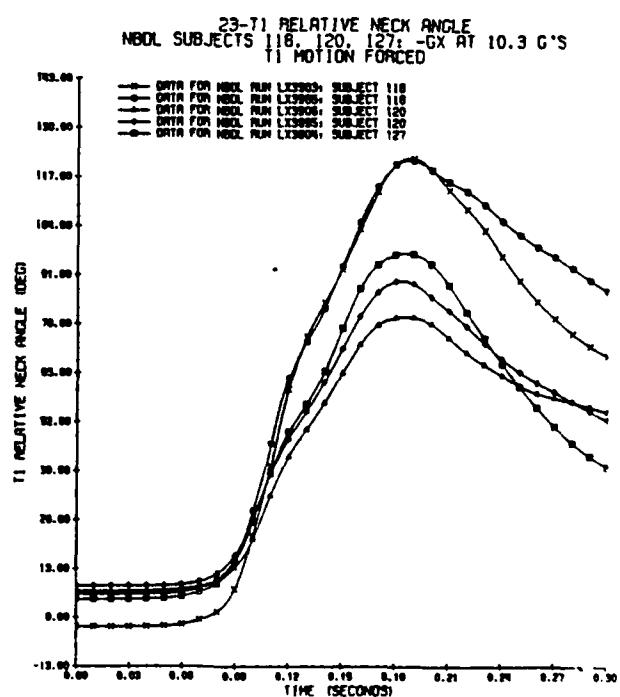
Figure 48. T1 Relative Angle-Time History at -10Gx, NBDL Subjects 118, 120, and 127.

30
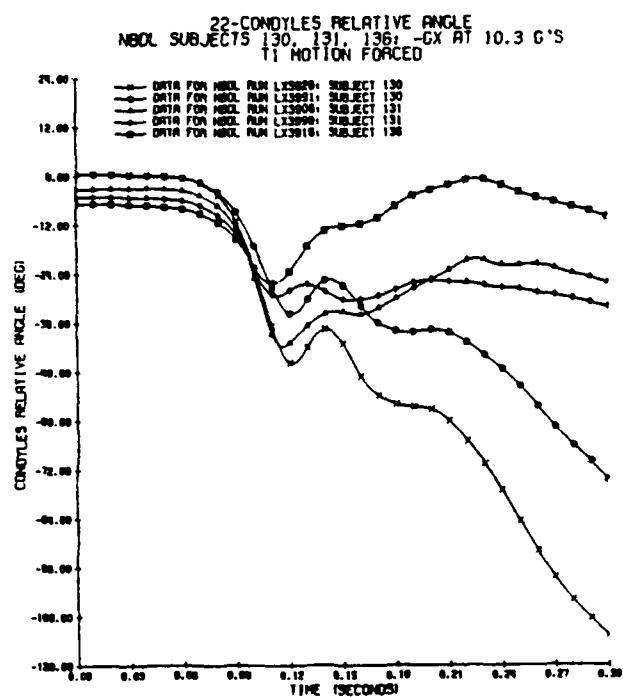
Figure 49. Condyles Relative Angle-Time History at -10Gx, NBDL Subjects 130, 131, and 136.
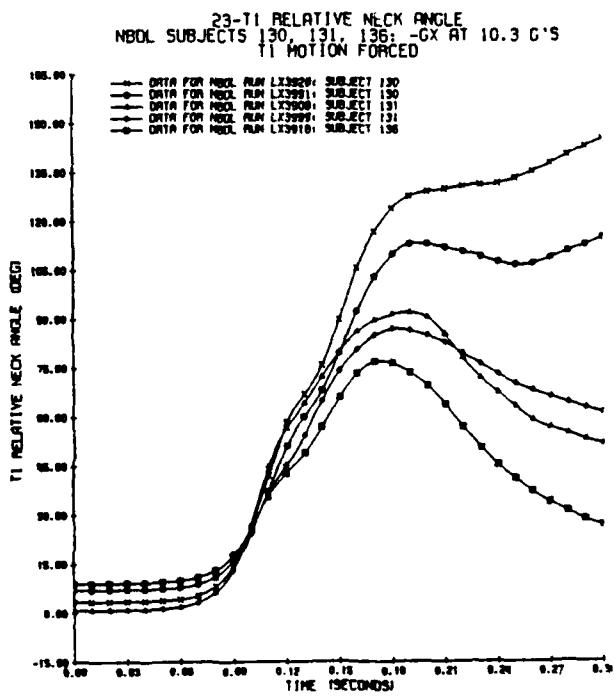


Figure 50. T1 Relative Angle-Time History at -10Gx, NBDL Subjects 130, 131, and 136.
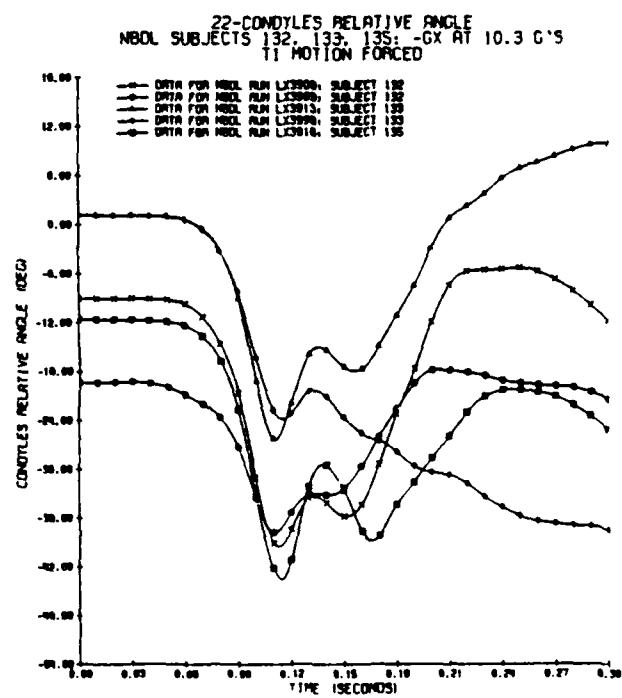


Figure 51. Condyles Relative Angle-Time History at -10Gx, NBDL Subjects 132, 133, and 135.
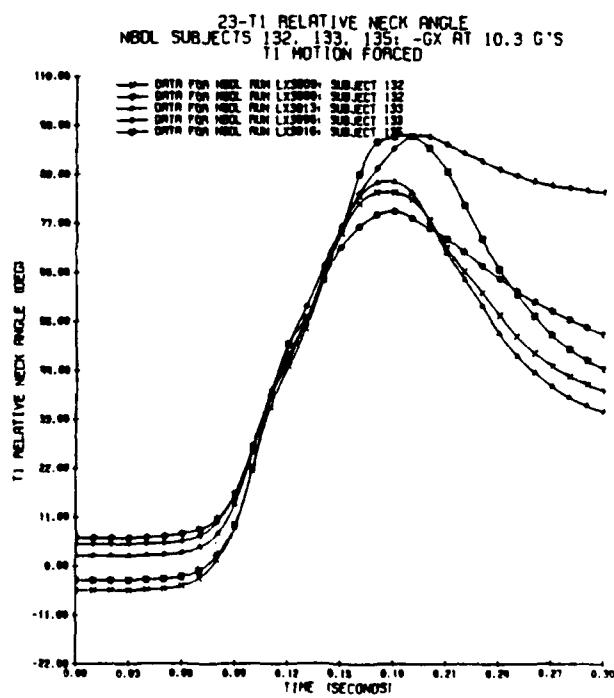


Figure 52. T1 Relative Angle-Time History at -10Gx, NBDL Subjects 132, 133, and 135.

31
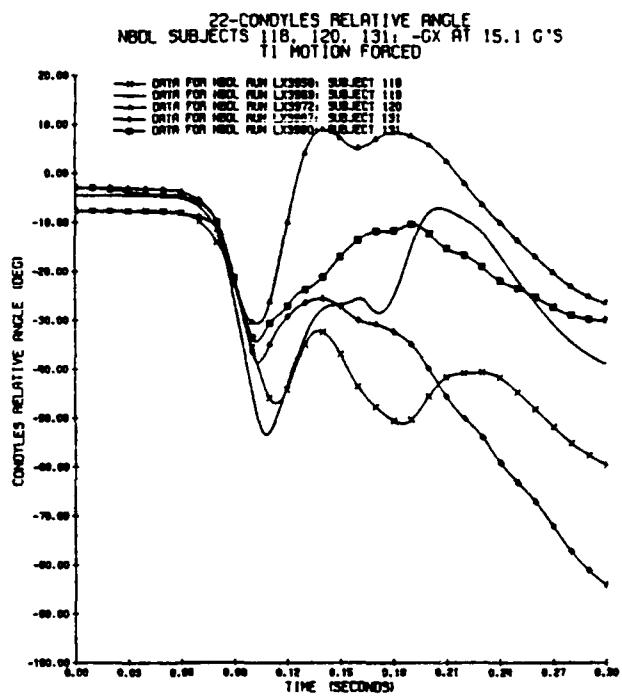
Figure 53. Condyles Relative Angle-Time History at -15Gx, NBDL Subjects 118, 120, and 131.
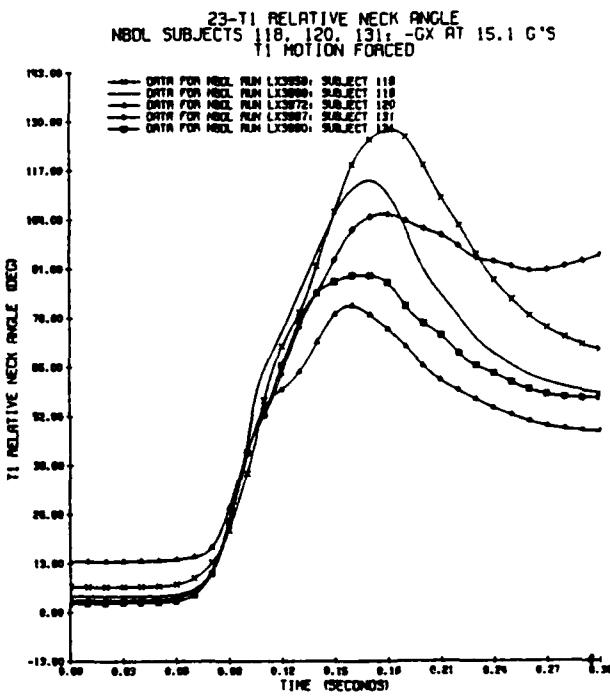


Figure 54. T1 Relative Angle-Time History at -15Gx, NBDL Subjects 118, 120, and 131.
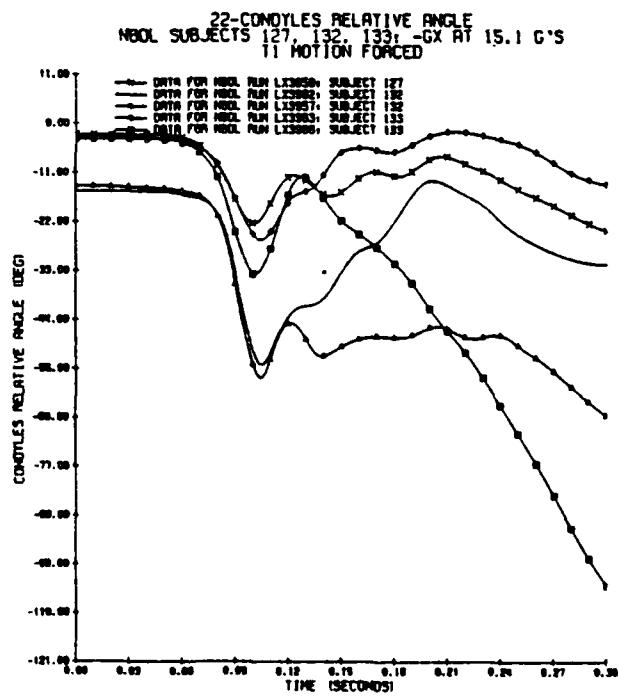


Figure 55. Condyles Relative Angle-Time History at -15Gx, NBDL Subjects 127, 132, and 133.
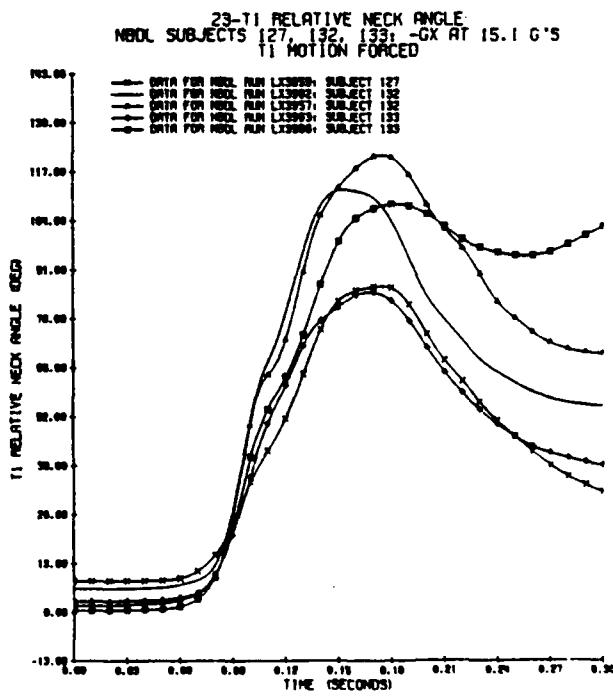


Figure 56. T1 Relative Angle-Time History at -15Gx, NBDL Subjects 127, 132, and 133.

32
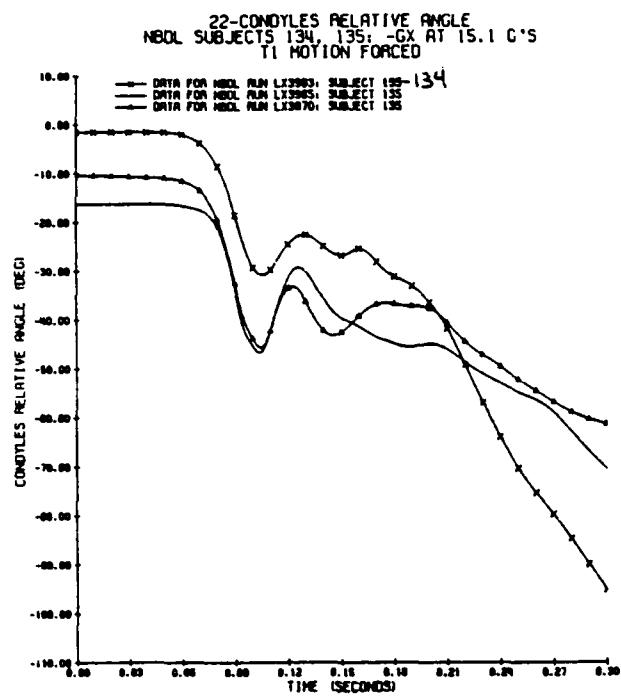
Figure 57.  Condyles Relative Angle-Time History at -15Gx, NBDL Subjects 134, 135.
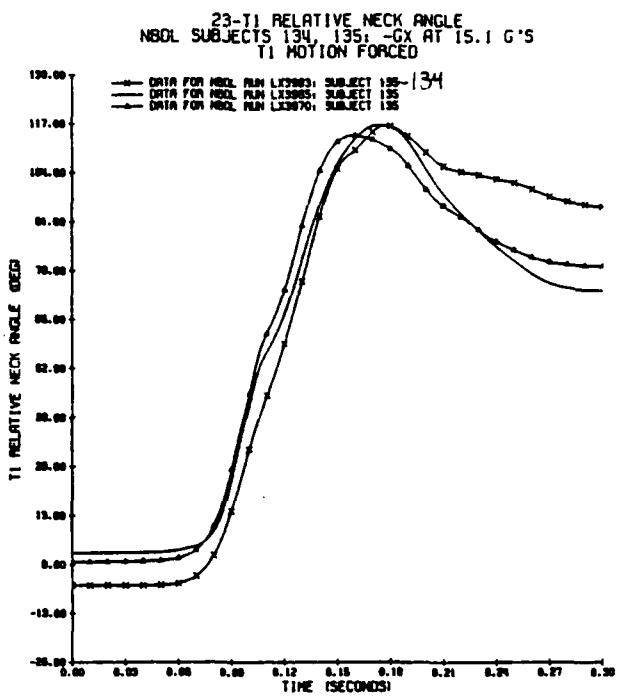
Figure 58.  T1 Relative Angle-Time History History at -15Gx, NBDL Subjects 134, 135.

# V. RESULTS AND DISCUSSION

In Phase II it was shown that a two-joint neck model could produce satisfactory linear and angular acceleration response for −Gx and +Gy. It was subsequently seen, however, that the neck model did not predict linear displacements well. Also, neck relative angles were not well predicted. Therefore, the modeling efforts in Phase III focussed on achieving better biofidelity in the neck model for linear and angular displacements in simulations of −Gx data while maintaining satisfactory acceleration response. In addition, preliminary simulations for +Gy were carried out to test the biofidelity of neck models having modified pivot point locations.

The simulation results discussed in the following sections are concerned with the improvement of the input model data for the −Gx vector. The input model data were modified by changes to 1) joint parameter values and 2) the location of the pivot points.

Simulations made to date show that variation of a limited set of neck model parameters is sufficient to tune several dynamic response variables. These parameters are:

1. condyles stiffness (linear)
2. condyles damping
3. condyles energy restitution coefficient
4. C7/T1 stiffness (linear and bilinear)
5. C7/T1 damping
6. C7/T1 energy restitution coefficient
7. neck length stiffness (linear and bilinear)
8. neck length damping
9. neck length energy restitution coefficient
10. coordinates of upper neck ("condyles") hinge point
11. coordinates of the lower neck hinge point

Neck joint parameters for bending stiffnesses, damping, and restitution coefficients affect the peak, phase, and rebound for the head/neck dynamic response. The location of the neck pivot points, however, also significantly affects the joint torques and simulation acceleration responses.

The two-joint neck of the MVMA 2-D model is shown in Figure 59. It is a one-link element with articulation at the head and torso. In normal use in crash simulation research, the upper and lower neck joints are assumed to be at the anatomic condyles and C7-T1 locations, as illustrated in the figure. There is no

model constraint, however, that requires the articulations to be at these anatomic locations, and in the current study the upper and lower neck articulations were moved away from anatomic condyles and C7-T1 locations in various simulations.

Figure 60 illustrates the definition of upper neck and lower neck relative angles used in this report. (In the figure they are labeled with "con" and "C7" subscripts, but in general, as previously indicated, the articulation points in simulations may be different from anatomic condyles and C7-T1.) Figures 61 and 62 illustrate the definitions used for flexion and extension at the neck joints.

The effect of modified neck joint data and neck linkages for −Gx simulations with the MVMA 2-D model is discussed below.

## -Gx Simulations with Phase II Neck Parameter Data

In Phase II work, experimental head angular motion and head linear resultant acceleration were the only time history data used to assess the biofidelity of the simulation results. On this basis, the Phase II simulations adequately predicted head motion. It is appropriate to re-evaluate the neck model data by considering additional response variables plotted in Phase III.

At the beginning of Phase III, the neck joint stiffnesses and damping data determined for Phase II were used in simulations of the Phase III NBDL averaged volunteer data at −6Gx, −10Gx, and −15Gx. Several plots not obtained during Phase II were obtained in these simulations —specifically: head/neck relative angles, linear head displacements, and the neck length. The simulation and experimental response data are shown in Figures 63–72 for −6Gx, Figures 73–82 for −10Gx, and Figures 83–92 for −15Gx.

The −Gx simulations show that head angular velocity and acceleration response are satisfactorily predicted by the neck model at all g-levels. However, the head angular position shows increasing error in peak magnitude at −10Gx and −15Gx. At −6Gx, the low T1 angulation and low condyles extension are in error by compensating amounts that result in a peak head angle of the correct magnitude. At −10Gx and −15Gx, the T1 angulation is improved, so the error in condyles angle also appears as an error in the head angle. Plotting additional response variables, viz., linear head displacement and condyles and T1 relative angles, shows that the condyles angular deflection is not adequately predicted in the simulation. Specifically, far too little condyles extension is obtained.
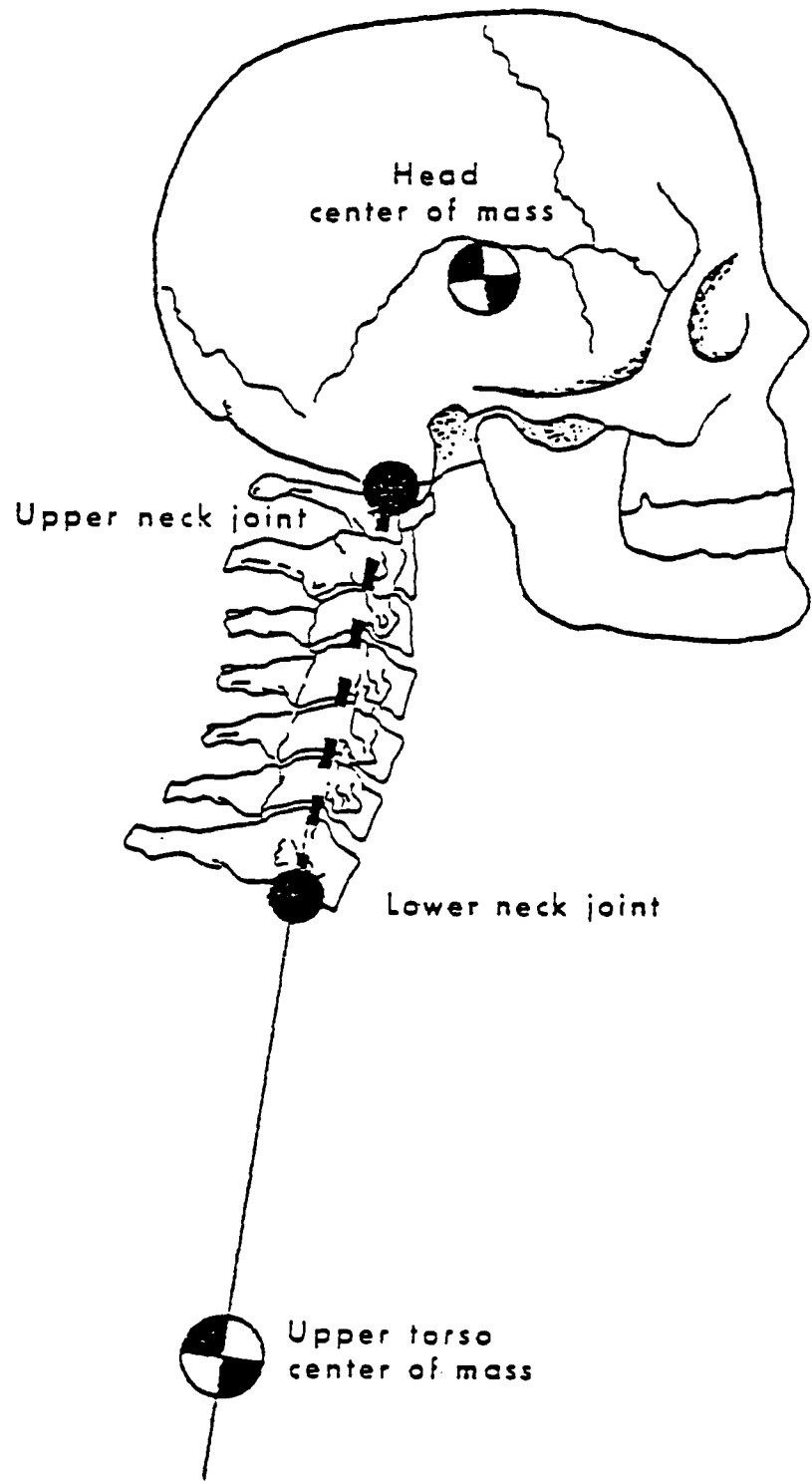
Figure 59. The Two-Joint Neck in the MVMA 2-D CVS Model
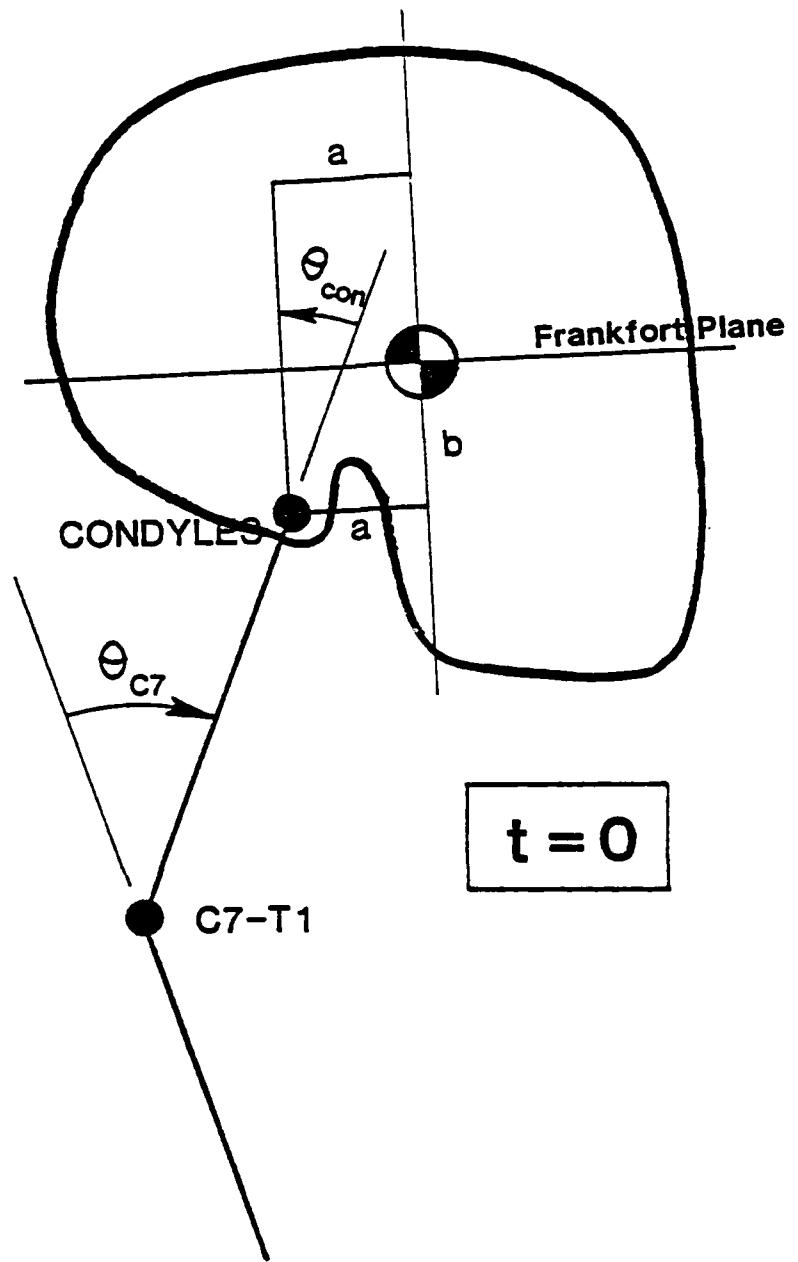
Angular deflection at each joint = 0

Flexion and extension at each joint
are zero, by definition, at t=0.

Figure 60.   C7-T1 and Condyles Angles at t=0.

$\theta_{con}$

$\theta_{con}^{|0|}$

b

a

a

Condyles Flexion
$$= -[\theta_{con} - \theta_{con}^{|0|}]$$

Flexion at either joint is the amount of forward (clockwise) angulation of the upper link with respect to the lower, relative to the time zero relative orientation.

Figure 62. Definition of Flexion Angle in MVMA 2-D Simulations.

C7 Extension
$$= -[\theta_{C7} - \theta_{C7}^{|0|}]$$

C7-T1

$\theta_{C7}$

$\theta_{C7}^{|0|}$
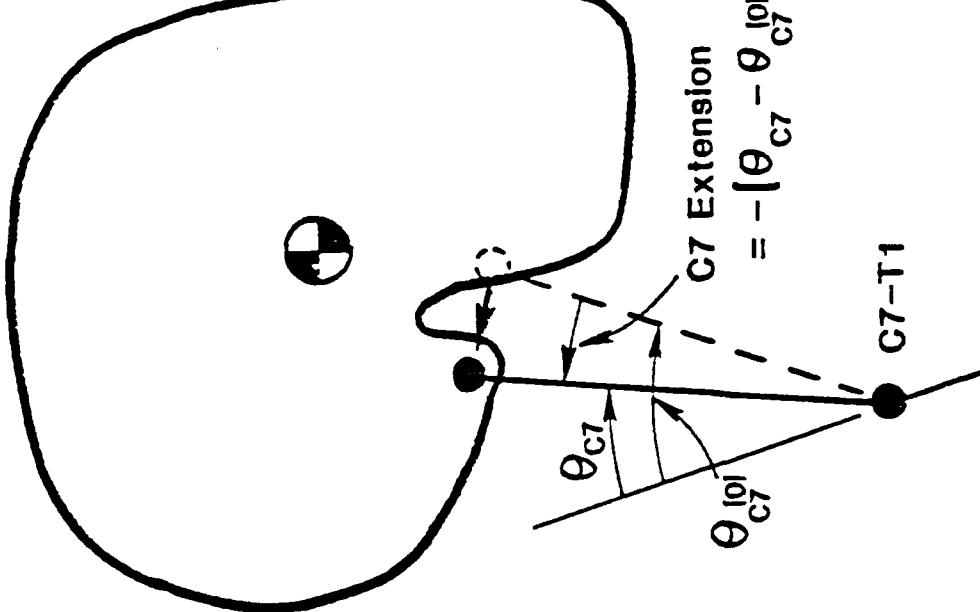
Extension at either joint is the amount of rearward (counter-clockwise) angulation of the upper link with respect to the lower, relative to the time zero relative orientation.

39

Figure 61. Definition of Extension Angle in MVMA 2-D Simulations.

The load-deflection characteristics of the Phase II neck model data are shown in Figure 93. The upper neck joint damping coefficients were .026 N-m sec/deg in flexion loading and unloading (.50 energy restitution coefficient). Damping was zero for extension loading and .026 N-m sec/deg for unloading (.95 restitution coefficient). The lower neck joint damping coefficients were zero in flexion loading and unloading (.11 restitution coefficient), and .0034 N-m sec/deg damping in extension loading and unloading (.11 restitution coefficient). Neck length damping was 7.34 N-sec/cm in tension loading and 3.62 N-sec/cm in tension unloading. Compression loading damping was 3.62 N-sec/cm; it was 7.34 N sec/cm in compression unloading. The restitution coefficients for neck length tension and compression were .99.

In initial modeling efforts, attention was focussed on the improvement of the condyles extension motion through adjustment of the neck joint parameters. Three simulations with modified neck data are discussed below for −6Gx.

## Joint Parameter Adjustment of Neck Model at −6Gx

It was important to determine whether the linear displacements and relative angle deflections of the neck (condyles extension in particular) could be significantly improved by modifying the neck joint data. The simulation results at −6Gx showed the largest error in condyles extension to be in peak and duration of condylar extension motion. Therefore, neck model adjustment focussed on −6Gx simulations.

The adjustment of the joint stop stiffness and joint stop angle for condyles extension loading may seem appropriate to improve extension at the upper neck joint. It was previously shown, however, that even the elimination of all resistance to angulation at the upper pivot point was not sufficient to improve condyles extension motion in the simulation for −Gx (14). Therefore, parameter adjustment focussed on increasing the initial neck angulation to improve the simulation of condyles relative angle.

The first trial neck model adjustment was to decrease C7 flexion stiffness and thereby allow greater neck flexion at C7 during the onset of condyles extension motion. With this modification, a larger condyles extension was anticipated. Figure 72 shows that Phase II neck model values for bending stiffness do not allow a sufficient angular deflection at the lower neck joint for −6Gx. The C7 stiffness was decreased from 1.6 N-m/deg to .8 N-m/deg to allow the neck to achieve a larger

angular deflection. The neck tension stiffness was also decreased to improve the prediction of the resultant linear acceleration for the head. The stiffness was changed from 1644 N/cm to 411 N/cm.

The results for this run are shown in Figures 94–103. The head z-displacement peak and T1 relative angle peak are in better agreement with the experimental data in Figures 99 and 103, but the condyles relative angle was only slightly improved, displaying −17.1 degrees maximum extension versus −12.4 degrees in Figure 71.

The joint stop torques for the upper and lower pivot points are shown in Figures 100 and 101, respectively. The flexion and extension stops are immediately on either side of the time zero joint stop angle. In Figure 100, the peak condyles loading for the extension joint stop corresponds to peak condyles extension and peak head angular acceleration. The head subsequently rebounds from extension rapidly and loads the flexion joint stop. At C7, the joint stop displays flexion loading up to 240 ms (Figure 101).

Reducing the C7 flexion stiffness did not produce the desired improvement in condyles extension motion. Furthermore, the resulting head angular excursion (Figure 94) is significantly worse. The peak head angle in Figure 94 is thirty degrees in error for the simulation due to the poor modeling of condyles extension versus the improved T1 relative angle peak. This result is seen in the simulation of −10Gx and −15Gx NBDL data with the Phase II neck model, where T1 relative angle is adequate but the condyles relative angle and head angle are not modeled well.

A second attempt at improving the biofidelity of head/neck angular motion was made by using a bilinear C7 flexion stiffness. The bilinear stiffness allows the neck to rapidly angulate downward during condyles extension. The neck model data were similar to the previous simulation except for decreased initial C7 flexion stiffness. The loading curve had a slope of .5 N-m/deg over the first forty degrees deflection and 1.8 N-m/deg after forty degrees of deflection. Figures 104–113 show the simulation results for the bilinear C7 flexion stiffness data. Here, the condyles relative angle displayed only minor improvement over the results shown in Figure 71. The head angular position, head angular velocity, and head z-displacement were actually somewhat worse, as shown in Figures 104–105, than the first simulation with decreased C7 bending stiffness.

41

The forty degree bilinear breakpoint at C7 allowed rapid neck angulation for the duration of the condyles extension action, but this was not sufficient to produce the desired head/neck motion. With regard to the location of the breakpoint between the first and second stiffness regions, forty degrees of angular excursion at C7 is too much angulation prior to the second stiffness region. This is evidenced by the spike in the head angular acceleration, which is due to joint stop deflection into the second stiffness region at C7 (Figure 111). Subsequently it was found that a breakpoint of approximately 20-25 degrees for C7 bilinear stiffness eliminates this type of undesirable acceleration response.

Another modification of the model input data tested the effect of including T1 angular acceleration. This allowed greater neck angulation early in the simulation by delaying the joint stop loading for C7 flexion stiffness. Also, the lower pivot was located 3 cm posterior to anatomic T1 to improve the simulation of head x-displacement. The neck model data were similar to the first −6Gx simulation with decreased C7 bending stiffness except for the T1 angular driver. The results for −6GX simulation with T1 angular acceleration input are shown in Figures 114–123. The condyles relative angle decreased to five degrees excursion for peak extension from eight degrees extension excursion seen in the previous simulation (Figure 112). Overall, the condyles extension motion was not of a satisfactory magnitude or duration when T1 angular acceleration was used as a forcing excitation in addition to T1 x- and z-acceleration.

Frisch and Cooper (24) have discussed the effect of T1 angular acceleration input for the simulation of −Gx NBDL data. In the current study it was found that T1 angular acceleration changes the character of the moment-time history at the lower neck joint. The inclusion of T1 angular acceleration as a forcing excitation results in a sequential no-load, load, and unload response at the C7 flexion joint stop between 90 and 150 ms in the simulation. As shown above, the condyles extension is actually decreased because the lower neck joint experiences a rapid C7 flexion loading at the same time that peak condyles extension occurs. This is shown in plots of the lower neck joint stop torque for no T1 angular acceleration input (Figure 101), and for T1 angular acceleration input (Figure 121). The effect of T1 angular acceleration input causes an earlier head angular acceleration peak, but it also improved the resultant linear head acceleration (Figure 117). At −6Gx, T1 angular acceleration input did not have a significant positive effect for other

responses nor did it lead to improved condyles extension response. These results agree with Frisch and Cooper's finding (24) that simulation results are better overall if the T1 angular acceleration input is not used.

Limitations of Occipital Condyles-Anatomic T1 Neck Model. Thus, it was concluded that parameter value adjustment was insufficient to significantly improve the magnitude and duration for condyles extension motion in − Gx simulations. The head z-displacement and the T1 relative angle were improved at − 6Gx by simple adjustment of the C7 flexion stiffness, but the neck model was not able to achieve significant condyles extension nor could it maintain the extension condition for the duration seen in the experimental data.

It was clear that the neck model exhibited only a limited range of angular deflection in extension and flexion when the upper neck joint was positioned at the true anatomical location of the occipital condyles. The neck tension forces of the model act on the upper pivot point such that a forward moment on the head cg does not allow a significant condyles extension to develop. That moment, developed after the peak condyles extension, pulls the head into flexion relative to the neck. This observation indicated that it was necessary to consider alternate pivot points to improve head/neck angulation, and condyles extension in particular. In the − Gx experimental data, condyles extension is observed in all tests. Condyles flexion following peak extension is observed in only six volunteer tests out of a total of forty-two tests examined.

Becker Neck Model at − 6Gx and − 15Gx. Becker (25) described a two-joint neck with the head pivot point located 1.9 cm anterior and 3.4 cm superior to the head center of mass for an instrumented head. In investigative simulations during Phase III, a Becker-like pivot point was modeled. The upper pivot point (with coordinates as described above) was 3.08 cm anterior and 6.32 cm superior to the head origin. Since instrumentation moves the cg anteriorly by about .35 cm and inferiorly by about .20 cm, it is a reasonable assumption that the "Becker pivot" for an uninstrumented head would be about 2.73 cm anterior and 6.52 cm superior to the head origin. Becker provides new estimates of the pivot point locations in reference (26), but we did not feel that results would differ significantly using upper pivot point locations specified in (25) or in (26).

Simulations for which the upper neck pivot point is superior to the head center of mass resulted in good agreement for several response variables (Figures 124–132). The relative angles at the condyles and C7-T1 are in good agreement with

NBDL data at −6Gx, as can be seen from Figures 131-132. (The relative angles are determined from a neck chord between the occipital condyles and anatomic T1.) The x- and z-direction displacement of the head origin are satisfactory for the Becker pivot as well. The experimental and simulation data are not in good agreement, however, for the head angular acceleration. The peak head angular acceleration is quite low in the simulation.

The upper pivot point is superior to the head cg for a Becker-type hinge. As a result of the pivot location, neck tension forces rotate the head backward about the cg and limit the head angular acceleration peak. The upper neck joint stop torque displays extension loading (Figure 130).

The neck model data determined for moment-deflection stiffnesses for the Becker link are shown in Figure 133. The upper neck joint damping coefficients were .026 N-m sec/deg in flexion loading and unloading (.50 energy restitution coefficient). Damping was zero for extension loading and .026 N-m sec/deg for unloading (.20 restitution coefficient). The lower neck joint damping coefficients were zero in flexion loading and unloading (.11 restitution coefficient), and .0034 N-m sec/deg damping in extension loading and unloading (.11 restitution coefficient). Neck length damping was 7.34 N-sec/cm in tension loading and 3.62 N-sec/cm in tension unloading. Compression loading damping was 3.62 N-sec/cm; it was 7.34 N sec/cm in compression unloading. The restitution coefficients for neck length tension and compression were .99.

A simulation at −15Gx was also made for the same Becker hinge point that was used for the −6Gx simulation. At −15Gx, the Becker neck model required a larger C7 flexion stiffness of 1.85 N-m/deg to limit the lower neck joint deflection in the simulation. The simulation and experimental data are shown in Figures 134–141. Overall, even with the larger C7 stiffness, the simulation results are not in good agreement with experimental data at −15Gx. The head angular acceleration is quite low, similar to the head angular acceleration at −6Gx for the Becker hinge point. The waveform of the condyles relative angle at −15Gx is the same as in the −6Gx simulation, i.e., extension with rebound. The NBDL data for condyles extension, however, shows a rapid rebound followed by increasing extension at −15Gx — as opposed to extension with rebound at −6Gx. The signature for extension motion produced by the Becker neck model did not differ for low-g and high-g simulations in −Gx except for magnitude of peak extension.

44

The low peak head angular acceleration produced in the Becker model was not considered a good result. It has been suggested (27) that the head angular acceleration peak could be increased by setting the condyles joint stop rearward of the "zero" position. The effect of this is to cause the head to be stopped abruptly as it rotates in extension relative to the neck. As shown in Figures 142–149, the simulation peak acceleration was improved, but the waveform of the simulation curve no longer resembled the experimental acceleration time history. In addition, it was difficult to model the condyles extension motion with the upper pivot extension joint stop at a non-zero position and maintain a satisfactory head angular acceleration peak. A large overshoot in condyles extension is shown in Figure 148.

Simulations at −Gx with a Long Neck Linkage. While the Becker hinge improved the ability of the model to predict relative angle between the head and the neck, its detrimental effect on the simulation of other dynamic response variables was severe enough to cause us to look further for a satisfactory modeling approach. A primary negative effect was to make it impossible to obtain head angular accelerations of the proper magnitude and waveform. In addition, it was not possible to model higher g levels with the Becker model with good agreement for both −6Gx and −15Gx. The Becker hinge did free our thinking, on the other hand, and we saw that there are good justifications for not adhering rigidly to a head/neck model that has pivot points at the anatomical condyles and C7/T1.

We have found that it is possible to obtain satisfactory condyles relative angle response without using an upper neck pivot point superior to the head center of mass. This is an important result because a head-neck system for an anthropomorphic dummy − particularly an omnidirectional dummy − will be much easier to construct if the head-neck juncture is low on the head, i.e., at or near the inferior external surface. For a hinge high in the head, interference between the neck linkage and the head during angular motions (particularly non-sagittal plane motion) is a serious problem.

Two approaches were identified for modifying the extension response at the upper neck joint for a pivot point inferior to the head cg. Both approaches make use of a neck link that is longer than the Phase II neck chord (a chord defined by anatomic T1 and the occipital condyles). The "long neck model" retains the desirable acceleration response associated with an occipital condyles pivot while increasing the range of extension motion between the head and the neck chord.

The first approach was to place the lower pivot at T1 and the upper pivot superior and anterior to the anatomic condyles. In the first simulation, the upper pivot was located at the head origin, which is 2.92 cm inferior and 1.18 cm posterior to the head center of mass. The lower pivot was 3 cm posterior to anatomic T1. The load-deflection data were identical to the first modified simulation for −6Gx, Figures 94–103, except for an increased C7 bending stiffness of 1.0 N-m/deg. Moving the pivot point from the occipital condyles to the head origin produced a larger extension at −6Gx, as shown in Figures 150–157. The increase in the extension peak for Figure 156 was −36.7 degrees versus −19.6 degrees for a −6Gx simulation that used occipital condyles and anatomic T1 hinge points. The magnitude of the extension peak was improved, but the head rebounded rapidly from the extension peak and proceeded into flexion.

Although a larger extension peak was observed for the head origin pivot point, a significant condyles moment pulled the head rapidly into flexion after the extension peak. This linkage provided an extension peak of improved magnitude in comparison to Phase II results, but the duration of extension was not sufficient. It was seen that the neck link angulation was excessive during the onset of condyles extension for the neck model with a head origin pivot. The low neck angle resulted in the neck link pulling the head into flexion. The extension peak was followed by rapid rebound from extension. The short duration for condyles extension could not be improved through the adjustment of joint stiffnesses or restitution coefficients. It was felt that locating the lower pivot inferior and posterior to anatomic T1 could reduce the neck link angulation during condyles extension and thus prolong the extension motion.

The second approach was to place the upper pivot at the occipital condyles and locate the lower pivot point posterior and inferior to T1. Anatomic T1 was still used for driving the head and neck system. A neck model that has the upper pivot point at the occipital condyles and the lower pivot point inferior and posterior to T1 permits a larger range of possible pivot locations. A similar type of neck link has been described by Spenny and Wismans (28), but their lower pivot point was located via a graphical solution for the origin of a constant radius condyles trajectory. A graphical solution such as this does not account for T1 motion, however, and the lower pivot location was greatly different for two graphical solutions in (28). In this work, on the other hand, the location of the lower pivot point was varied empirically to determine a suitable location.

A number of MVMA 2-D simulations were made with a long neck linkage as a parsimonious approach to improving the condyles extension response. In Figures 158–165, a −6Gx simulation results are shown for a neck model with a lower pivot point 5.12 cm posterior and 7.5 cm inferior to T1. The neck model data are similar to the data used for results in Figures 94–103 with the exception of a C7 flexion stiffness of 2 N-m/deg versus .8 N-m/deg. The results for this simulation are quite good overall. The head angular position and displacement are in good agreement with the experimental data. The head angular acceleration is only slightly early and peaks at 470 rad/sec-sec versus 519 rad/sec-sec, and the waveform is satisfactory. Significantly, the model achieved adequate condyles extension angulation with an upper neck pivot at the anatomical location of the occipital condyles. The waveform for condyles extension and rebound were not well modeled, but a sufficiently large peak extension was achieved to produce satisfactory angular deflections for both the head and neck.

The success of the long neck link in increasing upper neck extension derives directly from the geometry of the linkage. Consider, for example, the approach in which the condyles location is retained for the upper neck articulation but the lower neck articulation is positioned inferiorly to T1. While the neck link angulation in a simulation occurs from the inferiorly located pivot, the relative angle for the lower neck is calculated for the line between anatomic T1 and the condyles, i.e., in the same manner that the angle is calculated from the experimental data. Since anatomic T1 is nearer to the head trajectory arc than is the relocated articulation point, the calculated relative angle for the lower neck is larger than the angle resulting at the articulation, upon which lower neck torques are based.

The joint parameter data for the first simulation of the long neck model were suited only to −6Gx NBDL data inasmuch as the same model data did not provide satisfactory results for −15Gx NBDL data. This was evidenced by the results for a −15Gx simulation (Figures 165–173) using the same input data as the −6Gx simulation discussed above. A significant overshoot of the head angle, head z-direction displacement, and T1 relative angle are shown in the −15Gx simulation results. The head angular velocity peak and peak head angular acceleration are both low in comparison to the experimental data.

47

The primary drawback in using a long neck link is the difficulty in controlling the angular excursion at the lower neck joint. The C7 flexion stiffness must be sufficiently large to stop the neck link at some angular deflection less than 90 degrees from the vertical in order to simulate satisfactorily the T1 relative angle, head angle, and head z-displacement. In addition, it was seen that the use of linear stiffnesses at the lower neck joint did not provide satisfactory angular deflections at both $-6Gx$ and $-15Gx$.

A number of simulations were subsequently made to improve the long neck model data at $-6Gx$ and $-15Gx$.

Bilinear Neck Joint Data for Long Neck Model. The simulation results for two sets of long neck model data are discussed below that make use of bilinear C7 flexion stiffnesses and bilinear neck tension stiffnesses. The first set of neck model data has a lower pivot point located at 5 cm posterior and 6 cm inferior to T1, i.e., T1($-5,6$). The second set of neck model data has a lower neck pivot point 4 cm posterior and 3 cm inferior to T1, i.e., T1($-4,3$).

A 1:3 ratio between the slopes of the lower and upper segments of a bilinear stiffness curve was used for the T1($-5,6$) lower neck pivot point. The results for the long neck model at $-6Gx$ are shown in Figures 174–181. The simulation of the head angular position and head angular velocity are satisfactory, as seen in Figures 174–175. The simulation of the head angular acceleration is quite good. The joint relative angles in the simulation are low in magnitude for both condyles extension and T1 relative angle, but the waveform and peak alignment are satisfactory. The key neck joint parameters that produced the desirable features of the simulation results were a "soft" break in the bilinear C7 flexion stiffness and the bilinear neck tension stiffness.

The identical neck model data were used in a simulation at $-15Gx$. The results of this simulation are shown in Figures 182–189. The head angular position, head z-displacement, and T1 relative angle show large errors that are characteristic of excess angulation at C7 for the long neck model. In addition, the peak head angular acceleration at $-15Gx$ is low and the peak is late compared to the experimental data (Figure 184). The head resultant acceleration shows an improved waveform at $-15Gx$, but the peak values are in error. The condyles relative angle and T1 relative angles both display too much angulation at $-15Gx$ (Figures 188–189), but the excess angular excursion are improved by relocation of the lower pivot and adjustment of the C7 joint stop stiffness.

48

The neck model data determined for moment-deflection stiffnesses for the T1(−5,6) pivot neck are shown in Figure 190. The upper neck joint damping coefficients were .026 N-m sec/deg in flexion loading and unloading (.95 energy restitution coefficient). Damping was zero for extension loading and .026 N-m sec/deg for unloading (.5 restitution coefficient). The lower neck joint damping coefficients were zero in flexion loading and unloading (.25 restitution coefficient), and .0034 N-m sec/deg damping in extension loading and unloading (.11 restitution coefficient). Neck length damping was 5.19 N-sec/cm in tension loading and 5.19 N-sec/cm in tension unloading. Compression loading damping was 1.81 N-sec/cm; it was 3.67 N sec/cm in compression unloading. The restitution coefficients for neck length tension and compression were .99.

A 1:5.33 ratio for the slopes of the bilinear C7 flexion loading curve was used for the second set of simulations at −6Gx and −15Gx. The lower pivot point was located at T1(−4,3).

The simulation results for −6Gx are shown in Figures 191–198. The neck link does not achieve an adequate peak angulation and the head z-displacement and T1 relative angle are low. The head angular position and head angular velocity were similar to the T1(−5.6) simulation, but the alignment of the peaks is slightly worse. The peak head angular acceleration is significantly higher than in the first bilinear simulation at −6Gx, which showed very good agreement for the head angular acceleration. The condyles relative angle does not reach the same peak in extension because of a slightly larger extension stiffness. Rebound from extension at the condyles is more pronounced due to head angular excursion that result from loading the second stiffnesses at C7.

At −15Gx, on the other hand, the T1(−4,3) bilinear neck data produced satisfactory simulation results as shown in Figures 199–206. The large overshoot in head angle, head z-displacement, and T1 relative angle are improved in comparison to the T1(−5,6) neck model data. The peak head angular acceleration is significantly improved at −15Gx for a pivot at T1(−4,3). The condyles relative angle at −15Gx also shows a satisfactory response (Figure 205).

The first set of bilinear neck model data show better agreement for simulations of −6Gx data. The second set of bilinear neck model data show better agreement for the −15Gx data. A comparison of the two sets of model input data indicate that a longer neck link and a "soft" break in C7 bilinear stiffness favors

simulations at $-6Gx$ over $-15Gx$ data. A shorter neck link and a larger break in the C7 bilinear stiffness values favors the simulation of $-15Gx$ data more than $-6Gx$ data.

Overall, the set of bilinear neck data for a T1($-4,3$) pivot is recommended as a preliminary base line neck model. The model with a T1($-$ 4,3) pivot point is selected over the model with a T1($-5,6$) pivot because satisfactory results were obtained in simulations at $-6Gx$ and $-15Gx$ with a T1($-4,3$) pivot. The $-6Gx$ simulation results for the T1($-4,3$) pivot are not as good as the results for the T1($-5,6$) pivot point, but they represent an improvement over the Phase II $-6Gx$ simulation results (Figures 65–72).

The neck model data determined for moment-deflection stiffnesses for the T1($-4,3$) pivot neck are shown in Figure 207. The upper neck joint damping coefficients were .026 N-m sec/deg in flexion loading and unloading (.95 energy restitution coefficient). Damping was zero for extension loading and .026 N-m sec/deg for unloading (.25 restitution coefficient). The lower neck joint damping coefficients were zero in flexion loading and unloading (.20 restitution coefficient), and .0034 N-m sec/deg damping in extension loading and unloading (.11 restitution coefficient). Neck length damping was 5.19 N-sec/cm in tension loading and 5.19 N-sec/cm in tension unloading. Compression loading damping was 1.81 N-sec/cm; it was 3.67 N sec/cm in compression unloading. The restitution coefficients for neck length tension and compression were .99.

## Simulations at +5Gy

Neck model constants for non-sagittal load-deflection data were determined in Phase II +5Gy simulations of test LX2313 (19). The simulation results for responses in +Gy were generally good, but significant problems existed for downward (+Z) head displacement, velocity, and acceleration (Figures 208–210). Also, the neck axial force (Figure 211) showed a large, completely unexpected peak in compression prior to the onset of neck tension. Late in Phase II work it was found that the anomalous neck compression force — and, in consequence, the anomalous head z motion — resulted from a likely error in NBDL data for the laboratory coordinates of T1. Specifically, T1 had an initial lateral offset of 3.75 cm with respect to the head origin position. A 3.75 cm lateral offset for a 12 cm neck length seemed unlikely, and subsequent simulations were made for initial condition data with no lateral offset between the head origin and T1. The complete

50

elimination of lateral offset in the VOM 3-D input data is an arbitrary specification, but it effectively removed the anomalies in head downward excursions noted above. The hypothesized error in T1 position data was subsequently verified by NBDL.

The neck model data determined for +5Gy in Phase II were used in Phase III in a simulation for averaged NBDL volunteer data of Subjects H00118 to H00142. The VOM 3-D simulation results are shown in Figures 212-238. The downward (+Z) head motion is much improved in the simulation in comparison to the earlier simulation results (Figures 217, 221, and 224) because the lateral offset between the head origin and T1 is negligible. All linear accelerations of the head show generally good fit for the simulation and experimental data. The head Euler angles for yaw and roll are satisfactory but a significant overshoot in head pitch is seen in Figure 226. This simulation uses neck pivot points at the occipital condyles and anatomical T1.

The long neck model has been used to obtain improved results for −Gx. It is therefore appropriate to determine whether the long neck model also performs adequately in +Gy.

The effect of relocating the upper neck pivot point from the occipital condyles to the head origin was investigated for +5Gy. The results of this simulation are shown in Figures 239-265. Improvement in the head lateral (-X) and downward (+Z) excursions results from using the head origin pivot point (Figures 246 and 248). The head pitch Euler angle peak is also improved for the head origin pivot, but the yaw and roll Euler angles do not show improvement over the occipital condyles pivot point (Figures 252-254). The simulation results for head angular velocity and head angular acceleration about the x- and z-axis are also improved for the head origin pivot point link in peak magnitudes. Overall, the results for the simulation of +5Gy averaged NBDL data with the head origin pivot point are improved over the occipital condyles pivot point with the primary exception of the head yaw Euler angle.

The +5Gy simulation with a head origin pivot demonstrates that increased neck length has beneficial effects for modeling the +Gy acceleration vector. This neck model was not the only long neck link investigated, however. Results for −Gx indicate that a long neck link with pivot points at at the occipital condyles and anatomic T1 provided better agreement with NBDL data than a neck model with a head origin pivot. Therefore, this second type of long neck model was investigated for modeling lateral flexion.

A simulation of +5Gy averaged data was made using a long neck model that has pivot points at the occipital condyles and 5 cm posterior and 6 cm inferior to anatomic T1. There was no lateral offset from T1. The neck model data were similar to the first simulation (occipital condyles and anatomic T1 pivot points) to provide a comparison of the T1(−5,6) lower pivot point versus the anatomic T1 pivot. The neck twist stops were positioned at 45 degrees instead of 35 degrees to improve head yaw.

The long neck model simulation results are shown in Figures 266–292. The simulation of the T1(−5,6) pivot neck model stopped at 206 ms, however, due to a singularity encountered in the calculation of head motion in the VOM 3-D model. Results through 206 ms are valid. The long neck model displayed slightly improved head lateral excursions, as shown in Figures 269, 273, and 276. The head yaw and roll Euler angles are not as good for the long neck model as they are for the anatomic T1 pivot, but head pitch is in very good agreement with the experimental data up to 206 ms. In addition, the long neck model demonstrates better angular acceleration response about x- and z- directions than the simulation for the anatomic T1 pivot (Figures 285–287).

The long neck model was used for the improvement of − Gx simulations, but the preliminary results for +Gy also show improved agreement with the experimental data. It was anticipated that the long neck model could demonstrate satisfactory omni-directionality, but it was not clear whether head acceleration response would show poorer results. This is not the case, however. The acceleration response for x- and z-direction head excursions were slightly improved for the long neck model simulations versus the Phase II neck model.

# VI. SUMMARY

<u>Effect of Pivot Point for Neck Model Response.</u> The Phase II version of the two-joint neck was exercised with NBDL averaged volunteer data for $-6Gx$, $-10Gx$, $-15Gx$, and $+5Gy$. The neck model produced satisfactory head angular velocities and accelerations for each g level in $-Gx$, but x- and z-direction displacements, head angle, and the neck joint relative angles were not satisfactory. It was subsequently concluded that a two-joint neck with pivot points at the occipital condyles and at T1 cannot produce a condylar extension motion of satisfactory magnitude or duration in $-Gx$ simulations. This result has also been reported by Frisch and Cooper (24). Condyles extension could not be improved significantly by adjusting neck joint parameters to increase the neck link angulation. Removing all joint stop resistance to extension at the upper pivot point did not improve the extension motion (14). Therefore, an alternative neck linkage was sought to improve the condyles articulation.

Becker has described a neck link that uses an upper pivot point superior to the head center of mass (25). Simulations were made with the upper pivot point at 1.9 cm anterior and 3.4 cm superior to the head center of mass. The Becker model provided very good results for head angular deflections and linear displacements at $-6Gx$, but the head angular acceleration response was not satisfactory. At $-15Gx$, the Becker neck linkage did not model any of the response variables well.

A Becker-type link produces condyles extension motion through the use of a positive mechanical advantage to rotate the head backward about the cg in the $-Gx$ acceleration vector. The upper pivot is a theorized hinge point in the head that is determined as that point which has the most nearly constant distance from the articulation at the base of the neck. This approach for modeling the neck ignores the moments and forces that drive the head/neck system, however. The upper pivot in the Becker neck model provides sufficient extension of the head, but it directly interferes with the peak head angular acceleration. This is evident in the strong negative influence the neck tension force has on the head angular acceleration for the Becker neck in $-Gx$ simulations.

The long neck model was used as an alternative to the Phase II neck model and the Becker neck model. The best results were obtained for a long neck model which used pivot points located at the occipital condyles and posterior and inferior to T1. The neck model produced improved head/neck angulation while maintaining satisfactory acceleration response.

Spenny and Wismans (28) describe a two-joint neck that resembles the long neck model used in this investigation. Assuming a neck of fixed length, they determined an "optimal" lower pivot point that best fit a radial displacement path of the occipital condyles. Their pivot point at $-10Gx$ was approximately 2 cm posterior and 4 cm inferior to T1 for subject H0093 and 2 cm posterior to T1 for subject H0083. The lower pivot points determined by the authors show significant variation for two subjects at $-10Gx$. Indeed, ignoring T1 translation at the lower pivot introduced an unknown amount of error in the estimate of the pivot location via the graphical technique (29).

Different pivot points were used to empirically assess the effect of lower hinge location in this investigation. Values examined for the x- and z-offset from T1 were $(-3,0)$, $(-4,3)$, $(-2,6)$, $(-5,6)$, and $(-5.12,7.5)$. A neck link 3 cm posterior from anatomic T1 improved the agreement for only head x-displacement. When the lower pivot was located inferiorly to T1, the simulation results for condyles extension and head angle were improved. A pivot point located at $T1(-4,3)$ yielded the best results over all g-levels, but a best lower pivot point location has not necessarily yet been established.

Increasing the inferior ($+Z$) location of the lower pivot point has beneficial effect on the magnitude of condyles extension. For a lower pivot inferior to T1, it is necessary to limit C7 angulation to avoid large overshoot in predicted head angle and T1 relative angle, and inadequate peak head angular acceleration. With regard to posterior-anterior position of the lower pivot, it was found necessary to locate the pivot posterior to T1 to maintain satisfactory agreement for head x-displacement. At this time, the consequences of using a long neck link are still being investigated.

A long neck model maintains satisfactory results for the simulation of the head angular acceleration while accomplishing an improvement in head origin x and z motion and the relative angle response at condyles and T1. Previously, it had not been possible to get more than modest amounts of condyles extension in $-Gx$ simulations with a pivot at the occipital condyles. The improved results mean that

a dummy neck designed on the basis of long neck model data would be much more capable of producing proper (human-like) neck moments while retaining the parsimony of the Phase II neck model.

Neck Model Load-Deflection Properties. Modeling high-g and low-g NBDL data for $-$Gx showed that a nonlinear C7 bending stiffness and a nonlinear neck elongation stiffness improved the overall agreement for the simulation and experimental data. Bilinear loading curves were used to introduce nonlinearity because this made it simple to parameterize the nonlinearity.

The load-deflection properties for the bilinear neck tension stiffness (Figure 207) are modeled such that $-$6Gx neck elongation occurs within the first stiffness region and $-$15Gx neck elongation occurs over both the first and second stiffness regions. A bilinear neck tension stiffness improved the simulation results primarily for the resultant head linear acceleration and head x-displacement. The neck deflection at $-$6Gx remained within the first stiffness region, but the neck deflection at $-$15Gx proceeded through both stiffness regions. The bilinear stiffness for $-$15Gx produced better results than any linear stiffness curve.

Appropriate load-deflection properties of the lower hinge point were more difficult to establish. The angulation at the lower pivot is only ten percent greater in $-$15Gx NBDL data than in $-$6Gx NBDL data while head angular and linear accelerations increase in proportion to the T1 driver acceleration. The load-deflection curve for neck elongation has two stiffness regions to accommodate different amounts of neck deflection at $-$6Gx and $-$15Gx. The angular deflections at C7, however, are comparable at $-$6Gx and $-$15Gx. Linear C7 bending stiffnesses were found inadequate to satisfactorily model both high-g and low-g $-$Gx NBDL data. Damping was investigated for controlling the angulations at C7, but this also proved inappropriate. Nonlinear stiffnesses are used for the loading-deflection curve because a nonlinear stiffness came closest to providing model fidelity for high- and low-g impacts. The breakpoint between the two stiffness regions was specified at twenty degrees for the C7 load-deflection curve (Figure 207). The early breakpoint in the C7 bending stiffness corresponds to two events of significance in the simulation: the peak head angular acceleration and peak condyles extension. It was found that head angular acceleration and condyles extension were improved for a breakpoint in the range of twenty to twenty-five degrees.

# VII. CONCLUSIONS

1. The iterative comparison of simulation results against NBDL test results for both high-g and low-g tests yielded neck model data that exceeded the performance of the Phase II neck model for $-Gx$.

2. Two modes of subject response for condyles extension can be characterized as: 1) extension with rebound, and 2) extension with no rebound. Most subjects demonstrated extension with rebound at $-6Gx$ and $-10Gx$. At $-15Gx$, more than half the test subjects displayed no-rebound extension. This was notable because the mode one extension is seen exclusively in passive two-joint neck models, i.e., extension with rebound. The extension motion after the peak does seem to be a factor of the pretest subject tensing, but it is not characterized by the "atypical" subject response described by Seemann, et al. (12).

3. Achieving an adequate condyles extension in $-Gx$ was necessary to obtain satisfactory prediction of head angle, neck angle, and head x- and z-displacement, and head trajectory. To produce a satisfactory condyles extension, the lower pivot point must be located inferior and posterior to the anatomical T1 point.

4. It is better to locate the upper pivot point of the two-joint neck at or near the occipital condyles to preserve adequate acceleration and displacement response. An omnidirectional head-neck system will be much easier to construct for an anthropomorphic dummy if the head-neck juncture is low on the head, i.e., at or near the inferior external surface. For a hinge high in the head, interference between the head and the neck linkage during angular motions (particularly non-sagittal plane motion) is a serious problem.

5. A nonlinear lower neck joint stiffness and neck elongation stiffness is necessary to obtain satisfactory simulation results over the range 6–15 g's for $-Gx$ tests.

6. The Phase II neck model simulations and simulations of the Becker neck model demonstrate that the linear and angular displacement response and the acceleration response can be decoupled.

7. Preliminary simulations in $+Gy$ demonstrate that a long neck link can adequately model non-sagittal plane motion as well as sagittal plane motion. In $+5Gy$, a long neck link for $T1(-5,6)$ showed improved results for downward $(+Z)$ and lateral $(-X)$ head excursions versus a neck link with pivot points at the occipital condyles and anatomic T1. The head pitch angle was significantly improved for the long neck. Head yaw and roll were not modeled quite as well.

8. The neck joint parameters determined for mathematical models of the neck are generally linkage specific. It is therefore necessary to reassess previously determined model parameters when new or different data are available. Exercising the mathematical model for different g levels and acceleration vectors is necessary to ensure the generality of the neck model data.

9. Responses to impact in the different vectors are governed most strongly by different subsets of neck parameters, but significant coupling through "cross terms" is present. It would be desirable to have $+Gz$ data as well so that mechanisms in this vector could be investigated in parallel with simulations in $-Gx$ and $+Gy$.

58

# VIII. RECOMMENDATIONS FOR ADDITIONAL RESEARCH

It is suggested that additional study of NBDL data be carried out through modeling and simulation before simulation results are applied in the final design specifications of the neck module of a Bio-Fidelic Manikin. Specifically, the following tasks are recommended:

1) +Gz data should be studied. It is important that, to the extent possible, data be used for the same subjects involved in simulations in the present study. The primary goal of this task would be to ascertain the mechanism for the two basically different modes of response seen in +Gz sled tests. Implications are expected to bear on neck design, torso-shoulder design, or initial conditions considerations.

2) Simulations in −Gx and +Gy need to be carried out in parallel with the +Gz simulations. Since neck model parameter changes resulting from examination of simulations in any vector affect results in other vectors as well, all vectors must be dealt with together in the procedure of refining the model.

3) Once a baseline neck configuration is established from simulations of −Gx, +Gy, and +Gz data a parameter sensitivity study can be performed for the neck model parameters. Results will have a bearing on mechanical design tolerances. Additionally, the parameter sensitivity study would indicate which neck model specifications can be modified to obtain a maximally simplified neck design. The resulting parsimonious neck model will include only those joint characteristics shown to be pertinent by the sensitivity study.

# IX. APPENDIX

## Condyles Lockup

There was concern whether it was necessary to develop a neck model mechanism for condyles lockup in Phase III.

"Condyles lockup" has been described as an atypical test condition in which the subject "locks" the occipital condyles in anticipation of the impact event. Seemann, et al. (12), state that the condyles remain locked until a force of significant magnitude forces an "unlocking" of the condyles. Spenny and Wismans (28), however, use the term "condyles lockup" simply to describe a state of equal angular velocity motion for the head and neck that occurs after the peak head angular acceleration. $-10Gx$ condyles extension may give the appearance of lockup when there is minimal angulation at the condyles in the rebound from the extension peak, but the head and neck do not appear to be rigidly locked at any time.

Seemann, et al. (12), modeled the atypical response with the Becker neck model with the upper neck pivot point initially "locked". The Becker model was shown to model head angular acceleration for both the lock-up condition and the non-lockup condition. This was accomplished through the adjustment of the upper pivot point stop angle. The "lockup" condition of the model has a low joint stop angle of 1.61 degrees, whereas non-lockup has a joint stop angle of 9.1 degrees, which is a significant difference in the head angular deflection. In the model, however, bimodal angular acceleration response is a result of the pivot location and may not have much bearing on the pre-test condyles "lockup" condition. A Becker hinge with the pivot point posterior and superior to the head center of mass, analogous to the pivot location used by Seemann, et al., was found to yield a bimodal head angular acceleration peak of the type shown for the atypical response. It is recommended that the pre-test "lock-up" condition at the upper neck joint be tested for an occipital condyles joint location. This may yield more insight into the origin of the bimodal acceleration than simulations with a Becker hinge.

# X. REFERENCES

1. Ewing, C.L., Thomas, D.J., Beeler, G.W., Patrick, L.M., and Gillis,. D.B. "Dynamic Response of the Head and Neck of the Living Human to Gx Impact Acceleration." Proceedings, Twelfth Stapp Car Crash Conference. Society of Automotive Engineers, Inc., New York. SAE #680792, October 1968.

2. Ewing, C.L., Thomas, D.J., Patrick, L.M., Beeler, G.W., and Smith, M.J. "Living Human Dynamic Response to −Gx Impact Acceleration. II-Accelerations Measured on the Head and Neck." Proceedings, Thirteenth Stapp Car Crash Conference. Society of Automotive Engineers, Inc., New York. SAE #690817, December 1969.

3. Ewing, C.L. and Thomas, D.J. "Human Dynamic Response to −Gx Impact Acceleration." AGARD Conference Proceedings, AGARD-Cp-88-71, June 1972.

4. Ewing, C.L., and Thomas, D.J. Human Head and Neck Response to Impact Acceleration. NAMRL Monograph 21 USAMRL 73-1, August 1972.

5. Ewing, C.L. and Thomas, D.J. "Torque Versus Angular Displacement Response of Human Head to −Gx Impact Acceleration." Proceedings, Seventeenth Stapp Car Crash Conference, SAE #730976, November 1973.

6. Ewing, C.L., Thomas, D.J., Lustick, L., Becker, E., Willems, G., and Muzzy, W.H. III, "The Effect of the Initial Position of the Head and Neck on the Dynamic Response of the Human Head and Neck to −Gx Impact Acceleration." Proceedings of Nineteenth Stapp Car Crash Conference, SAE #751157, November 1975.

7. Ewing, C.L., Thomas, D.J., Lustick, L., Muzzy, W.H., Willems, G., Majewski, P.L. "The Effect of Duration, Rate of Onset and Peak Sled Acceleration on the Dynamic Response of the Human Head and Neck." Proceedings 20th Stapp Car Crash Conference, SAE #760800, October 1976.

8. Muzzy, W.H., and Lustick, L. "Comparison of Kinematic Parameters Between Hybrid II Head and Neck System with Human Volunteers for −Gx Acceleration." Proceedings, 20th Stapp Car Crash Conference, SAE #760801, October 1976.

9. Ewing, C.L., Thomas, D.J., Majewski, P.L., Black, R., and Lustick, L. "Measurements of Head, T1, and Pelvic Response to −Gx Impact Accelerations." Proceedings, 21st Stapp Car Crash Conference, SAE #770927, October 1977.

10. Ewing, C.L., Thomas, D.J., Lustick, L., Muzzy, W.H., Willems, G.C., and Majewski, P. "Dynamic Response of the Human Head and Neck to +Gy Impact Acceleration." Proceedings, 21st Stapp Car Crash Conference, SAE #770928, October 1977.

11. Ewing, C.L., Thomas, D.J., Lustick, L., Muzzy, W.H., Willems, G.C., and Majewski, P. "Effect of Initial Position on the Human Head and Neck Response to +Y Impact Acceleration." Proceedings, 22nd Stapp Car Crash Conference, SAE #780888, October 1978.

12. Seemann, M.R., Lustick, L.S., and Frisch, G.D., "Mechanism for Control of Head and Neck Dynamic Response." Proceedings, 28th Stapp Car Crash Conference, SAE #841669, November 1984.

13. Schneider, L.W., Bowman, B.M., Snyder, R.G., and Peck, L.S. A Prediction of Response of the Head and Neck of the U.S. Adult Military Population to Dynamic Impact Acceleration from Selected Dynamic Test Subjects. 12 Month Technical Report NR 105- 832, ONR Contract N00014-75-C-1077, May 1976.

14. Schneider, L.W., and Bowman, B.M., "Prediction of Head/ Neck Dynamic Response of Selected Military Subjects to -Gx Acceleration." Proceedings of Symposium on Biodynamic Models, Dayton, February 1977, Aviation, Space, and Environmental Medicine, Supplemental Issue, January 1978.

15. Bowman, B.M., and Schneider, L.W., Analysis of Head and Neck Dynamic Response of the U.S. Adult Military Population. Annual Report NR 207- 280, prepar   for Naval Medical Research and Development Command. ONR Contract No. N00014-81-K-0603. UM-HSRI-82-29. July 1982.

16. Bowman, B.M., and Schneider, L.W., "Analysis of Head and Neck Dynamic Response of the U.S. Adult Military Population: Phase II." Six-Month Status Report, prepared for Naval Medical Research and Development Command. ONR Contract No. N00014-81-K-0603. January 12, 1983.

17. Six-Month Status Report, January 27, 1982. "Analysis of Head and Neck Dynamic Response of the U.S. Adult Military Population" (Phase I), Contract No. N00014-81- K-0603. Submitted to Program Director, Office of Naval Research, Code 612B:JCE.

18. Proposal for Phase III: "Analysis of Head and Neck Dynamic Response of the U.S. Adult Military Population: Phase III." Submitted to Naval Biodynamics Laboratory, February 11, 1983. Transportation Research Institute, University of Michigan, Ann Arbor.

19. Bowman, B.M., Schneider, L.W., Lustick, L.S., Anderson, W.R., and Thomas, D.J. "Simulation Analysis of Head and Neck Dynamic Response." Proceedings, 28th Stapp Car Crash Conference., SAE #841668, November 1984.

20. Bowman, B.M., Robbins, D.H., and Bennett, R.O. MVMA Two-Dimensional Crash Victim Simulation Tutorial System: Self-Study Guide and Audio-Visual Program. Prepared for Motor Vehicle Manufacturers Association. UM-HSRI-77-18-1, 2 (2 volumes). April 1977.

21. Bowman, B.M., Bennett, R.O., and Robbins, D.H. MVMA Two-Dimensional Crash Victim Simulation, Version 4 Volumes 1, 2 and 3. Final Report No. UM-HSRI-79-5-1, 2,3, June 1979.

22. Bowman, B.M., Bennett, R.O., and Robbins, D.H. MVMA Two-Dimensional Crash Victim Simulation, Version 5 Volumes 1, 2 and 3. Final Report No. UMTRI-85-24-1,2,3, June 1985.

23. Bowman, B.M., Analytical Model of a Vehicle Occupant For Use in Crash Simulations. Ph.D. Thesis. The University of Michigan, 1971.

24. Frisch, G.D., Cooper, C., "Mathematical Modeling of the Head and Neck Response to -Gx Impact Acceleration (Minimum Articulation Requirements)", Proceedings of Symposium on Biodynamic Models, Dayton, February 1977, Aviation, Space, and Environmental Medicine, Supplemental Issue, January 1978.

25. Becker, E. B., "Preliminary Discussion of an Approach to Modeling Living Human Head and Neck to -Gx Impact Acceleration." Human Impact Response. King, W.F. and Mertz, H. J., ed., Plenum Publishing Corp., New York 1973.

26. Becker, E. B., "Head and Neck Kinematics for Frontal, Oblique, and Lateral Crash Impact", Research Report No. NBDL-80R009, New Orleans, 1980.

27. Private communication, Leonard S. Lustick, November 1985.

28. Wismans, J., Spenny, C.H., "Head-Neck Response in Frontal Flexion", Proceedings, 28th Stapp Car Crash Conference, SAE #841666, November 1984.

29. Private communication, Curt H. Spenny, April 1986.
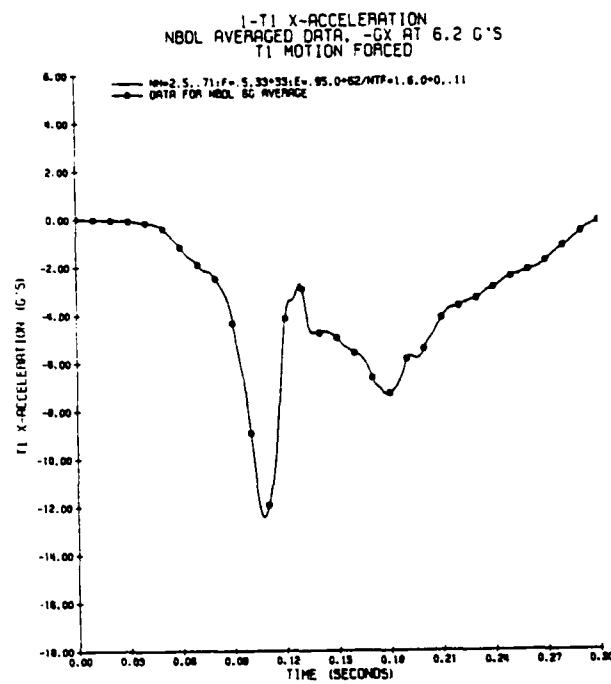
Figure 63. NBDL Averaged Data for T1 X-Axis Acceleration at -6Gx.
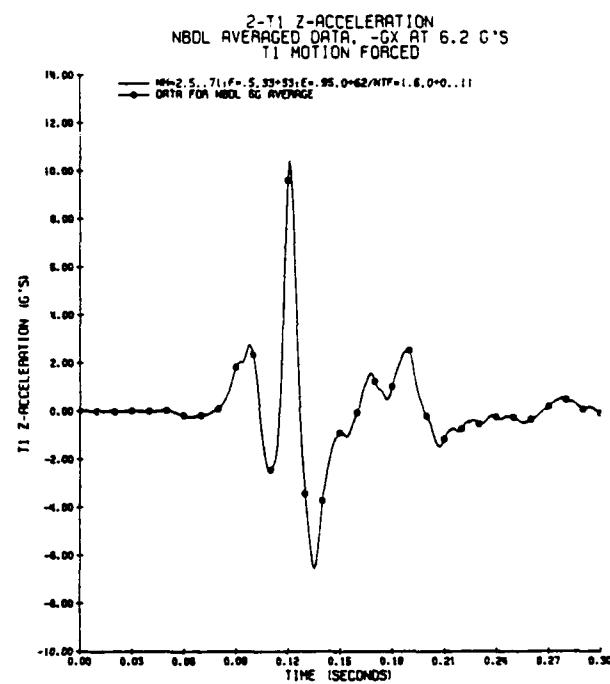


Figure 64. NBDL Averaged Data for T1 Z-Axis Acceleration at -6Gx.
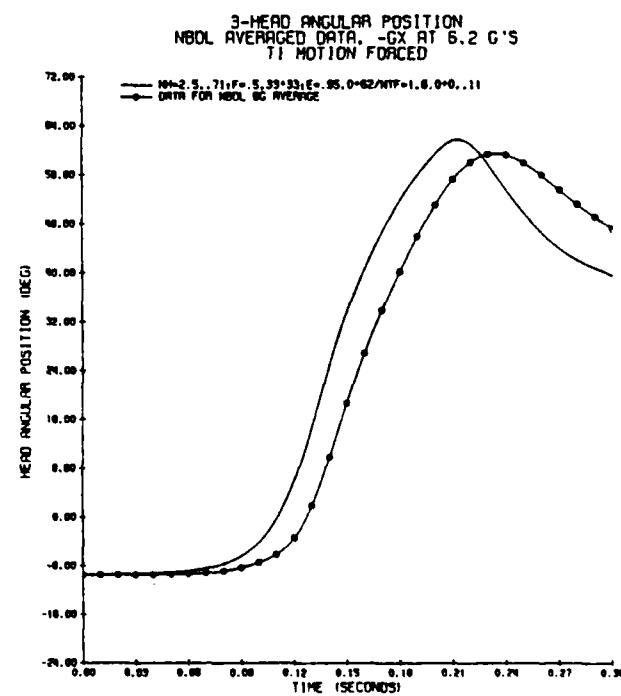


Figure 65. Head Angular Position for Phase II Neck Model Data at -6Gx.
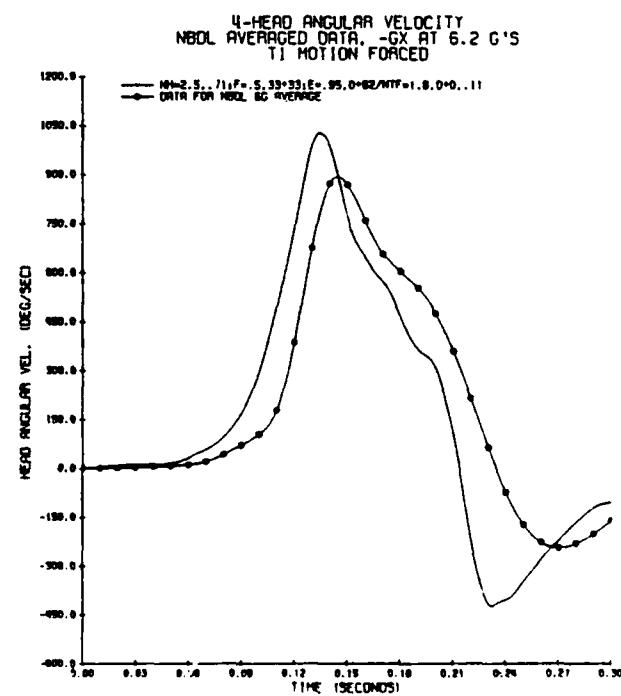


Figure 66. Head Angular Velocity for Phase II Neck Model Data at -6Gx.

67

5-HEAD ANGULAR ACCELERATION
NBDL AVERAGED DATA, -GX AT 6.2 G'S
T1 MOTION FORCED
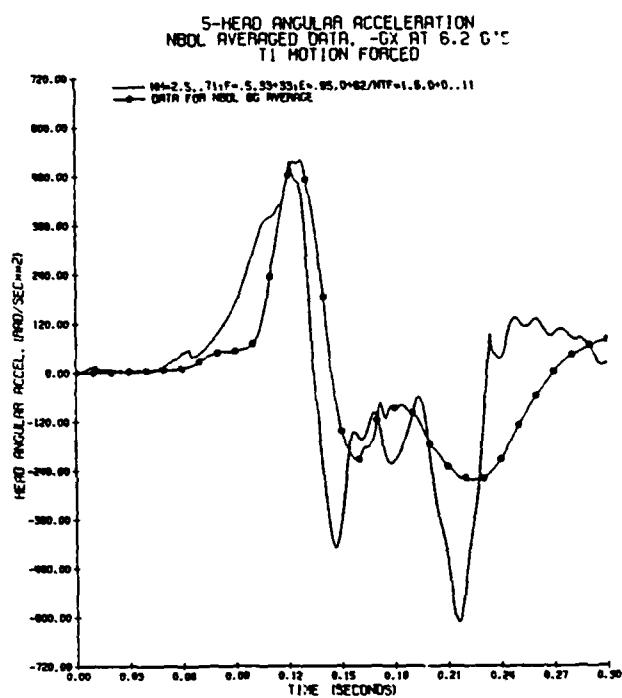
Figure 67.  Head Angular Acceleration for Phase II Neck Model Data at -6Gx.

6-RESUL. LINEAR ACCEL. OF HEAD ANATOMICAL ORIGIN
NBDL AVERAGED DATA, -GX AT 6.2 G'S
T1 MOTION FORCED
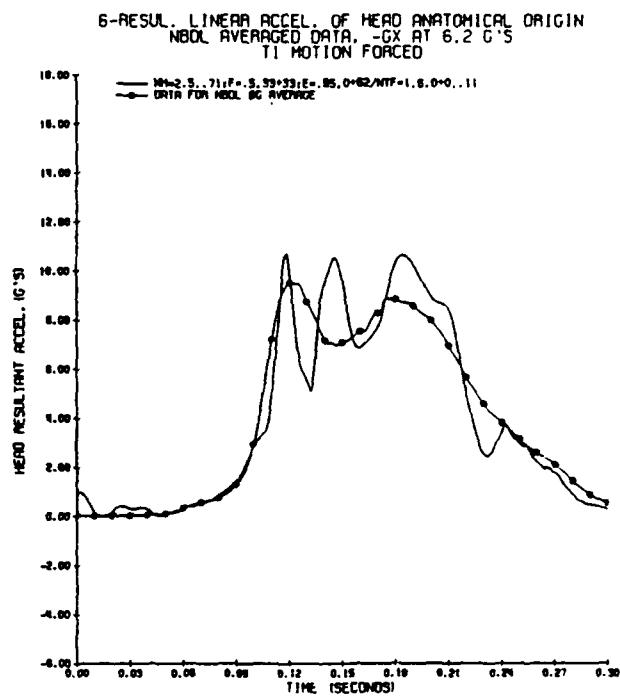
Figure 68.  Head Resultant Acceleration for Phase II Neck Model Data at -6Gx.

7-HEAD X-DISPL. REL. TO T1
NBDL AVERAGED DATA, -GX AT 6.2 G'S
T1 MOTION FORCED
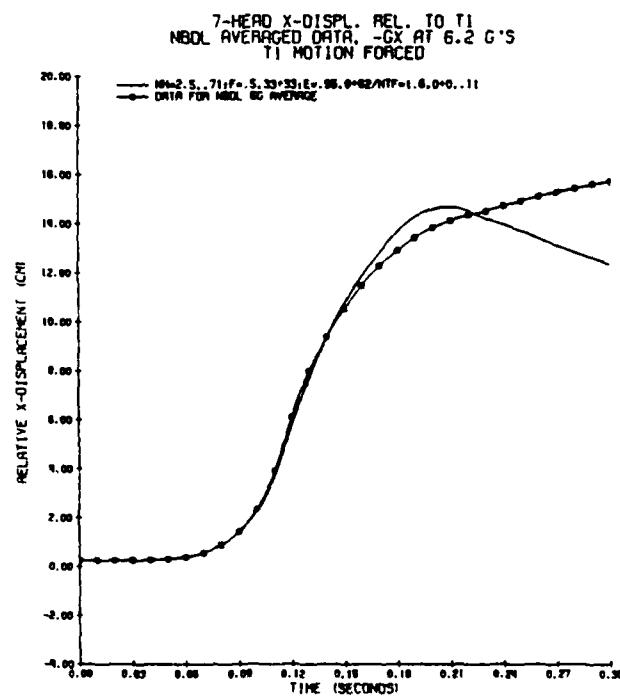
Figure 69.  Head Origin X-Axis Displacement for Phase II Neck Model Data at -6Gx.

8-HEAD Z-DISPL. REL. TO T1
NBDL AVERAGED DATA, -GX AT 6.2 G'S
T1 MOTION FORCED
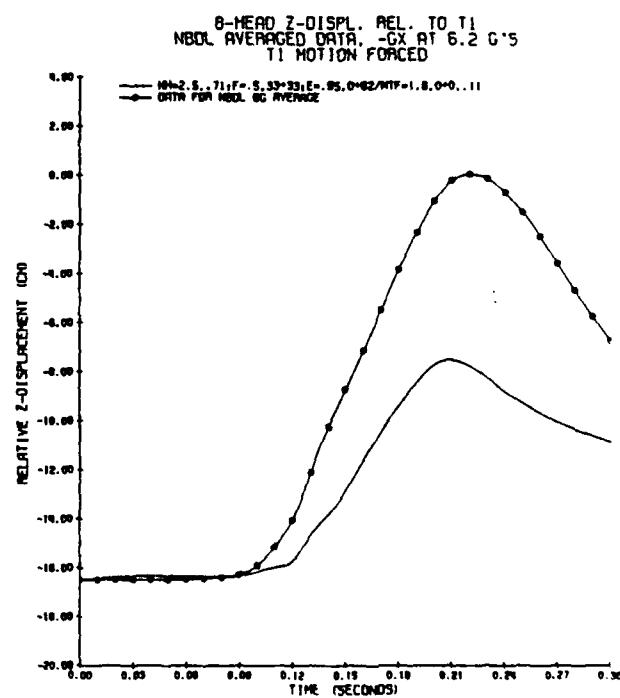
Figure 70.  Head Origin Z-Axis Displacement for Phase II Neck Model Data at -6Gx.

68
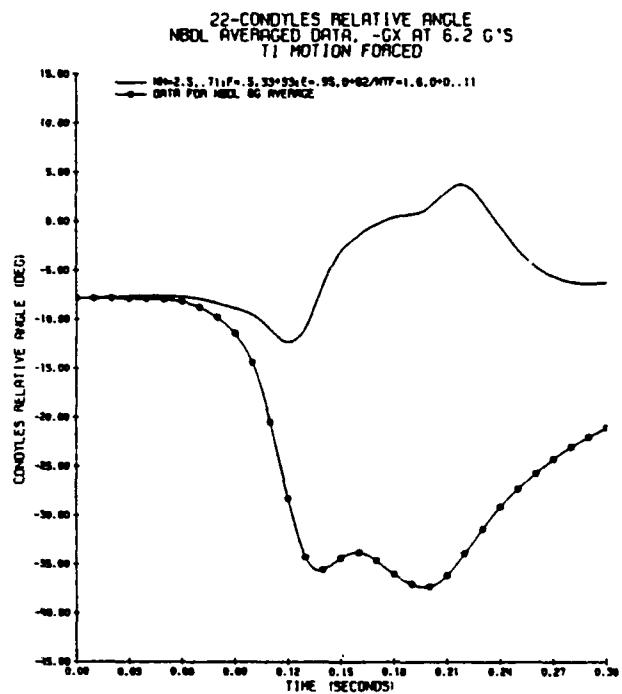
Figure 71. Condyles Relative Angle for Phase II Neck Model Data at -6Gx.
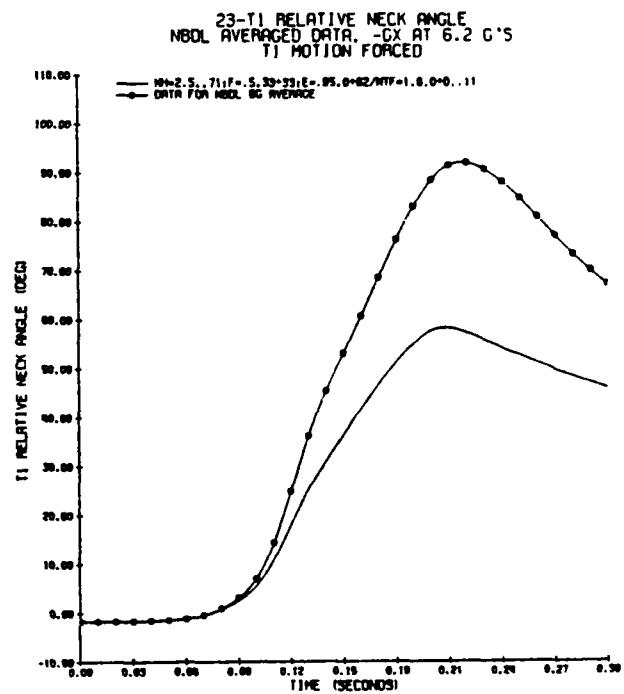
Figure 72. T1 Relative Angle for Phase II Neck Model Data at -6Gx.
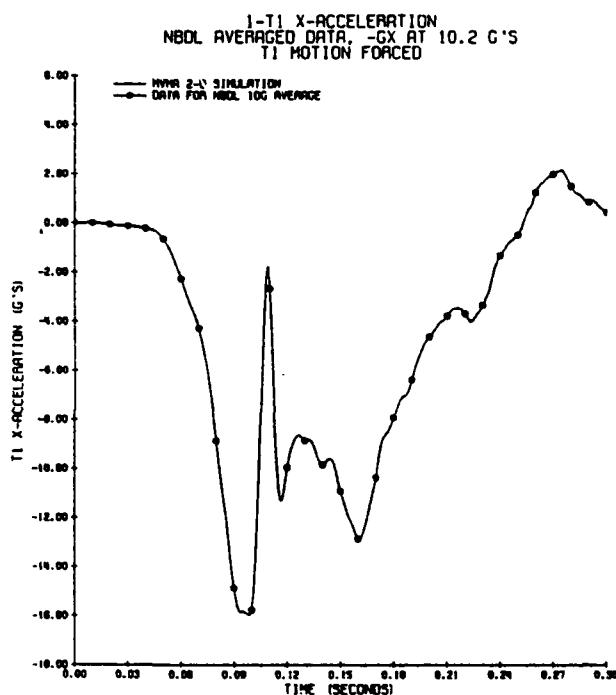
Figure 73. NBDL Averaged Data for T1 X-Axis Acceleration at -10Gx.
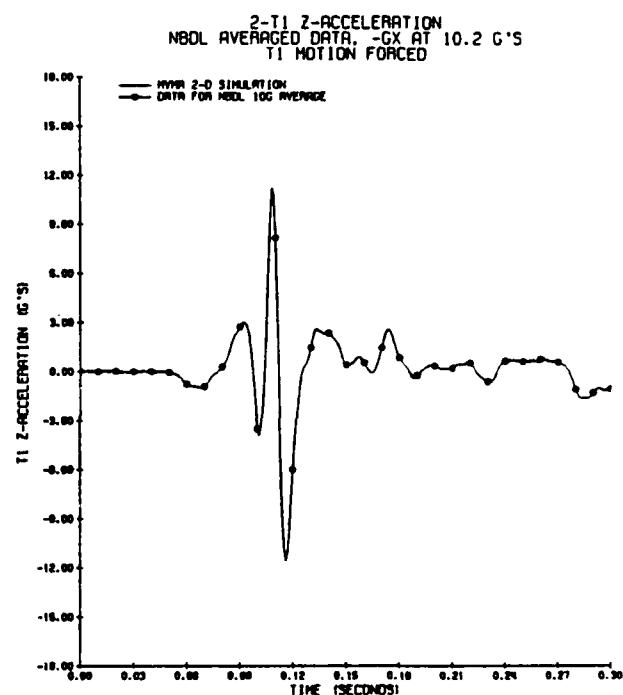


Figure 74. NBDL Averaged Data for T1 Z-Axis Acceleration at -10Gx.
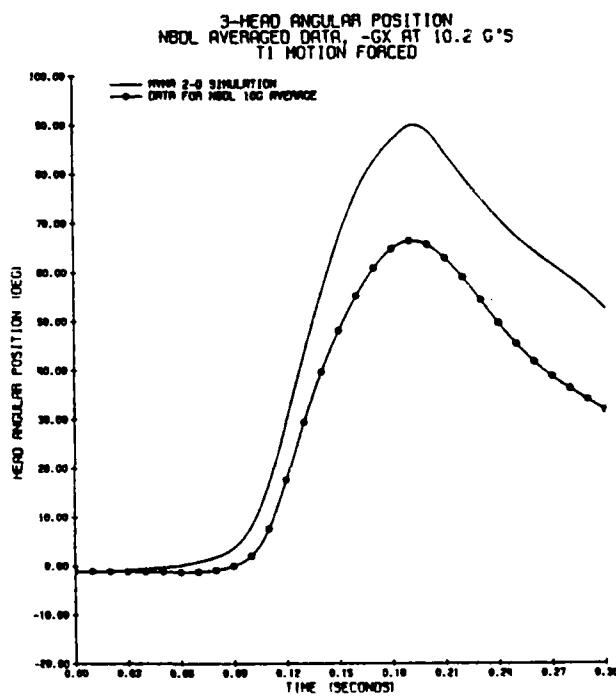


Figure 75. Head Angular Position for Phase II Neck Model Data at -10Gx.
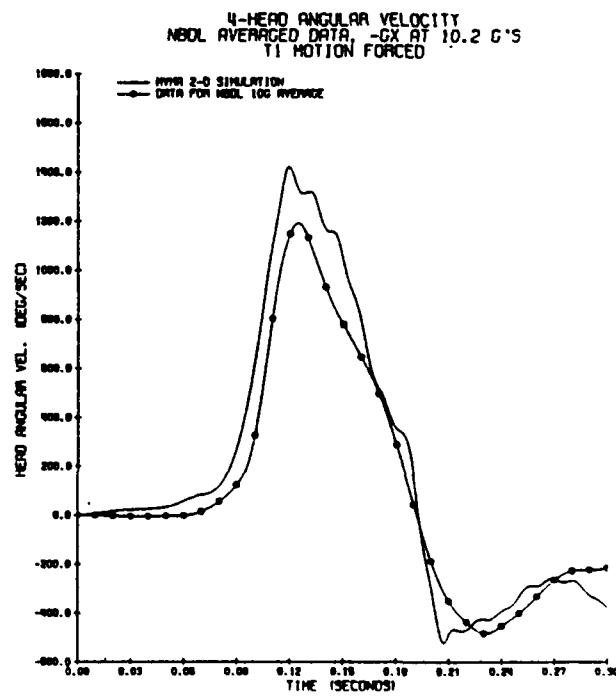


Figure 76. Head Angular Velocity for Phase II Neck Model Data at -10Gx.

## 5-HEAD ANGULAR ACCELERATION
### NBDL AVERAGED DATA, -GX AT 10.2 G'S
### T1 MOTION FORCED
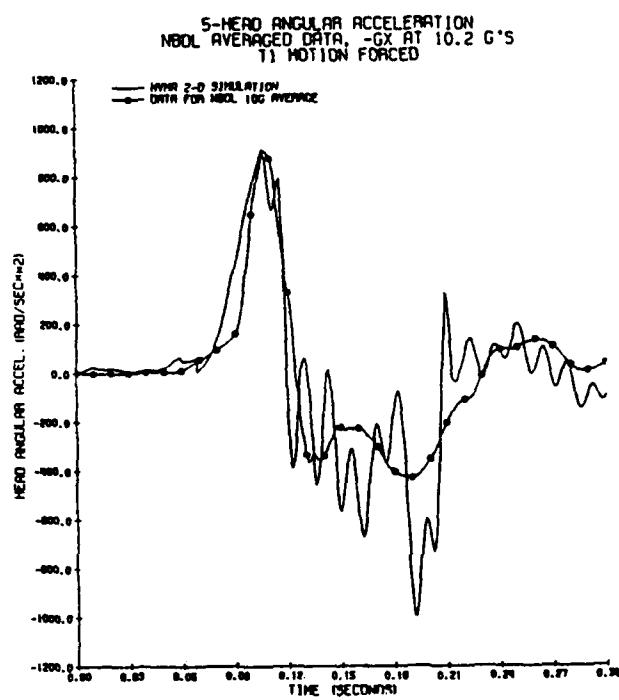
Figure 77. Head Angular Acceleration for Phase II Neck Model Data at -10Gx.

## 6-RESUL. LINEAR ACCEL. OF HEAD ANATOMICAL ORIGIN
### NBDL AVERAGED DATA, -GX AT 10.2 G'S
### T1 MOTION FORCED
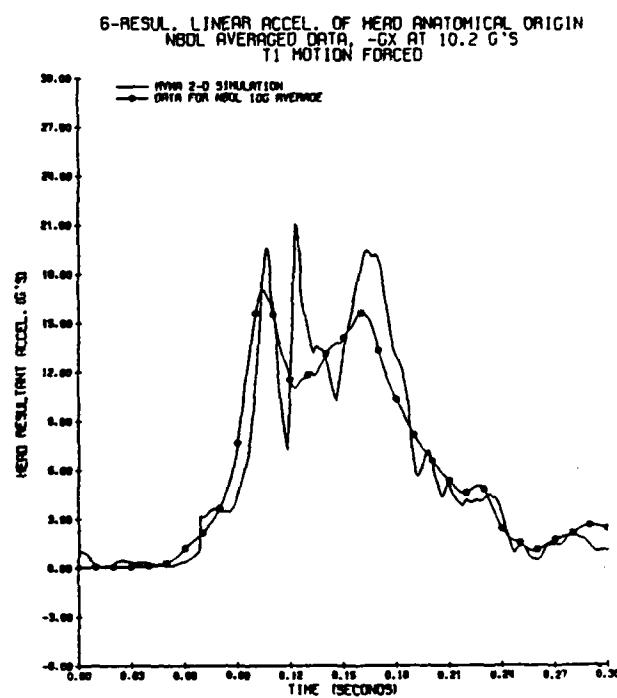
Figure 78. Head Resultant Acceleration for Phase II Neck Model Data at -10Gx.

## 7-HEAD X-DISPL. REL. TO T1
### NBDL AVERAGED DATA, -GX AT 10.2 G'S
### T1 MOTION FORCED
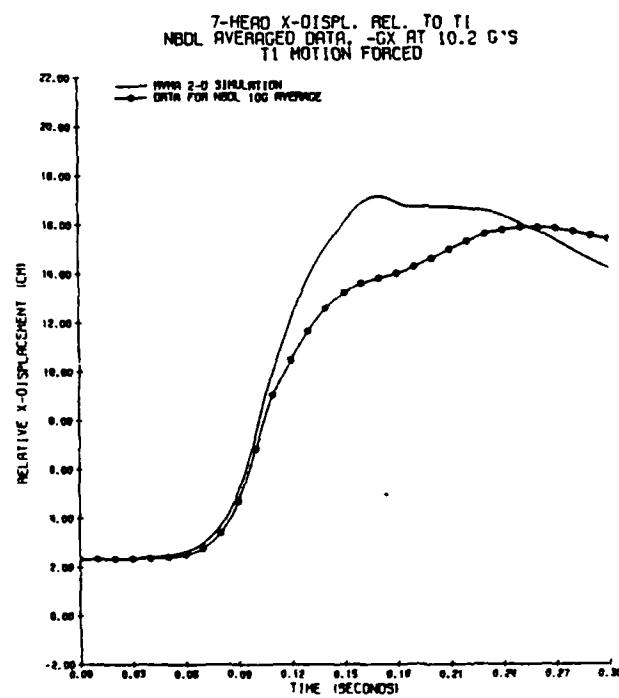
Figure 79. Head Origin X-Axis Displacement for Phase II Neck Model Data at -10Gx.

## 8-HEAD Z-DISPL. REL. TO T1
### NBDL AVERAGED DATA, -GX AT 10.2 G'S
### T1 MOTION FORCED
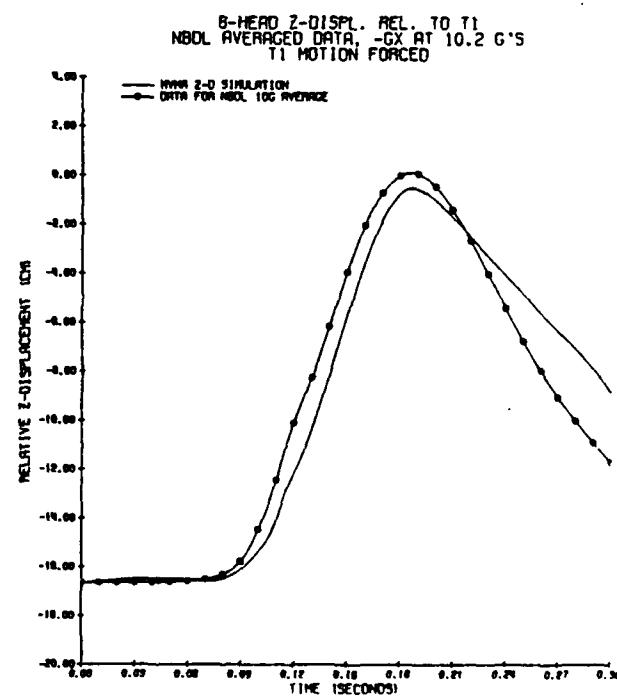
Figure 80. Head Origin Z-Axis Displacement for Phase II Neck Model Data at -10Gx.

71
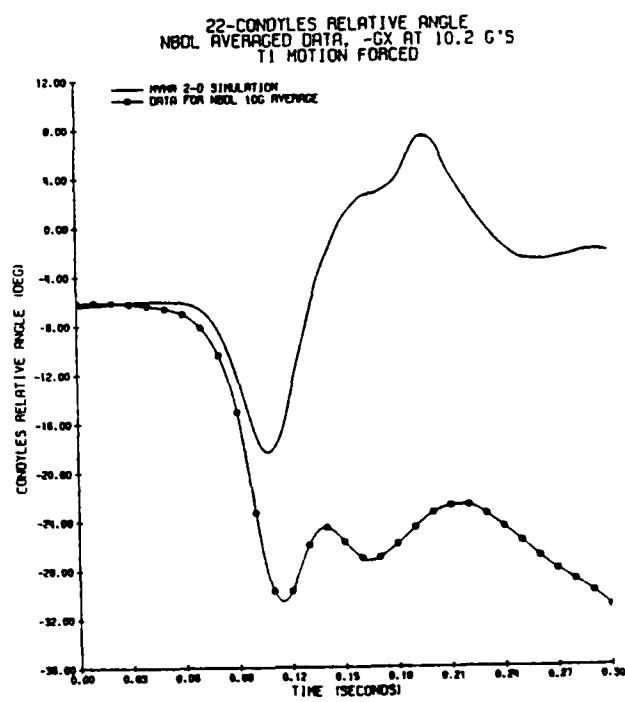
Figure 81. Condyles Relative Angle for Phase II
Neck Model Data at -10Gx.
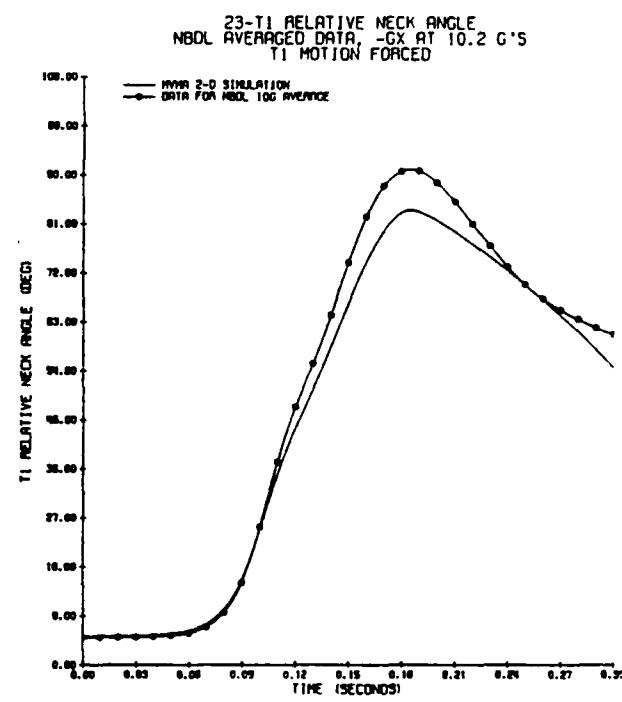
Figure 82. T1 Relative Angle for Phase II Neck
Model Data at -10Gx.
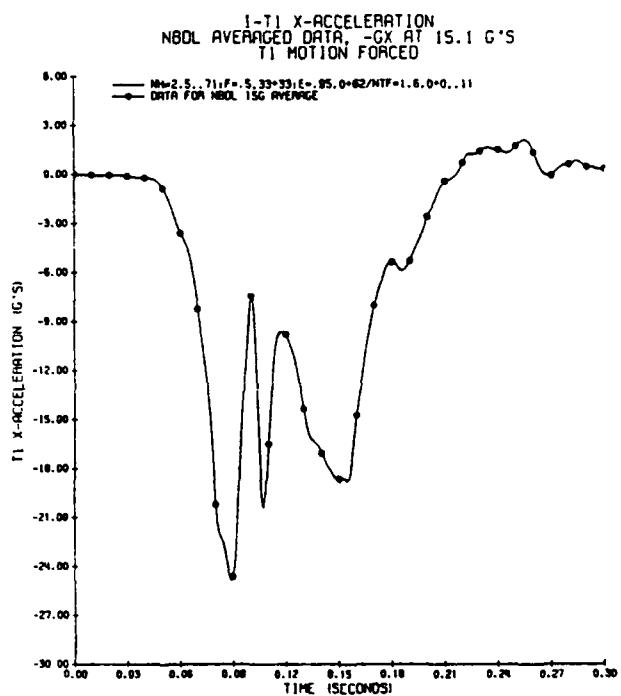
**1-T1 X-ACCELERATION**
**NBDL AVERAGED DATA, -GX AT 15.1 G'S**
**T1 MOTION FORCED**

Figure 83. NBDL Averaged Data for T1 X-Axis Acceleration at -15Gx.

**2-T1 Z-ACCELERATION**
**NBDL AVERAGED DATA, -GX AT 15.1 G'S**
**T1 MOTION FORCED**

Figure 84. NBDL Averaged Data for T1 Z-Axis Acceleration at -15Gx.
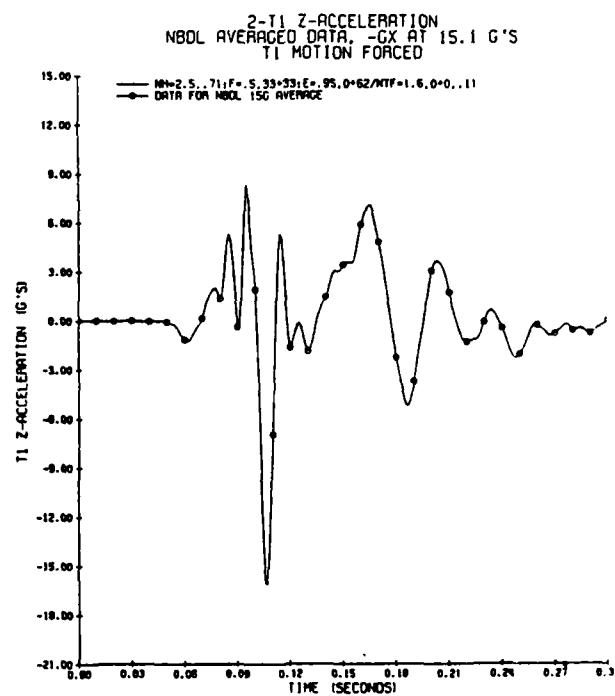
**3-HEAD ANGULAR POSITION**
**NBDL AVERAGED DATA, -GX AT 15.1 G'S**
**T1 MOTION FORCED**
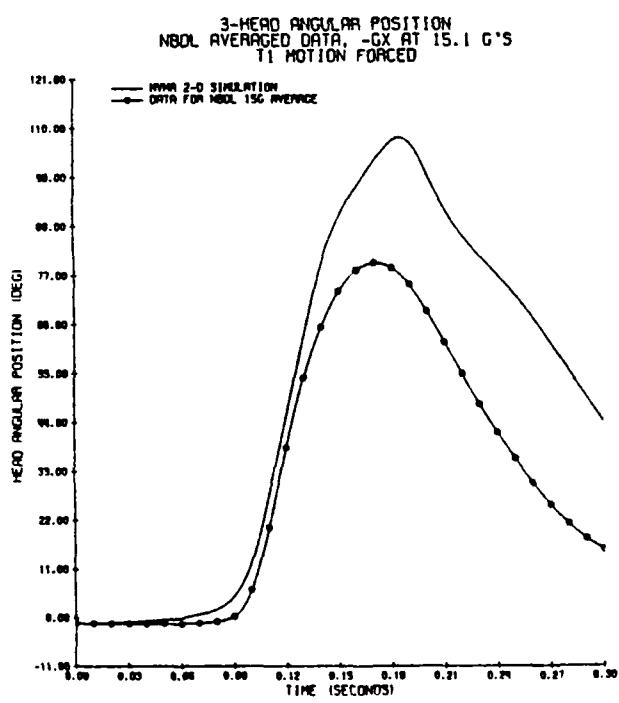
Figure 85. Head Angular Position for Phase II Neck Model Data at -15Gx.

**4-HEAD ANGULAR VELOCITY**
**NBDL AVERAGED DATA, -GX AT 15.1 G'S**
**T1 MOTION FORCED**
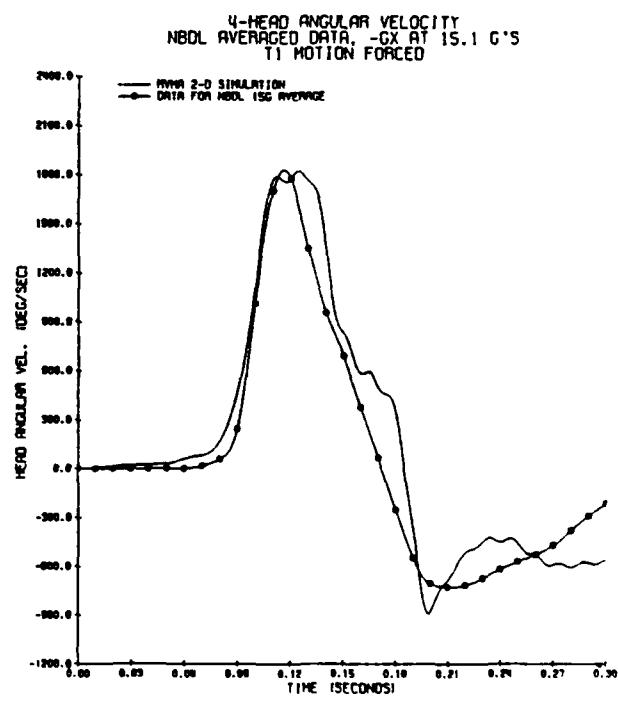
Figure 86. Head Angular Velocity for Phase II Neck Model Data at -15Gx.

73
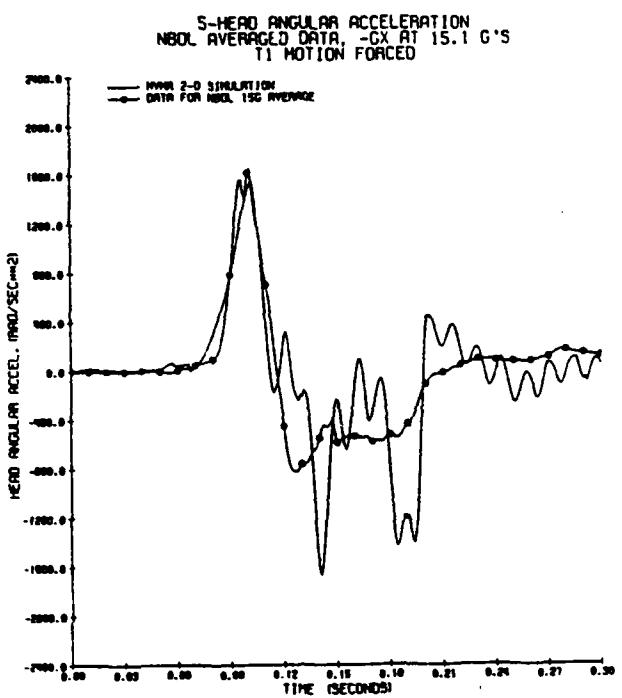
Figure 87. Head Angular Acceleration for Phase II Neck Model Data at -15Gx.
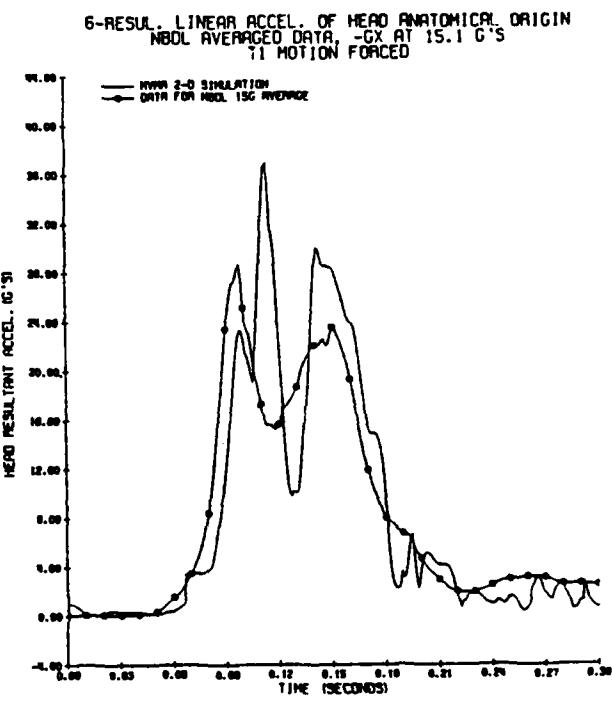


Figure 88. Head Resultant Acceleration for Phase II Neck Model Data at -15Gx.
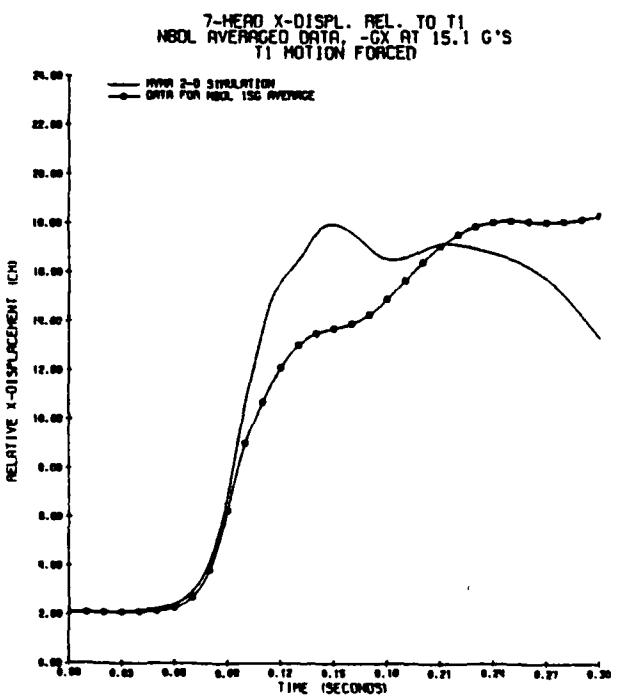


Figure 89. Head Origin X-Axis Displacement for Phase II Neck Model Data at -15Gx.
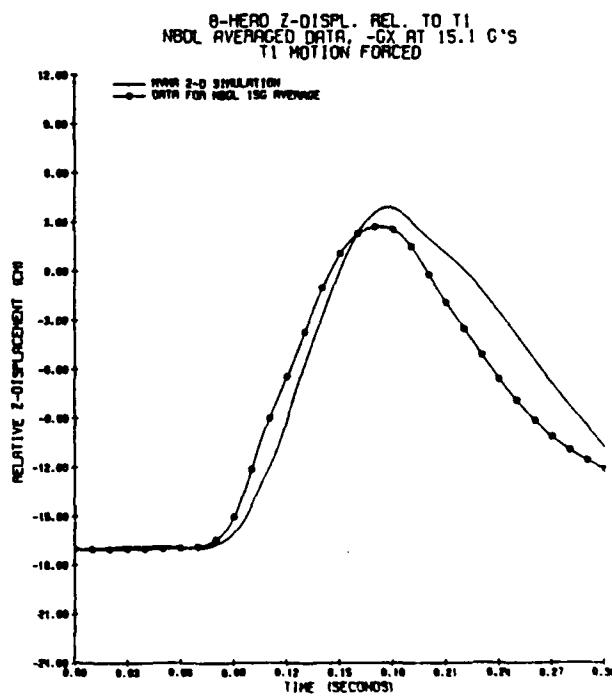


Figure 90. Head Origin Z-Axis Displacement for Phase II Neck Model Data at -15Gx.

74
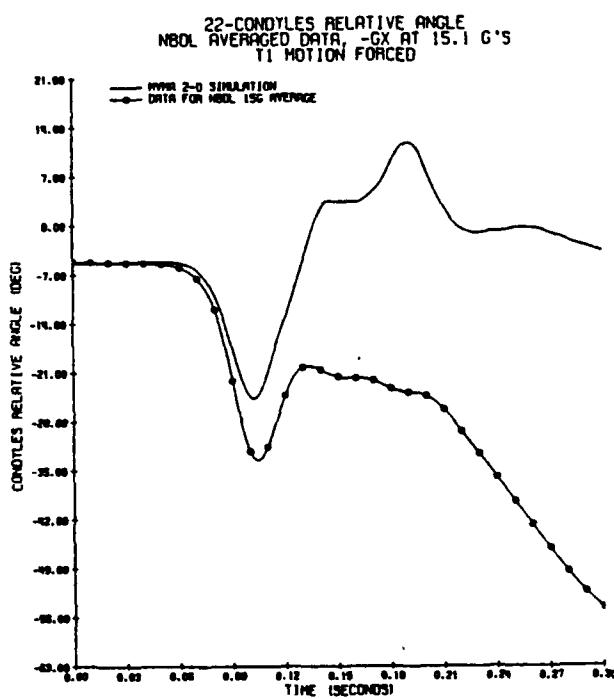
Figure 91.   Condyles Relative Angle for Phase II
Neck Model Data at -15Gx.
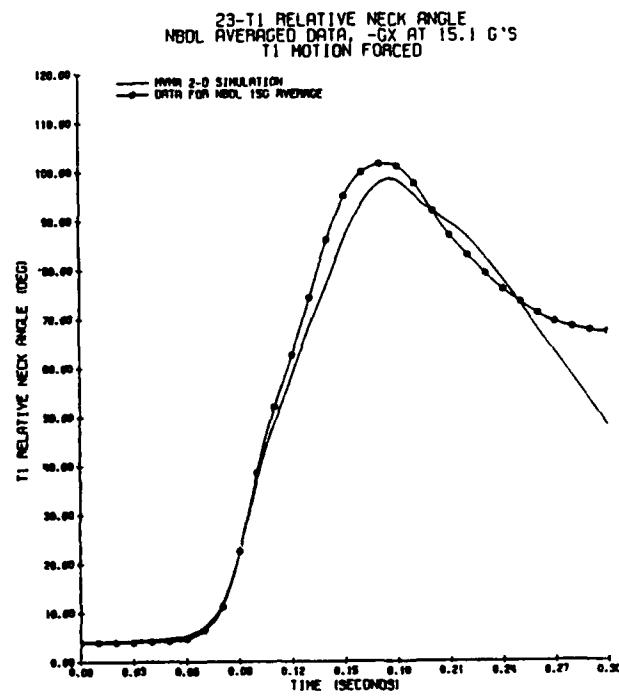
Figure 92.   T1 Relative Angle for Phase II Neck
Model Data at -15Gx.

75

NECK MODEL LOAD-DEFLECTION DATA

CONDYLES BENDING STIFFNESS

$M_\theta$ (Nm)

2.5 N-m/deg

EXTENSION          $\theta$ (degrees)          FLEXION

.714 N-m/deg

C7 BENDING STIFFNESS

$M_\theta$ (Nm)

1.6 N-m/deg

EXTENSION          $\theta$ (degrees)          FLEXION

.457 N-m/deg

NECK ELONGATION STIFFNESS

F(N)

1644 N/cm

(cm)

COMPRESSION          TENSION

400 N/cm
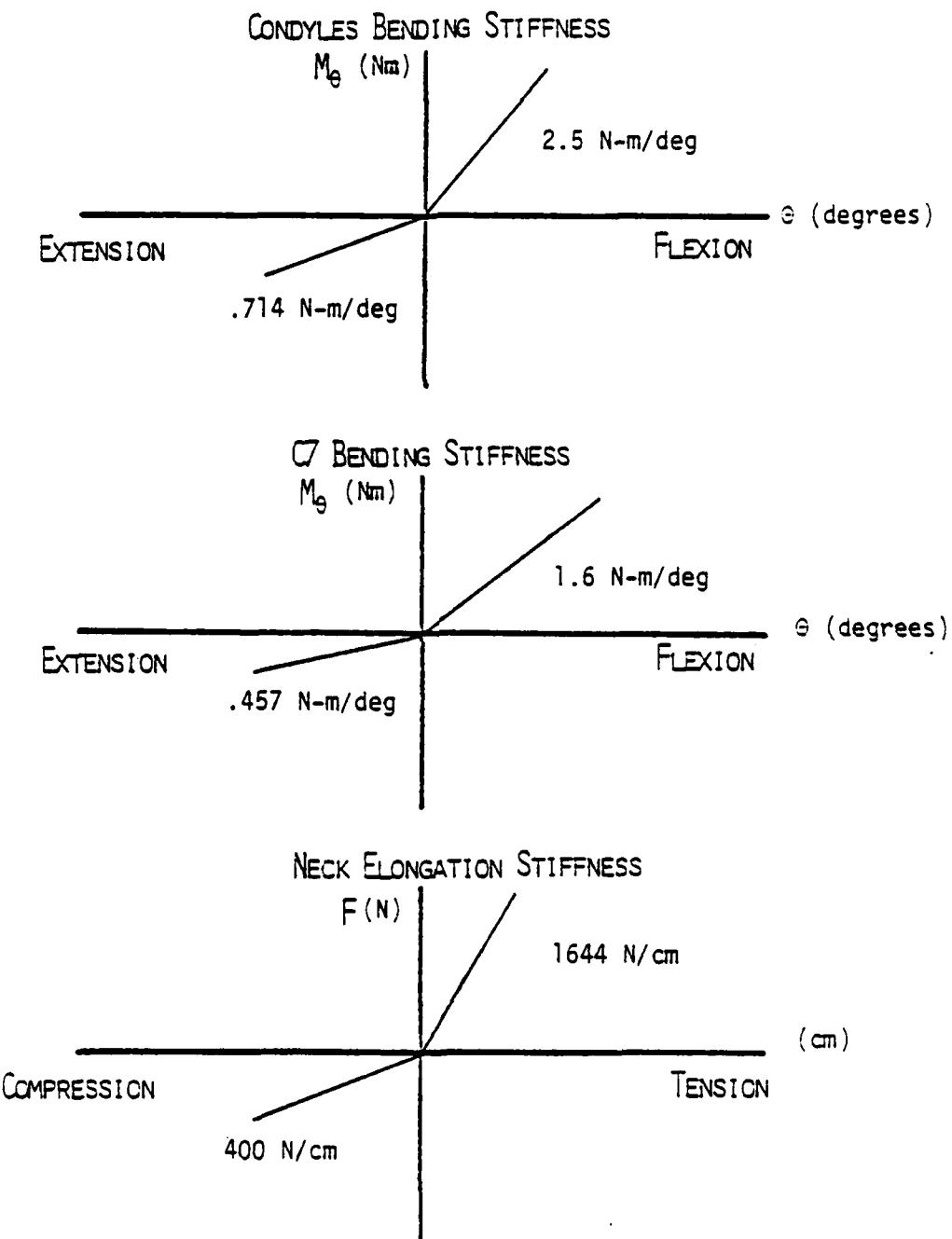
Figure 93.    Neck Model Load-Deflection Data for
the Phase II Neck Model Data.

3-HEAD ANGULAR POSITION
NBDL AVERAGED DATA, -GX AT 6.2 G'S
TI MOTION FORCED
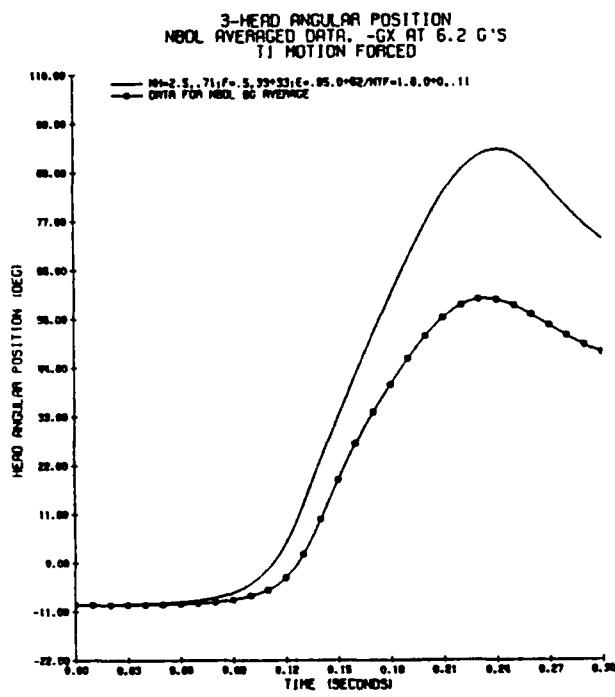
Figure 94. Head Angular Position for Decreased
C7 Bending Stiffness at -6Gx.

4-HEAD ANGULAR VELOCITY
NBDL AVERAGED DATA, -GX AT 6.2 G'S
TI MOTION FORCED
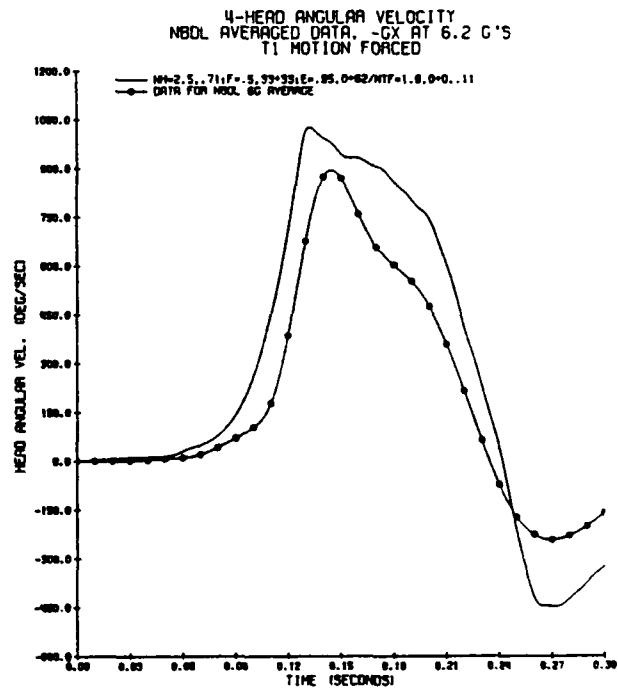
Figure 95. Head Angular Velocity for Decreased
C7 Bending Stiffness at -6Gx.

5-HEAD ANGULAR ACCELERATION
NBDL AVERAGED DATA, -GX AT 6.2 G'S
TI MOTION FORCED
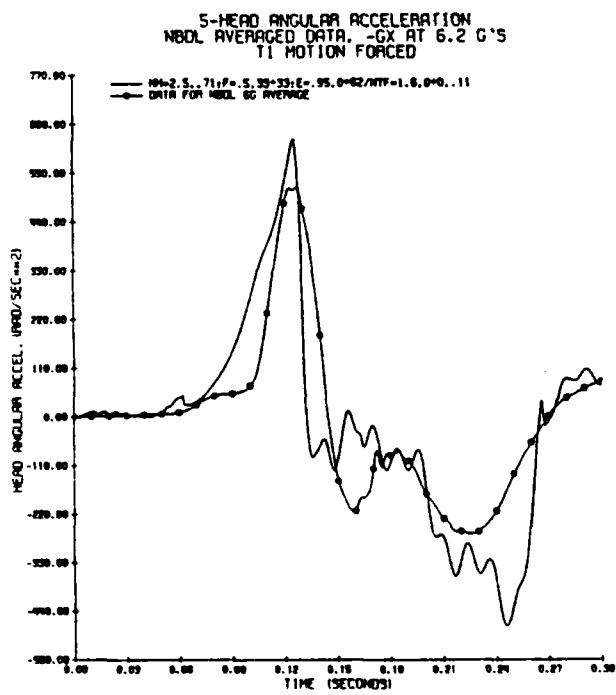
Figure 96. Head Angular Acceleration for
Decreased C7 Bending Stiffness at -6Gx.

6-RESUL. LINEAR ACCEL. OF HEAD ANATOMICAL ORIGIN
NBDL AVERAGED DATA, -GX AT 6.2 G'S
TI MOTION FORCED
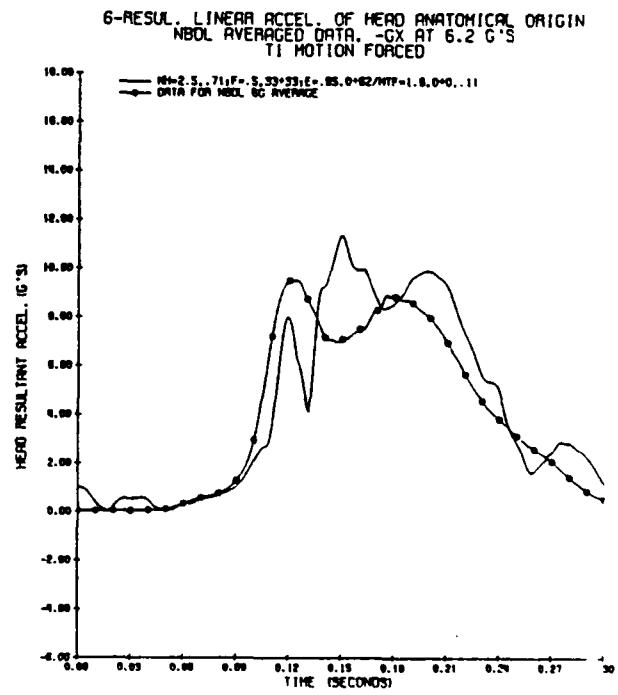
Figure 97. Head Resultant Acceleration for
Decreased C7 Bending Stiffness at -6Gx.

77
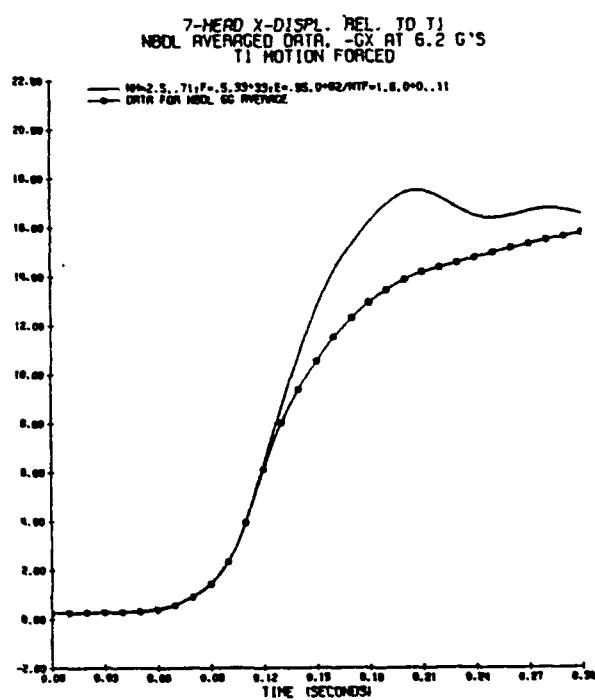
Figure 98. Head Origin X-Axis Displacement for Decreased C7 Bending Stiffness at -6Gx.
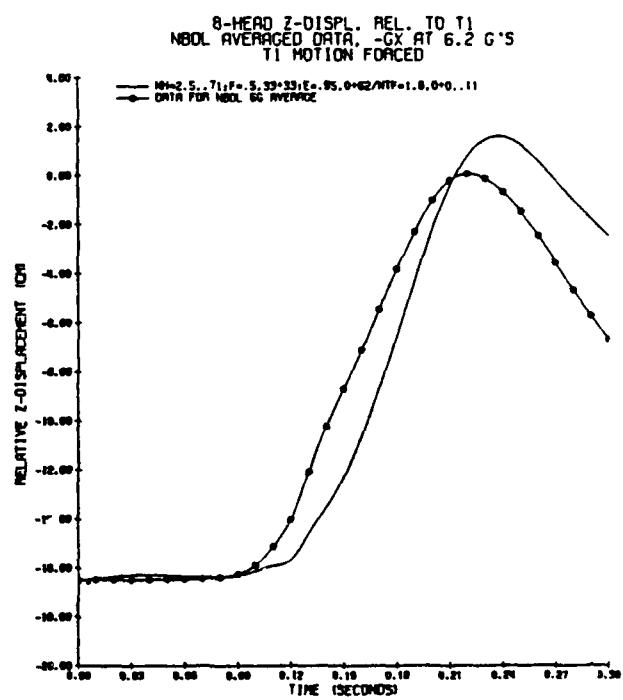


Figure 99. Head Origin Z-Axis Displacement for Decreased C7 Bending Stiffness at -6Gx.
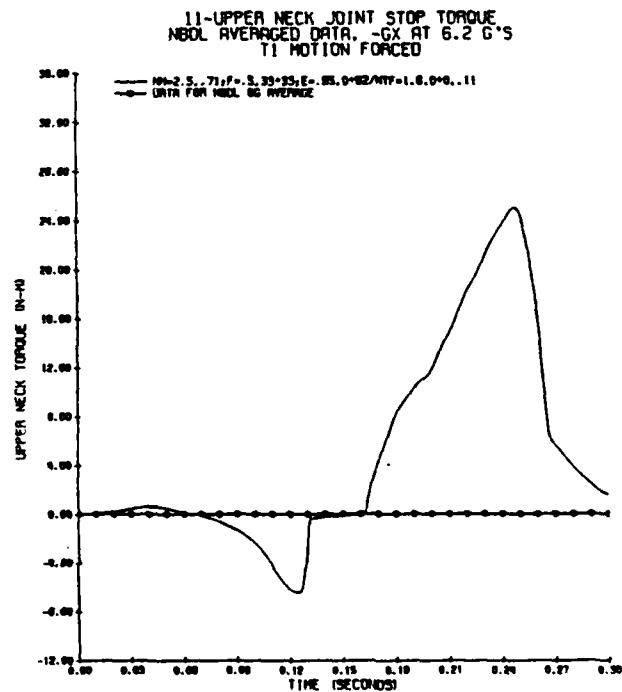


Figure 100. Upper Neck Joint Stop Torque for Decreased C7 Bending Stiffness at -6Gx.
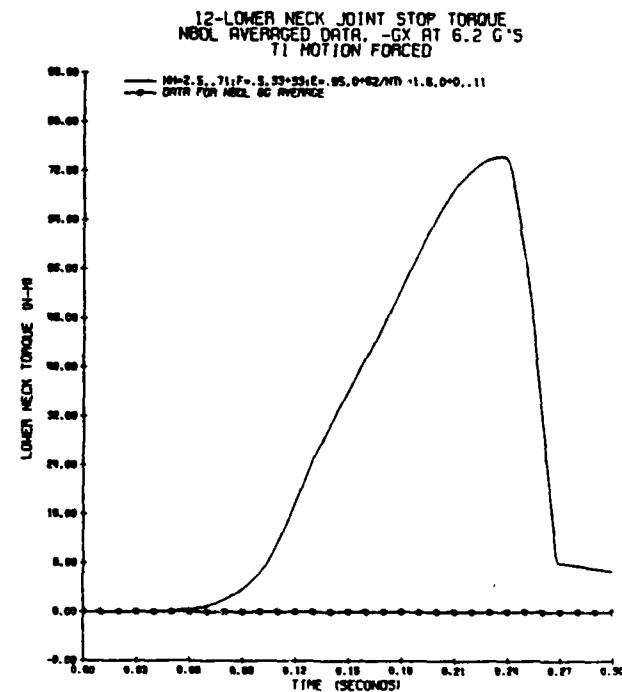


Figure 101. Lower Neck Joint Stop Torque for Decreased C7 Bending Stiffness at -6Gx.

78

22-CONDYLES RELATIVE ANGLE
NBDL AVERAGED DATA. -GX AT 6.2 G'S
T1 MOTION FORCED

23-T1 RELATIVE NECK ANGLE
NBDL AVERAGED DATA. -GX AT 6.2 G'S
T1 MOTION FORCED
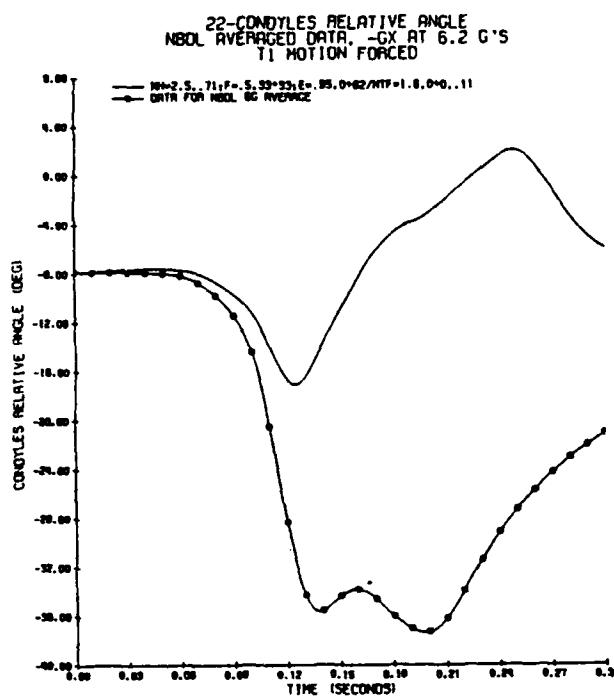
Figure 102. Condyles Relative Angle for
Decreased C7 Bending Stiffness at -6Gx.
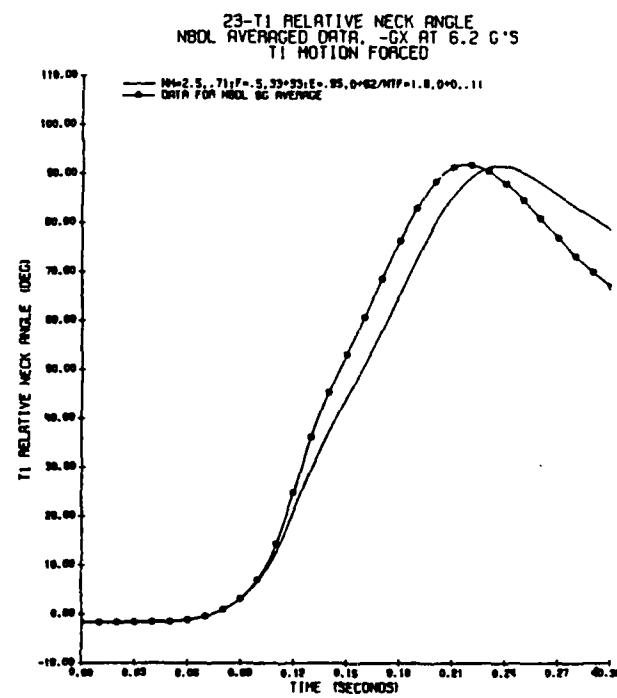
Figure 103. T1 Relative Angle for Decreased C7
Bending Stiffness at -6Gx.

79
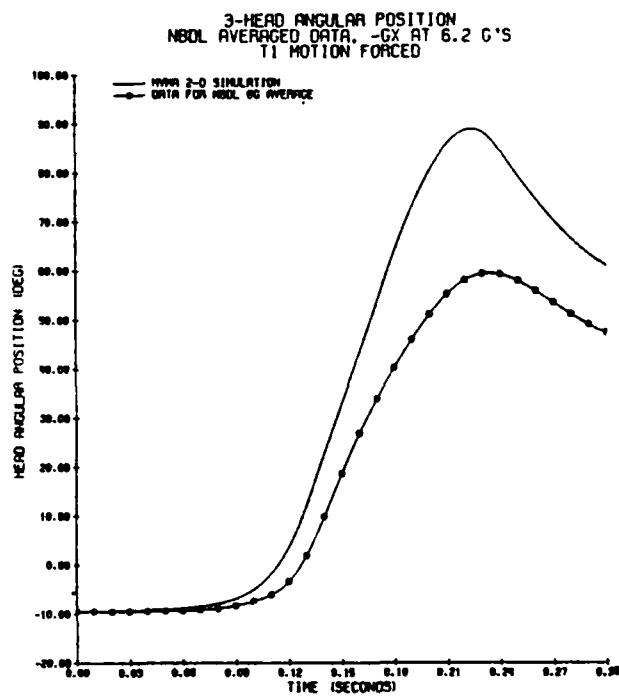
Figure 104. Head Angular Position for Bilinear C7 Bending Stiffness at -6Gx.
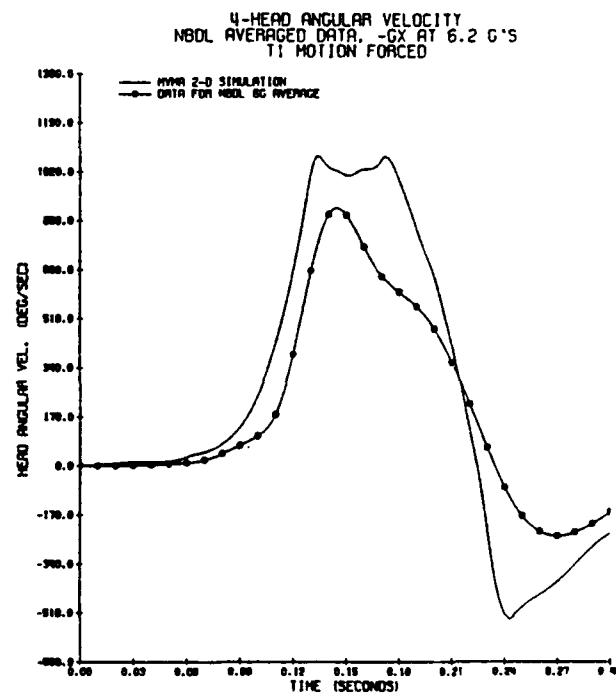


Figure 105. Head Angular Velocity for Bilinear C7 Bending Stiffness at -6Gx.
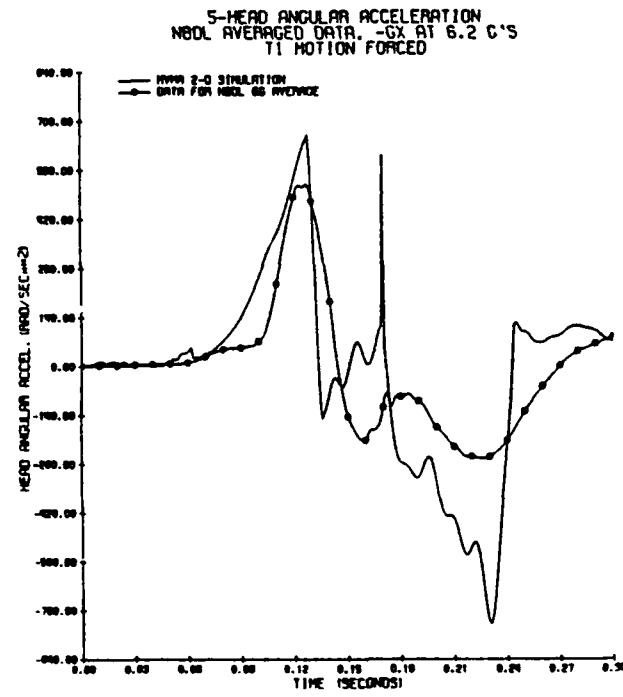


Figure 106. Head Angular Acceleration for Bilinear C7 Bending Stiffness at -6Gx.
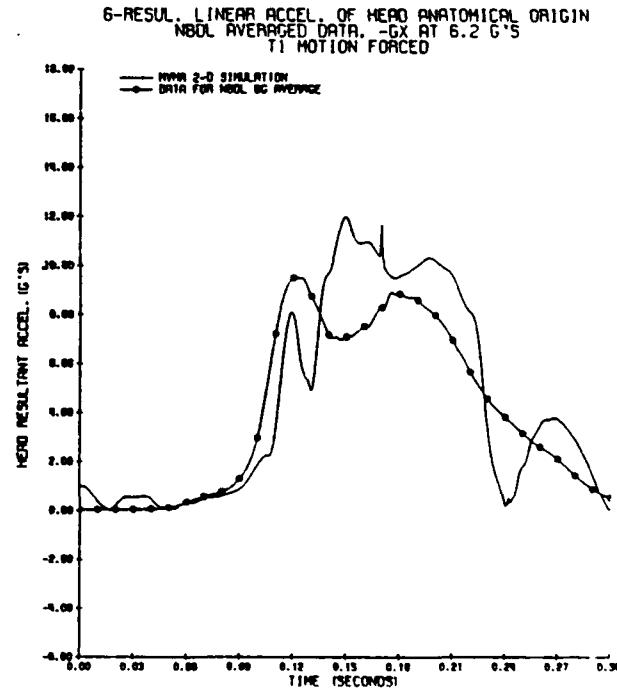


Figure 107. Head Resultant Acceleration for Bilinear C7 Bending Stiffness at -6Gx.

7-HEAD X-DISPL. REL. TO T1
NBDL AVERAGED DATA. -GX AT 6.2 G'S
T1 MOTION FORCED
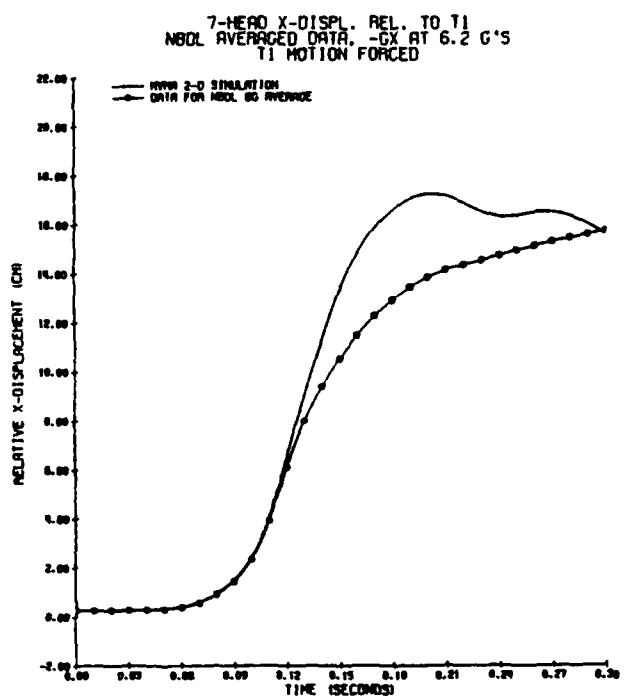
Figure 108. Head Origin X-Axis Displacement for Bilinear C7 Bending Stiffness at -6Gx.

8-HEAD Z-DISPL. REL. TO T1
NBDL AVERAGED DATA. -GX AT 6.2 G'S
T1 MOTION FORCED
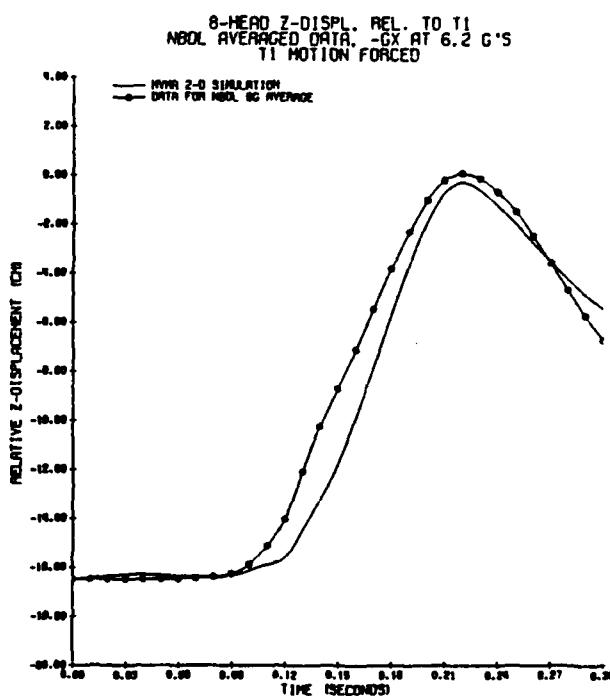
Figure 109. Head Origin Z-Axis Displacement for Bilinear C7 Bending Stiffness at -6Gx.

11-UPPER NECK JOINT STOP TORQUE
NBDL AVERAGED DATA. -GX AT 6.2 G'S
T1 MOTION FORCED
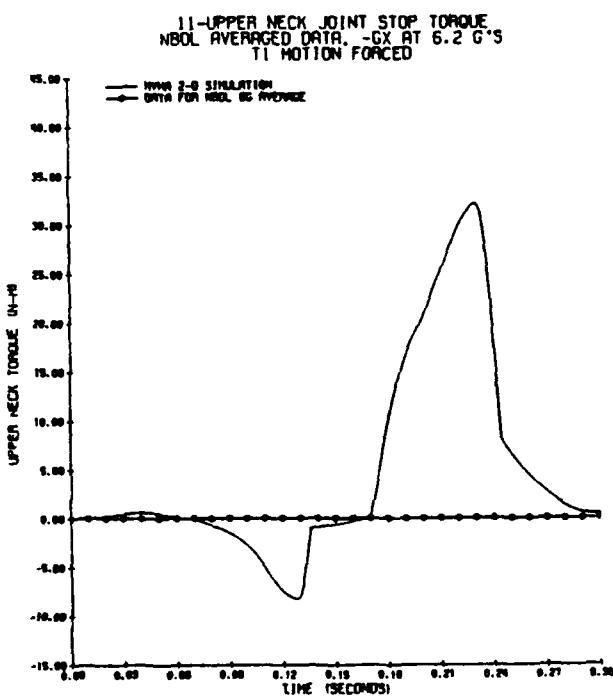
Figure 110. Upper Neck Joint Stop Torque for Bilinear C7 Bending Stiffness at -6Gx.

12-LOWER NECK JOINT STOP TORQUE
NBDL AVERAGED DATA. -GX AT 6.2 G'S
T1 MOTION FORCED
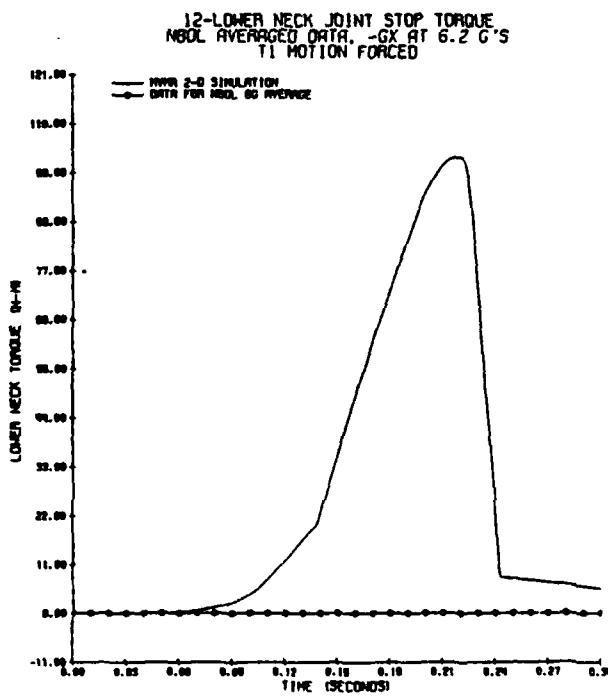
Figure 111. Lower Neck Joint Stop Torque for Bilinear C7 Bending Stiffness at -6Gx.

81
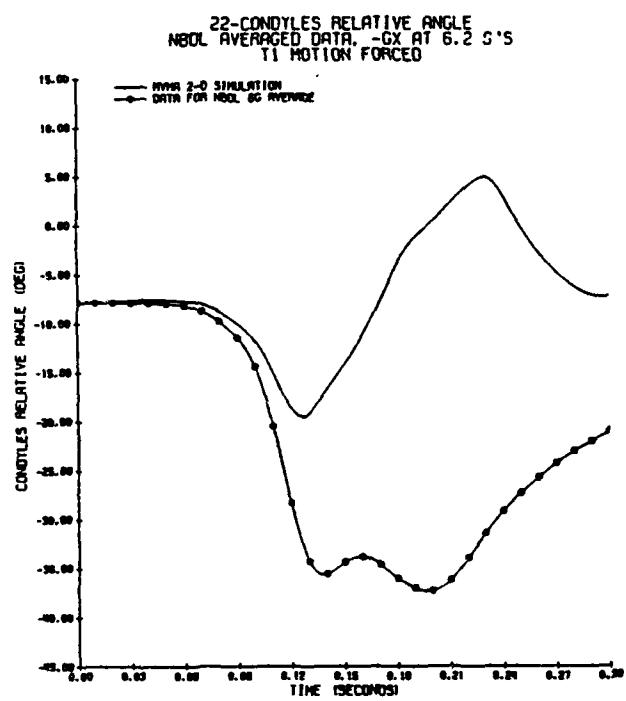
Figure 112. Condyles Relative Angle for
Bilinear C7 Bending Stiffness at -6Gx.
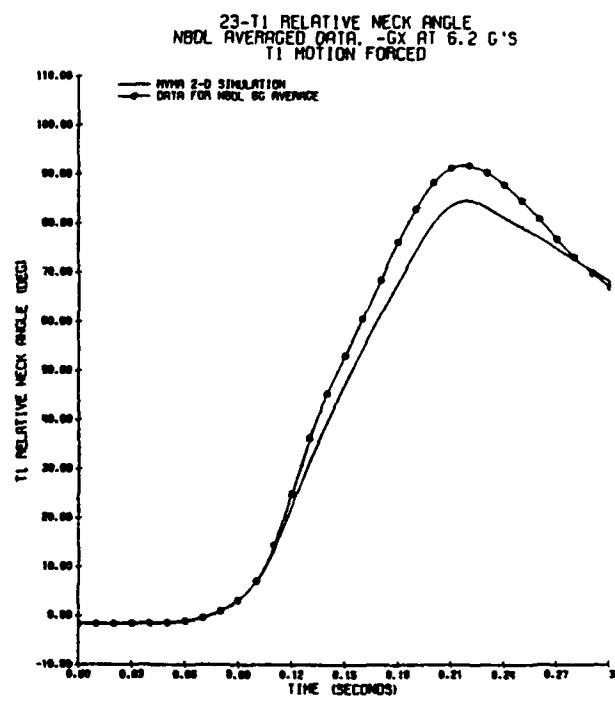
Figure 113. T1 Relative Angle for Bilinear C7
Bending Stiffness at -6Gx.

## 4-HEAD ANGULAR POSITION
### NBDL AVERAGED DATA. -GX AT 6.2 G'S
### T1 MOTION FORCED
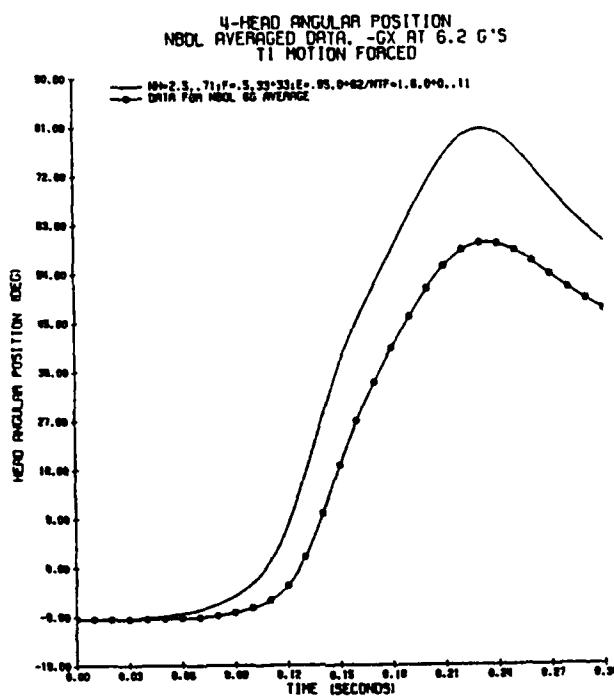
Figure 114. Head Angular Position for T1
Angular Acceleration Input at -6Gx.

## 5-HEAD ANGULAR VELOCITY
### NBDL AVERAGED DATA. -GX AT 6.2 G'S
### T1 MOTION FORCED
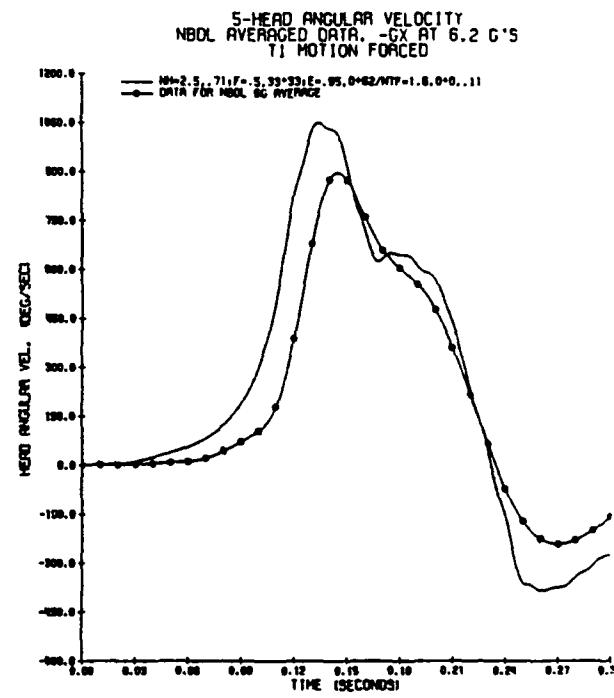
Figure 115. Head Angular Velocity for T1
Angular Acceleration Input at -6Gx.

## 6-HEAD ANGULAR ACCELERATION
### NBDL AVERAGED DATA. -GX AT 6.2 G'S
### T1 MOTION FORCED
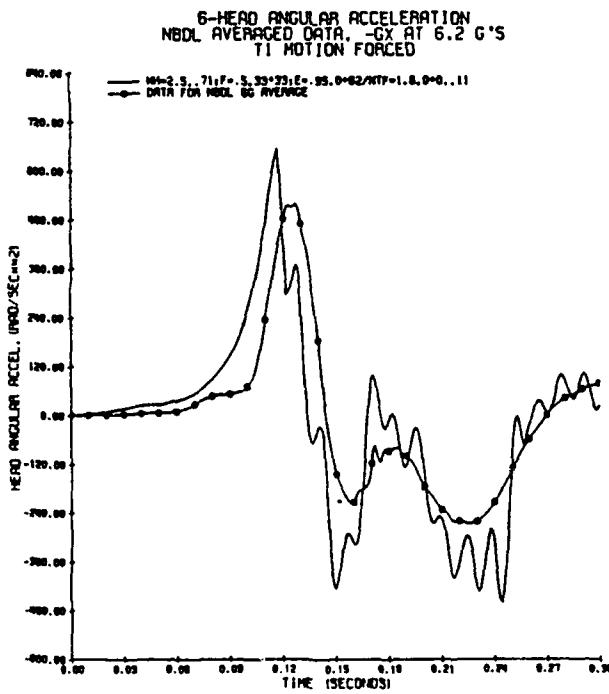
Figure 116. Head Angular Acceleration for T1
Angular Acceleration Input at -6Gx.

## 7-RESUL. LINEAR ACCEL. OF HEAD ANATOMICAL ORIGIN
### NBDL AVERAGED DATA. -GX AT 6.2 G'S
### T1 MOTION FORCED
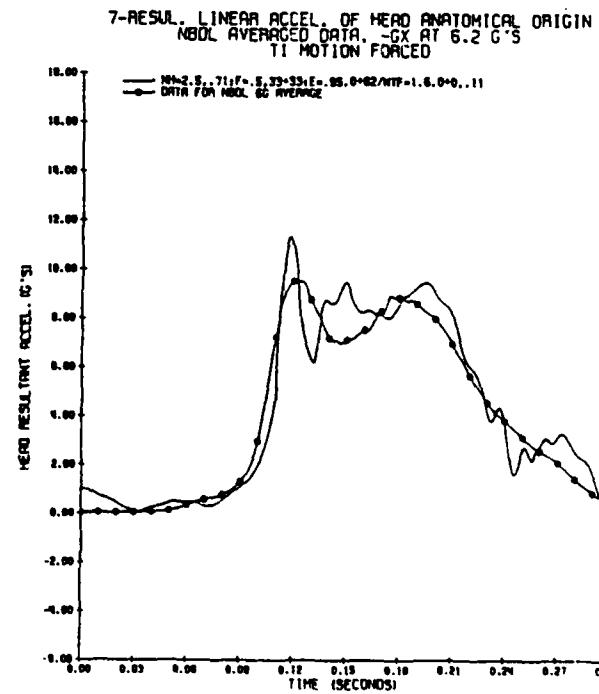
Figure 117. Head Resultant Acceleration for T1
Angular Acceleration Input at -6Gx.

83
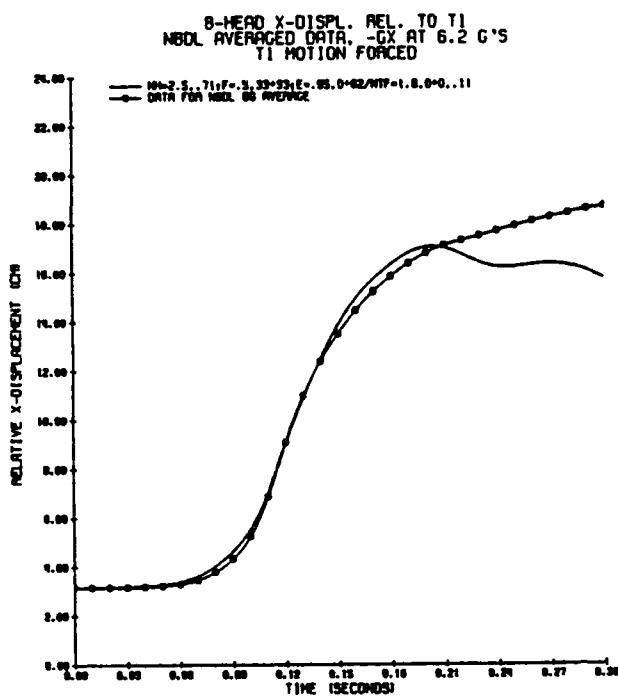
Figure 118. Head Origin X-Axis Displacement for T1 Angular Acceleration Input at -6Gx.
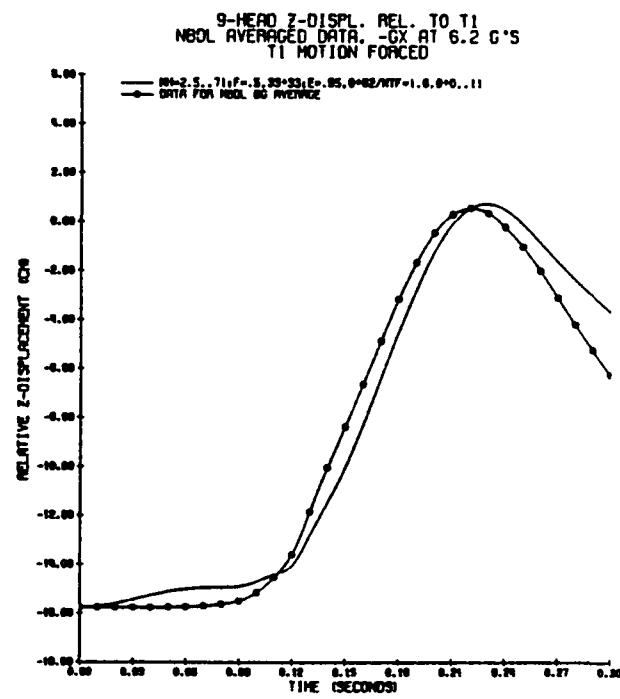


Figure 119. Head Origin Z-Axis Displacement for T1 Angular Acceleration Input at -6Gx.
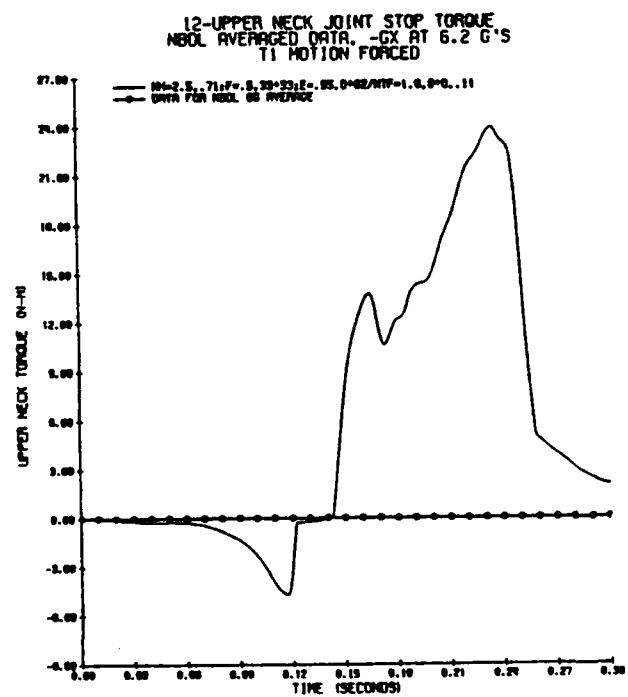


Figure 120. Upper Neck Joint Stop Torque for T1 Angular Acceleration Input at -6Gx.
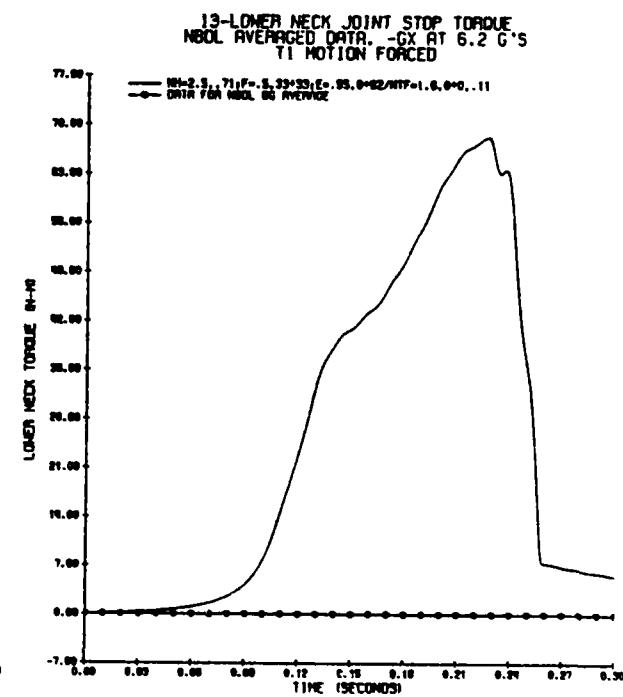


Figure 121. Lower Neck Joint Stop Torque for T1 Angular Acceleration Input at -6Gx.
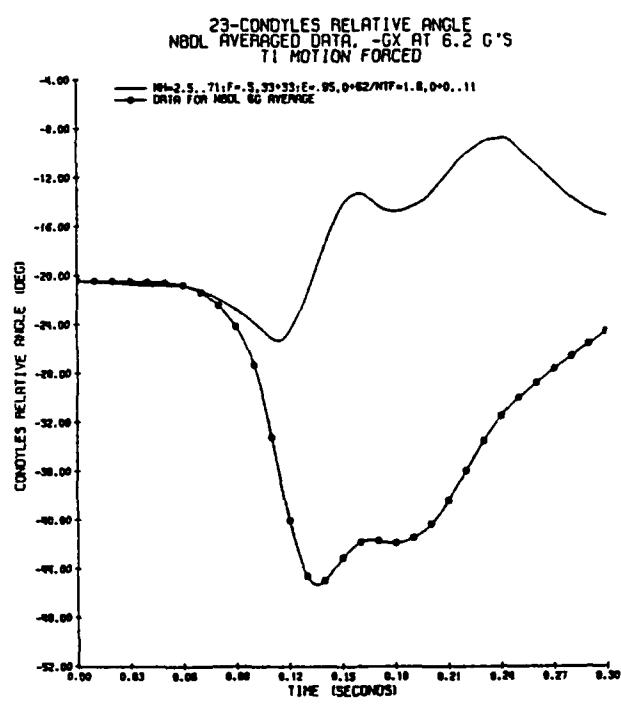
Figure 122. Condyles Relative Angle for T1
Angular Acceleration Input at -6Gx.
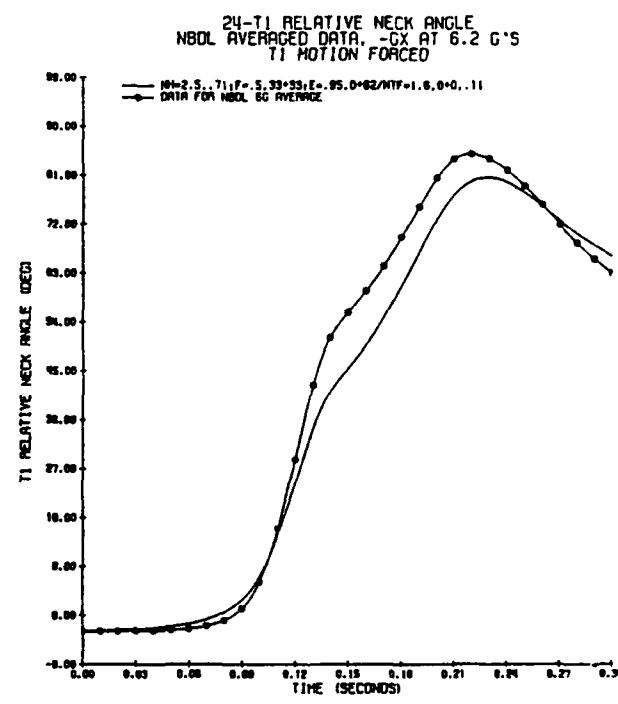
Figure 123. T1 Relative Angle for T1
Angular Acceleration Input at -6Gx.
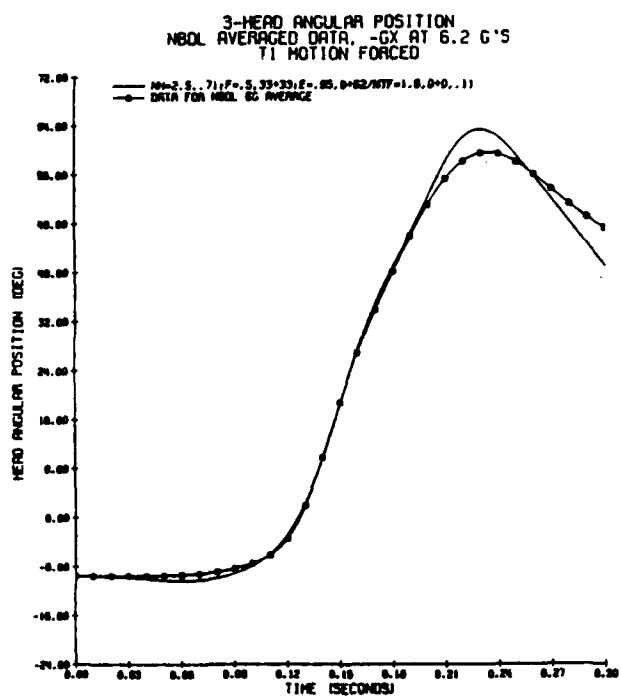
Figure 124. Head Angular Position for Becker Neck Model at -6Gx.
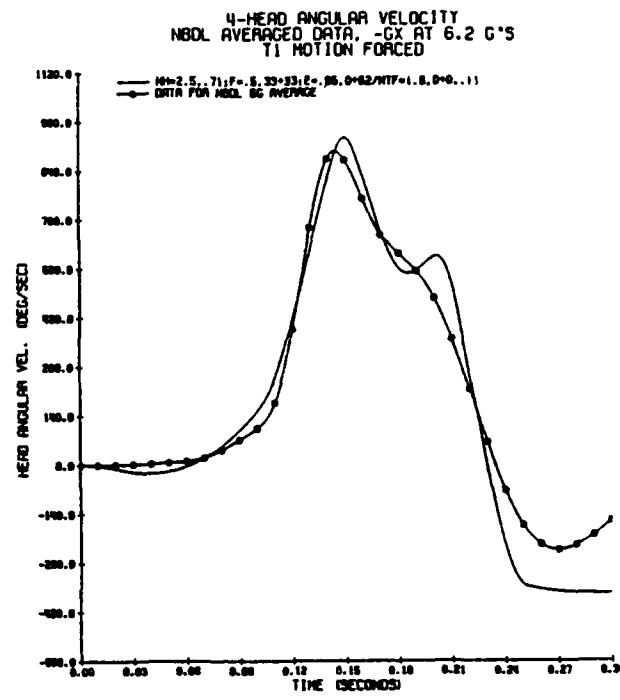


Figure 125. Head Angular Velocity for Becker Neck Model at -6Gx.
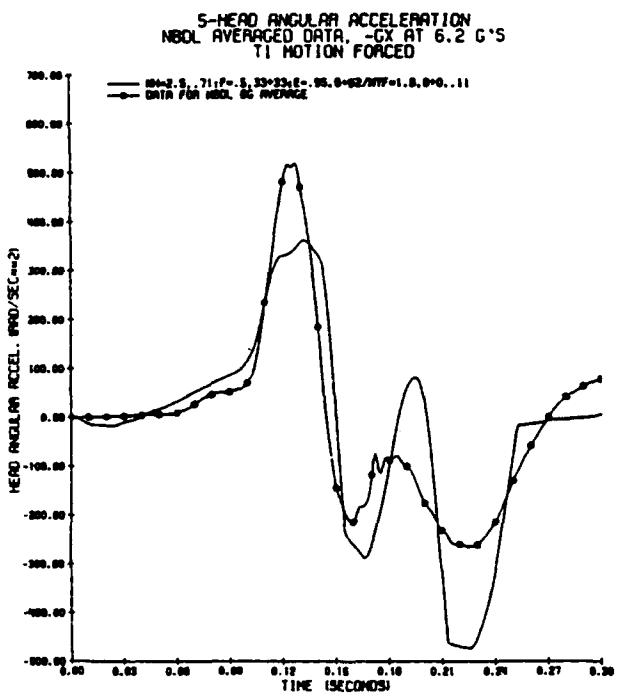


Figure 126. Head Angular Acceleration for Becker Neck Model at -6Gx.
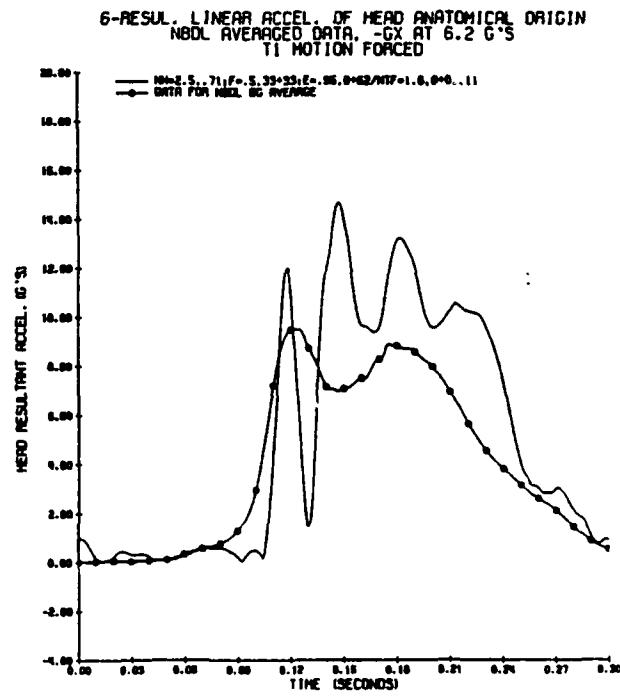


Figure 127. Head Resultant Acceleration for Becker Neck Model at -6Gx.

86
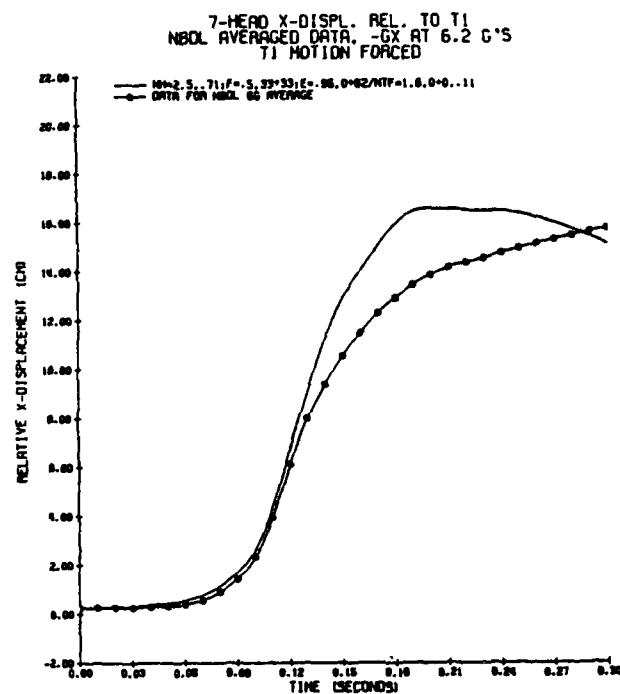
Figure 128.  Head Origin X-Axis Displacement for Becker Neck Model at -6Gx.
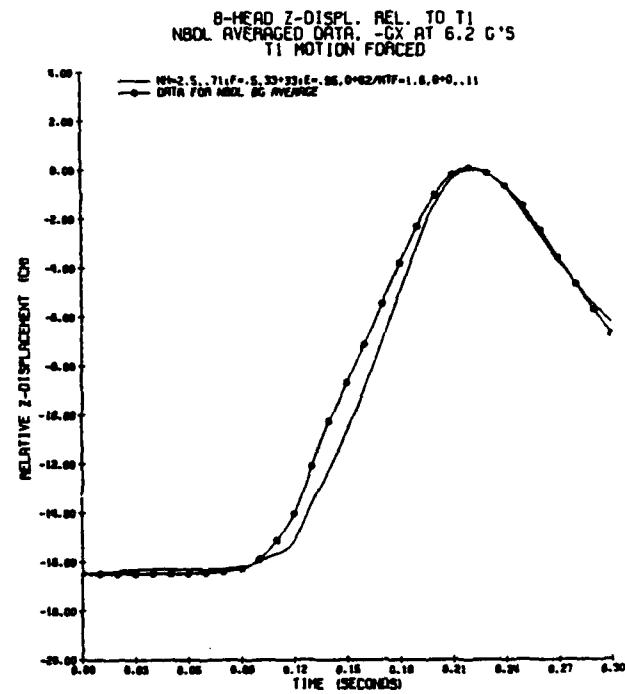


Figure 129.  Head Origin Z-Axis Displacement for Becker Neck Model at -6Gx.
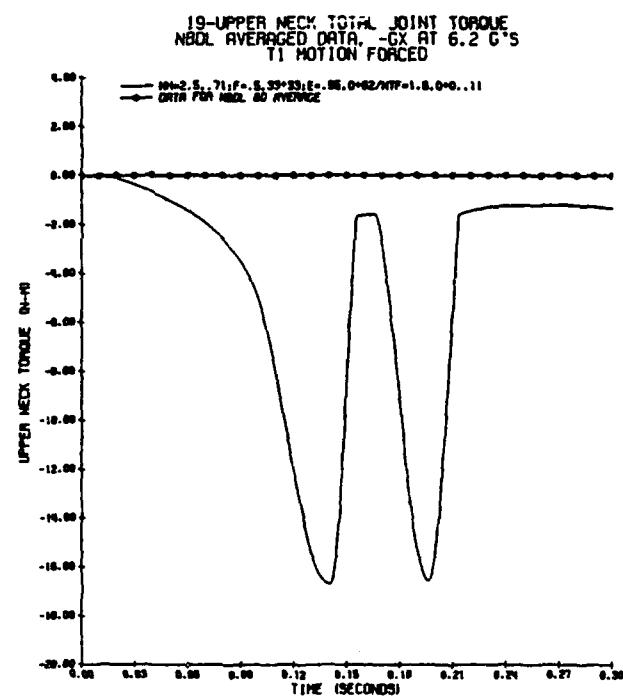


Figure 130.  Upper Neck Joint Stop Torque for Becker Neck Model at -6Gx.
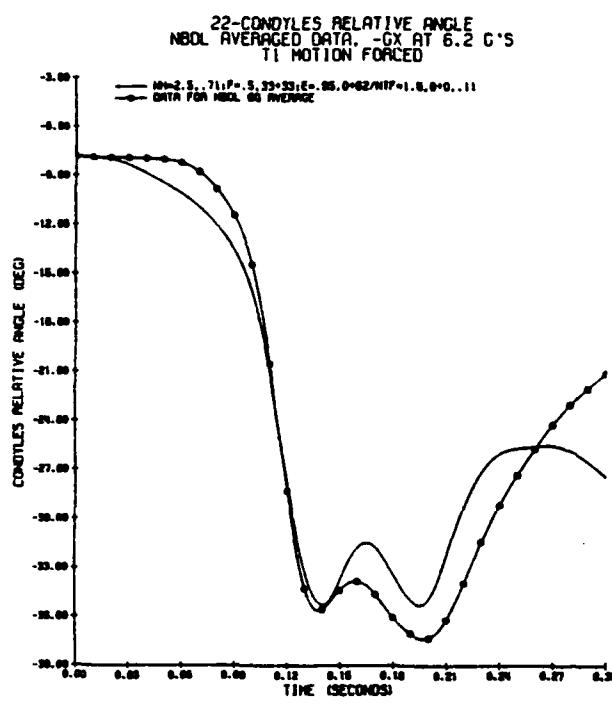
Figure 131. Condyles Relative Angle for for Becker Neck Model at -6Gx.
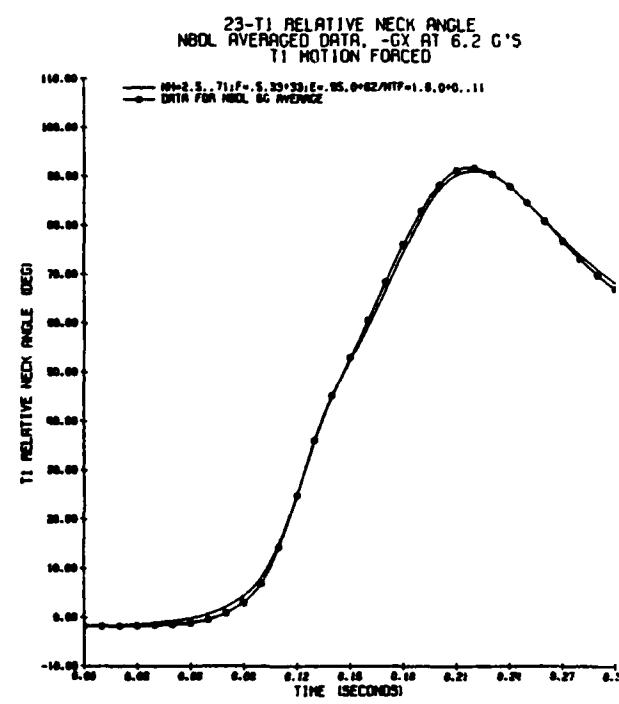


Figure 132. T1 Relative Angle for for Becker Neck Model at -6Gx.

NECK MODEL LOAD-DEFLECTION DATA

CONDYLES BENDING STIFFNESS

$M_\theta$ (Nm)

2.5 N-m/deg

$\theta$ (degrees)

EXTENSION                    FLEXION

1.0 N-m/deg

C7 BENDING STIFFNESS

$M_\theta$ (Nm)

1.1 N-m/deg

$\theta$ (degrees)

EXTENSION                    FLEXION

.457 N-m/deg

NECK ELONGATION STIFFNESS

F(N)

1644 N/cm

(cm)

COMPRESSION                  TENSION

400 N/cm
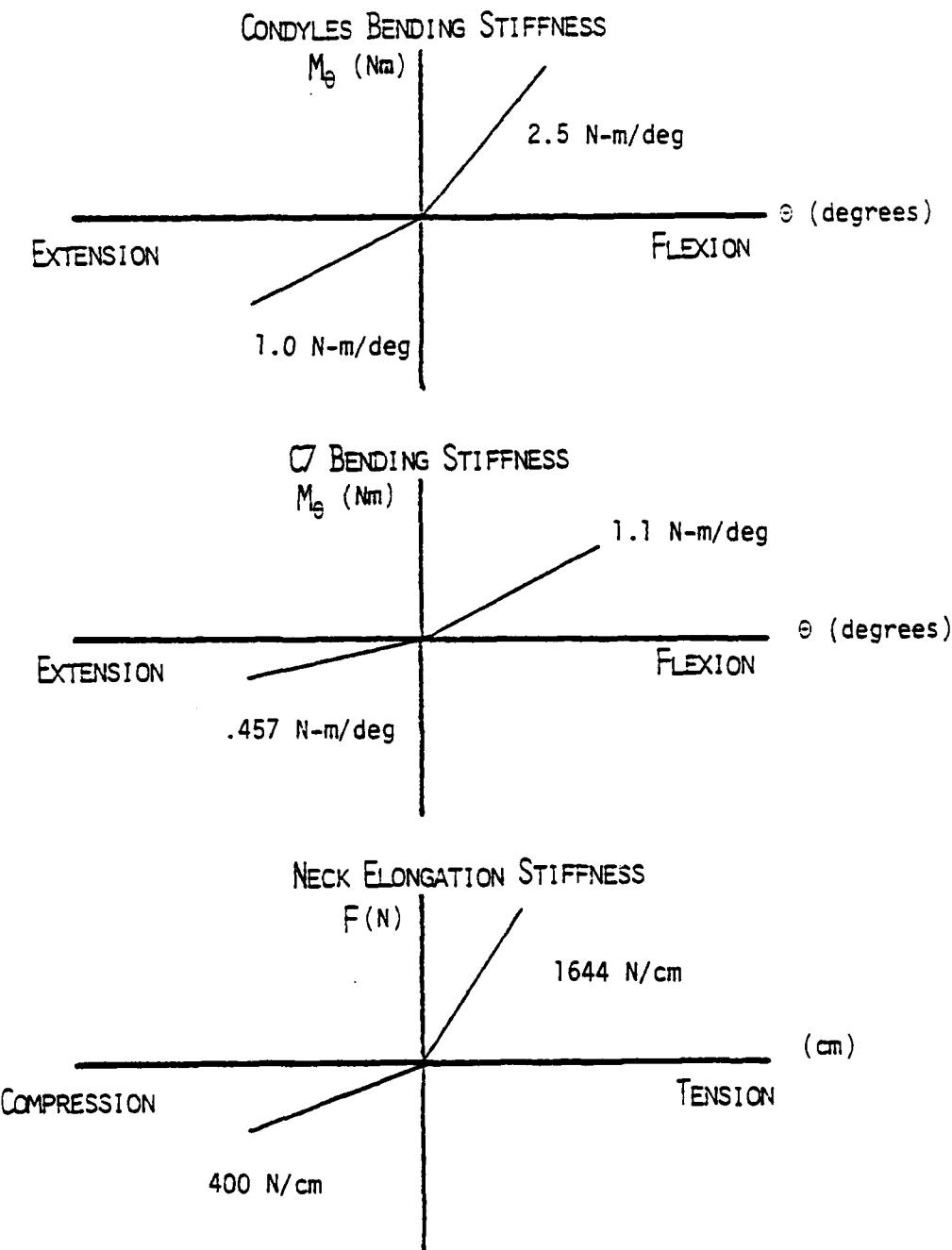
Figure 133. Neck Model Load-Deflection Data for
the Becker Neck Model Data.

**4-HEAD ANGULAR POSITION**
**NBDL AVERAGED DATA, -GX AT 15.1 G'S**
**T1 MOTION FORCED**
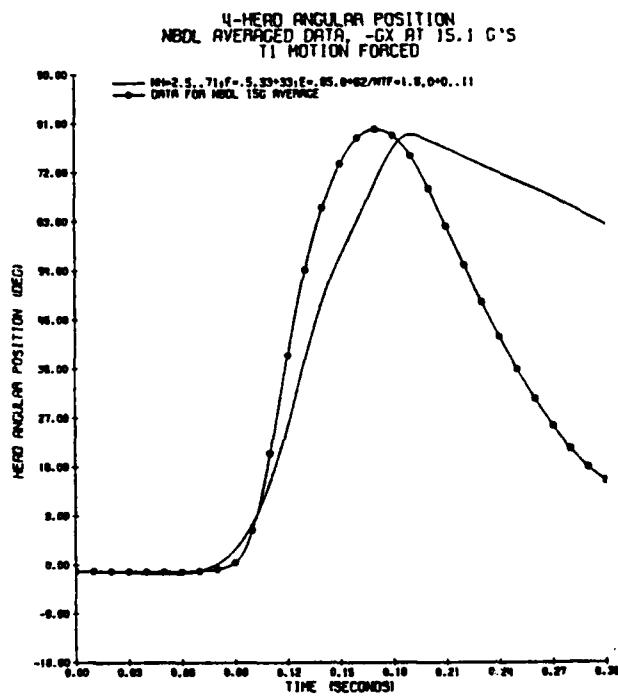
Figure 134. Head Angular Position for Becker
Neck Model at -15Gx.



**5-HEAD ANGULAR VELOCITY**
**NBDL AVERAGED DATA, -GX AT 15.1 G'S**
**T1 MOTION FORCED**
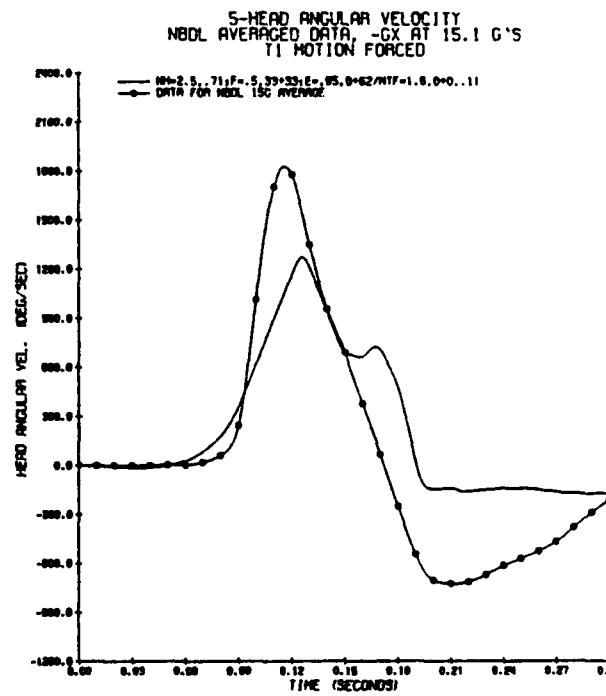
Figure 135. Head Angular Velocity for Becker
Neck Model at -15Gx.



**6-HEAD ANGULAR ACCELERATION**
**NBDL AVERAGED DATA, -GX AT 15.1 G'S**
**T1 MOTION FORCED**
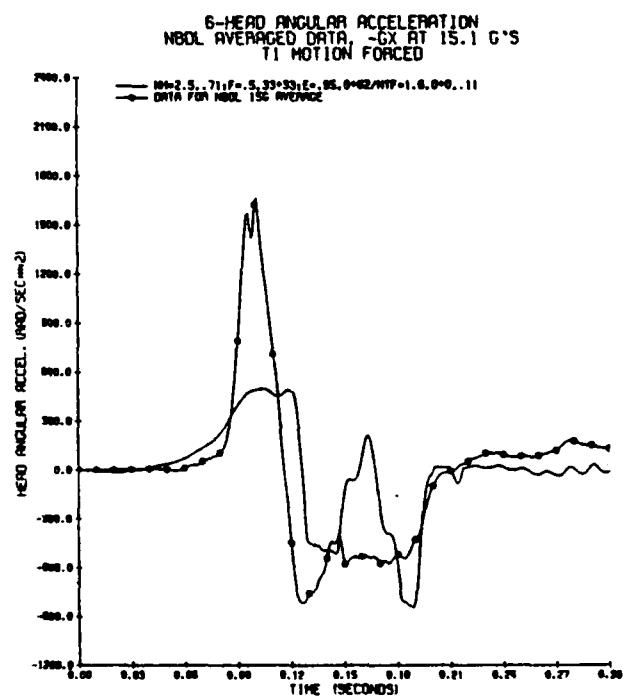
Figure 136. Head Angular Acceleration for
Becker Neck Model at -15Gx.



**7-RESUL. LINEAR ACCEL. OF HEAD ANATOMICAL ORIGIN**
**NBDL AVERAGED DATA, -GX AT 15.1 G'S**
**T1 MOTION FORCED**
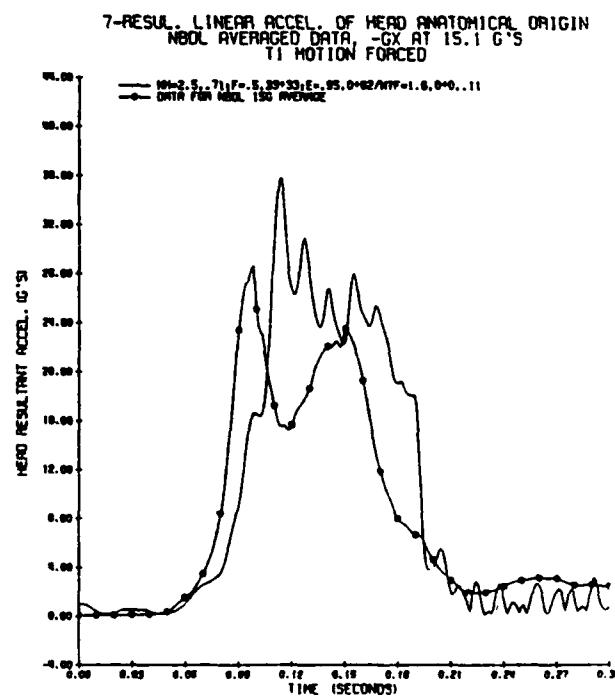
Figure 137. Head Resultant Acceleration for
Becker Neck Model at -15Gx.

90

8-HEAD X-DISPL. REL. TO T1
NBDL AVERAGED DATA, -GX AT 15.1 G'S
T1 MOTION FORCED
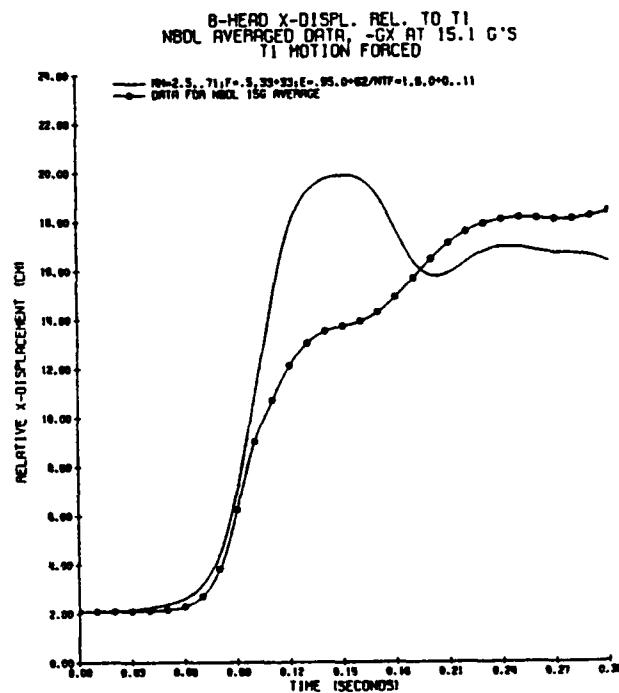
Figure 138.   Head Origin X-Axis Displacement for
Becker Neck Model at -15Gx.

9-HEAD Z-DISPL. REL. TO T1
NBDL AVERAGED DATA, -GX AT 15.1 G'S
T1 MOTION FORCED
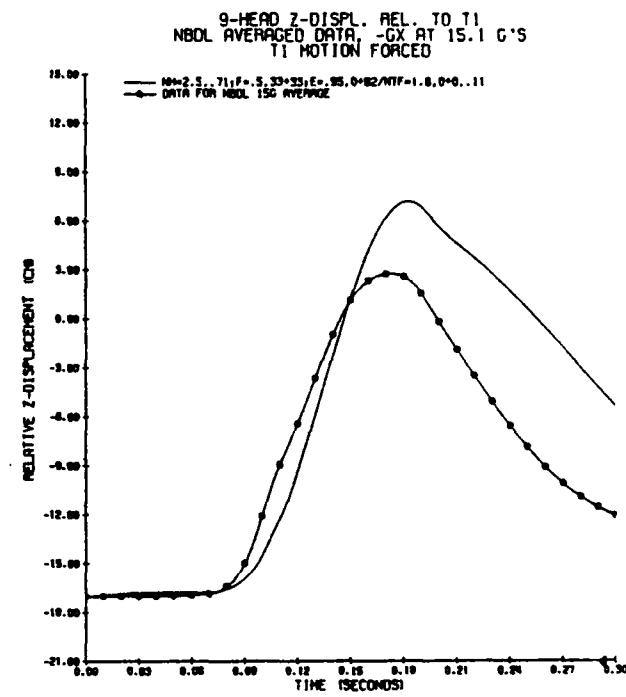
Figure 139.   Head Origin Z-Axis Displacement for
Becker Neck Model at -15Gx.

23-CONDYLES RELATIVE ANGLE
NBDL AVERAGED DATA, -GX AT 15.1 G'S
T1 MOTION FORCED
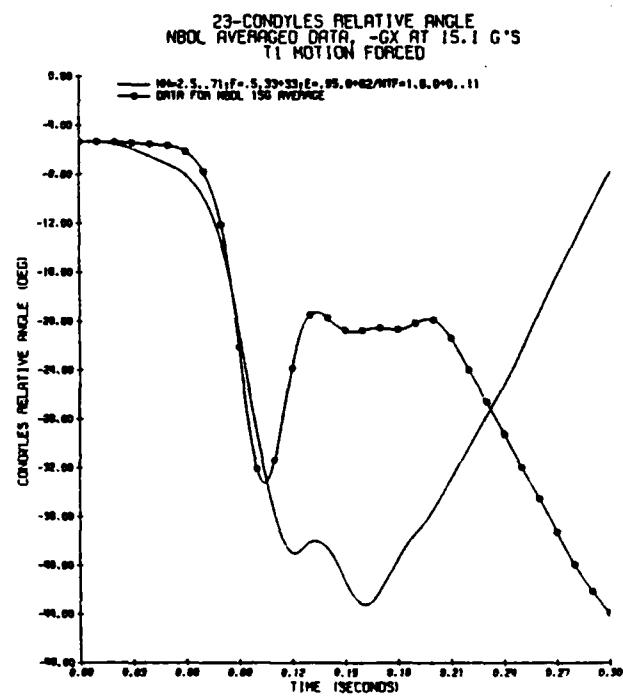
Figure 140.   Condyles Relative Angle for
Becker Neck Model at -15Gx.

24-T1 RELATIVE NECK ANGLE
NBDL AVERAGED DATA, -GX AT 15.1 G'S
T1 MOTION FORCED
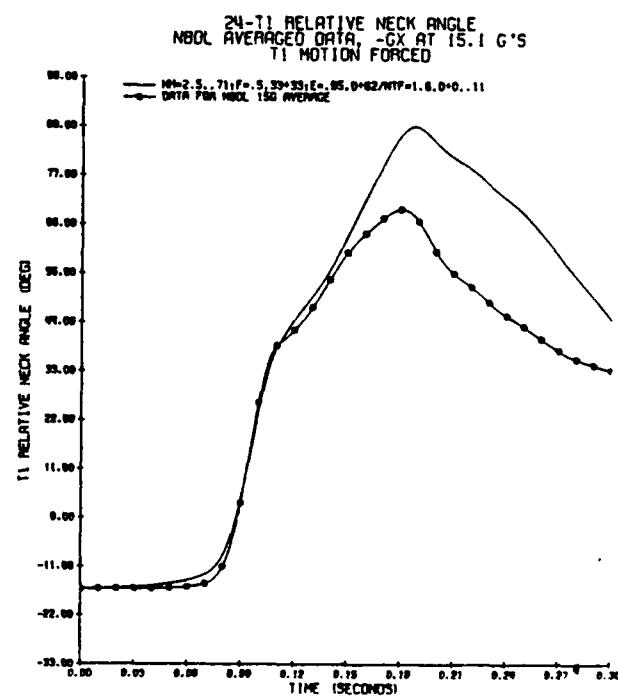
Figure 141.   T1 Relative Angle for Becker
Neck Model at -15Gx.
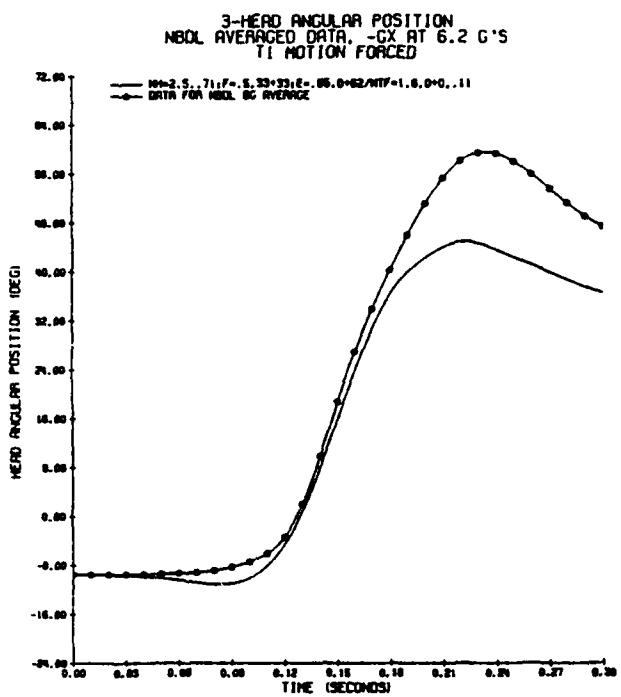
Figure 142. Head Angular Position for Becker Neck Model with nonzero condyles joint stop at -6Gx.
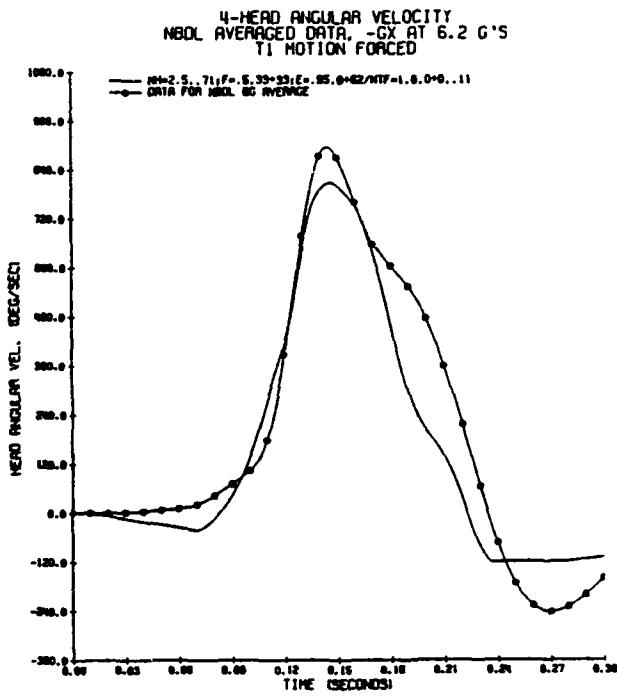


Figure 143. Head Angular Velocity for Becker Neck Model with nonzero condyles joint stop at -6Gx.
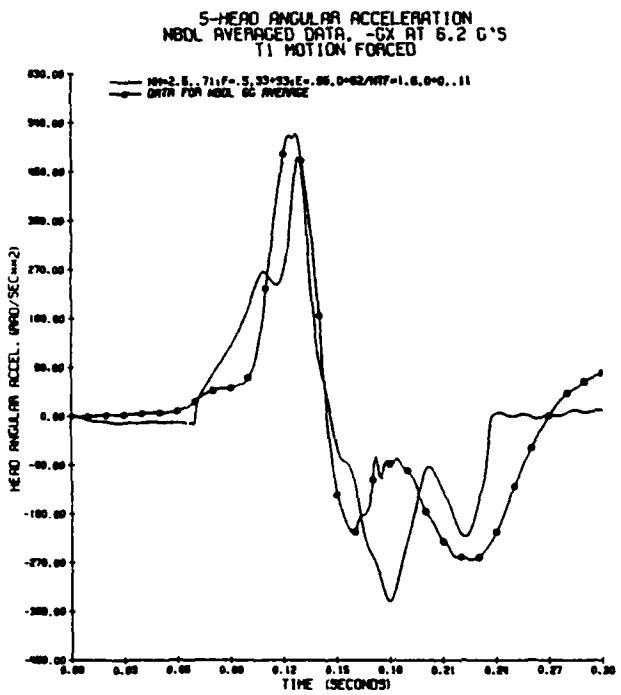


Figure 144. Head Angular Acceleration for Becker Neck Model with nonzero condyles joint stop at -6Gx.
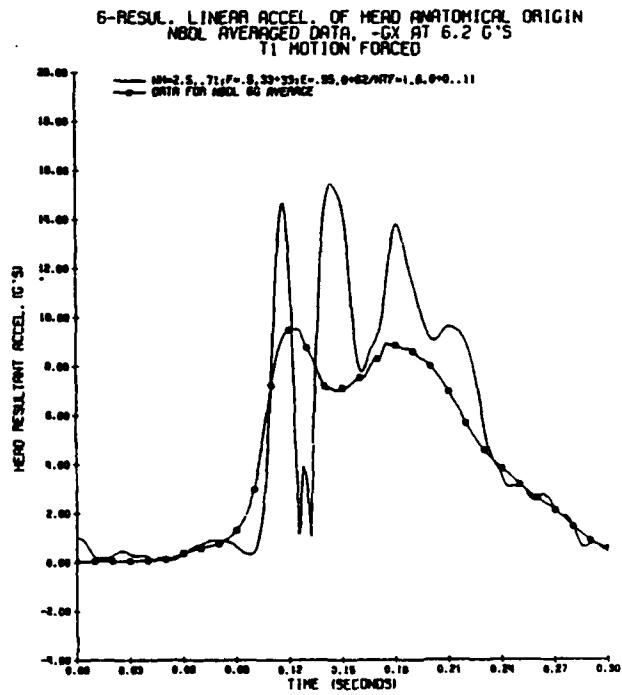


Figure 145. Head Resultant Acceleration for Becker Neck Model with nonzero condyles joint stop at -6Gx.
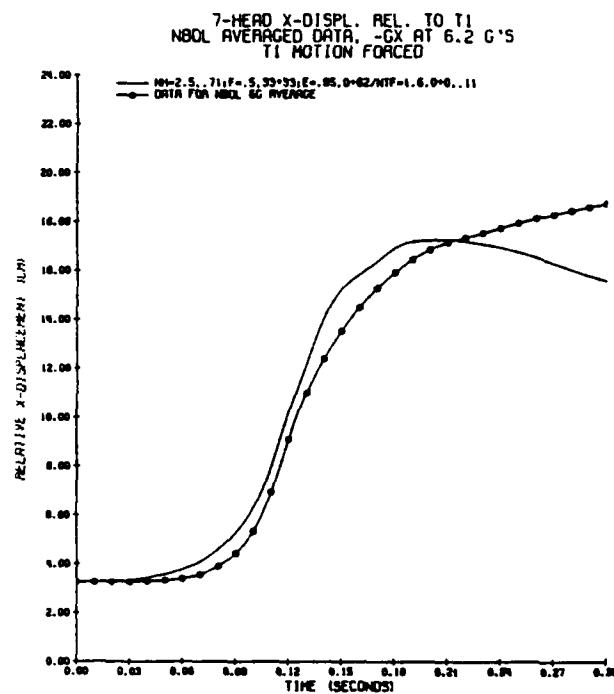
Figure 146. Head Origin X-Axis Displacement for Becker Neck Model with nonzero condyles joint stop at -6Gx.
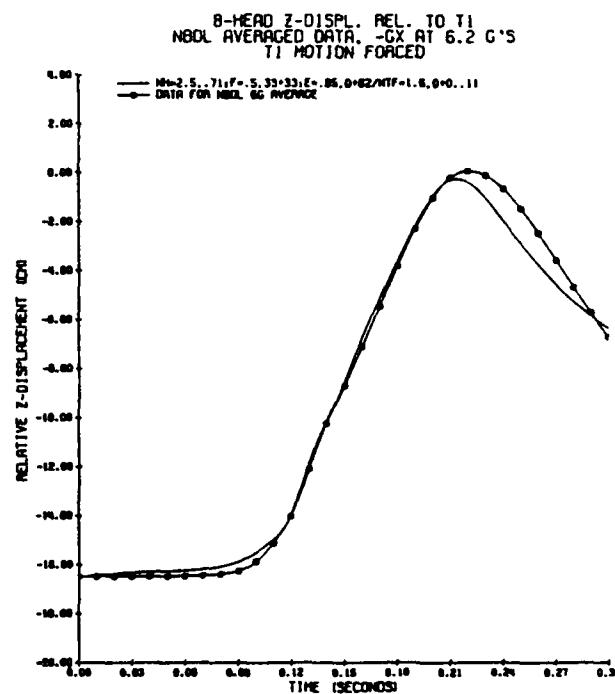


Figure 147. Head Origin Z-Axis Displacement for Becker Neck Model with nonzero condyles joint stop at -6Gx.
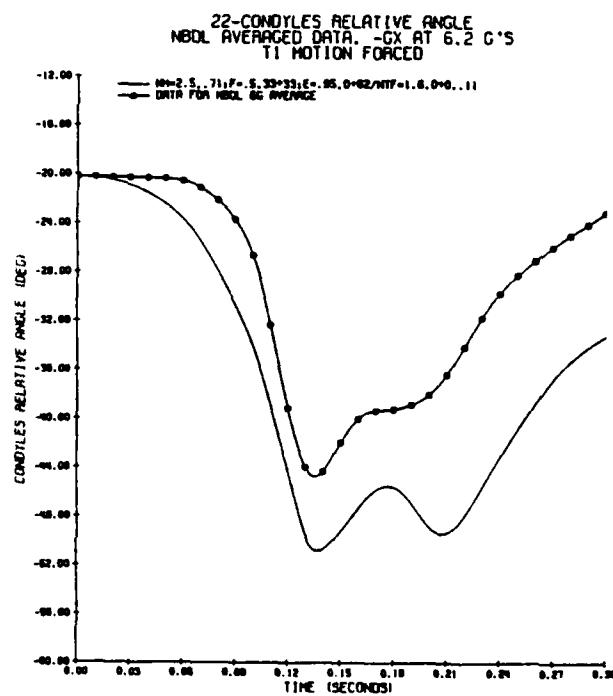


Figure 148. Condyles Relative Angle for Becker Neck Model with nonzero condyles joint stop at -6Gx.
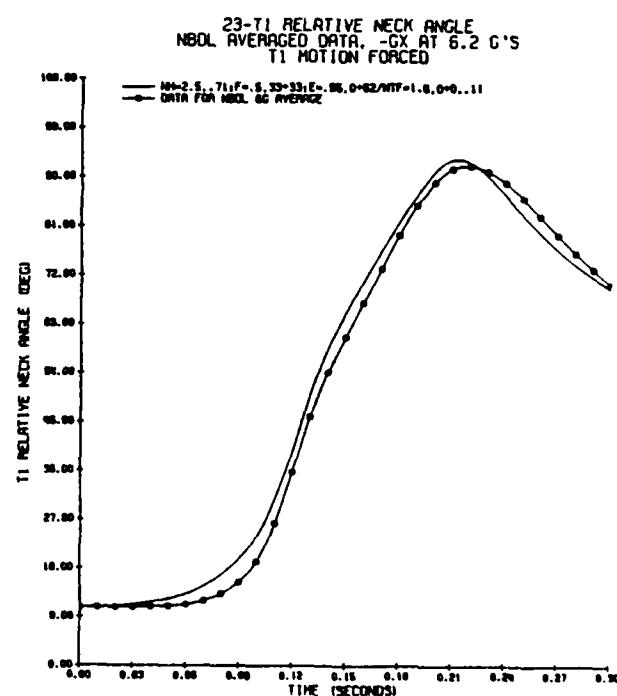


Figure 149. T1 Relative Angle for Becker Neck Model with nonzero condyles joint stop at -6Gx.

93
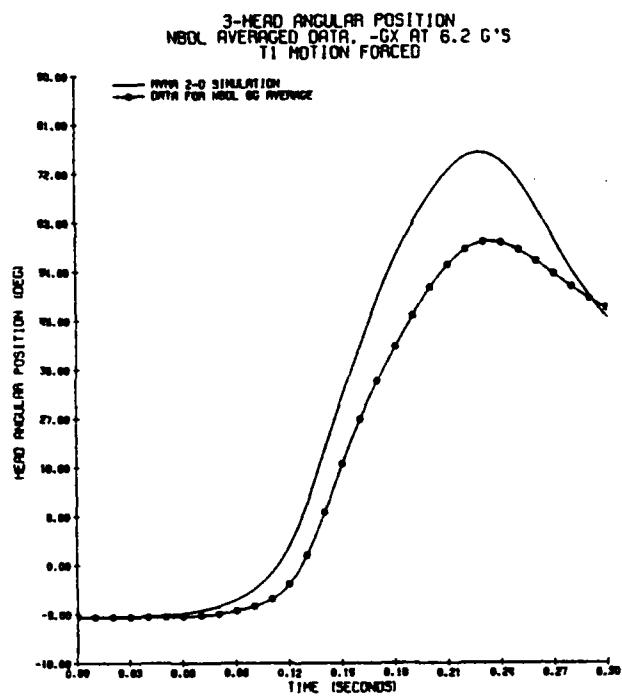
Figure 150. Head Angular Position for Neck Model with Head Origin Pivot at -6Gx.
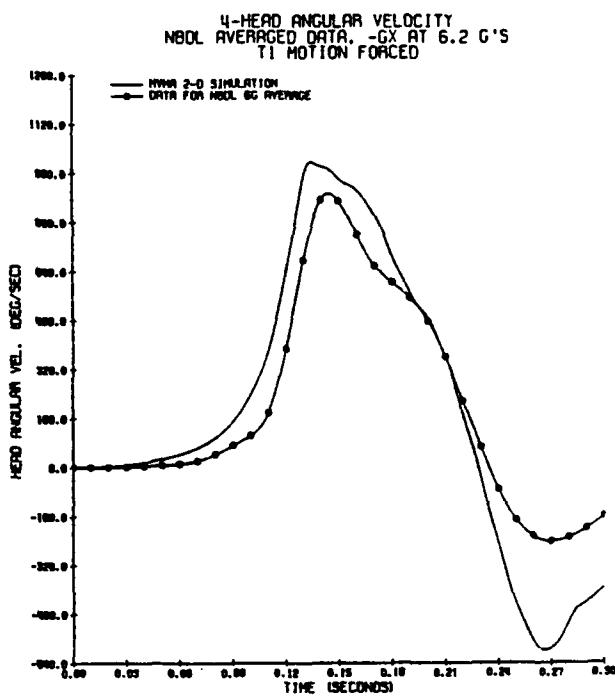


Figure 151. Head Angular Velocity for Neck Model with Head Origin Pivot at -6Gx.
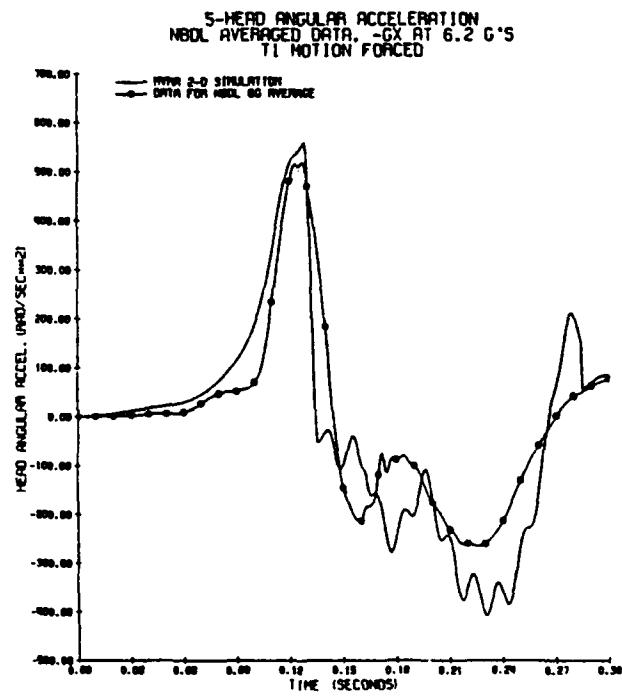


Figure 152. Head Angular Acceleration for Neck Model with Head Origin Pivot at -6Gx.
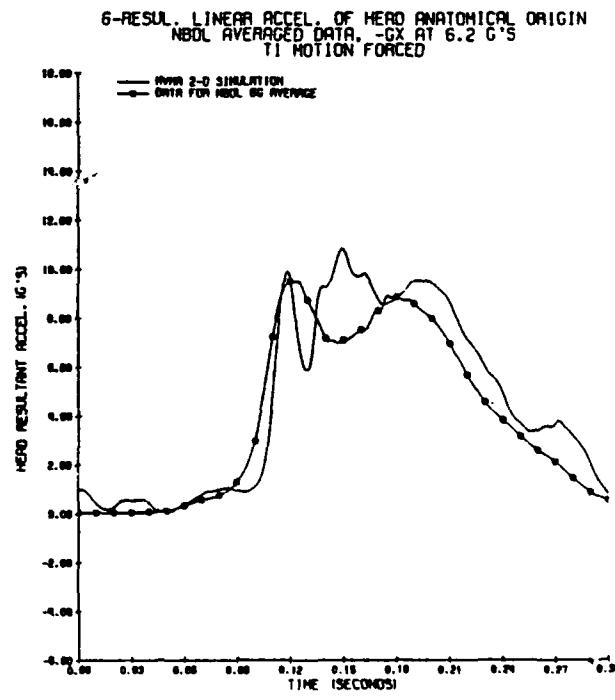


Figure 153. Head Resultant Acceleration for Neck Model with Head Origin Pivot at -6Gx.

94
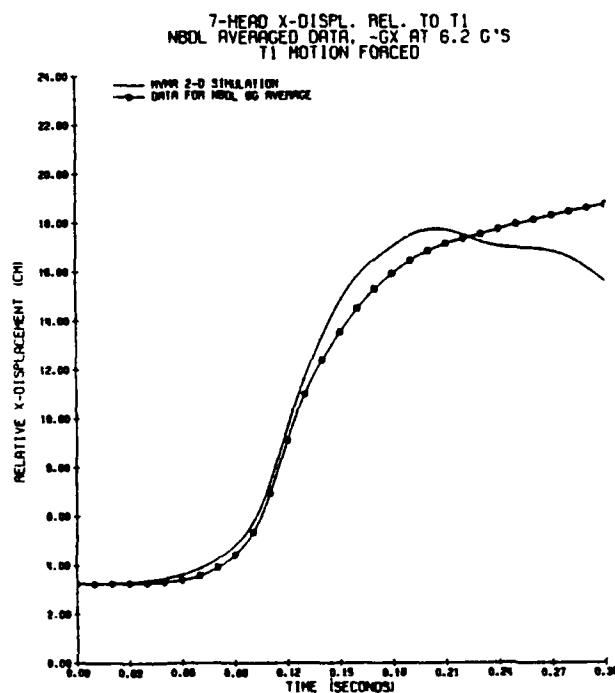
Figure 154. Head Origin X-Axis Displacement for Neck Model with Head Origin Pivot at -6Gx.
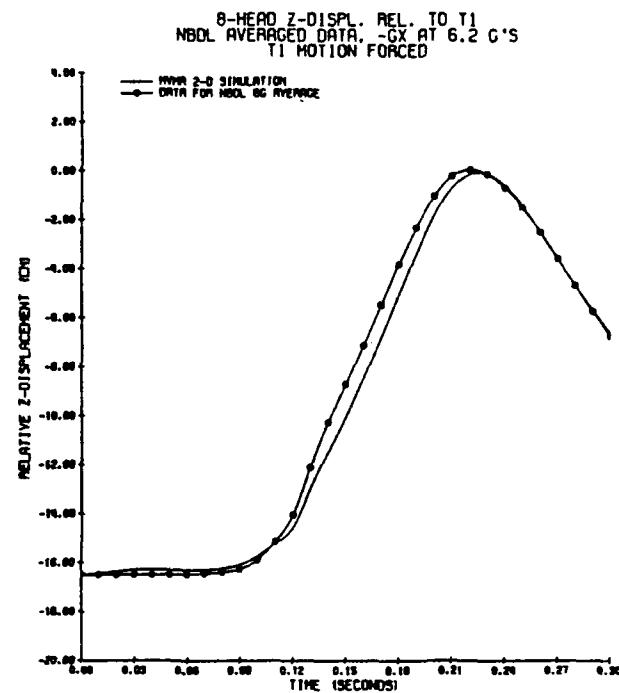


Figure 155. Head Origin Z-Axis Displacement for Neck Model with Head Origin Pivot at -6Gx.
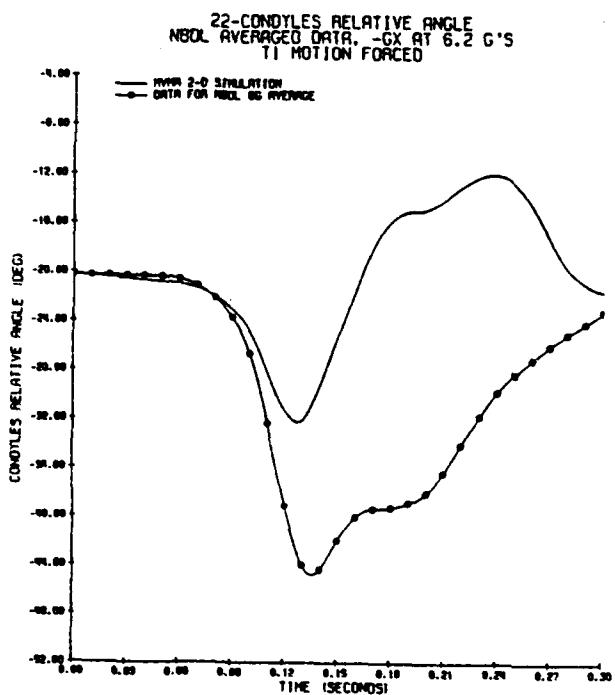


Figure 156. Condyles Relative Angle for Neck Model with Head Origin Pivot at -6Gx.
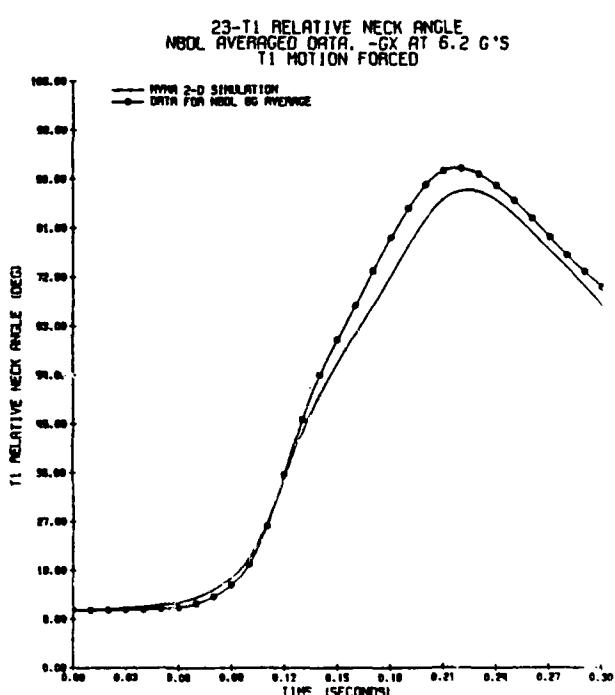


Figure 157. T1 Relative Angle for Neck Model with Head Origin Pivot at -6Gx.

95

3-HEAD ANGULAR POSITION
NBDL AVERAGED DATA. -GX AT 6.2 G'S
TI MOTION FORCED
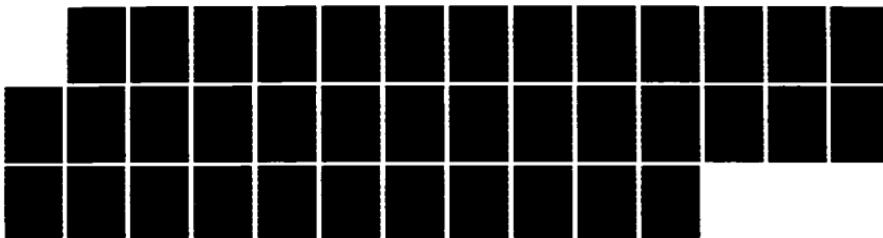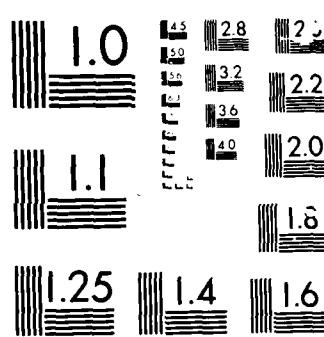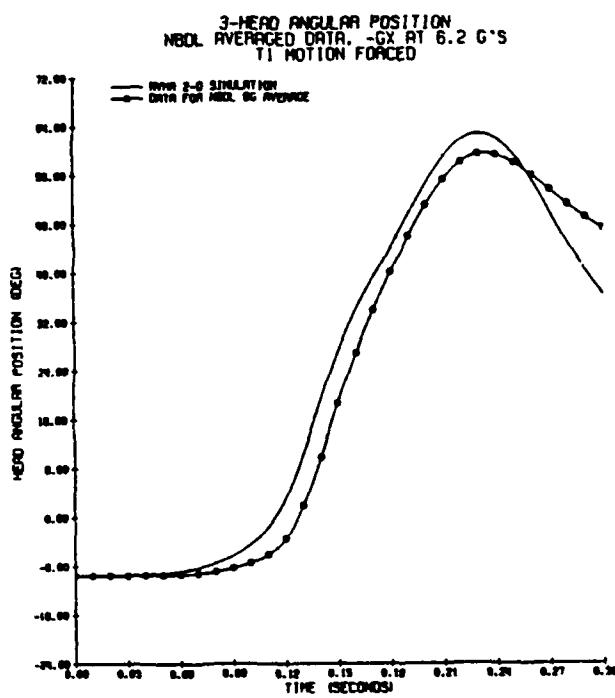
Figure 158. Head Angular Position for Long Neck Model with T1(-5.12,7.5) Pivot at -6Gx.

4-HEAD ANGULAR VELOCITY
NBDL AVERAGED DATA. -GX AT 6.2 G'S
TI MOTION FORCED
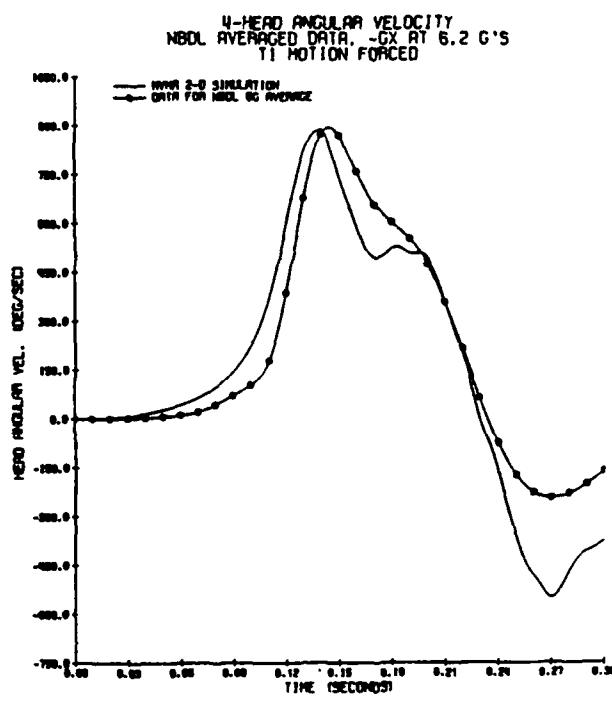
Figure 159. Head Angular Velocity for Neck Model with T1(-5.12,7.5) Pivot at -6Gx.

5-HEAD ANGULAR ACCELERATION
NBDL AVERAGED DATA. -GX AT 6.2 G'S
TI MOTION FORCED
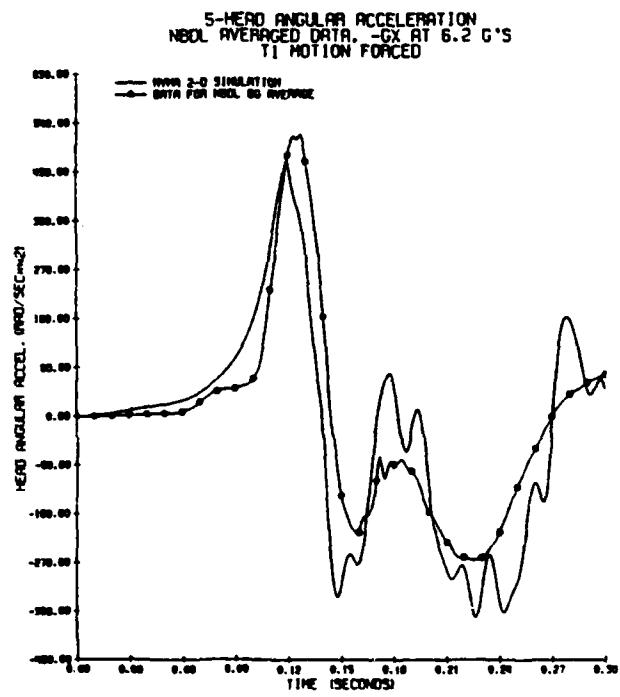
Figure 160. Head Angular Acceleration for Neck Model with T1(-5.12,7.5) Pivot at -6Gx.

6-RESUL. LINEAR ACCEL. OF HEAD ANATOMICAL ORIGIN
NBDL AVERAGED DATA. -GX AT 6.2 G'S
TI MOTION FORCED
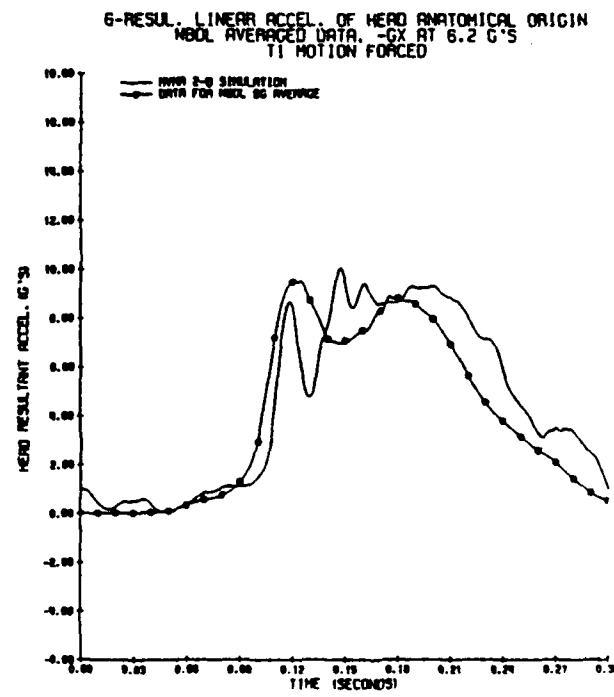
Figure 161. Head Resultant Acceleration for Neck Model with T1(-5.12,7.5) Pivot at -6Gx.

96
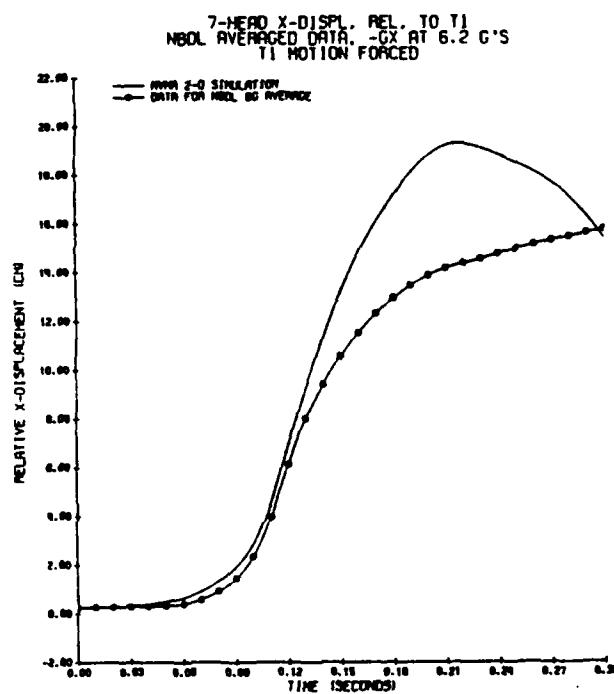
Figure 162. Head Origin X-Axis Displacement
Neck Model with T1(-5.12,7.5) Pivot at -6Gx.
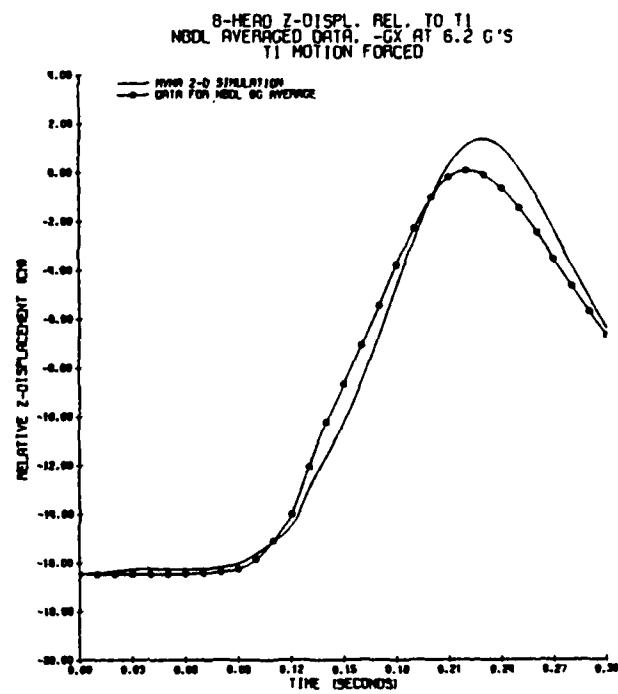


Figure 163. Head Origin Z-Axis Displacement
Neck Model with T1(-5.12,7.5) Pivot at -6Gx.
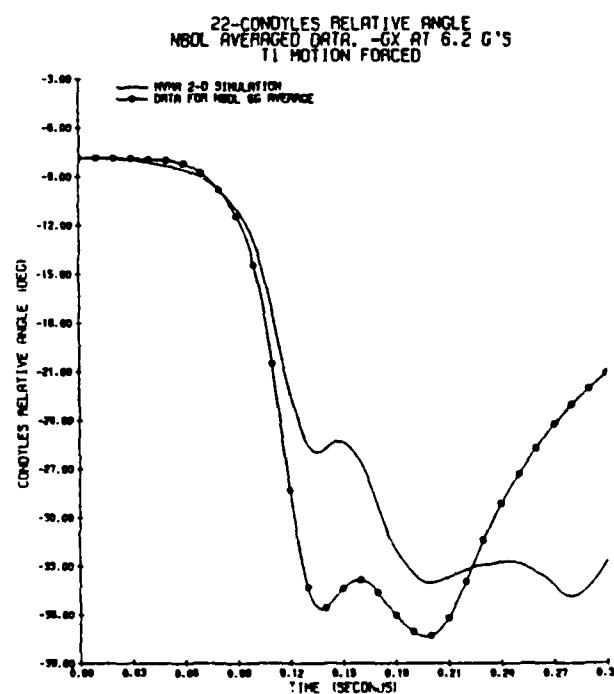


Figure 164. Condyles Relative Angle for Neck
Model with T1(-5.12,7.5) Pivot at -6Gx.
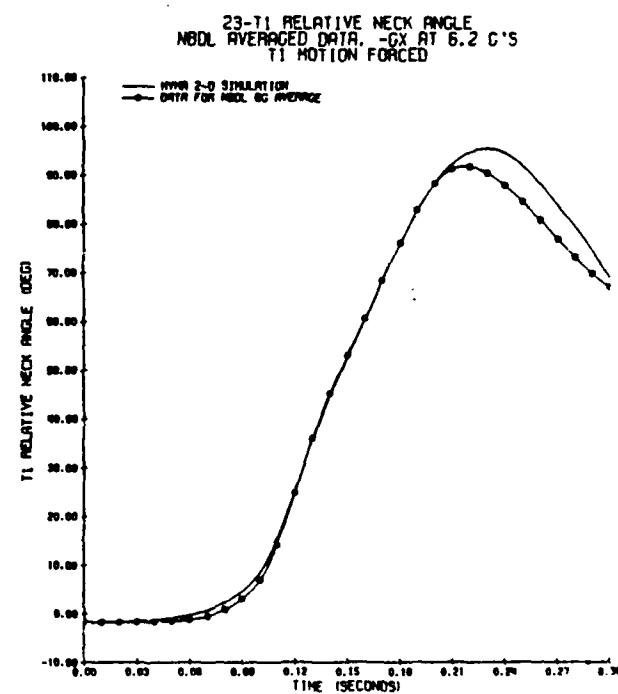


Figure 165. T1 Relative Angle for Neck Model
with T1(-5.12,7.5) Pivot at -6Gx.

97
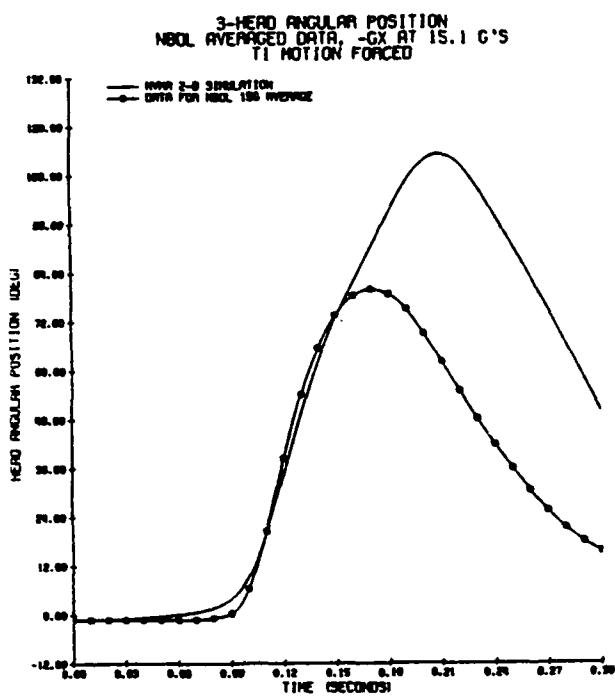
Figure 166. Head Angular Position for Long Neck Model with T1(-5.12,7.5) Pivot at -15Gx.
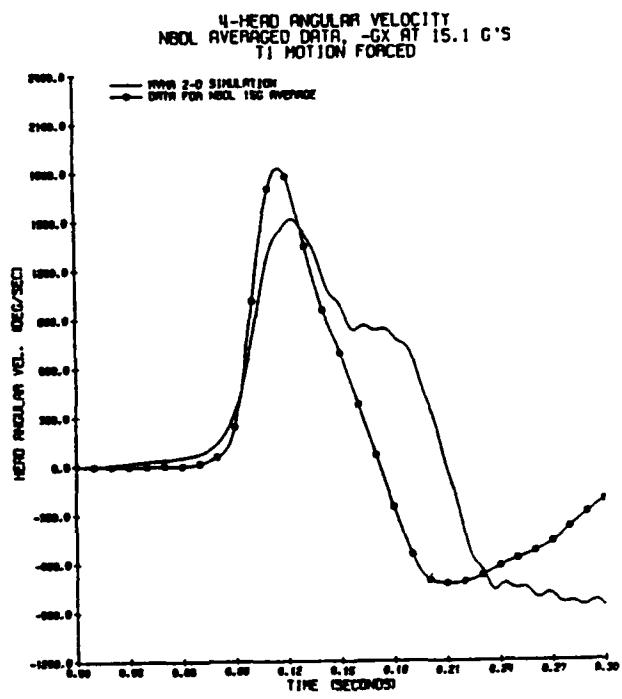


Figure 167. Head Angular Velocity for Neck Model with T1(-5.12,7.5) Pivot at -15Gx.
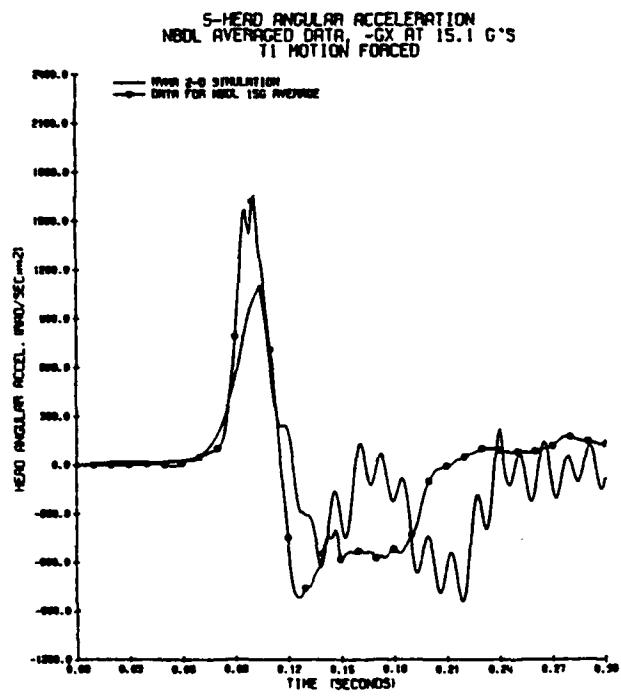


Figure 168. Head Angular Acceleration for Neck Model with T1(-5.12,7.5) Pivot at -15Gx.
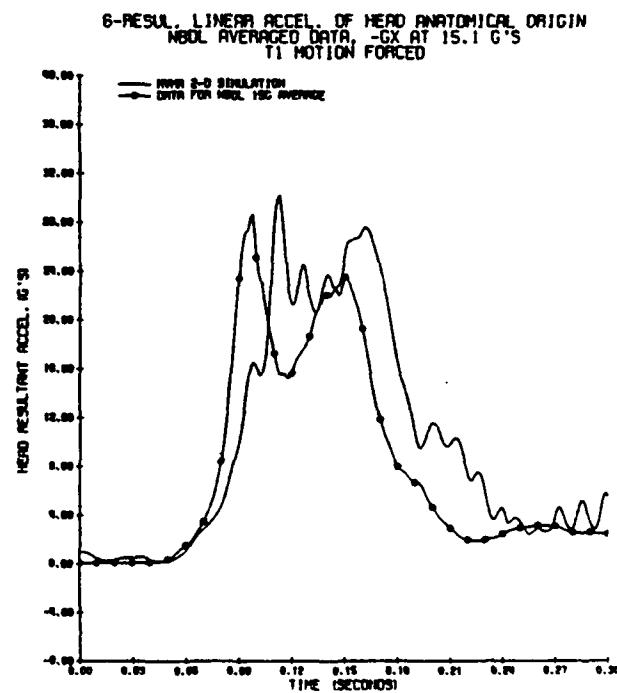


Figure 169. Head Resultant Acceleration for Neck Model with T1(-5.12,7.5) Pivot at -15Gx.
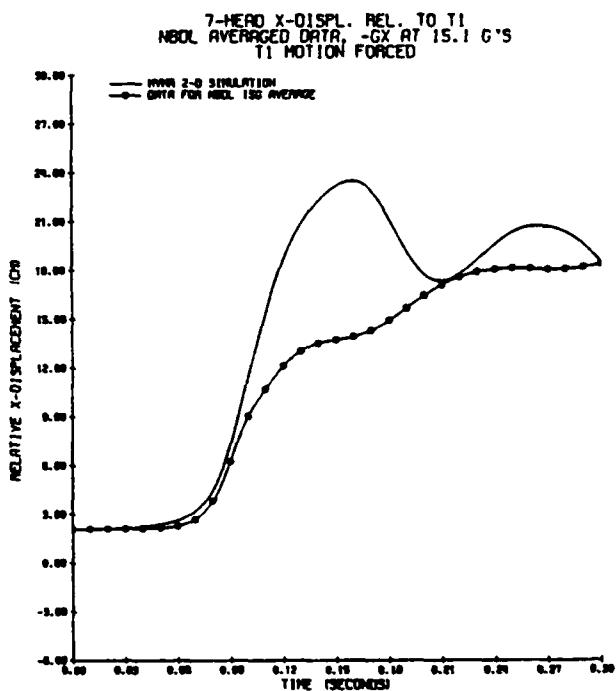
Figure 170.   Head Origin X-Axis Displacement
Neck Model with T1(-5.12,7.5) Pivot at -15Gx.
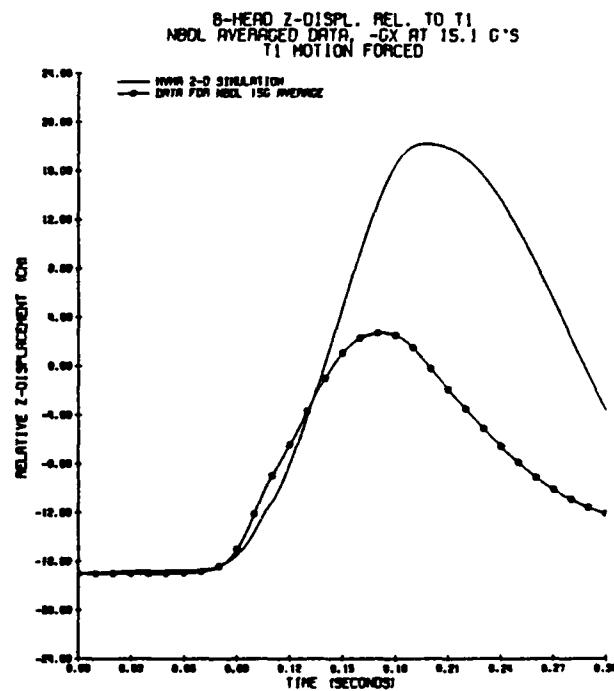


Figure 171.   Head Origin Z-Axis Displacement
Neck Model with T1(-5.12,7.5) Pivot at -15Gx.
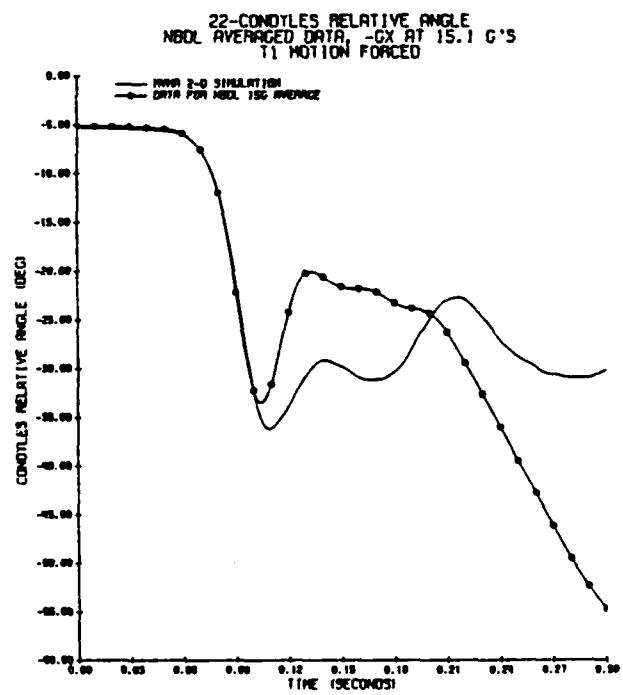


Figure 172.   Condyles Relative Angle for Neck
Model with T1(-5.12,7.5) Pivot at -15Gx.
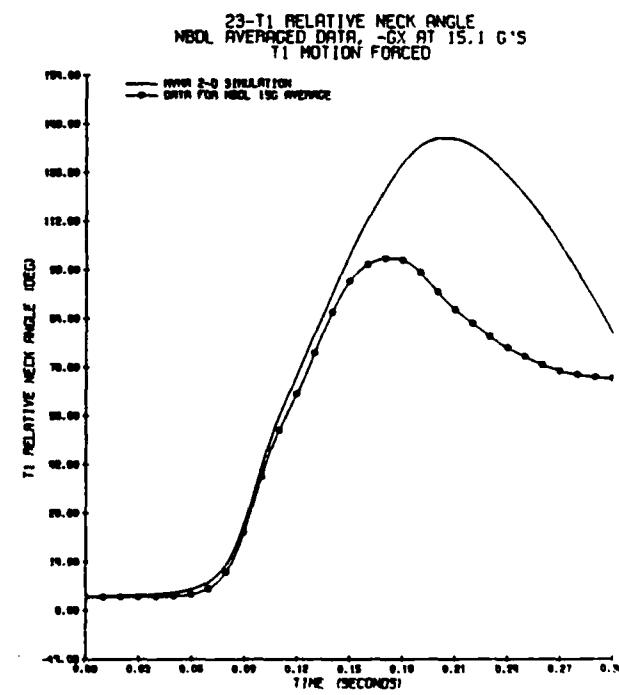


Figure 173.   T1 Relative Angle for Neck Model
with T1(-5.12,7.5) Pivot at -15Gx.

99
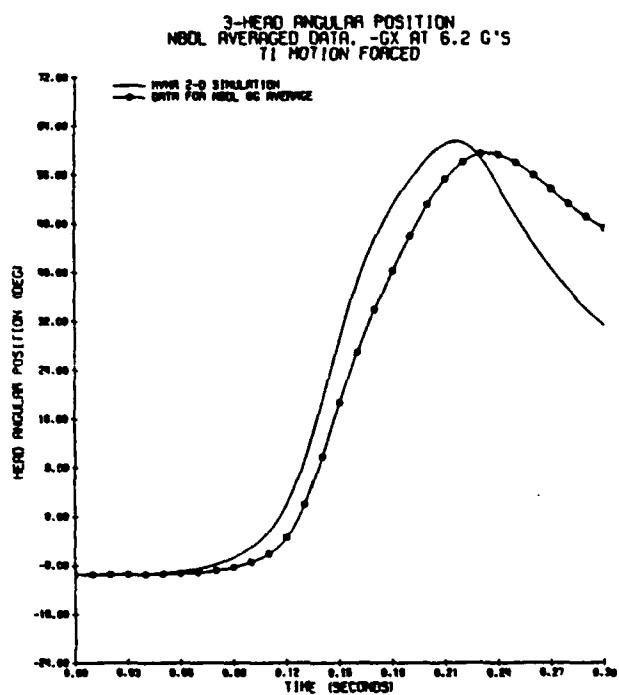
Figure 174. Head Angular Position for Long Neck Model with T1(-5,6) Pivot at -6Gx.
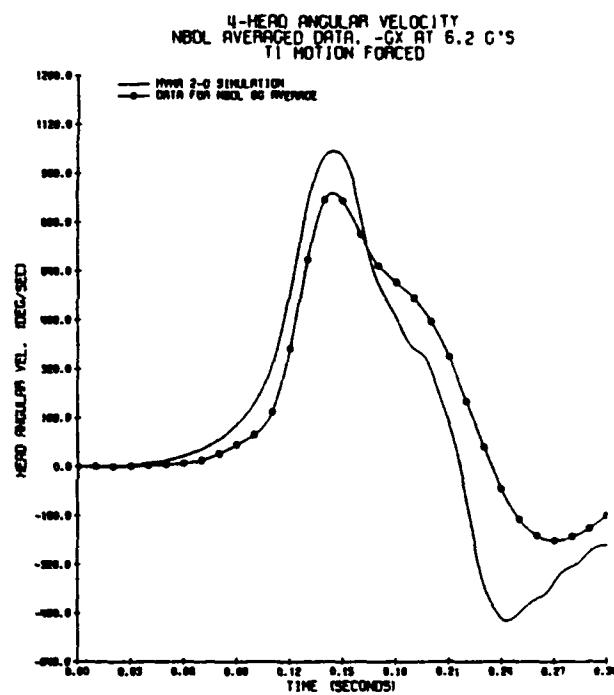
Figure 175. Head Angular Velocity for Neck Model with T1(-5,6) Pivot at -6Gx.
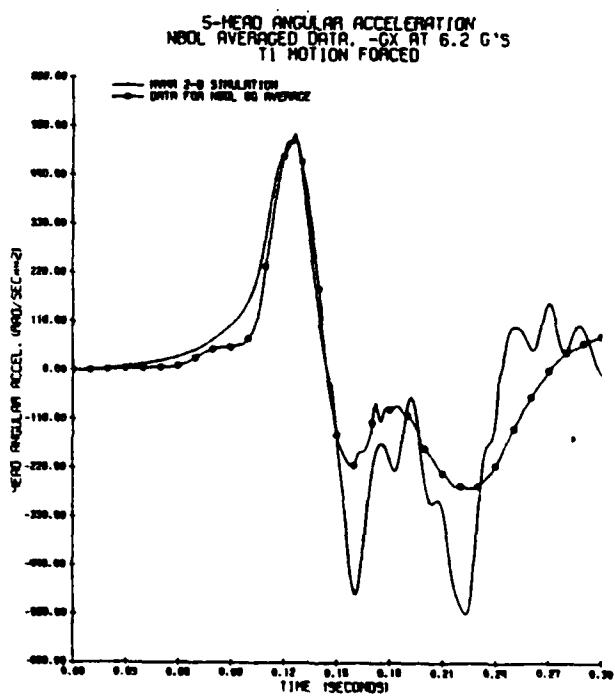
Figure 176. Head Angular Acceleration for Neck Model with T1(-5,6) Pivot at -6Gx.
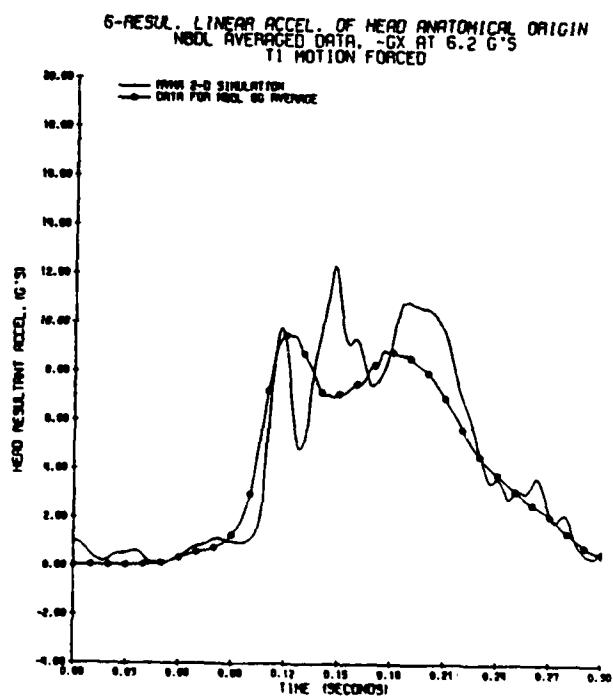
Figure 177. Head Resultant Acceleration for Neck Model with T1(-5,6) Pivot at -6Gx.
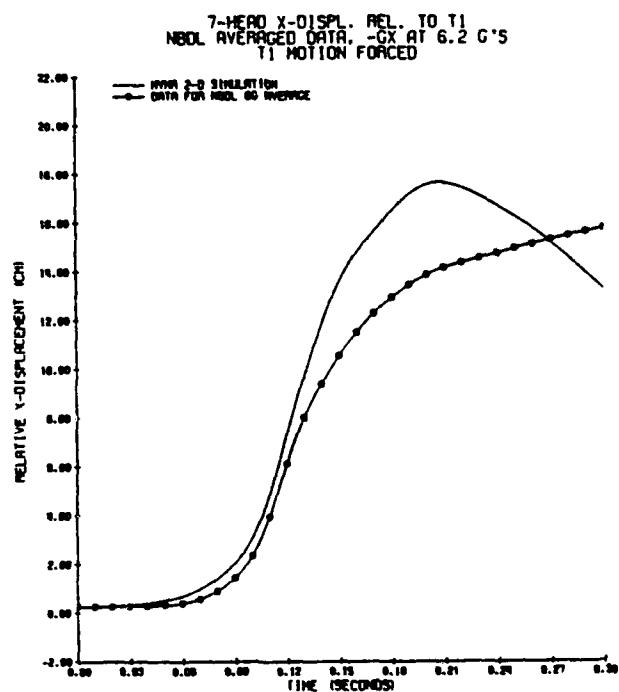
Figure 178. Head Origin X-Axis Displacement Neck Model with T1(-5,6) Pivot at -6Gx.
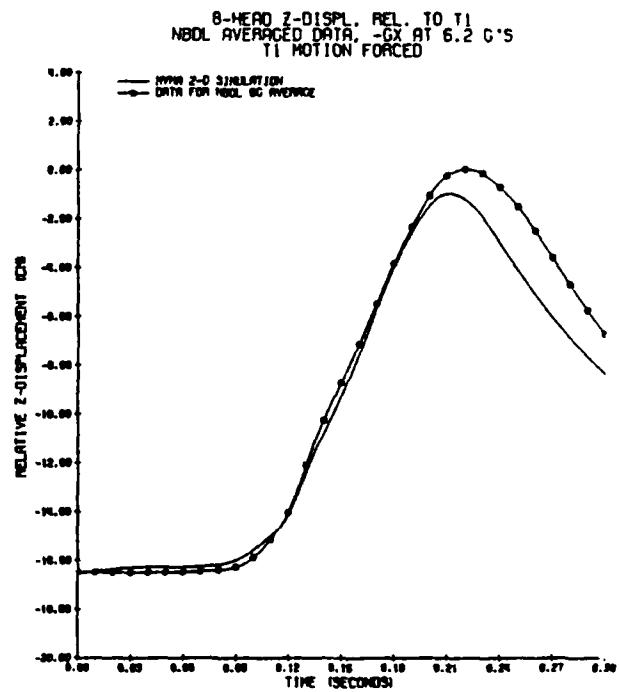


Figure 179. Head Origin Z-Axis Displacement Neck Model with T1(-5,6) Pivot at -6Gx.
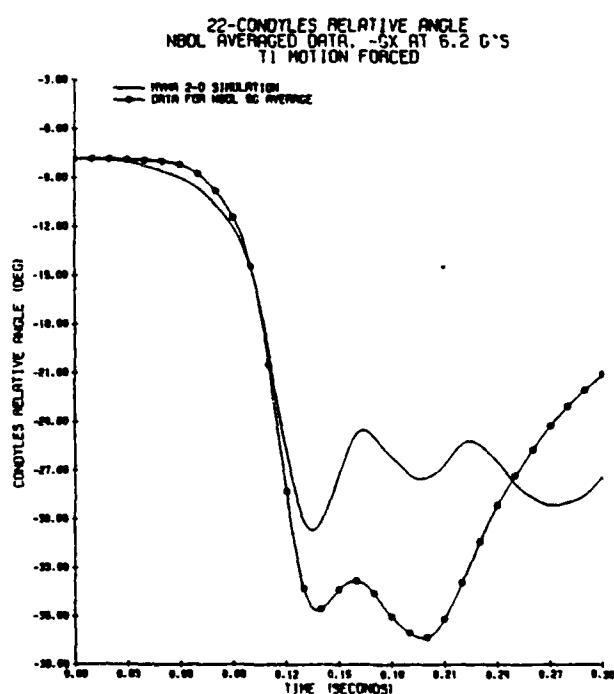


Figure 180. Condyles Relative Angle for Neck Model with T1(-5,6) Pivot at -6Gx.
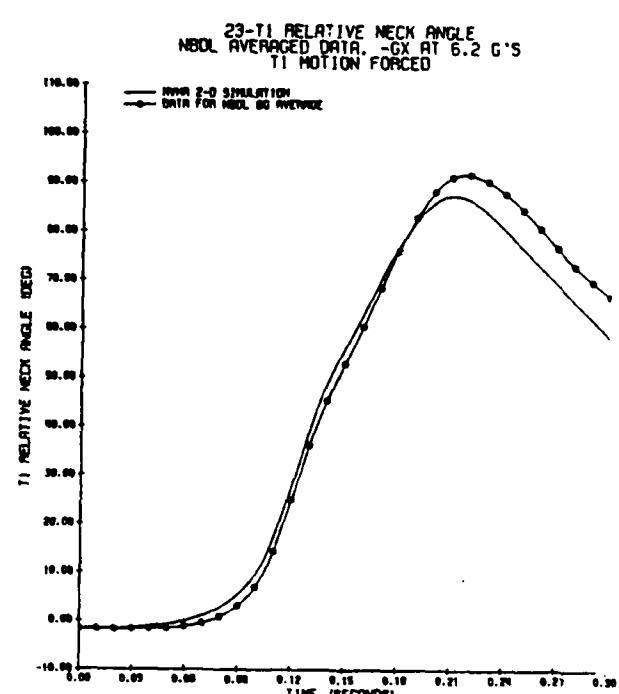


Figure 181. T1 Relative Angle for Neck Model with T1(-5,6) Pivot at -6Gx.

101
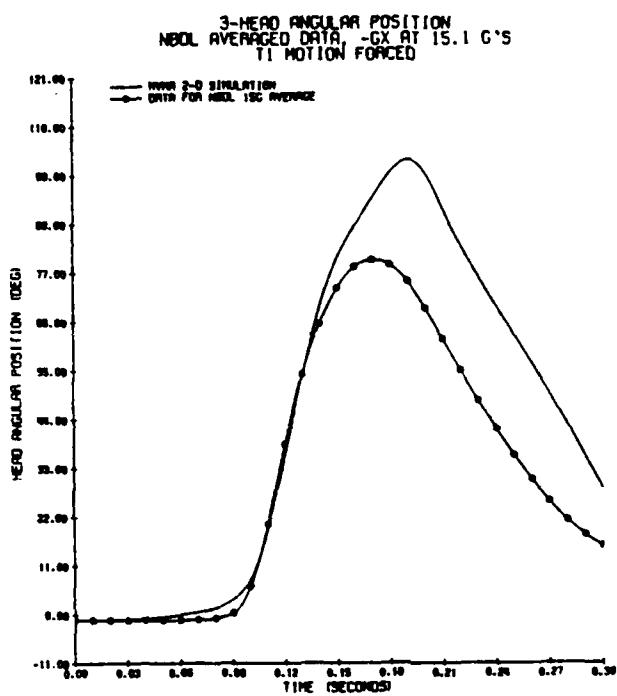
Figure 182. Head Angular Position for Long Neck
Model with T1(-5,6) Pivot at -15Gx.
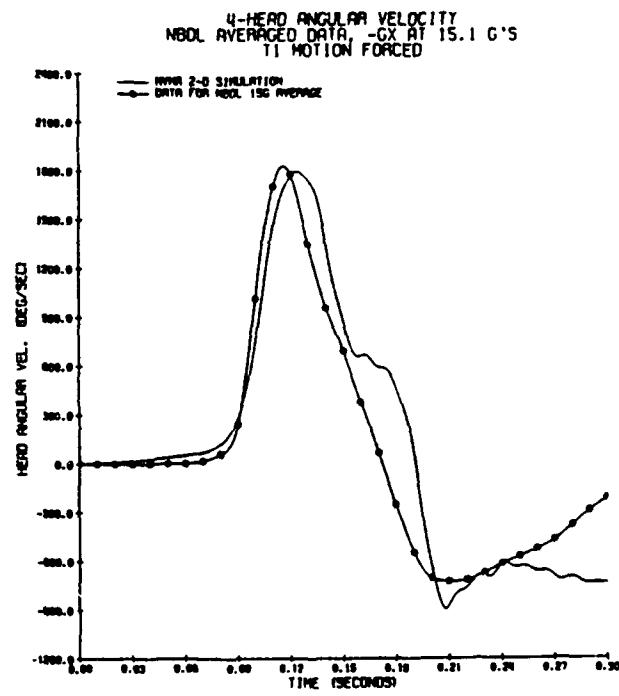
Figure 183. Head Angular Velocity for Neck
Model with T1(-5,6) Pivot at -15Gx.
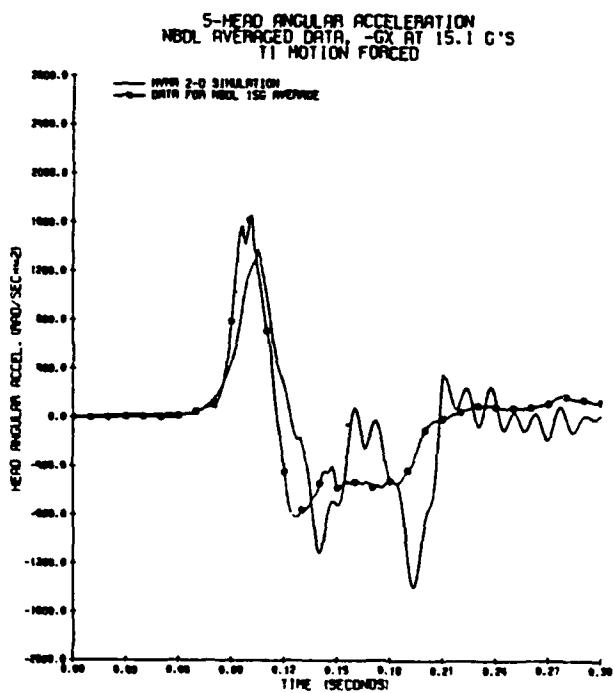
Figure 184. Head Angular Acceleration for Neck
Model with T1(-5,6) Pivot at -15Gx.
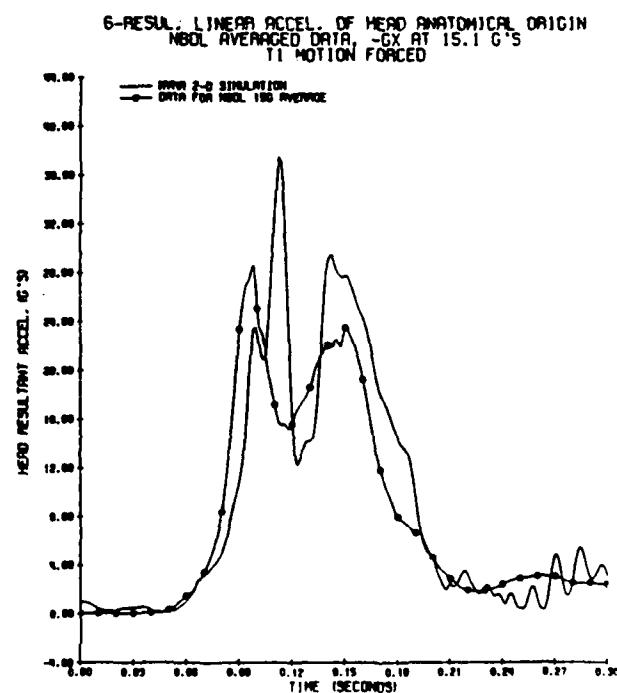
Figure 185. Head Resultant Acceleration for
Neck Model with T1(-5,6) Pivot at -15Gx.
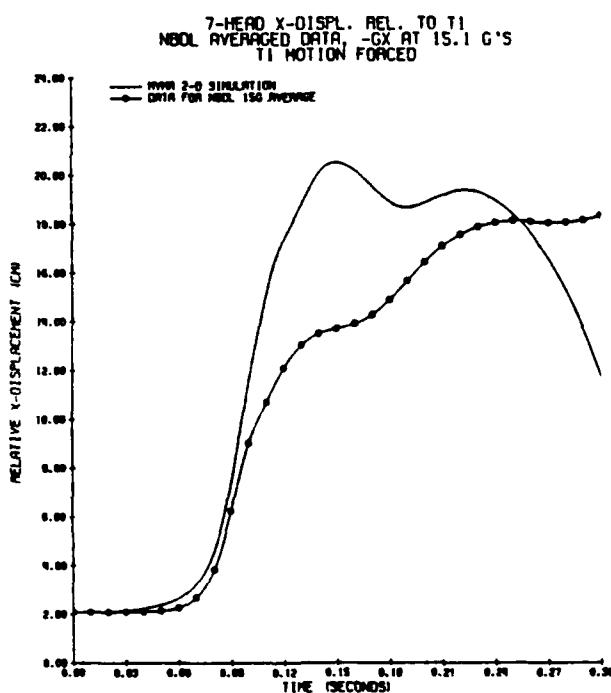
Figure 186. Head Origin X-Axis Displacement Neck Model with T1(-5,6) Pivot at -15Gx.
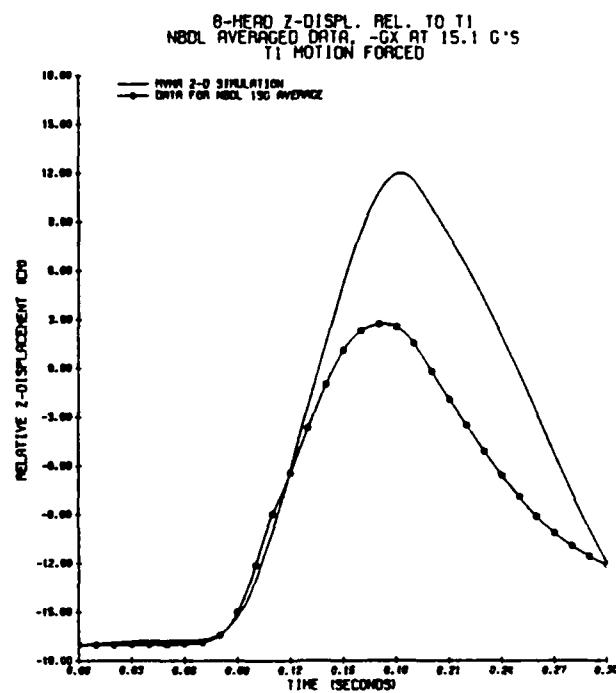


Figure 187. Head Origin Z-Axis Displacement Neck Model with T1(-5,6) Pivot at -15Gx.
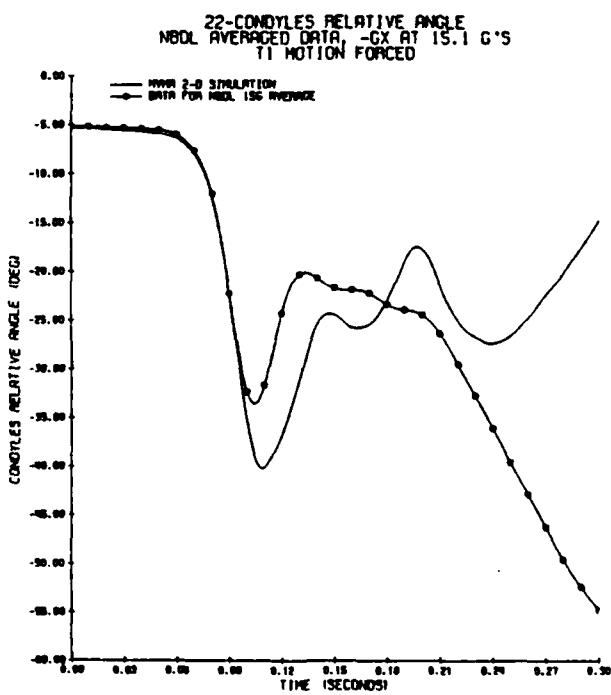


Figure 188. Condyles Relative Angle for Neck Model with T1(-5,6) Pivot at -15Gx.
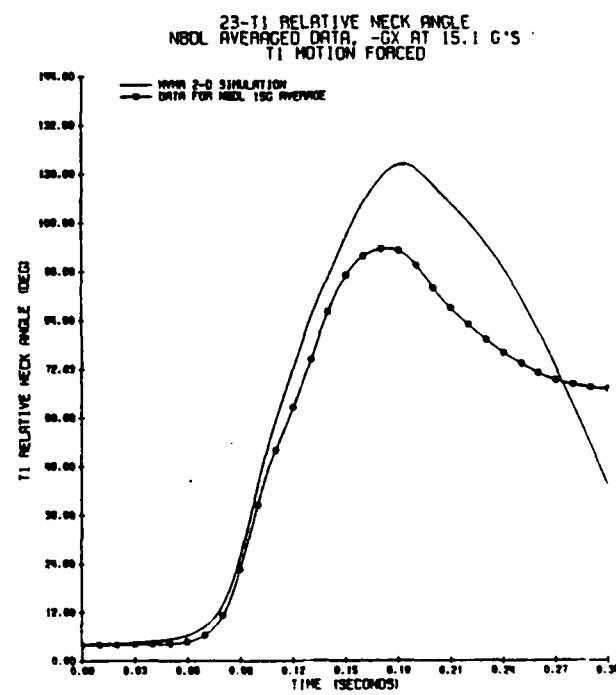


Figure 189. T1 Relative Angle for Neck Model with T1(-5,6) Pivot at -15Gx.

103

# NECK MODEL LOAD-DEFLECTION DATA

## CONDYLES BENDING STIFFNESS

$M_\theta$ (Nm)

2.5 N-m/deg

$\theta$ (degrees)

EXTENSION

FLEXION

.5 N-m/deg

## C7 BENDING STIFFNESS

$M_\theta$ (Nm)

3. N-m/deg

1. N-m/deg

$\theta$ (degrees)

EXTENSION

20°

FLEXION

.457 N-m/deg

## NECK ELONGATION STIFFNESS

F(N)

1644 N/cm

411 N/cm

(cm)

COMPRESSION

.8 cm

TENSION

400 N/cm
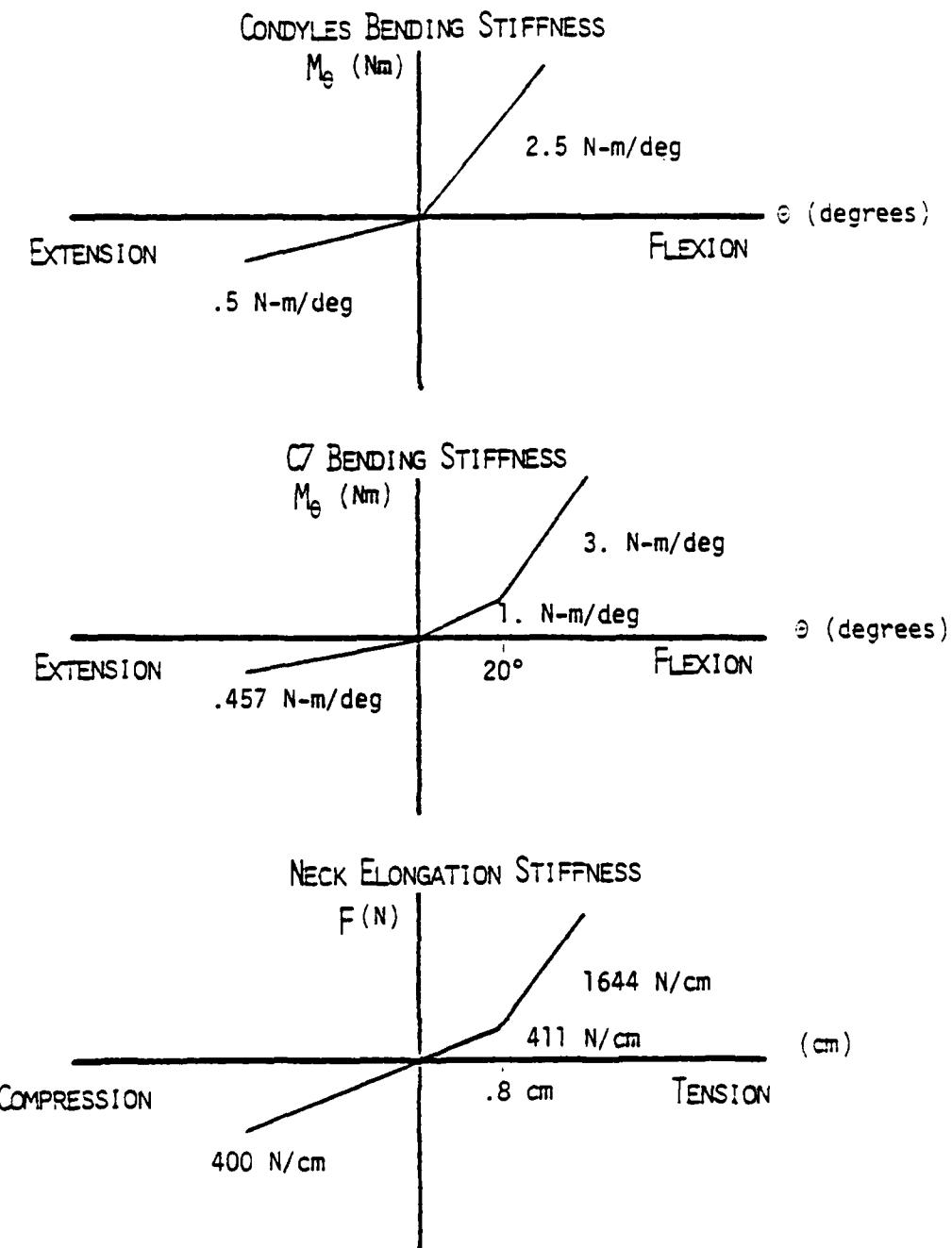
Figure 190.  Bilinear Load-Deflection Data for
Long Neck Model with T1(-5,6) Pivot.

## 3-HEAD ANGULAR POSITION
### NBOL AVERAGED DATA, -GX AT 6.2 G'S
### T1 MOTION FORCED
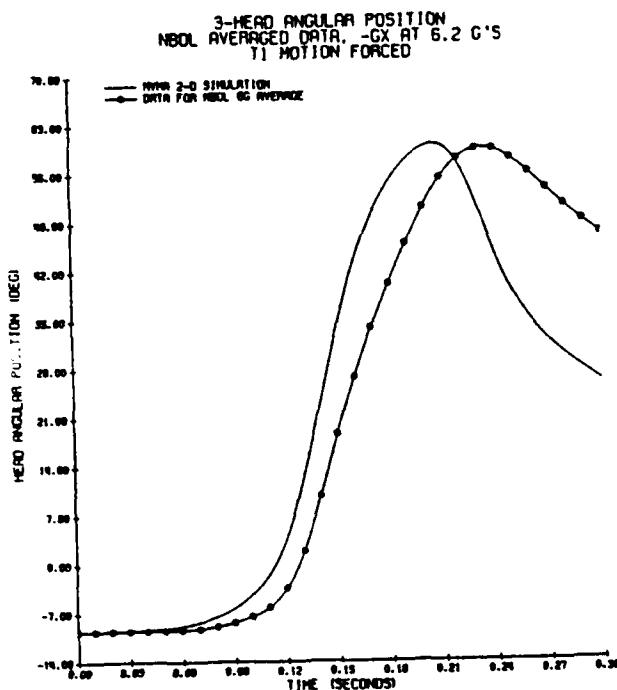
Figure 191. Head Angular Position for Long Neck Model with T1(-4,3) Pivot at -6Gx.

## 4-HEAD ANGULAR VELOCITY
### NBOL AVERAGED DATA, -GX AT 6.2 G'S
### T1 MOTION FORCED
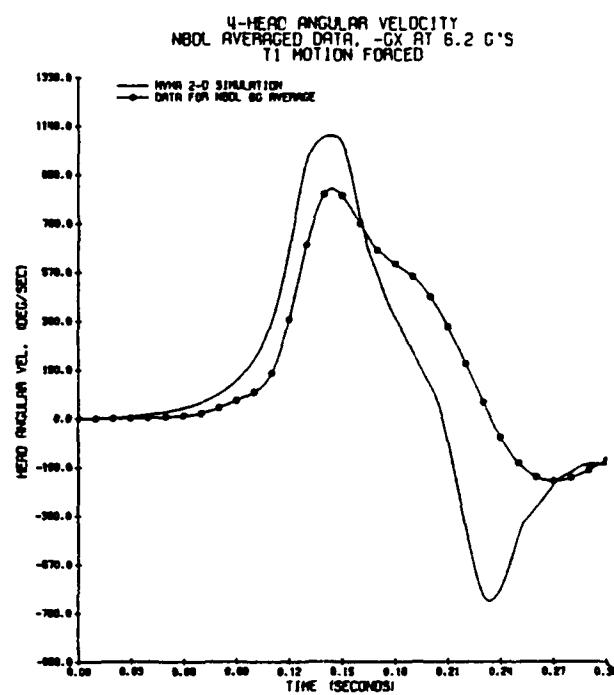
Figure 192. Head Angular Velocity for Neck Model with T1(-4,3) Pivot at -6Gx.

## 5-HEAD ANGULAR ACCELERATION
### NBOL AVERAGED DATA, -GX AT 6.2 G'S
### T1 MOTION FORCED
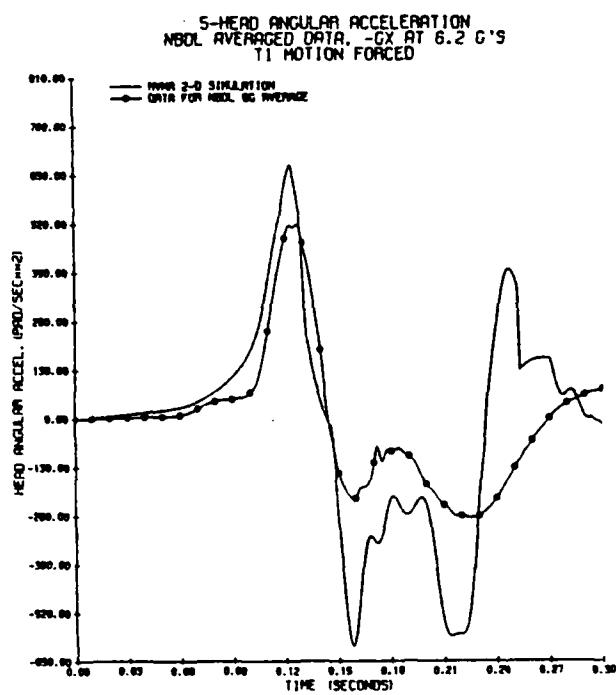
Figure 193. Head Angular Acceleration for Neck Model with T1(-4,3) Pivot at -6Gx.

## 6-RESUL. LINEAR ACCEL. OF HEAD ANATOMICAL ORIGIN
### NBOL AVERAGED DATA, -GX AT 6.2 G'S
### T1 MOTION FORCED
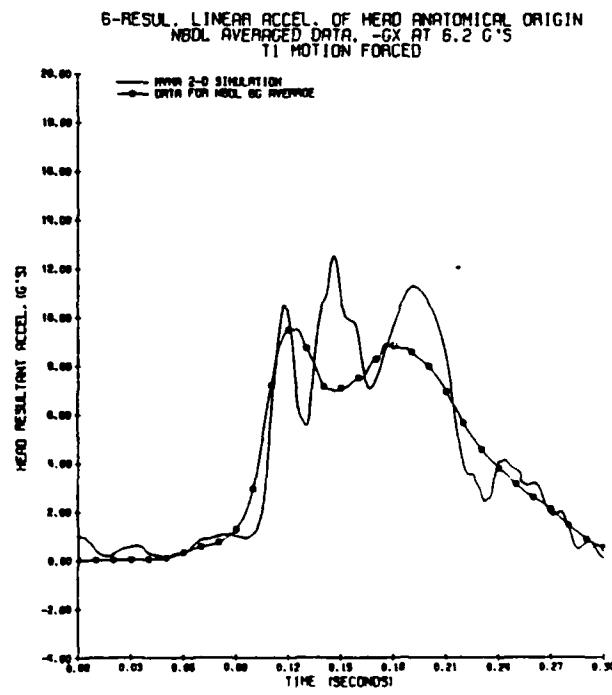
Figure 194. Head Resultant Acceleration for Neck Model with T1(-4,3) Pivot at -6Gx.

105
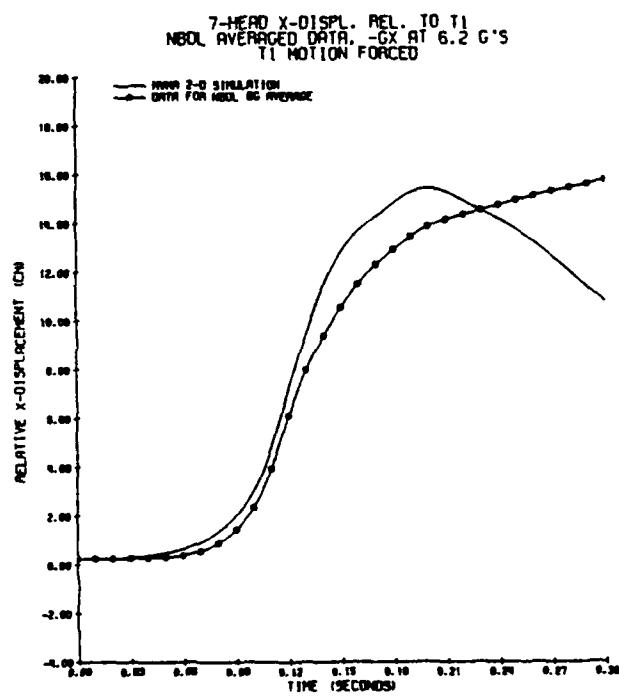
Figure 195. Head Origin X-Axis Displacement
Neck Model with T1(-4,3) Pivot at -6Gx.
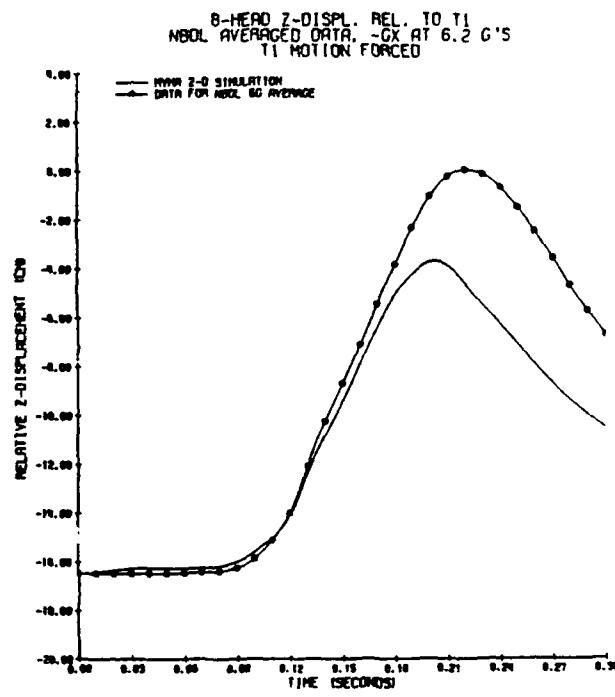


Figure 196. Head Origin Z-Axis Displacement
Neck Model with T1(-4,3) Pivot at -6Gx.
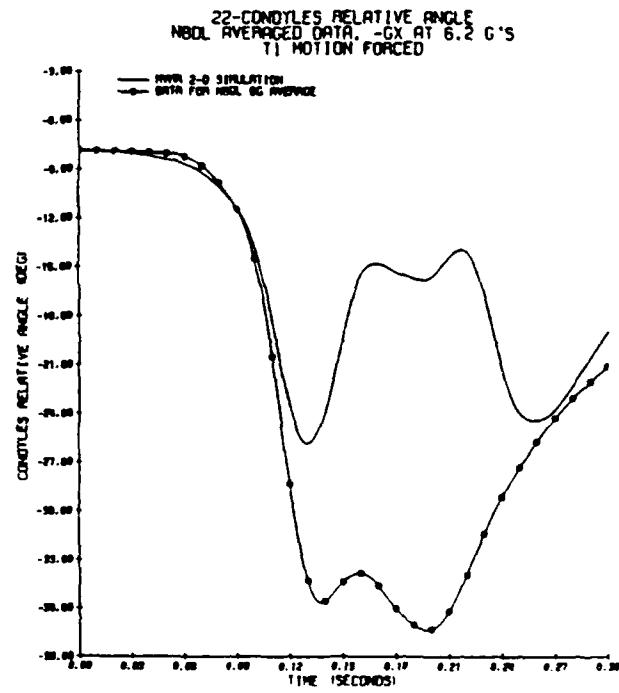


Figure 197. Condyles Relative Angle for Neck
Model with T1(-4,3) Pivot at -6Gx.
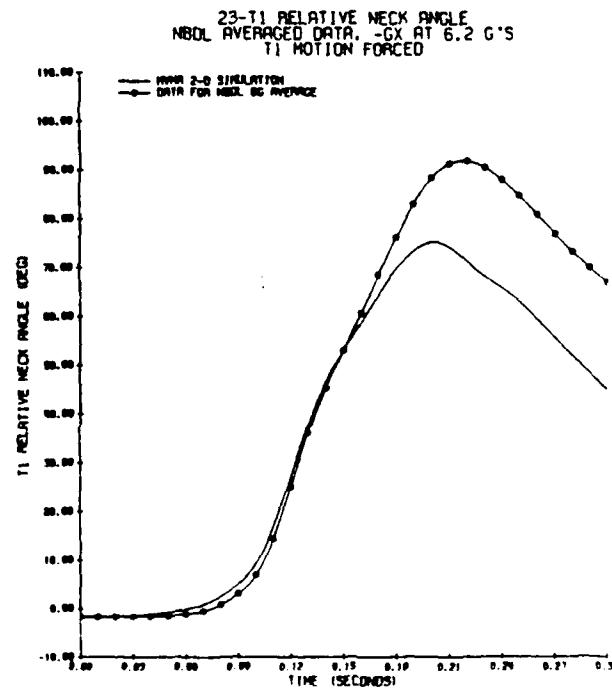


Figure 198. T1 Relative Angle for Neck Model
with T1(-4,3) Pivot at -6Gx.
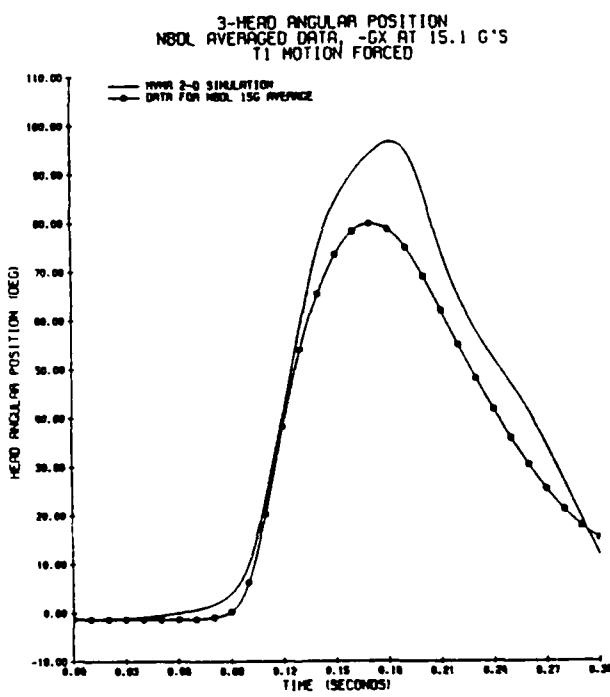
Figure 199.  Head Angular Position for Long Neck Model with T1(-4,3) Pivot at -15Gx.
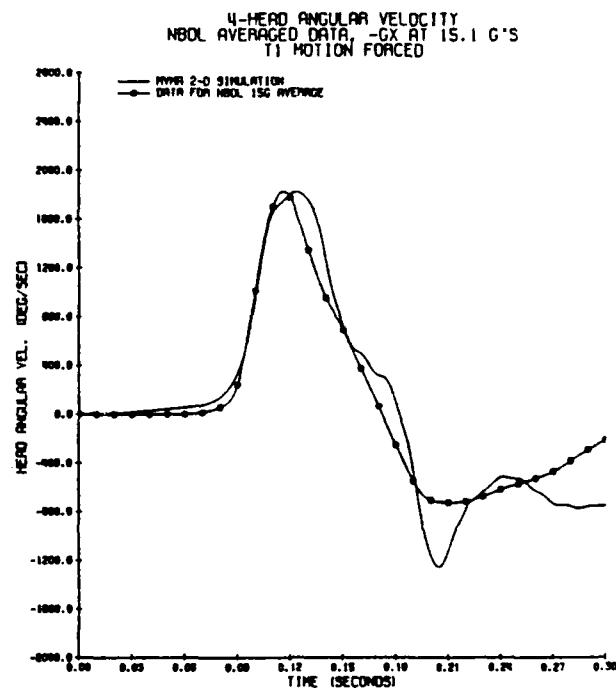


Figure 200.  Head Angular Velocity for Neck Model with T1(-4,3) Pivot at -15Gx.
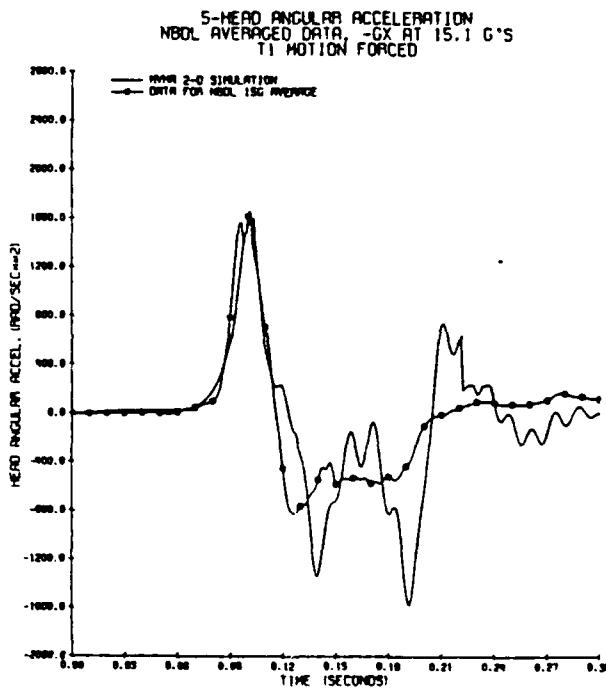


Figure 201.  Head Angular Acceleration for Neck Model with T1(-4,3) Pivot at -15Gx.
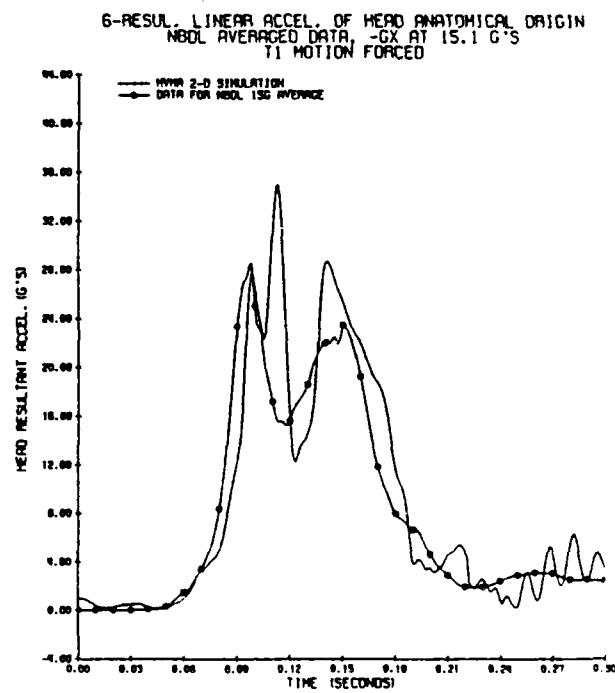


Figure 202.  Head Resultant Acceleration for Neck Model with T1(-4,3) Pivot at -15Gx.

107
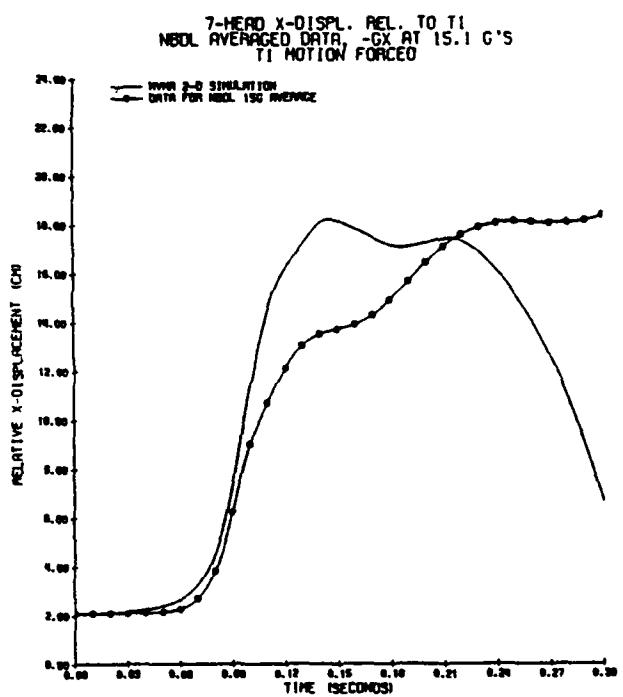
Figure 203. Head Origin X-Axis Displacement
Neck Model with T1(-4,3) Pivot at -15Gx.
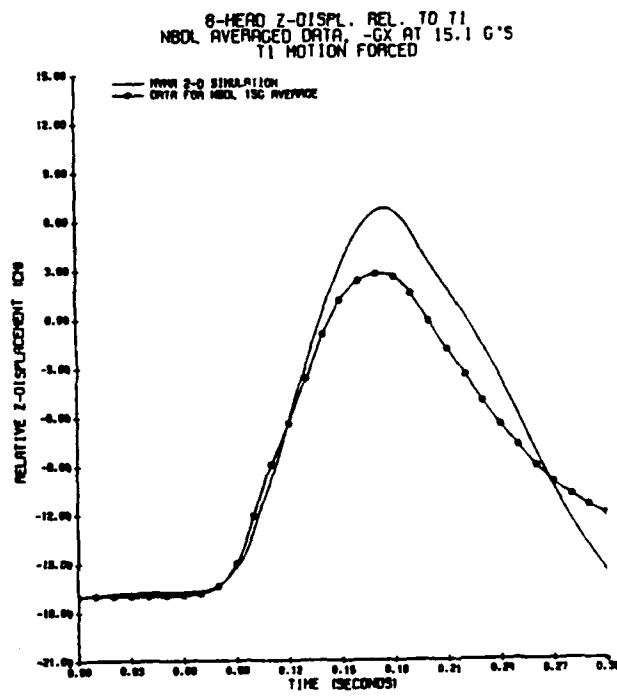


Figure 204. Head Origin Z-Axis Displacement
Neck Model with T1(-4,3) Pivot at -15Gx.
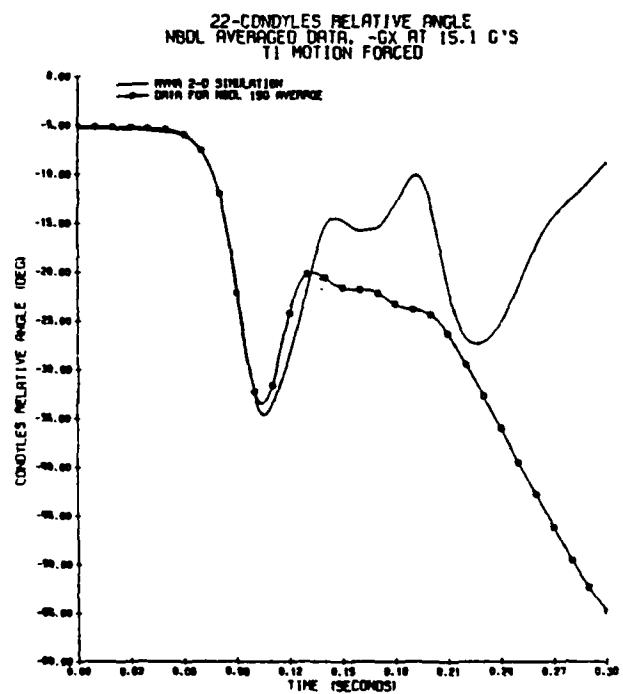


Figure 205. Condyles Relative Angle for Neck
Model with T1(-4,3) Pivot at -15Gx.
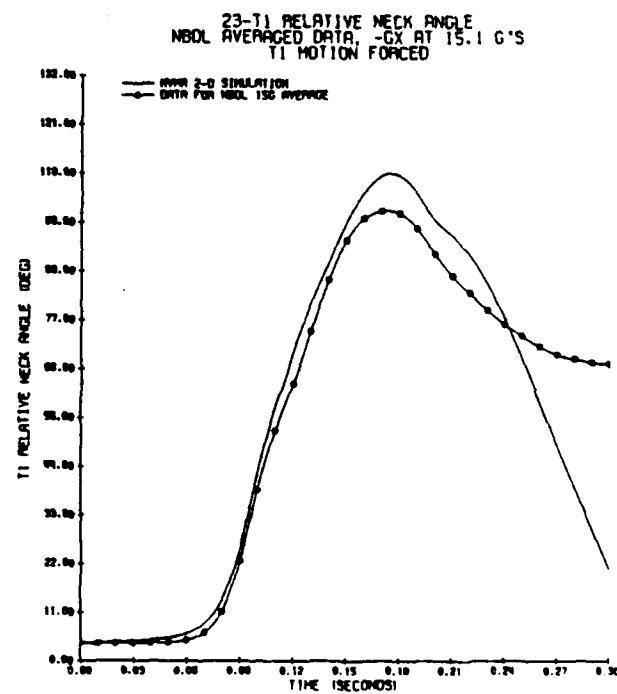


Figure 206. T1 Relative Angle for Neck Model
with T1(-4,3) Pivot at -15Gx.

NECK MODEL LOAD-DEFLECTION DATA

CONDYLES BENDING STIFFNESS

$M_\theta$ (Nm)

2.5 N-m/deg

$\theta$ (degrees)

EXTENSION          FLEXION

.62 N-m/deg

C7 BENDING STIFFNESS

$M_\theta$ (Nm)

3.2 N-m/deg

.6 N-m/deg

$\theta$ (degrees)

EXTENSION          FLEXION

20°

.457 N-m/deg

NECK ELONGATION STIFFNESS

F (N)

1644 N/cm

411 N/cm

(cm)

COMPRESSION          TENSION

.8 cm

400 N/cm
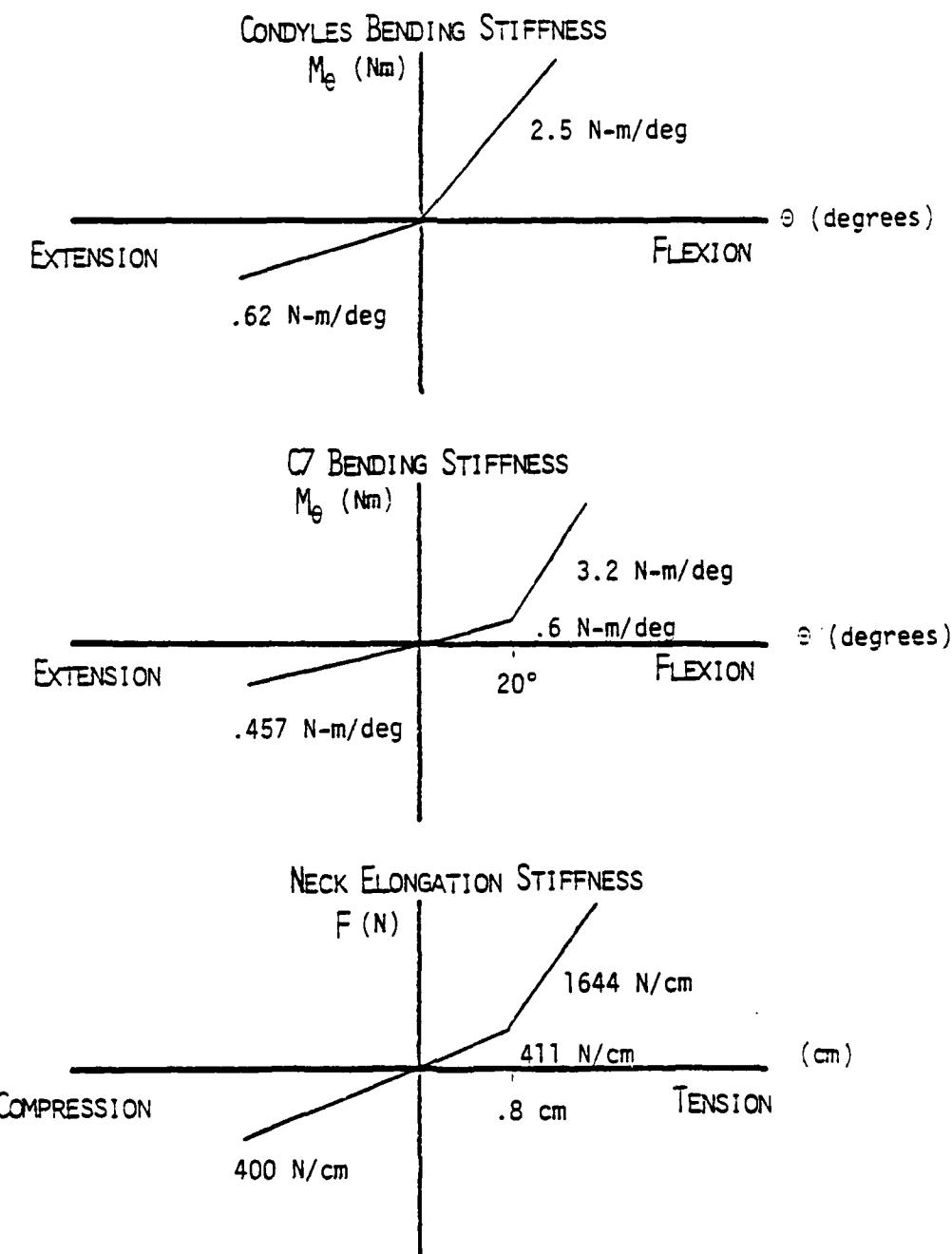
Figure 207.   Bilinear Load-Deflection Data for
Long Neck Model with T1(-4,3) Pivot.

109
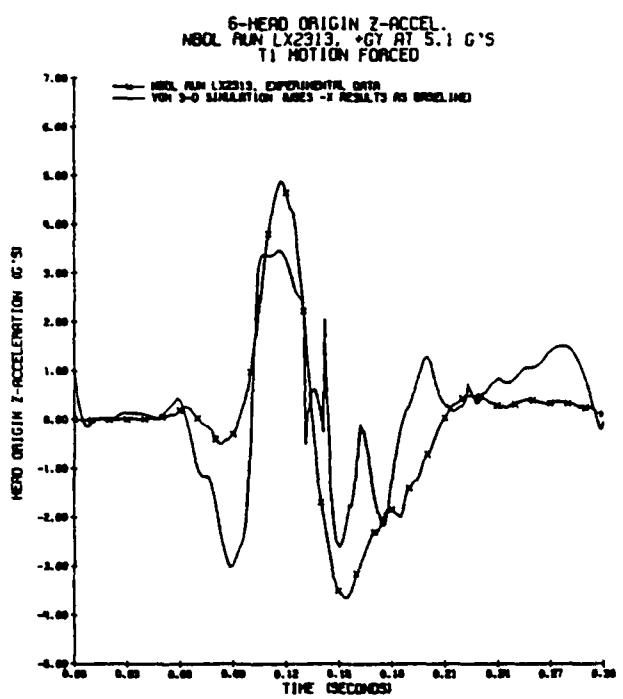
Figure 208. Head Z-Acceleration for +5Gy with Initial Lateral Offset at T1, LX2313.
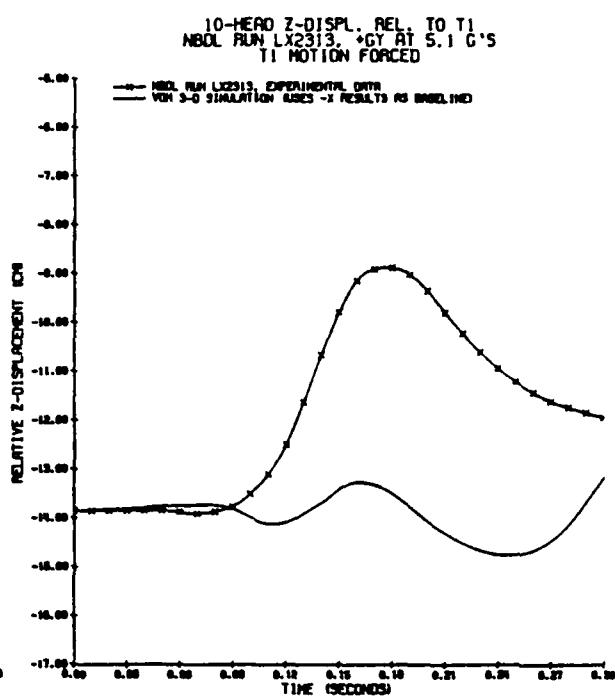


Figure 209. Head Z-Displacement for +5Gy with Initial Lateral Offset at T1, LX2313.
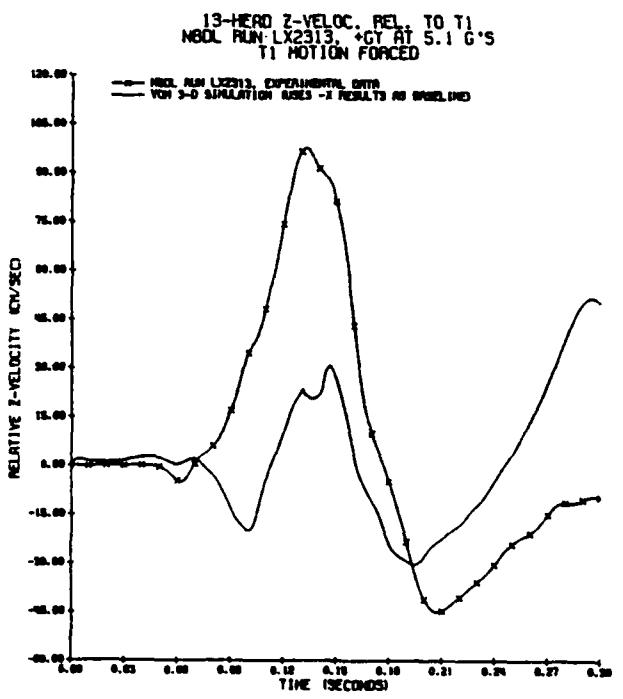


Figure 210. Head Z-Velocity for +5Gy with Initial Lateral Offset at T1, LX2313.
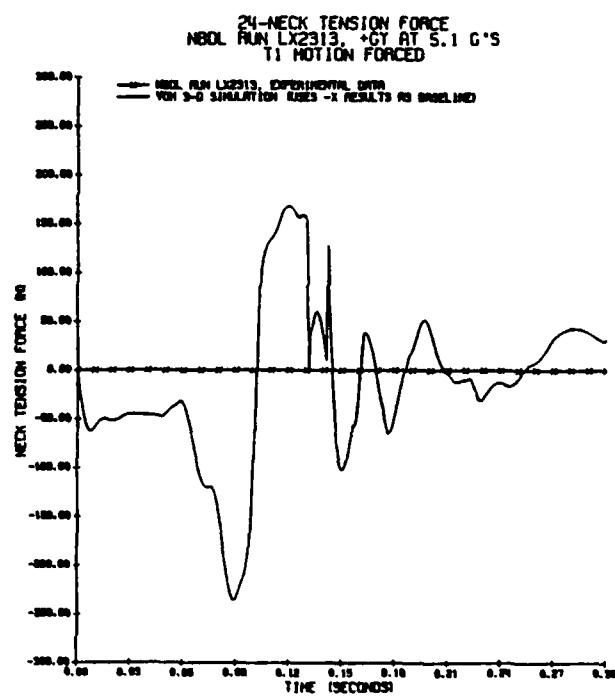


Figure 211. Neck Tension Force for +5Gy with Initial Lateral Offset at T1, LX2313.
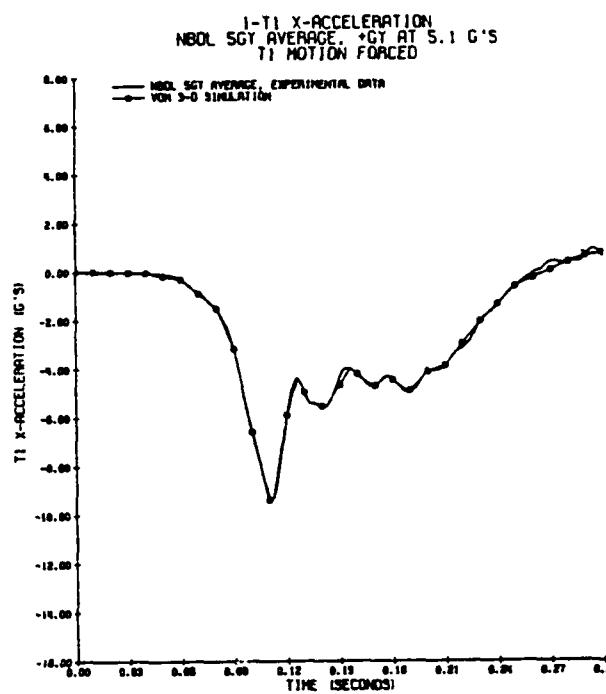
110

1-T1 X-ACCELERATION
NBDL SGY AVERAGE, +GY AT 5.1 G'S
T1 MOTION FORCED

2-T1 Y-ACCELERATION
NBDL SGY AVERAGE, +GY AT 5.1 G'S
T1 MOTION FORCED

Figure 212. NBDL Averaged Data for T1 X-Axis
Acceleration at +5Gy.

Figure 213. NBDL Averaged Data for T1 Y-Axis
Acceleration at +5Gy.

3-T1 Z-ACCELERATION
NBDL SGY AVERAGE, +GY AT 5.1 G'S
T1 MOTION FORCED
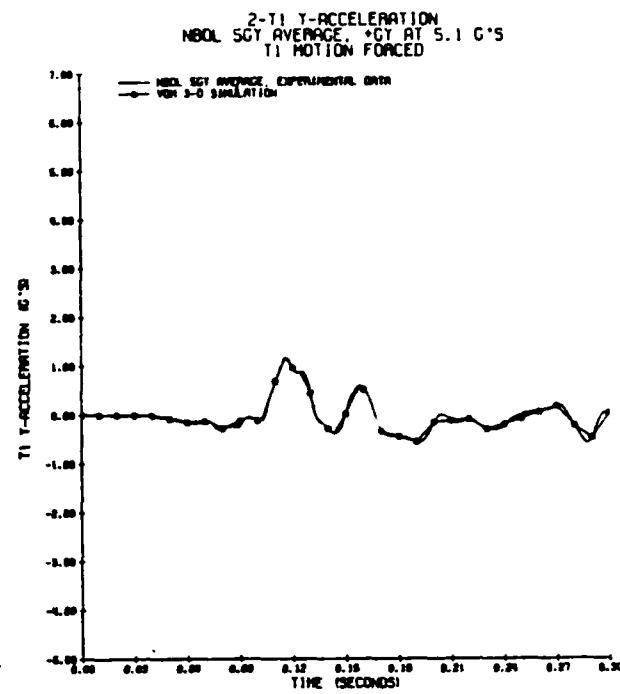
4-HEAD ORIGIN X-ACCEL.
NBDL SGY AVERAGE, +GY AT 5.1 G'S
T1 MOTION FORCED
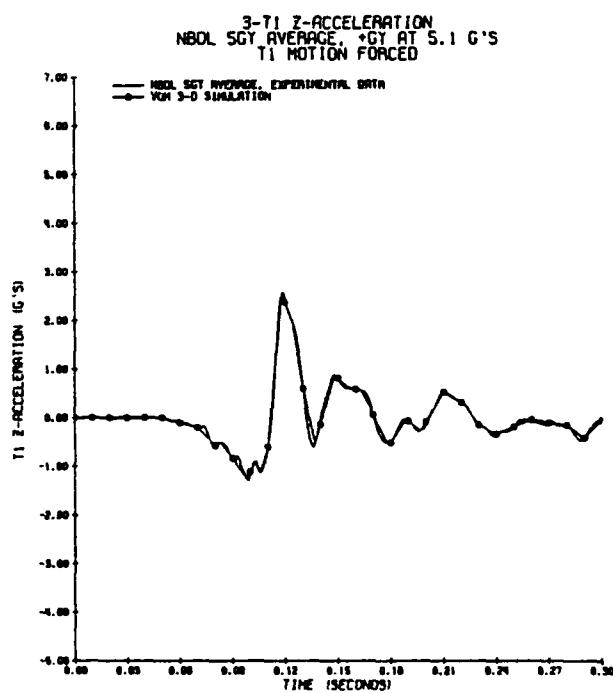
Figure 214. NBDL Averaged Data for T1 Z-Axis
Acceleration at +5Gy.
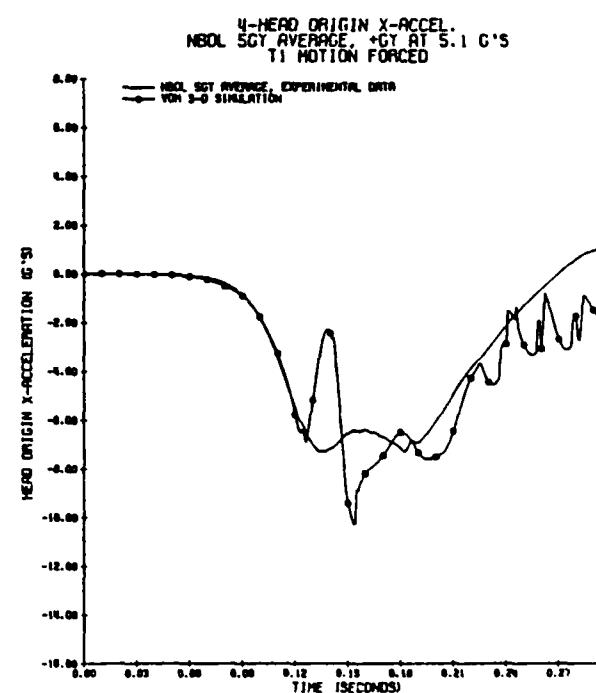
Figure 215. Head Origin X-Acceleration for
Phase II Neck Model Data at +5Gy.

111
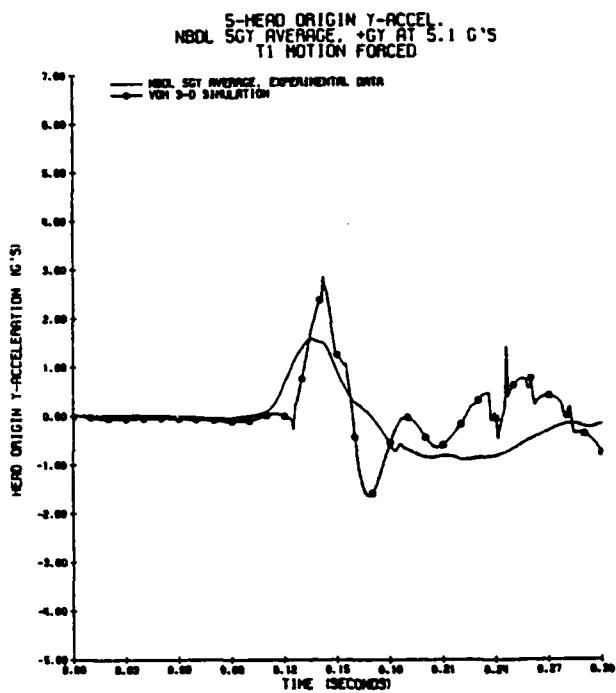
**Figure 216.** Head Origin Y-Acceleration for Phase II Neck Model Data at +5Gy.
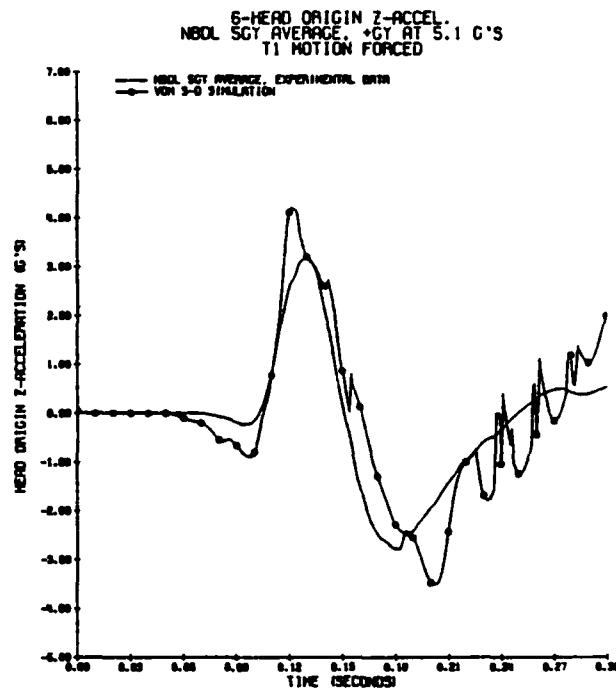


**Figure 217.** Head Origin Z-Acceleration for Phase II Neck Model Data at +5Gy.
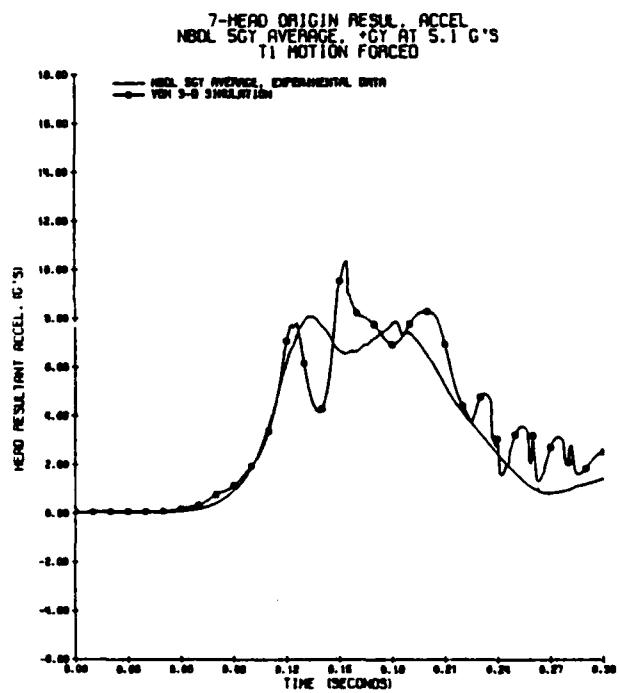


**Figure 218.** Head Resultant Acceleration for Phase II Neck Model Data at +5Gy.
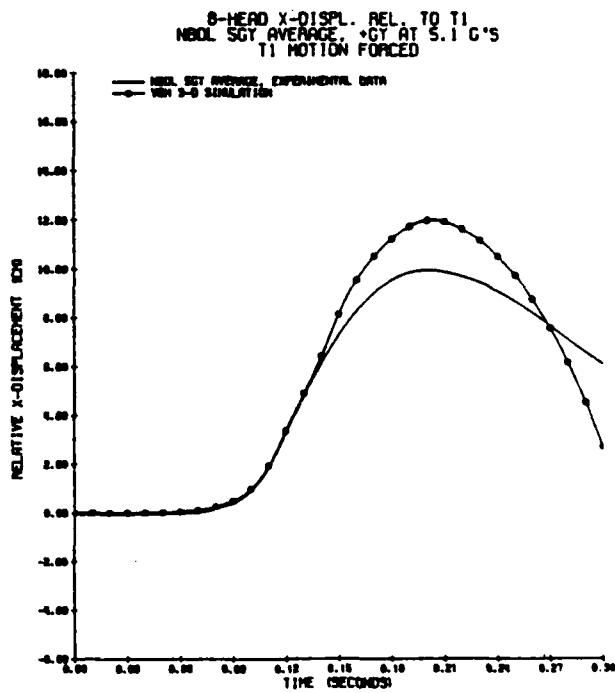


**Figure 219.** Head X-Displacement for Phase II Neck Model Data at +5Gy.

112
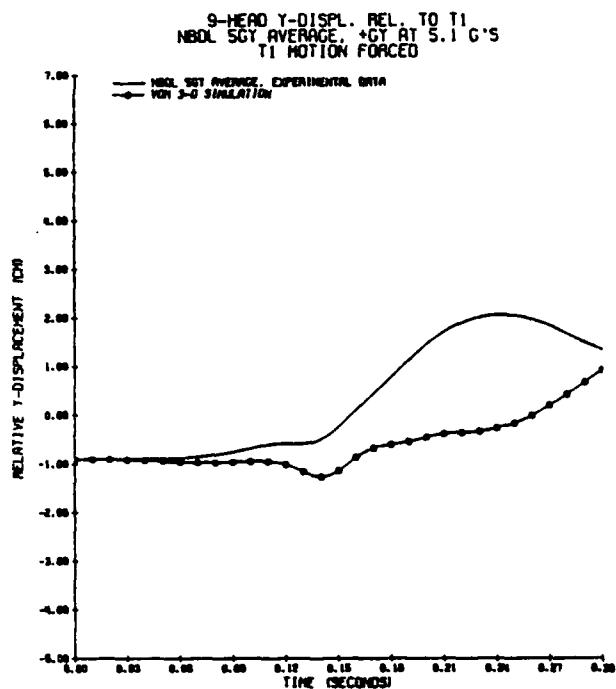
Figure 220. Head Y-Displacement for Phase II
Neck Model Data at +5Gy.
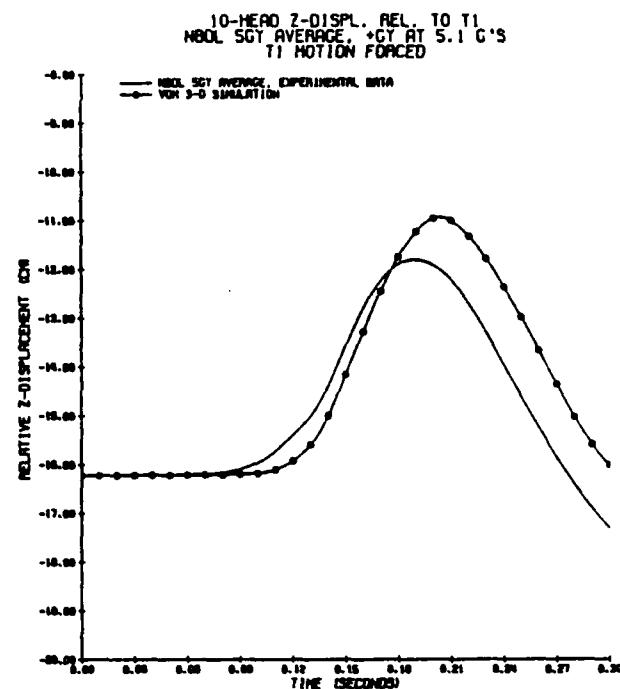


Figure 221. Head Z-Displacement for Phase II
Neck Model Data at +5Gy.
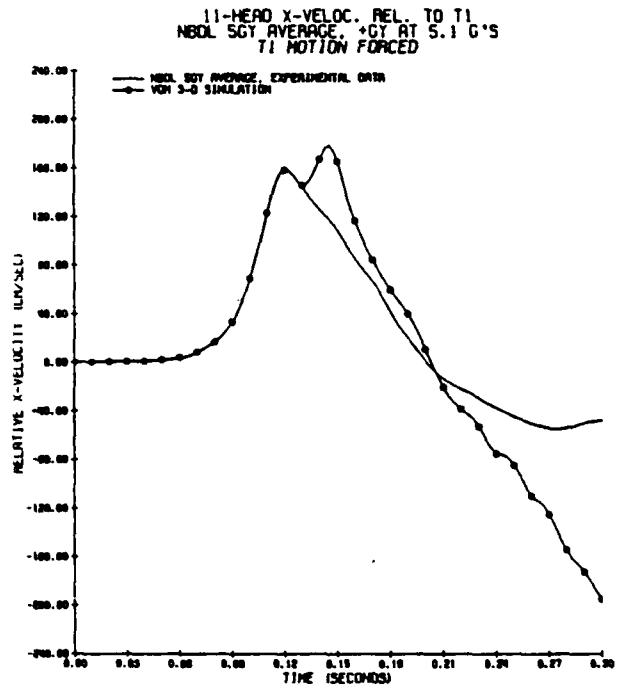


Figure 222. Head X-Velocity for Phase II Neck
Model Data at +5Gy.
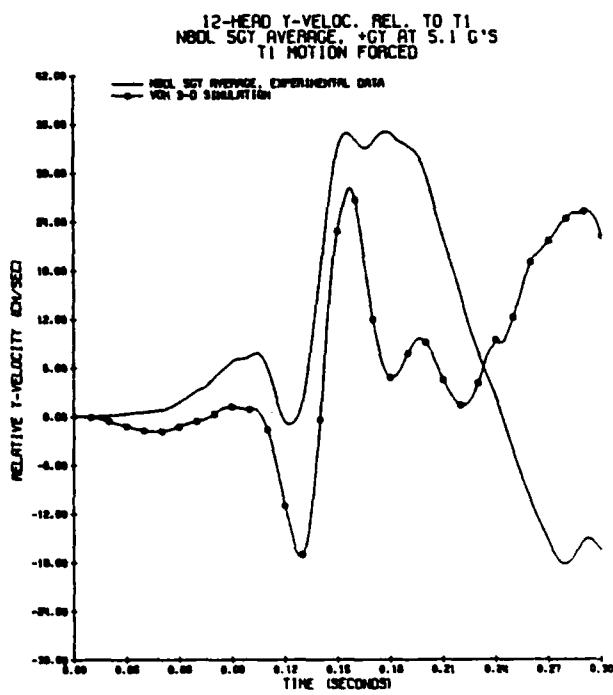


Figure 223. Head Y-Velocity for Phase II Neck
Model Data at +5Gy.

113
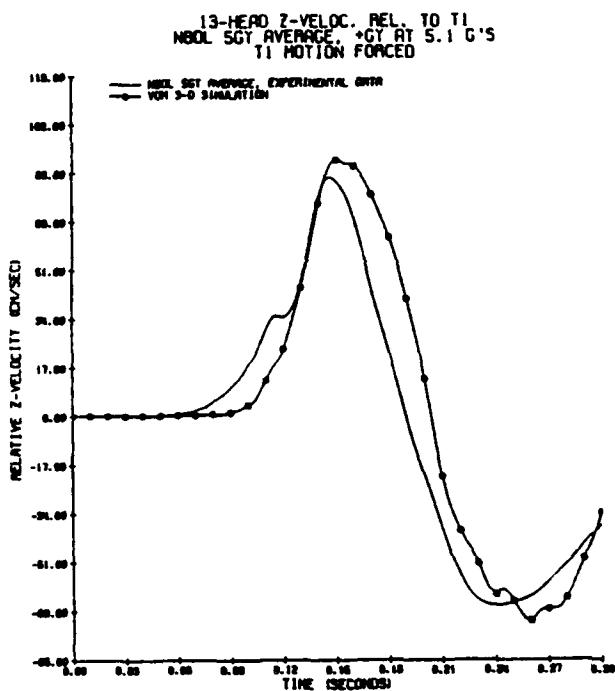
Figure 224. Head Z-Velocity for Phase II Neck Model Data at +5Gy.
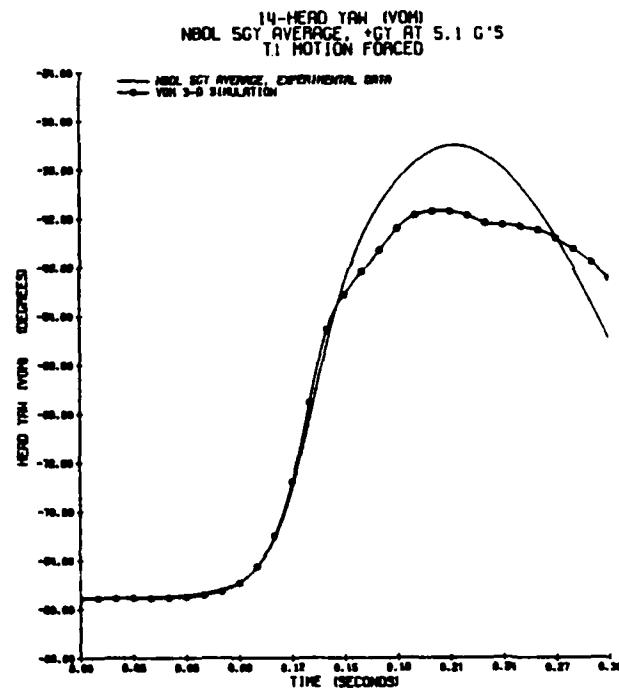


Figure 225. Head Yaw for Phase II Neck Model Data at +5Gy.
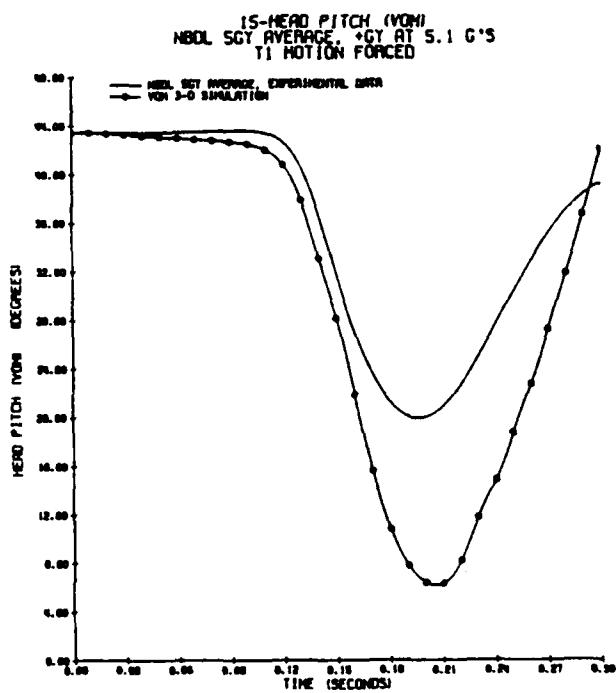


Figure 226. Head Pitch for Phase II Neck Model Data at +5Gy.
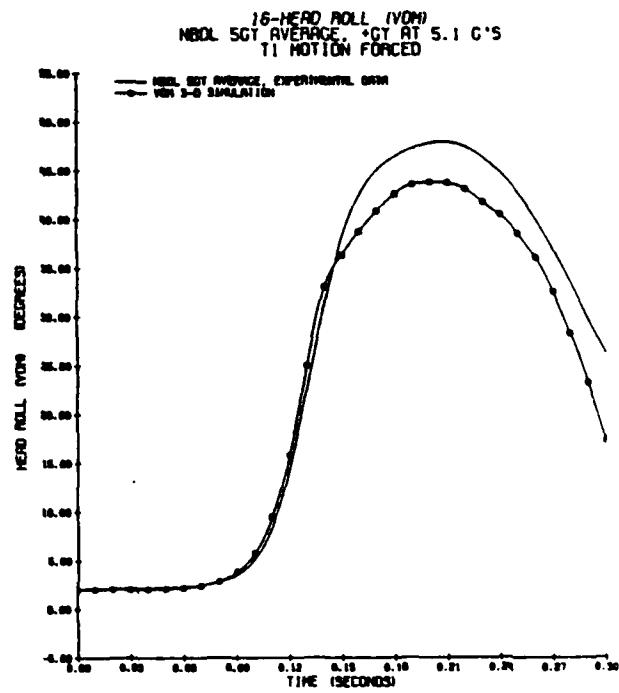


Figure 227. Head Roll for Phase II Neck Model Data at +5Gy.

114
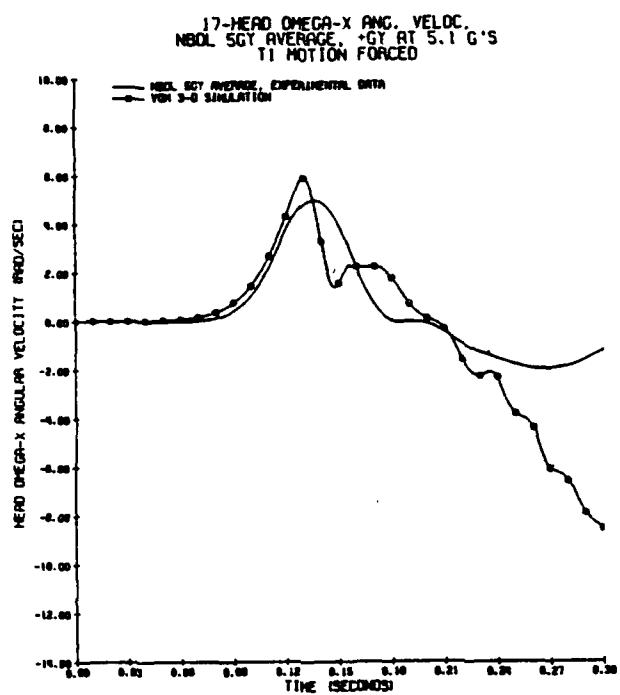
Figure 228. Head X-Axis Angular Velocity for Phase II Neck Model Data at +5Gy.
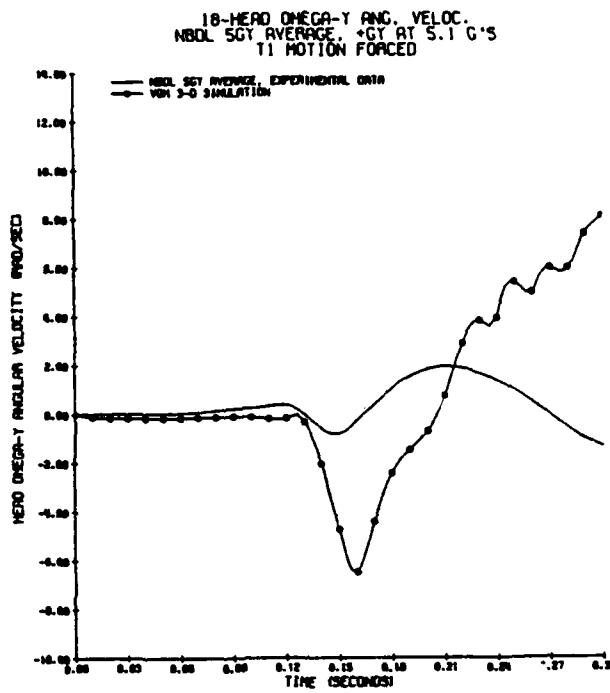


Figure 229. Head Y-Axis Angular Velocity for Phase II Neck Model Data at +5Gy.
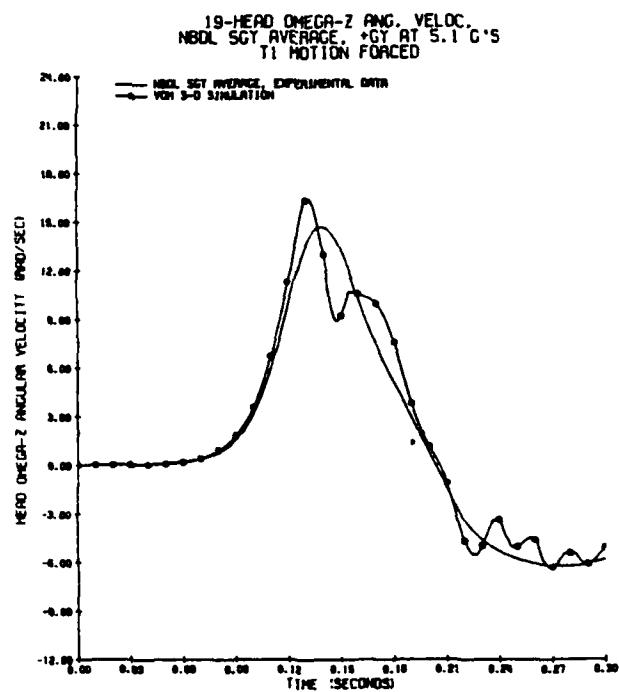


Figure 230. Head Z-Axis Angular Velocity for Phase II Neck Model Data at +5Gy.
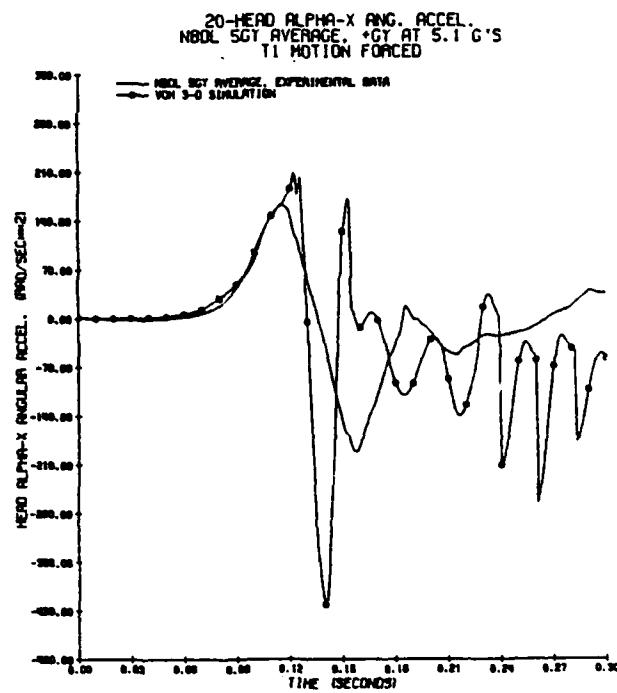


Figure 231. Head X-Axis Angular Acceleration for Phase II Neck Model Data at +5Gy.
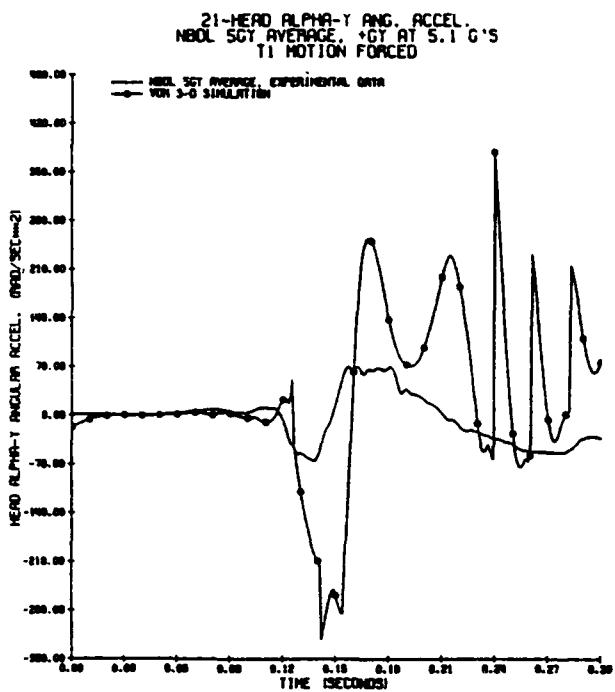
Figure 232. Head Y-Axis Angular Acceleration for Phase II Neck Model Data at +5Gy.
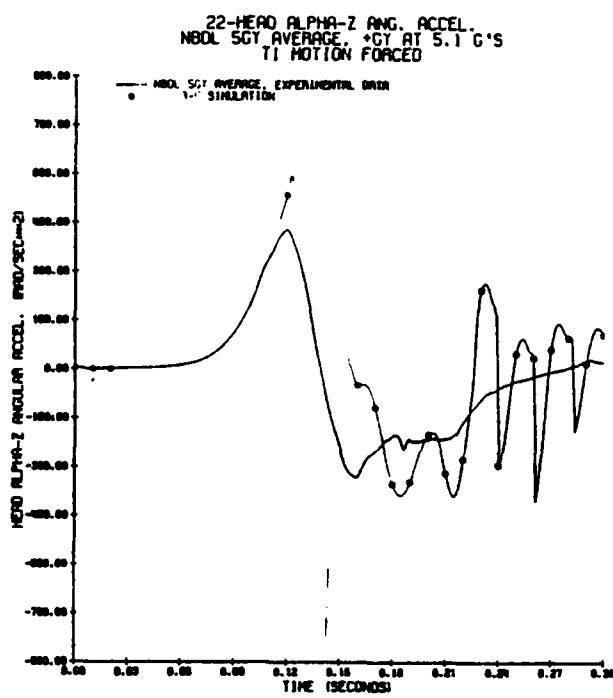


Figure 233. Head Z-Axis Angular Acceleration for Phase II Neck Model Data at +5Gy.
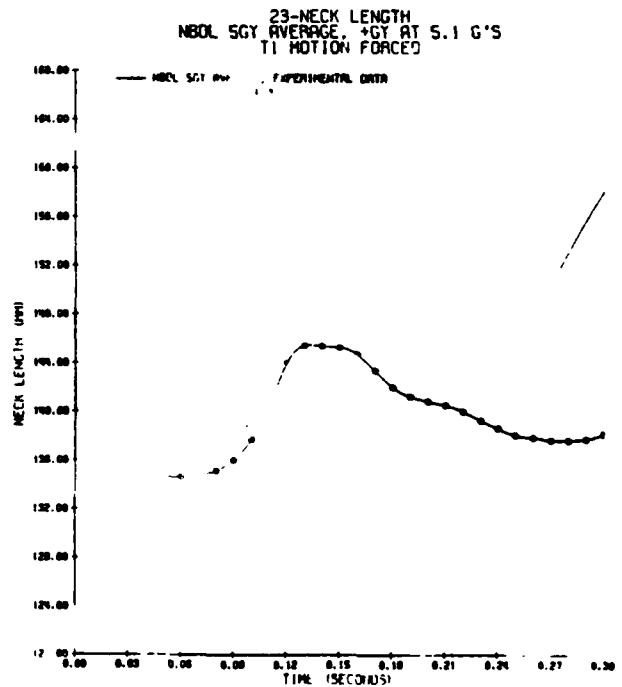


Figure 234. Neck Length for Phase II Neck Model Data at +5Gy.
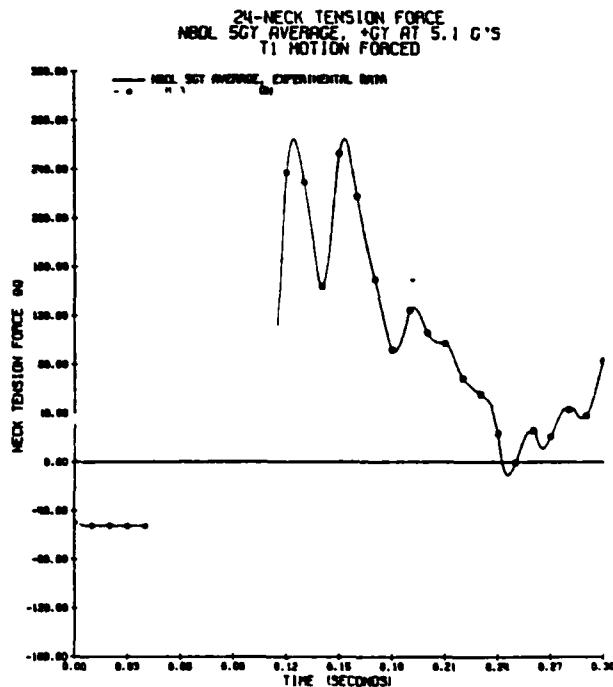


Figure 235. Neck Tension Force for Phase II Neck Model Data at +5Gy.
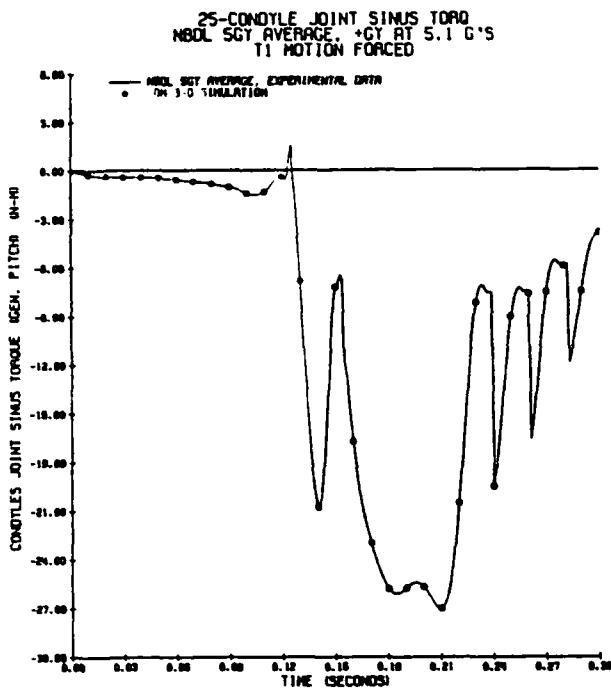
Figure 236. Condyle Joint Sinus Torque for Phase II Neck Model Data at +5Gy.
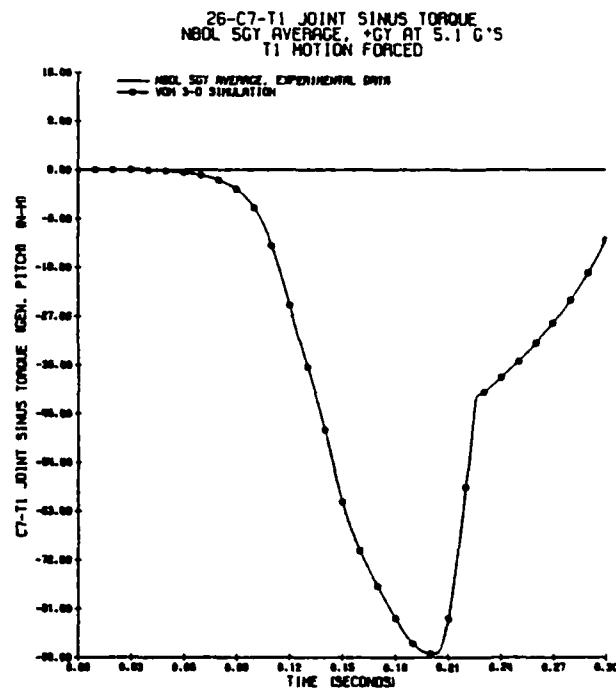
Figure 237. C7-T1 Joint Sinus Torque for Phase II Neck Model Data at +5Gy.
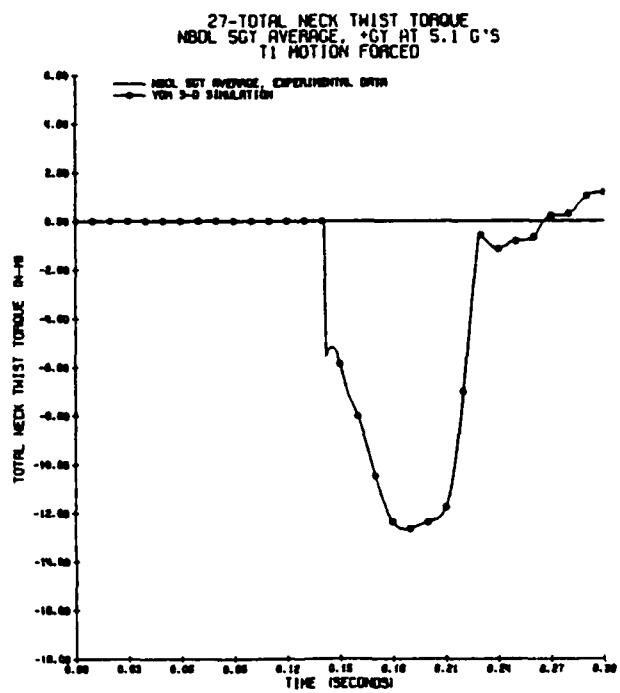
Figure 238. Total Neck Twist Torque for Phase II Neck Model Data at +5Gy.

117
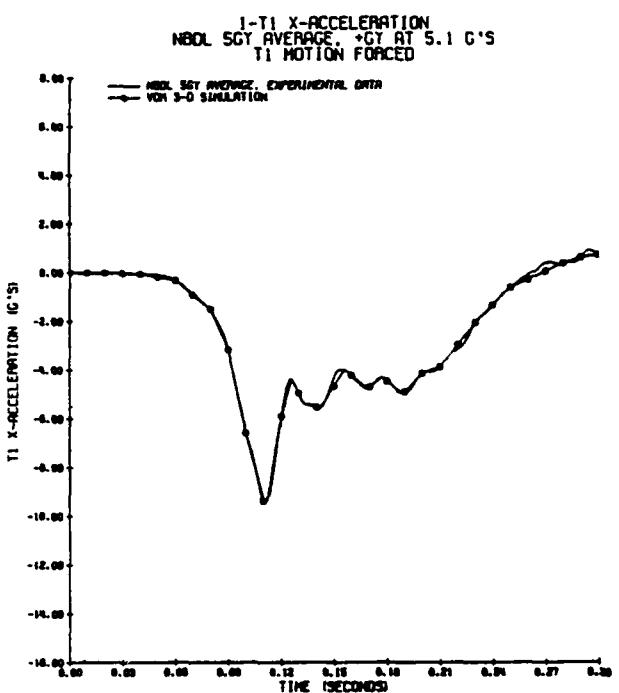
Figure 239. NBDL Averaged Data for T1 X-Axis Acceleration at +5Gy.
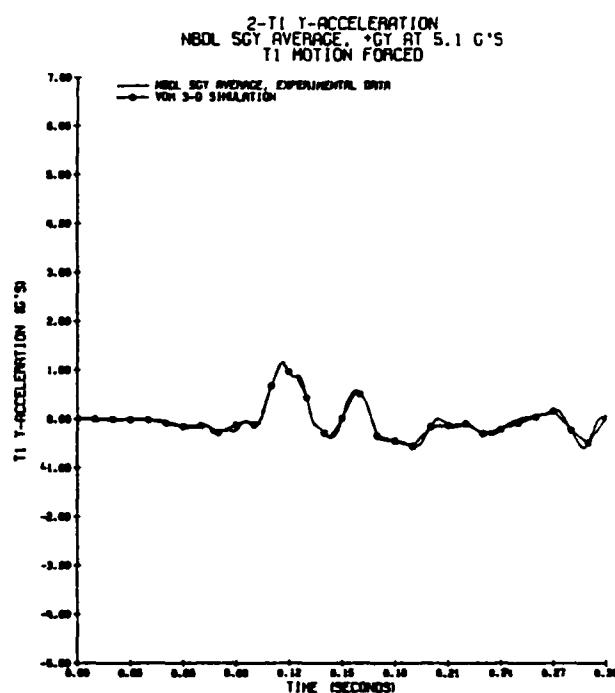


Figure 240. NBDL Averaged Data for T1 Y-Axis Acceleration at +5Gy.
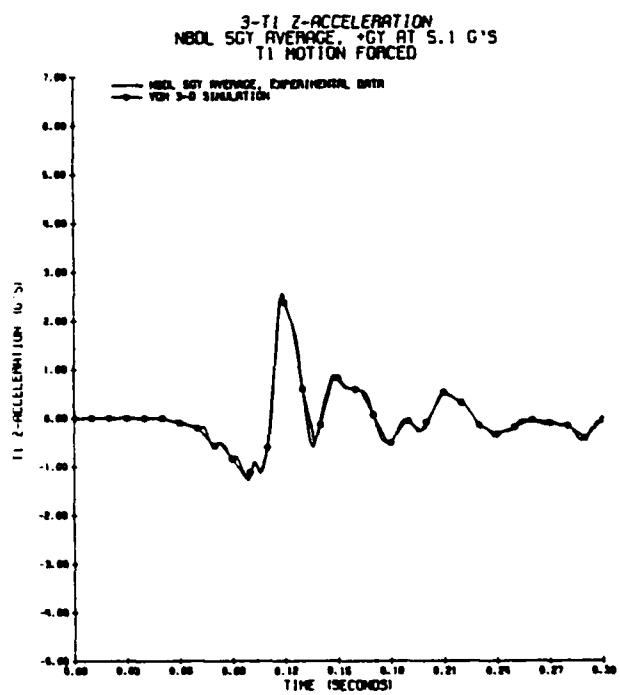


Figure 241. NBDL Averaged Data for T1 Z-Axis Acceleration at +5Gy.
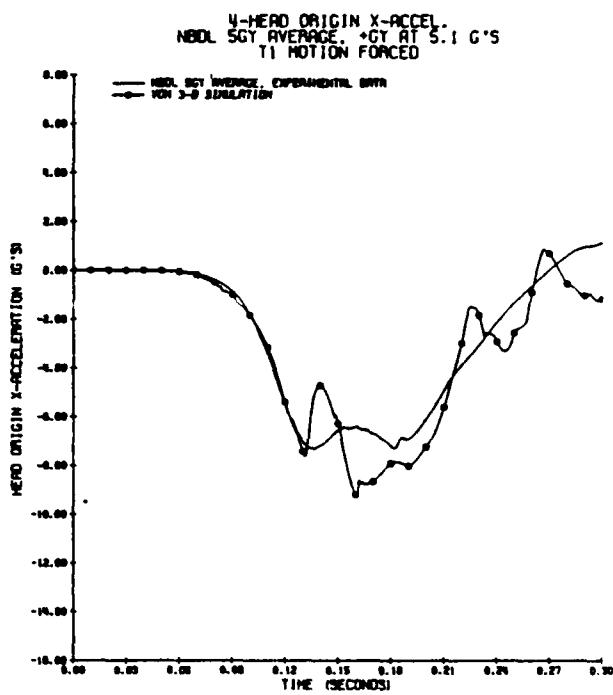


Figure 242. Head X-Acceleration for Head Origin Upper Pivot Point Data at +5Gy.

118
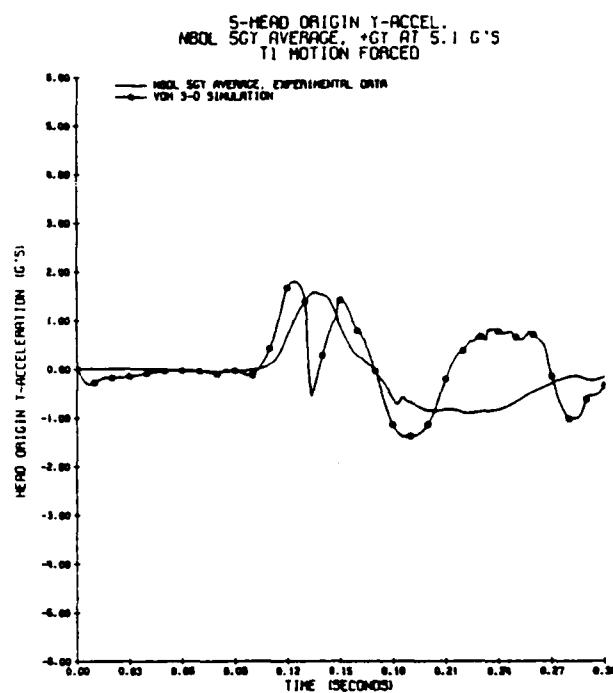
Figure 243.   Head Y-Acceleration for Head Origin
Upper Pivot Point Data at +5Gy.
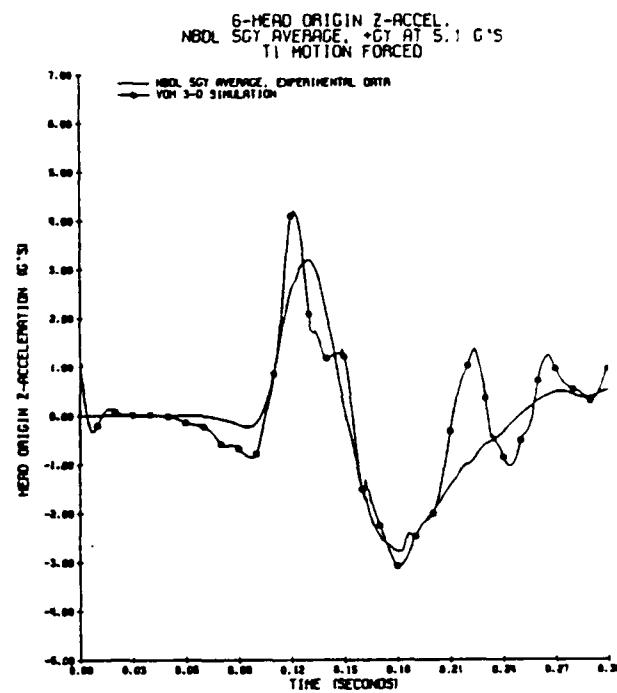


Figure 244.   Head Z-Acceleration for Head Origin
Upper Pivot Point Data at +5Gy.
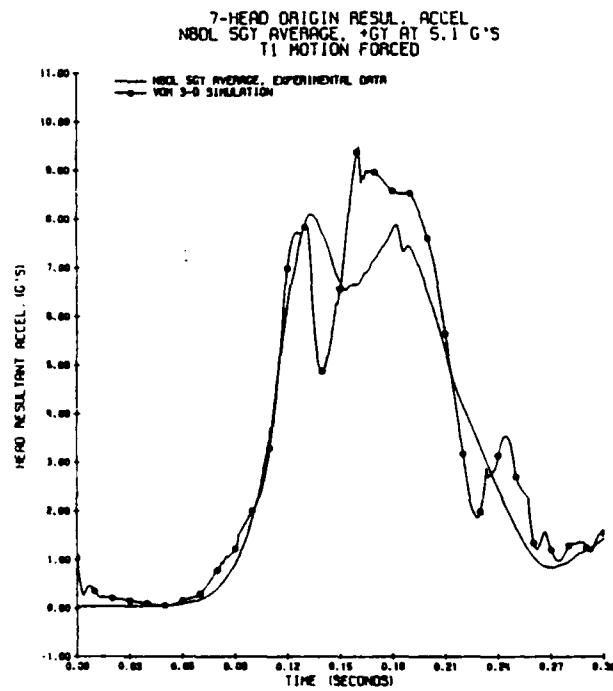


Figure 245.   Head Resultant Acceleration for
Head Origin Upper Pivot Point Data at +5Gy.
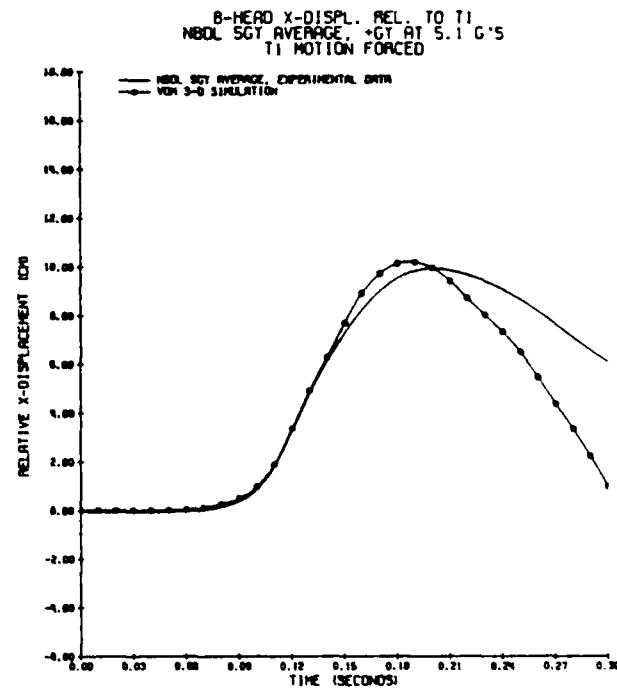


Figure 246.   Head X-Displacement for Head Origin
Upper Pivot Point Data at +5Gy.

119
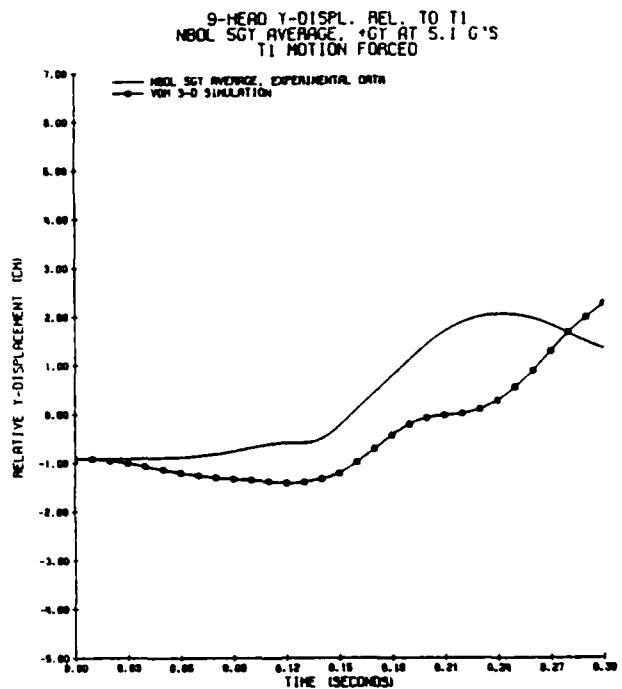
Figure 247. Head Y-Displacement for Head Origin Upper Pivot Point Data at +5Gy.
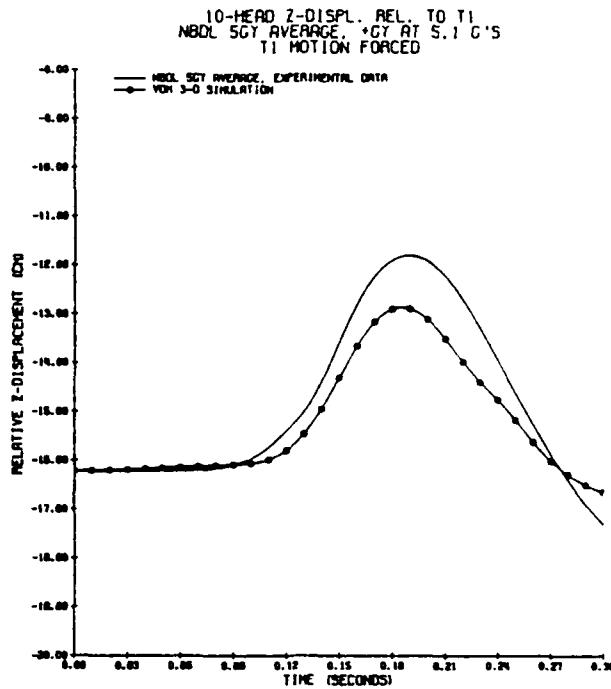


Figure 248. Head Z-Displacement for Head Origin Upper Pivot Point Data at +5Gy.
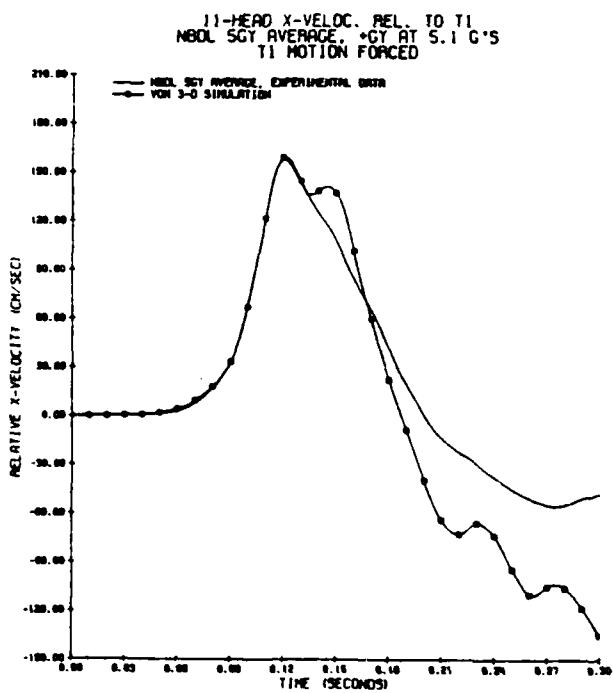


Figure 249. Head X-Velocity for Head Origin Upper Pivot Point Data at +5Gy.
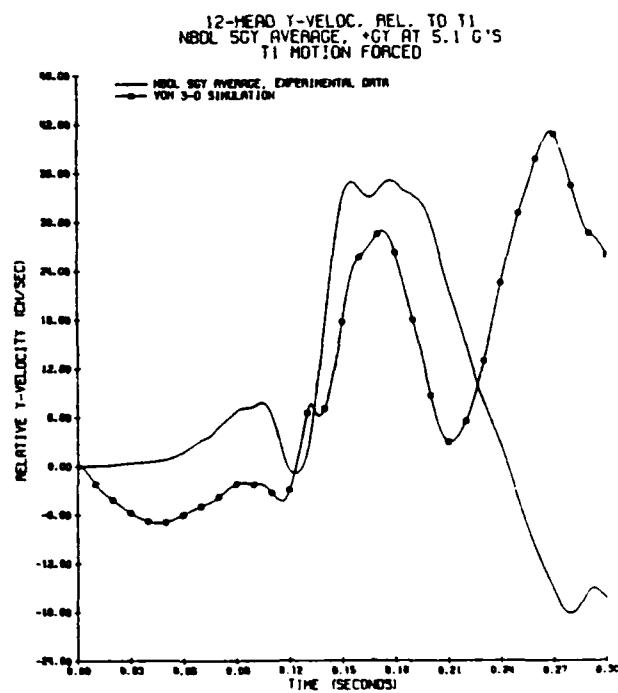


Figure 250. Head Y-Velocity for Head Origin Upper Pivot Point Data at +5Gy.

120

13-HEAD Z-VELOC. REL. TO T1
NBDL SGT AVERAGE, +GY AT 5.1 G'S
T1 MOTION FORCED

14-HEAD YAW (VOM)
NBDL SGT AVERAGE, +GY AT 5.1 G'S
T1 MOTION FORCED
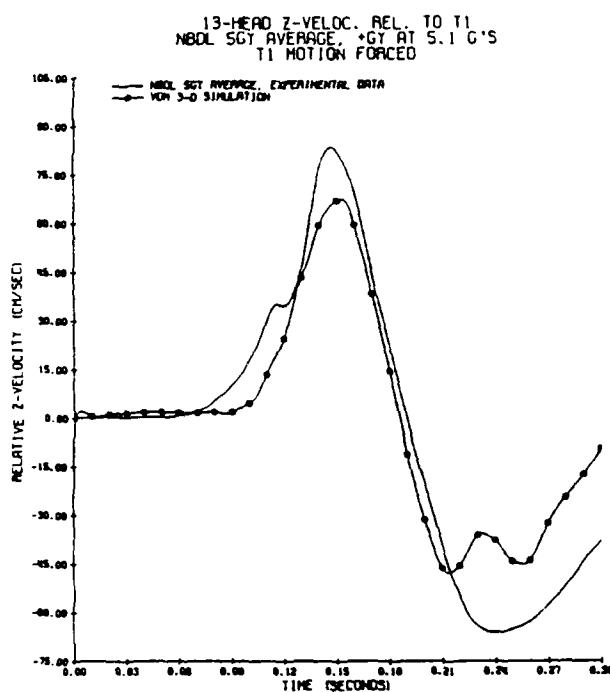
Figure 251.  Head Z-Velocity for Head Origin
Upper Pivot Point Data at +5Gy.
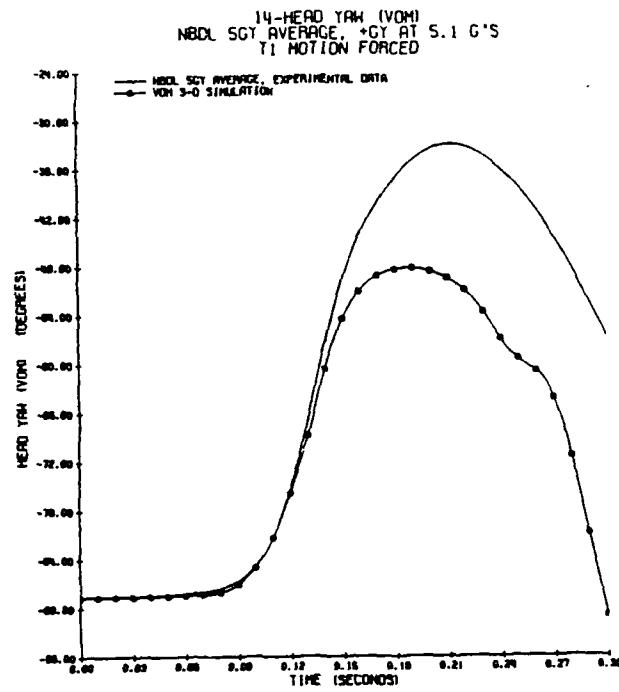
Figure 252.  Head Yaw for Head Origin Upper
Pivot Point Data at +5Gy.

15-HEAD PITCH (VOM)
NBDL SGT AVERAGE, +GY AT 5.1 G'S
T1 MOTION FORCED

16-HEAD ROLL (VOM)
NBDL SGT AVERAGE, +GY AT 5.1 G'S
T1 MOTION FORCED
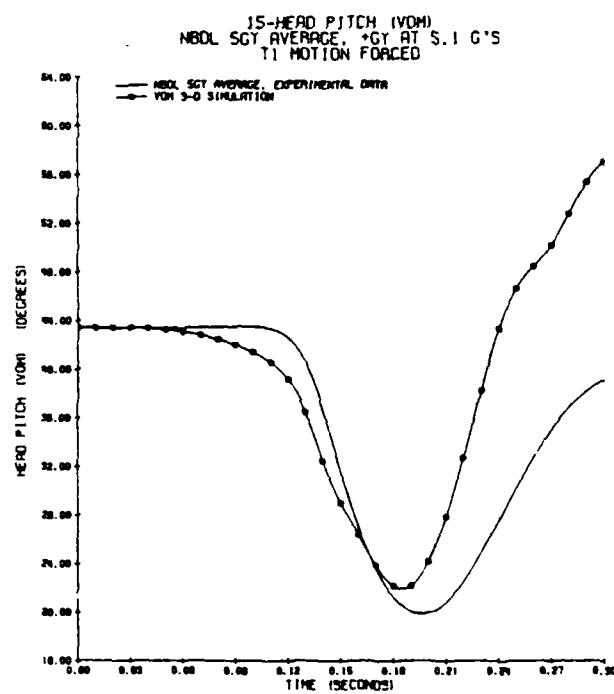
Figure 253.  Head Pitch for Head Origin Upper
Pivot Point Data at +5Gy.
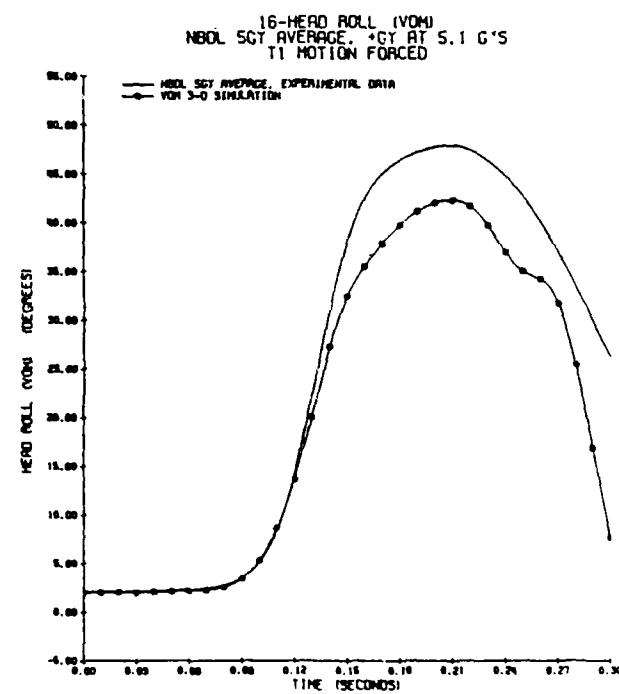
Figure 254.  Head Roll for Head Origin Upper
Pivot Point Data at +5Gy.

121

17-HEAD OMEGA-X ANG. VELOC.
NBDL 5GY AVERAGE, +GY AT 5.1 G'S
TI MOTION FORCED
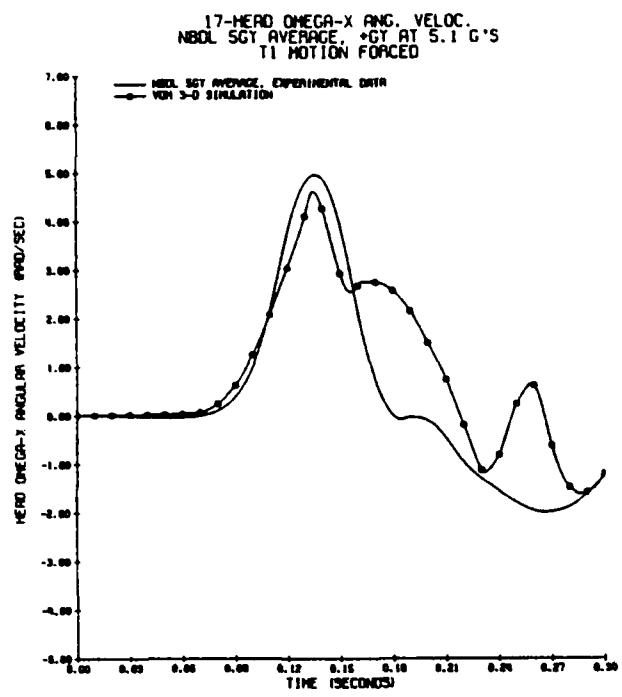
Figure 255. Head X-Axis Angular Velocity for
Head Origin Upper Pivot Point Data at +5Gy.



18-HEAD OMEGA-Y ANG. VELOC.
NBDL 5GY AVERAGE, +GY AT 5.1 G'S
TI MOTION FORCED
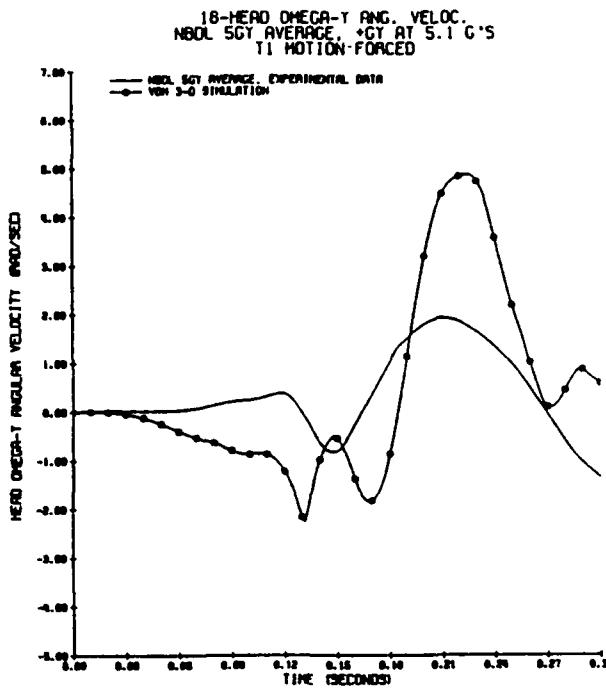
Figure 256. Head Y-Axis Angular Velocity for
Head Origin Upper Pivot Point Data at +5Gy.



19-HEAD OMEGA-Z ANG. VELOC.
NBDL 5GY AVERAGE, +GY AT 5.1 G'S
TI MOTION FORCED
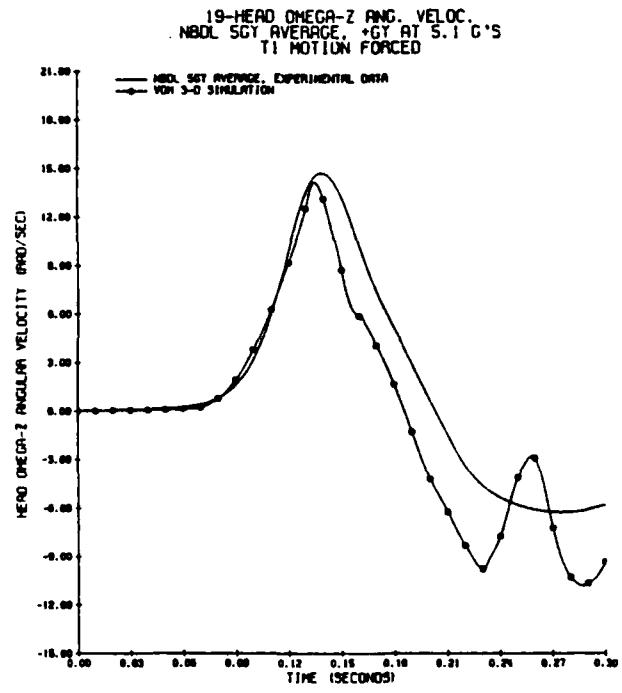
Figure 257. Head Z-Axis Angular Velocity for
Head Origin Upper Pivot Point Data at +5Gy.



20-HEAD ALPHA-X ANG. ACCEL.
NBDL 5GY AVERAGE, +GY AT 5.1 G'S
TI MOTION FORCED
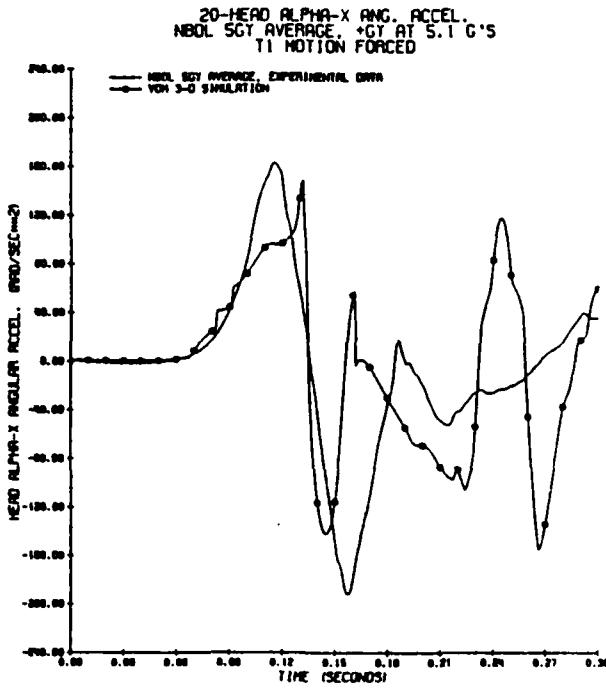
Figure 258. Head X-Axis Angular Acceleration
for Head Origin Upper Pivot Point Data at +5Gy.

122
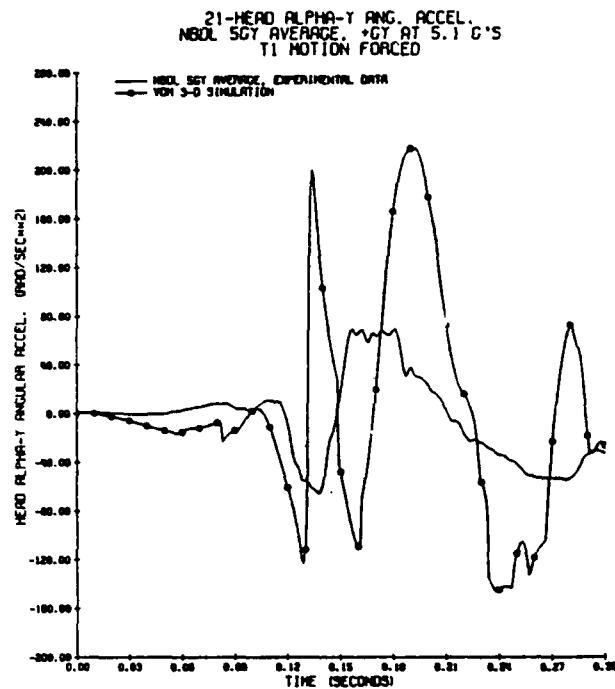
Figure 259. Head Y-Axis Angular Acceleration for Head Origin Upper Pivot Point Data at +5Gy.
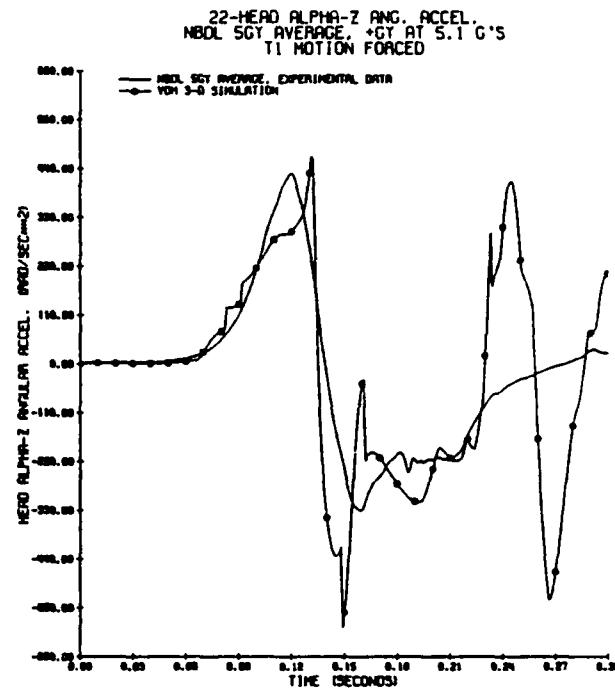


Figure 260. Head Z-Axis Angular Acceleration for Head Origin Upper Pivot Point Data at +5Gy.
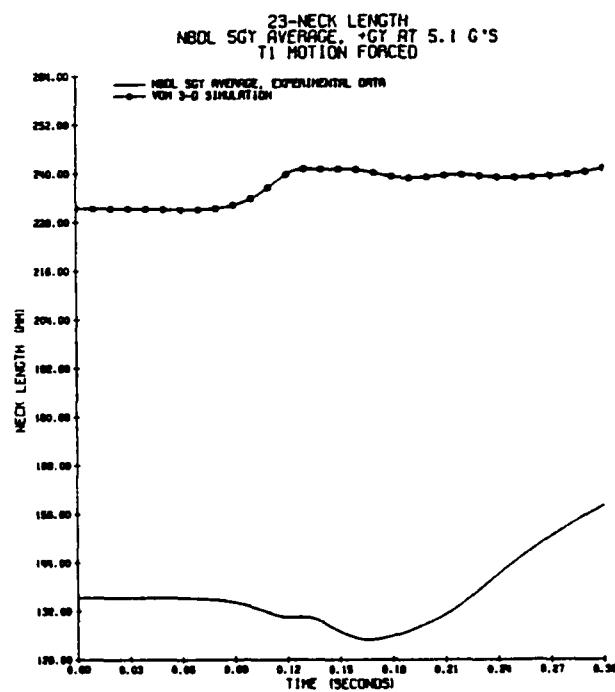


Figure 261. Neck Length for Head Origin Upper Pivot Point Data at +5Gy.
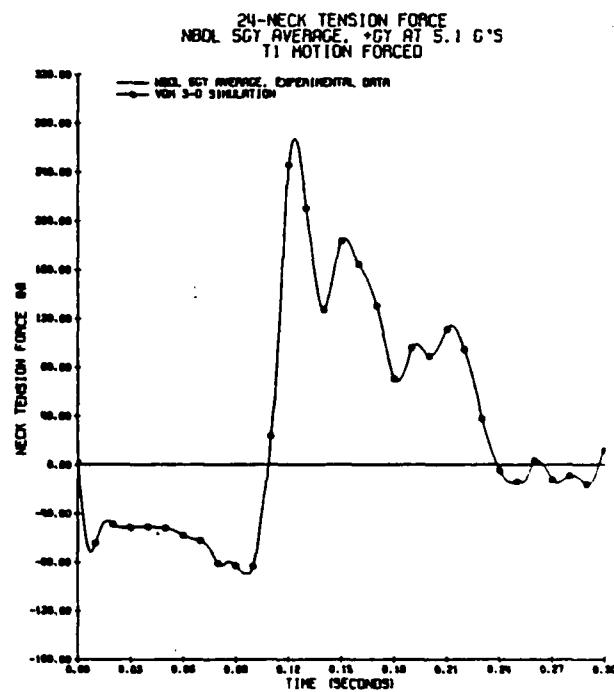


Figure 262. Neck Tension Force for Head Origin Upper Pivot Point Data at +5Gy.
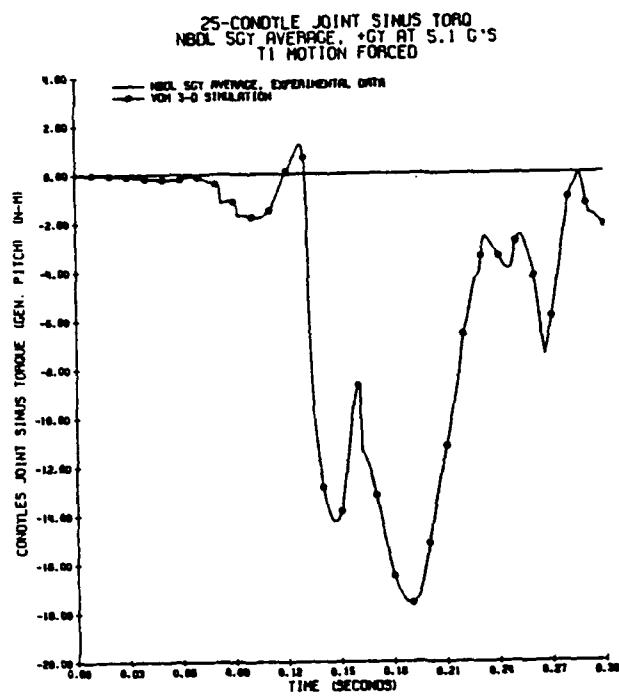
Figure 263. Condyle Joint Sinus Torque for Head Origin Upper Pivot Point Data at +5Gy.
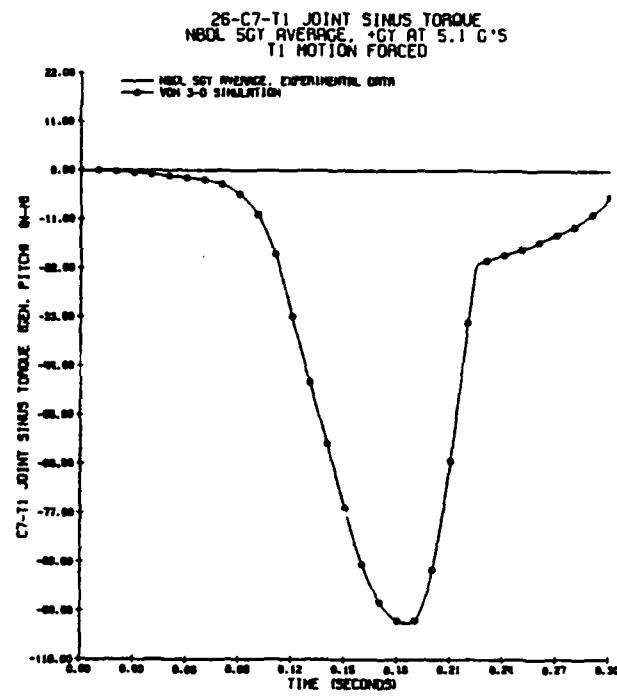


Figure 264. C7-T1 Joint Sinus Torque for Head Origin Upper Pivot Point Data at +5Gy.
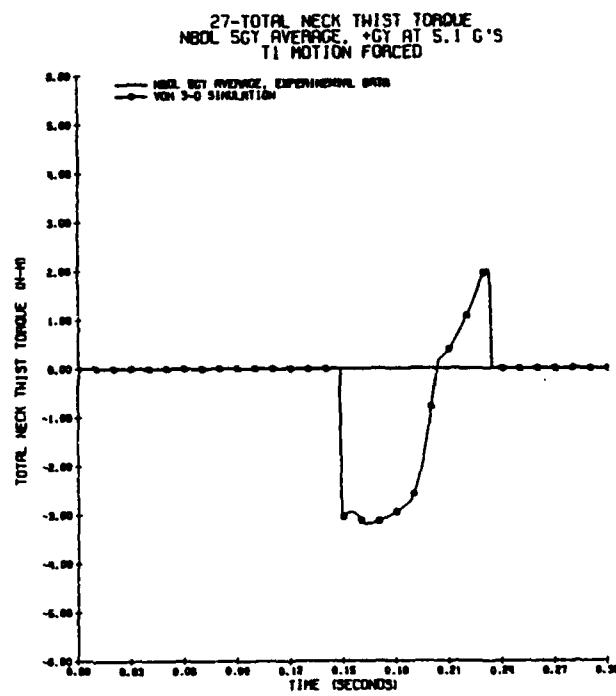


Figure 265. Total Neck Twist Torque for Head Origin Upper Pivot Point Data at +5Gy.
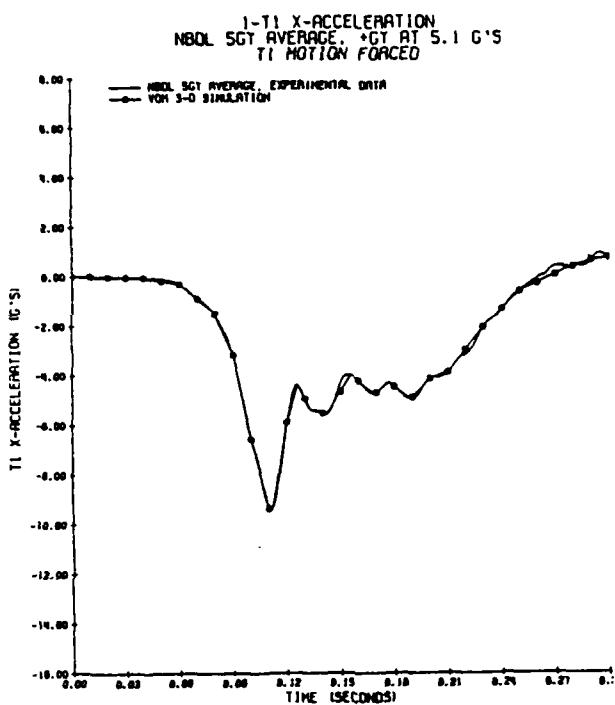
Figure 266. NBDL Averaged Data for T1 X-Axis Acceleration at +5Gy.
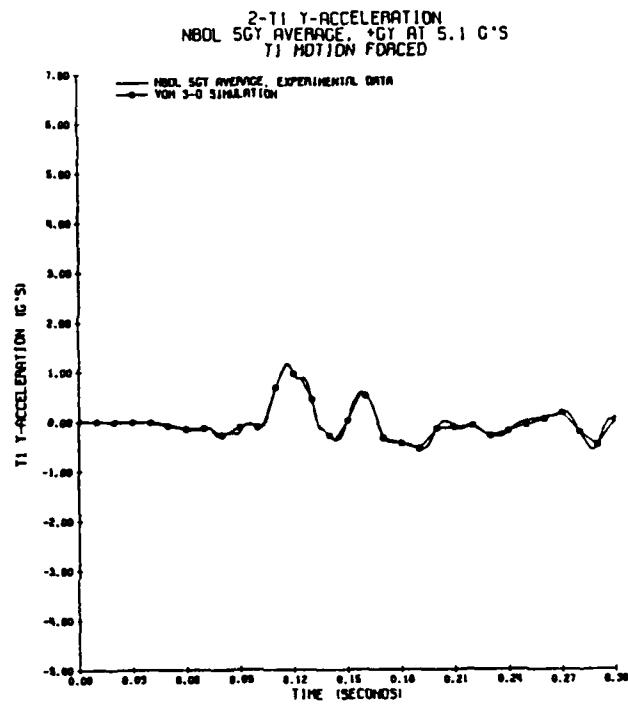


Figure 267. NBDL Averaged Data for T1 Y-Axis Acceleration at +5Gy.
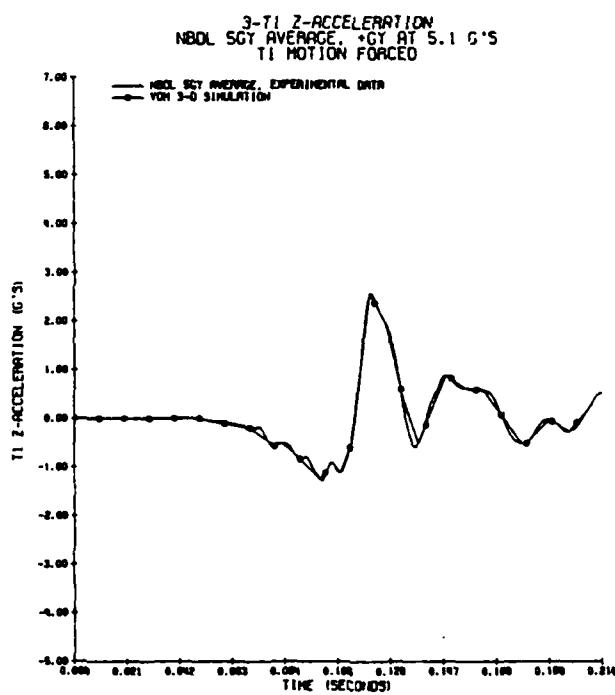


Figure 268. NBDL Averaged Data for T1 Z-Axis Acceleration at +5Gy.
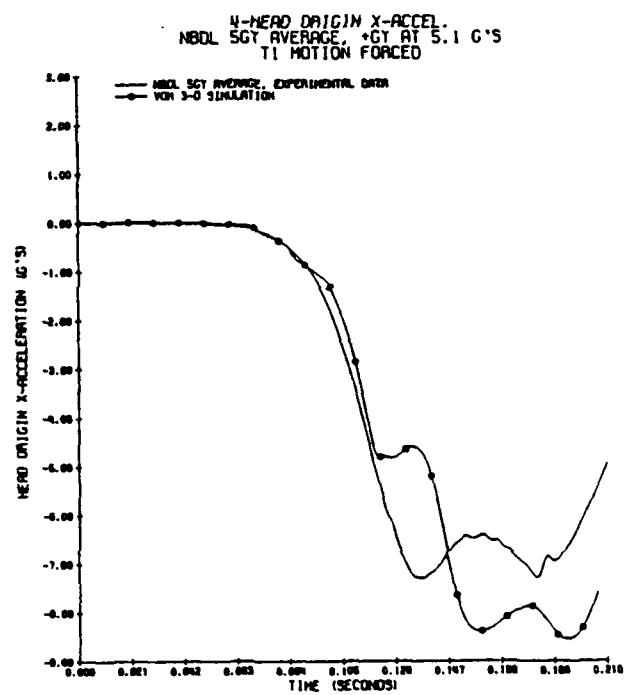


Figure 269. Head X-Acceleration for Long Neck Model with T1(-5,6) Pivot at +5Gy.

125
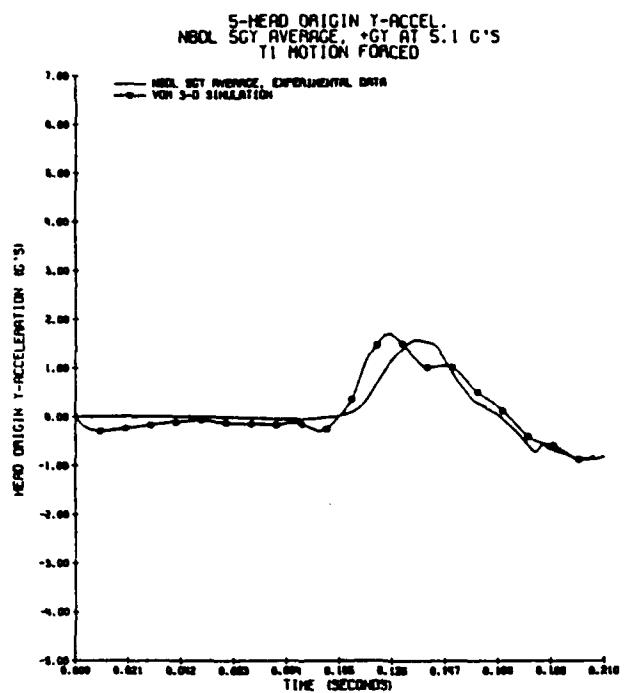
Figure 270. Head Y-Acceleration for Long Neck Model with T1(-5,6) Pivot at +5Gy.
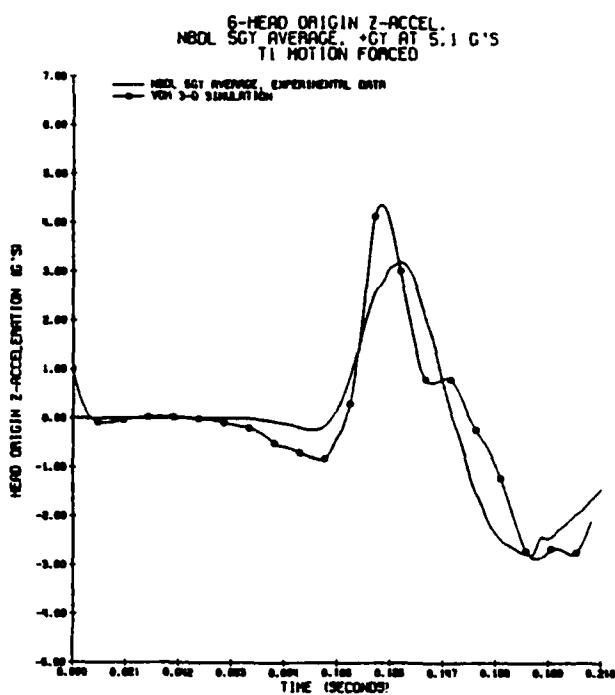


Figure 271. Head Z-Acceleration for Long Neck Model with T1(-5,6) Pivot at +5Gy.
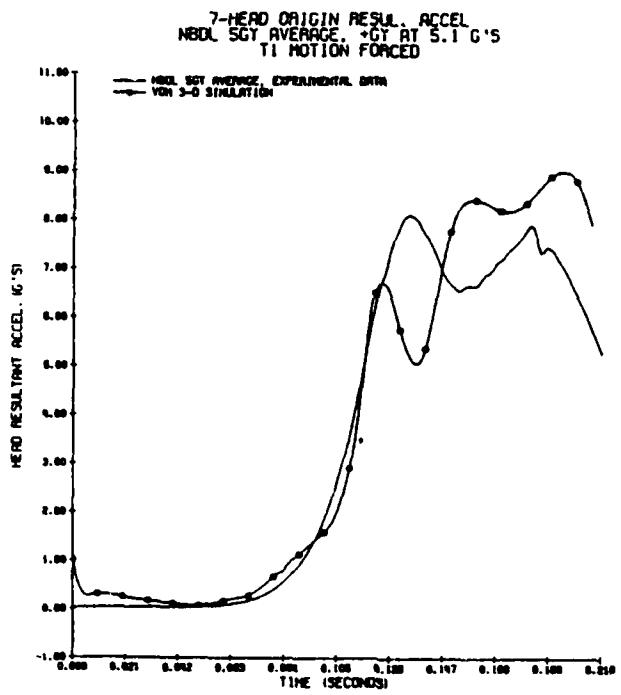


Figure 272. Head Resultant Acceleration for Long Neck Model with T1(-5,6) Pivot at +5Gy.
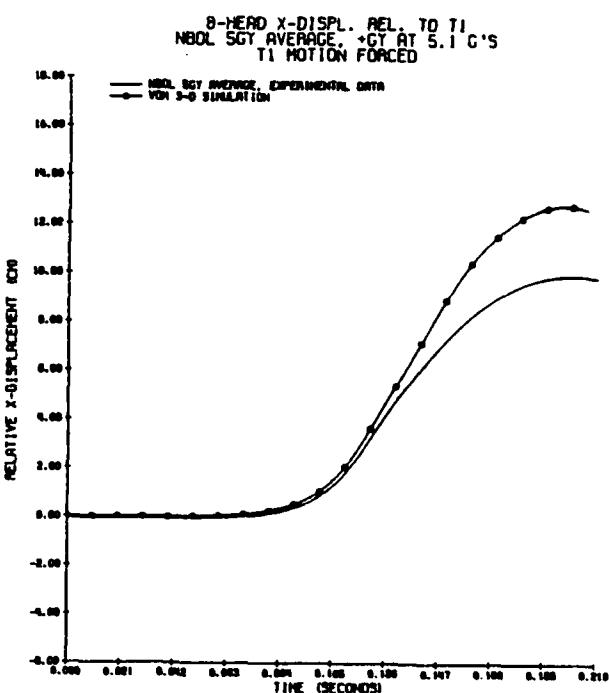


Figure 273. Head X-Displacement for Long Neck Model with T1(-5,6) Pivot at +5Gy.

9-HEAD Y-DISPL. REL. TO T1
NBDL SGT AVERAGE, +GY AT 5.1 G'S
T1 MOTION FORCED
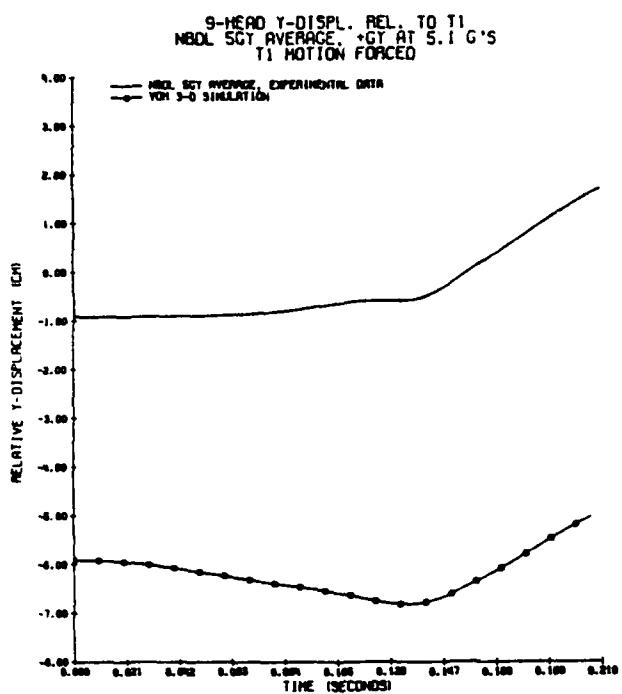
Figure 274. Head Y-Displacement for Long Neck
Model with T1(-5,6) Pivot at +5Gy.



10-HEAD Z-DISPL. REL. TO T1
NBDL SGT AVERAGE, +GY AT 5.1 G'S
T1 MOTION FORCED
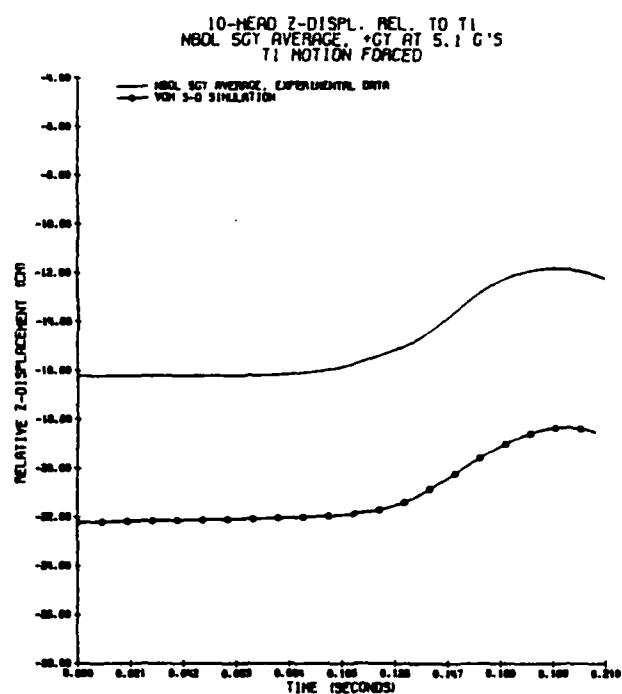
Figure 275. Head Z-Displacement for Long Neck
Model with T1(-5,6) Pivot at +5Gy.



11-HEAD X-VELOC. REL. TO T1
NBDL SGT AVERAGE, +GY AT 5.1 G'S
T1 MOTION FORCED
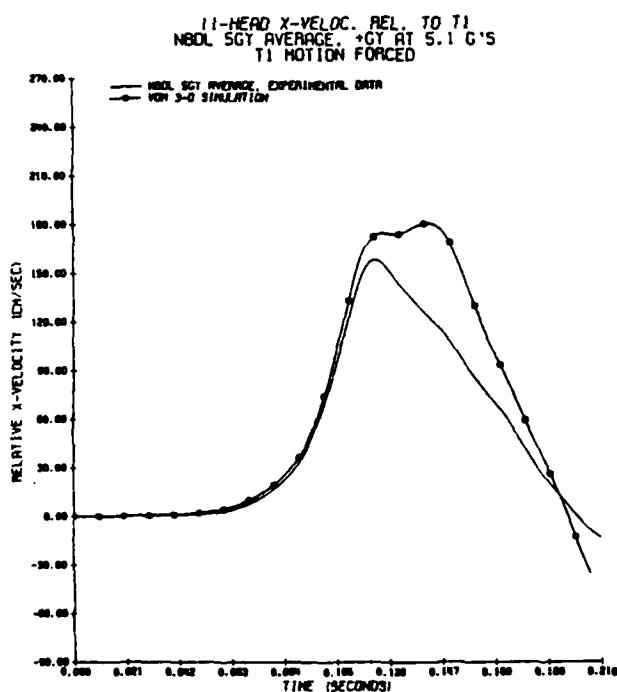
Figure 276. Head X-Velocity for Long Neck Model
with T1(-5,6) Pivot at +5Gy.



12-HEAD Y-VELOC. REL. TO T1
NBDL SGT AVERAGE, +GY AT 5.1 G'S
T1 MOTION FORCED
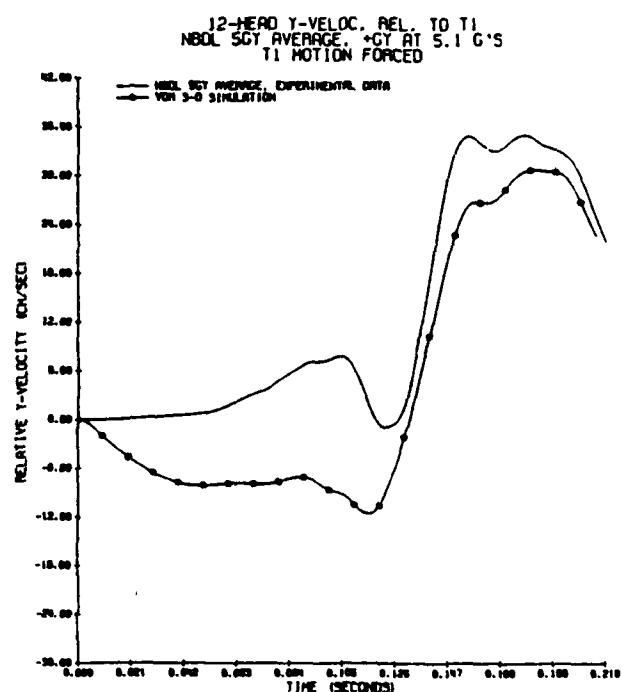
Figure 277. Head Y-Velocity for Long Neck Model
with T1(-5,6) Pivot at +5Gy.

127
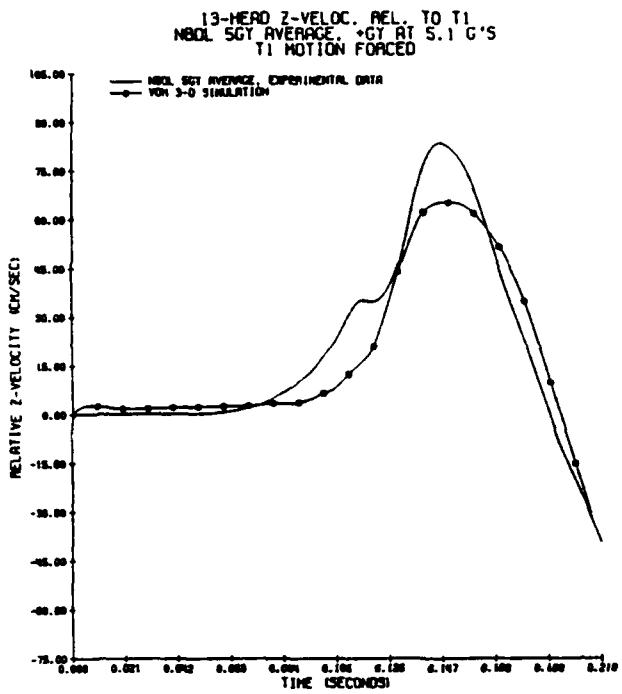
Figure 278. Head Z-Velocity for Long Neck Model with T1(-5.6) Pivot at +5Gy.
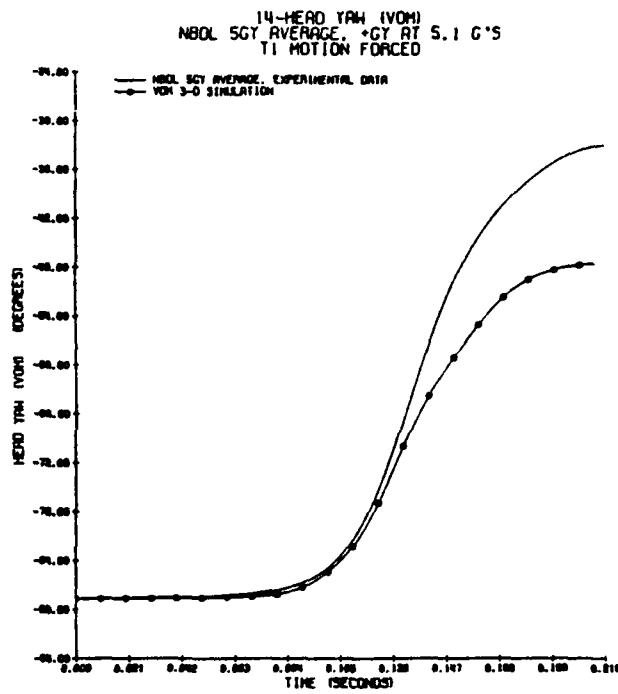


Figure 279. Head Yaw for Long Neck Model with T1(-5.6) Pivot at +5Gy.
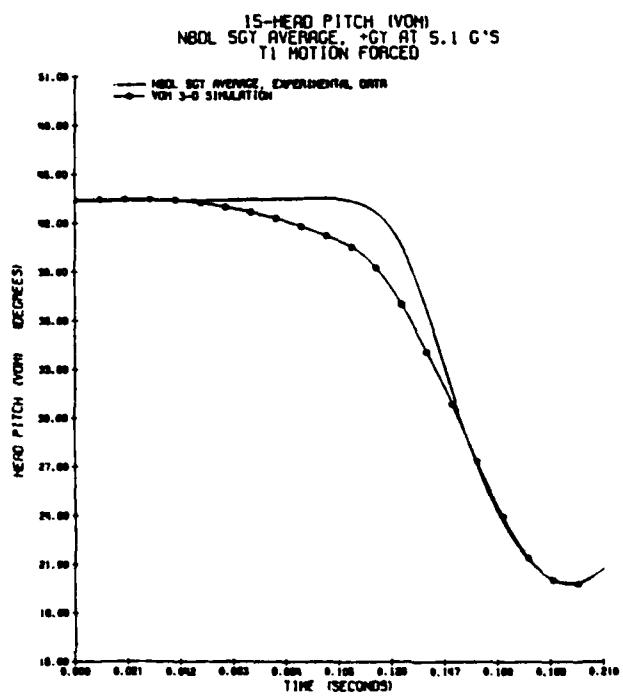


Figure 280. Head Pitch for Long Neck Model with T1(-5.6) Pivot at +5Gy.
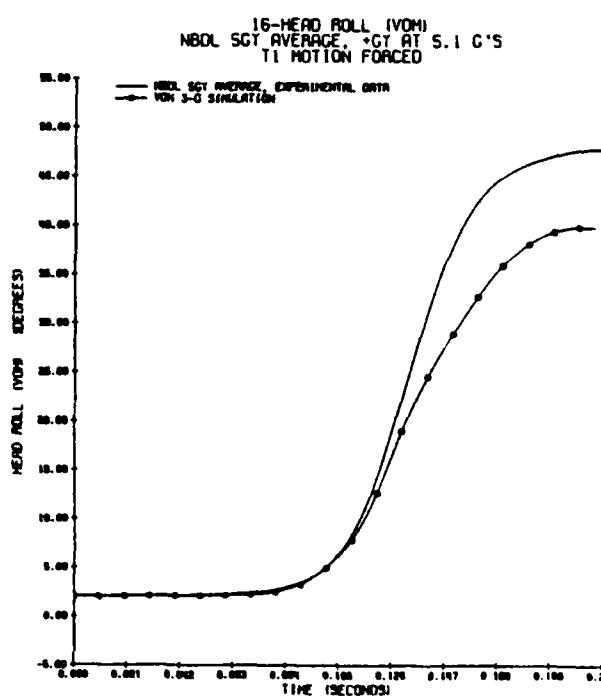


Figure 281. Head Roll for Long Neck Model with T1(-5.6) Pivot at +5Gy.
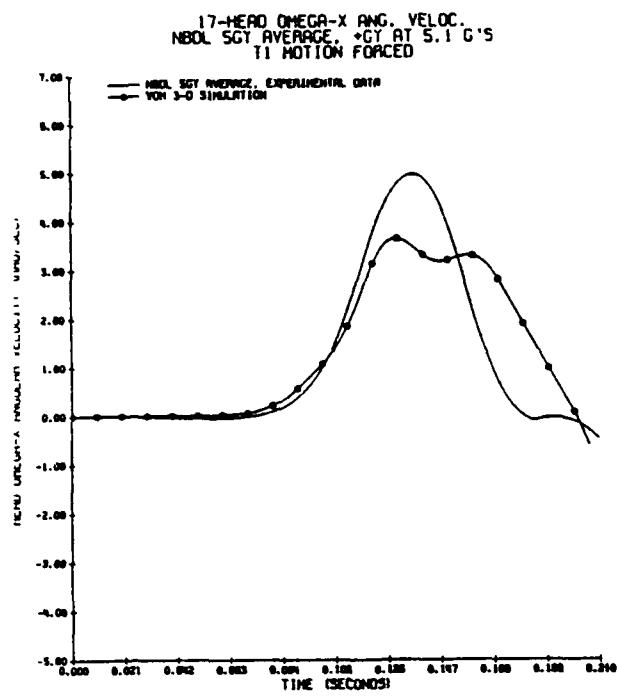
Figure 282. Head X-Axis Angular Velocity for Long Neck Model with T1(-5,6) Pivot at +5Gy.
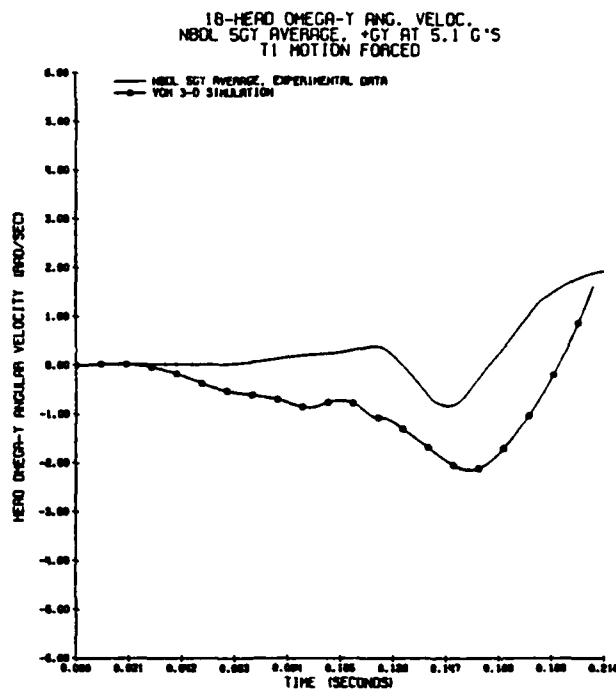


Figure 283. Head Y-Axis Angular Velocity for Long Neck Model with T1(-5,6) Pivot at +5Gy.
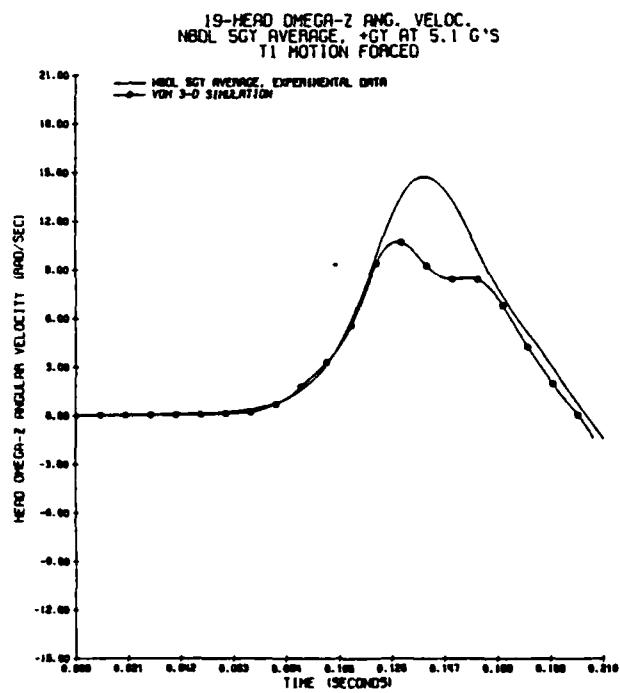


Figure 284. Head Z-Axis Angular Velocity for Long Neck Model with T1(-5,6) Pivot at +5Gy.
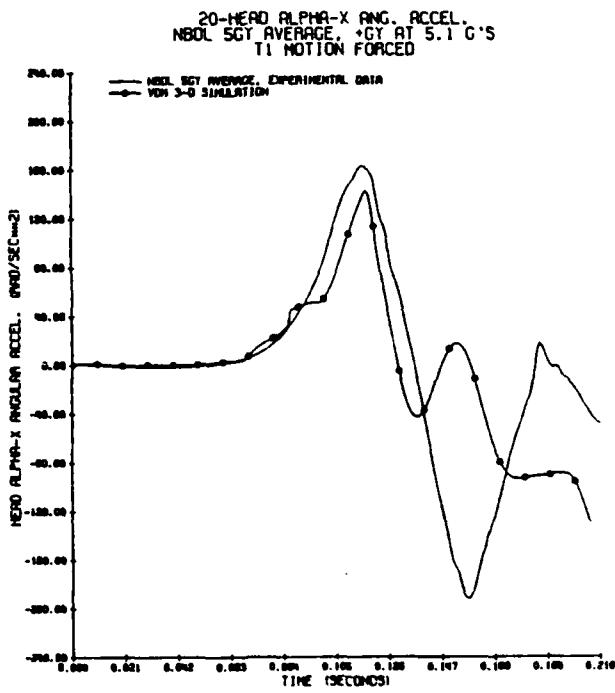


Figure 285. Head X-Axis Angular Acceleration for Long Neck Model with T1(-5,6) Pivot at +5Gy.
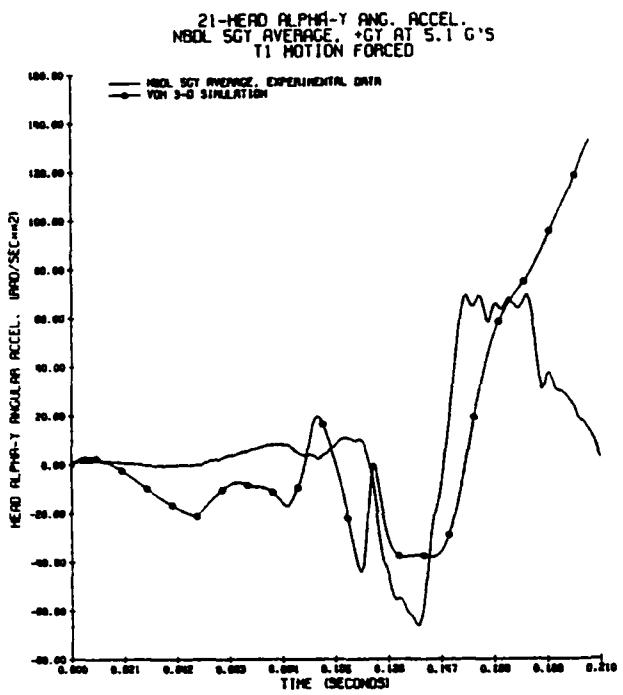
Figure 286. Head Y-Axis Angular Acceleration
for Long Neck Model with T1(-5,6) Pivot at +5Gy.
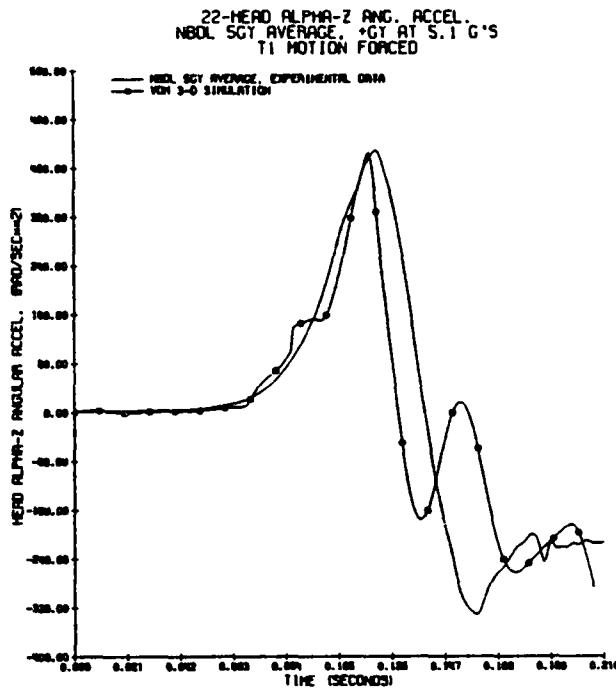


Figure 287. Head Z-Axis Angular Acceleration
for Long Neck Model with T1(-5,6) Pivot at +5Gy.
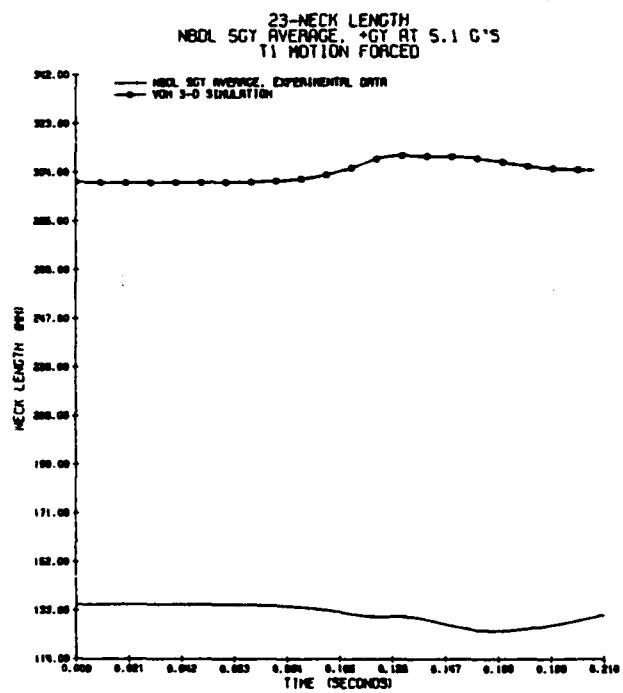


Figure 288. Neck Length for Long Neck Model
with T1(-5,6) Pivot at +5Gy.
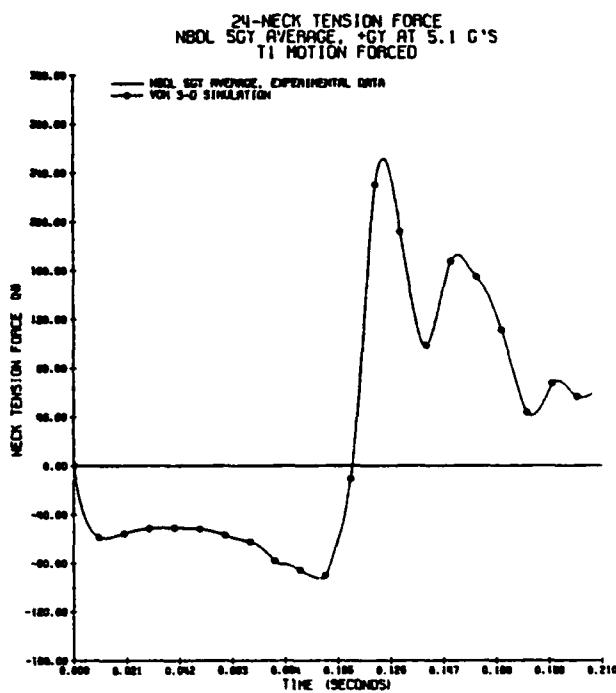


Figure 289. Neck Tension Force for Long Neck
Model with T1(-5,6) Pivot at +5Gy.

25-CONDYLE JOINT SINUS TORQ
NBDL SGT AVERAGE, +GY AT 5.1 G'S
T1 MOTION FORCED

26-C7-T1 JOINT SINUS TORQUE
NBDL SGT AVERAGE, +GY AT 5.1 G'S
T1 MOTION FORCED
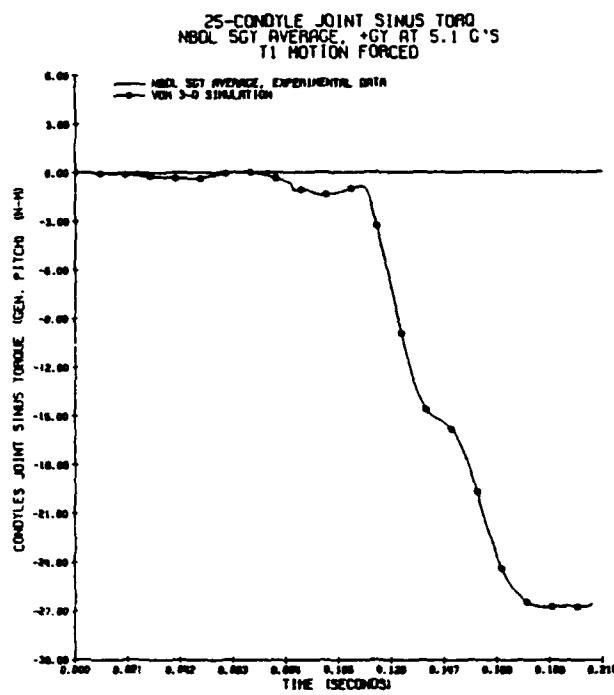
Figure 290. Condyle Joint Sinus Torque for Long
Neck Model with T1(-5,6) Pivot at +5Gy.
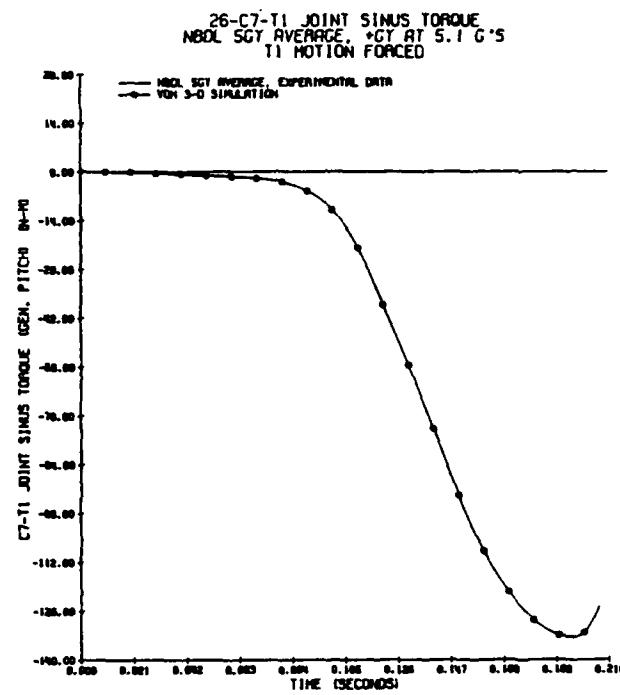
Figure 291. C7-T1 Joint Sinus Torque for Long
Neck Model with T1(-5,6) Pivot at +5Gy.

27-TOTAL NECK TWIST TORQUE
NBDL SGT AVERAGE, +GY AT 5.1 G'S
T1 MOTION FORCED
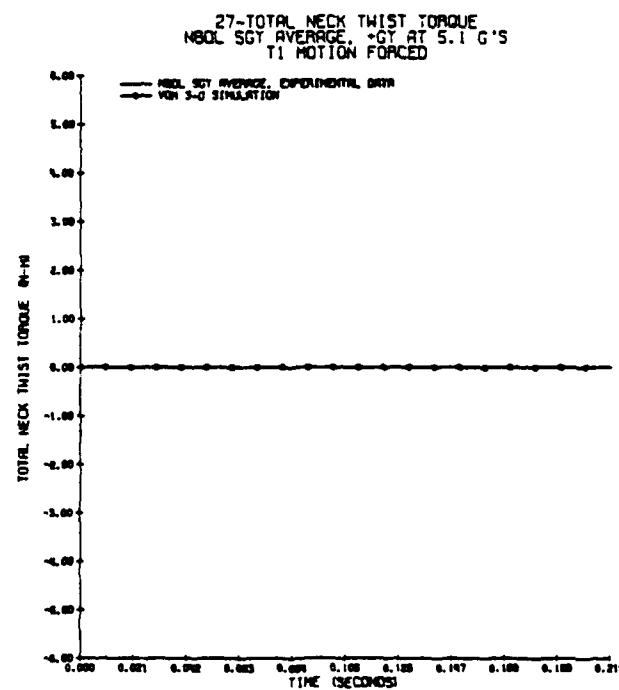
Figure 292. Total Neck Twist Torque for Long
Neck Model with T1(-5,6) Pivot at +5Gy.

131

END

DTIC

8-86